Phytoplankton and water color : multiscale analysis of the adaptive advantage conferred by chromatic acclimation in marine cyanobacteria

Louison Dufour

THESE DE DOCTORAT DE SORBONNE UNIVERSITE

Spécialité Ecologie Microbienne
« Sciences de la Nature et de l'Homme : évolution et écologie » (ED227)

Présentée par

DUFOUR LOUISON

En vue de l'obtention du grade de
DOCTEURE de SORBONNE UNIVERSITE

Phytoplankton and water color: Multiscale analysis of the adaptive advantage conferred by chromatic acclimation in marine cyanobacteria

Soutenue le 8 septembre 2023, devant le jury composé de :

Pr. Dr. Nicole FRANKENBERG-DINKEL ..... Rapportrice
Technische Universität Kaiserlautern-Landau

Pr. David J. SCANLAN ..... Rapporteur
University of Warwick

Dr. Cristiana CALLIERI ..... Examinatrice
Water Research Institute of Verbania

Pr. Stéphane EGEE ..... Président du jury
Sorbonne Université, Roscoff

Dr. Frédéric PARTENSKY ..... Directeur de thèse
CNRS, Roscoff

Dr. Laurence GARCZAREK ..... Co-directrice de thèse
CNRS, Roscoff

Station Biologique de Roscoff
UMR 7144 Adaptation et Diversité en Milieu Marin
Equipe ECOMAP (Ecology of Marine Plankton)

Abstract

Global change is predicted to have numerous impacts on the physico-chemical properties of the ocean. This includes a rapid expansion of warm, nutrient-poor areas that in turn alters the underwater light field, and subsequently impacts the competition between phytoplankton species that have an obligate requirement for light to produce energy. As the second organism in the world's ocean, and the most diversified with regard to its pigmentation, *Synechococcus* constitutes an excellent model to assess the consequences of on-going changes in water optical properties on the distribution, dynamics and composition of marine phytoplanktonic communities. To date, seven *Synechococcus* pigment types (PTs) have been identified based on the composition and chromophorylation of their light-harvesting complexes, called phycobilisomes. While PTs 3a and 3c have a fixed pigmentation that enable them to efficiently collect either green (GL) or blue light (BL), respectively, PT 3d are capable of Type IV chromatic acclimation (CA4). In other words, they can reversibly modify their phycobilisome pigmentation in order to capture either green or blue photons, according to the ambient light color. Two genetically distinct types of chromatic acclimaters (PTs 3dA and 3dB) have been evidenced and found to be equally abundant in the ocean. Together, they constitute the most prevalent *Synechococcus* PT at the global scale. However, the reasons for their prevalence in natural populations remain unclear. Both PTs 3dA and 3dB possess one genomic island involved in CA4, with partially distinct gene content (CA4-A and CA4-B islands, respectively). While the molecular bases of CA4-A begin to be well understood, CA4-B is less well known. One objective of my thesis was therefore to characterize genes of the CA4-B island using CRISPR-Cas12 technology. Partial characterization of one of these genes (*fciB*) suggested that the regulation of CA4 process in PT 3dB cells may be reversed compared to that of PT 3dA strains, since FciB appears to act as an activator or a repressor of the process. To investigate phenotypic differences between the two types of chromatic acclimaters, I also examined their response to various conditions of temperature, light quantity and quality. Interestingly, I found that both differ in the ratio of blue to green light required to trigger chromatic acclimation. The second objective consisted in better characterize the advantage conferred by chromatic acclimation over fixed pigmentation. For this purpose, I conducted mono- and co-cultures of PTs 3a, 3c and 3dB representatives in various light qualities and quantities, and demonstrated that blue (PT 3c) and green (PT 3a) light specialists where the best competitors in low BL and GL, respectively. At high light, the chromatic acclimater won the competition in BL, while the green light specialist was the winner in GL. In a mixture of both lights, co-existence of the chromatic acclimater and the green light specialist was achieved. Finally, the last objective was to refine our knowledge of the temporal and spatial dynamics of *Synechococcus*. To do so, I participated in a two-year time series at two oceanographically distinct sites (the SOMLIT-Astan station in the English Channel and the BOUSSOLE station in the Mediterranean Sea). Analysis of the picocyanobacteria cell concentration and ancillary parameters (nutrients availability, pigments, seawater optical characteristics) strongly suggests a seasonal succession of PT 3 subtypes at both sites, with variations in timing and relative proportion of PTs 3a, 3c and 3d cells. Upcoming metagenomic analyses should provide further insights into the relative abundance of the different *Synechococcus* PTs.

Résumé

Les propriétés physico-chimiques des océans sont particulièrement affectées par le changement climatique. Une expansion rapide des zones chaudes et pauvres en nutriments a notamment été remarquée, modifiant la couleur de l'eau et, par conséquent, la compétition entre les diverses espèces du phytoplancton qui ont besoin de lumière pour produire de l'énergie. En tant que deuxième organisme le plus abondant des océans, *Synechococcus* constitue un excellent modèle pour évaluer les conséquences de l'altération des propriétés optiques de l'eau sur la distribution, la dynamique et la composition des communautés phytoplanctoniques marines. A ce jour, sept types pigmentaires (TPs) ont été identifiés chez *Synechococcus* sur la base de la composition et de la chromophorylation de leurs complexes collecteurs de lumière, appelés phycobilisomes. Alors que les TPs 3a et 3c ont une pigmentation fixe qui leur permet de collecter efficacement la lumière verte ou bleue, respectivement, le TP 3d est capable d'acclimatation chromatique de Type IV (CA4). En d'autres termes, il peut modifier de manière réversible la pigmentation de ses phycobilismes afin de capturer les photons verts ou bleus, en fonction de la couleur de la lumière ambiante. Deux types génétiquement distincts d'acclimateurs chromatiques également abondants dans l'océan (TPs 3dA et 3dB) ont été mis en évidence. Ensemble, ils constituent le TP de *Synechococcus* le plus répandu à l'échelle globale, bien que les raisons de leur prévalence dans les populations naturelles ne soient pas claires. Les TPs 3dA et 3dB possèdent chacun un îlot génomique impliqué dans la CA4 (îlots CA4-A et CA4-B). Alors que les bases moléculaires de la CA4-A commencent à être bien comprises, celles de la CA4-B sont moins connues. Un des objectifs de ma thèse a donc été de caractériser des gènes de l'îlot CA4-B en utilisant la technologie CRISPR-Cas12. La caractérisation partielle de l'un des gènes (*fciB*) a suggéré que la régulation de la CA4 chez les TPs 3dB pourrait être inversée par rapport à celle rencontrée chez les TPs 3dA. En effet, FciB semble agir comme un activateur chez l'un, et comme un répresseur chez l'autre. Pour étudier les différences phénotypiques entre les deux types d'acclimateurs chromatiques, j'ai également examiné leur réponse dans diverses conditions de température, quantité et qualité de lumière. De toute évidence, les TPs 3dA et 3dB diffèrent dans le rapport de lumière bleue et verte nécessaire pour déclencher la CA4. Le deuxième objectif a consisté à mieux caractériser l'avantage conféré par l'acclimatation chromatique par rapport à la pigmentation fixe. Pour cela, j'ai réalisé des mono-cultures et co-cultures de représentants des TPs 3a, 3c et 3dB dans différentes conditions de qualité et de quantité de lumière. J'ai démontré que les spécialistes de la lumière bleue (TP 3c) et verte (TP 3a) sont les meilleurs compétiteurs dans des conditions de faible lumière bleue et verte, respectivement. A plus forte intensité lumineuse, le spécialiste de la lumière verte a remporté la compétition en vert, et l'acclimateur chromatique en bleu. Dans un mélange des deux lumières, la coexistence des deux mêmes souches a été observée. Enfin, le dernier objectif a été d'affiner nos connaissances concernant la dynamique temporelle et spatiale des *Synechococcus*. Pour ce faire, j'ai participé à une série temporelle de deux ans au niveau de deux sites océanographiquement distincts : la station SOMLIT-Astan en Manche et la station BOUSSOLE en Méditerranée. L'analyse de l'abondance de picocyanobactéries, couplée à divers autres paramètres auxiliaires (disponibilité des nutriments, pigments, caractéristiques optiques de l'eau de mer), suggère fortement une succession saisonnière des TPs 3a, 3c et 3d au niveau des deux sites. Les prochaines analyses métagénomiques devraient permettre de mieux décrire l'abondance relative des différents TPs de *Synechococcus*, ainsi que leurs cycles saisonniers.

Acknowledgements/Remerciements

I would like to start by thanking Nicole Frankenberg-Dinkel, David Scanlan, Cristiana Callieri and Stéphane Egée for agreeing to read and evaluate my work. I also wish to thank Julia Uitz, Nathalie Simon, David Kehoe and Christophe Destombe for accepting to be part of my thesis committee and for giving me so much advice and feedback on my work.

Je souhaite également remercier Loh et Fred, sans qui tout ça n'aurait tout simplement pas été possible. Au-delà de superviser cette thèse et de me former à la recherche, vous avez su me donner envie de poursuivre en post-doc (et ce n'était pas gagné... !). Merci pour votre entrain, votre amour de la science, vos projets dantesques, et surtout d'avoir mis autant d'énergie dans ce projet.

J'ai une grande pensée pour Momo. Ca a été un immense plaisir de travailler avec toi. Merci de m'avoir formée, aidée, rassurée, soutenue et j'en passe. Merci aussi pour ton énergie matinale débordante, tes improvisations musicales, et pour les moments de détente à construire des murs en pierre. Je pense également à Julia et Bastian, qui m'ont grandement aidée. C'était une super expérience de vous former et de vous voir évoluer au sein de la Station. Merci beaucoup pour le grand coup de main que vous m'avez donné. Autre compère de labo, et pas des moindres, un grand merci à Mathilde. Tellement de temps passé à tes côtés à la Station, et en dehors, que j'en perds les mots. Je te remercie donc pour tous ces moments et pour ton amitié. Je pense aussi aux collègues de bureau, notamment Ulysse et Emile.

Je souhaite remercier très chaleureusement tous les membres de l'équipe PhytoPK avec qui j'ai eu le plaisir de partager de nombreuses pauses café, discussions et réunions. Un merci tout particulier à Flo, Fabienne, Pris et Domi pour votre bienveillance ; et à Martin pour les (?trop nombreuses?) analyses cyto. Merci également aux autres membres de la Station qui ont ensoleillé mes journées et/ou participé, de près ou de loin, à mes travaux. Je pense notamment à l'équipage de la Néomysis qui m'a emmené en mer pendant 2 ans, et par tout temps ! Le C-OPS n'aura jamais autant surfé, et moi été malade ! Je pense également à l'équipe du RAS qui m'a fait de la place au sein de ses locaux pendant plus d'un an. Merci aussi à l'équipe enseignante de m'avoir fait confiance au cours de mon monitorat.

Roscoff c'est aussi beaucoup d'ami.e.s, beaucoup trop pour être listé.e.s ici. Je me contente donc de vous remercier pour les nombreux moments de bonheur qui m'ont permis d'arriver au bout de cette aventure qu'est la thèse. Je pense aux balades, pique-niques, baignades dans l'eau glaciale, verres au Typ, festivals, et bien d'autres. Merci mille fois. J'ai une pensée toute spéciale pour Yasmine et Lisa. Merci à vous deux d'avoir fait de la coloc un cocon douillet, et bien plus encore...

Je pense aussi à mes copain.e.s d'ailleurs ainsi qu'à ma famille, à leur soutient sans bornes et aux efforts déployés pendant 4 ans pour comprendre ce que je faisais. Merci aussi à toi, Sam, pour ta patience, ta gentillesse et ta grande générosité.

Le mot final est évidemment dédié à Roscoff, merci pour ta beauté, tes couchers de soleils spectaculaires et pour tout ce que tu m'as offert.

Table of contents

List of figures

List of acronyms

APC: allophycocyanin
β-car: β-carotene
BL: blue light
CA4: type IV chromatic acclimation
Chl *a*: chlorophyll *a*
DOM: dissolved organic matter
FSC: forward scatter
GL: green light
gRNA: guide RNA
HBL: high blue light
HBGL: high blue green light
HGL: high green light
HL: high light
HTR: homologous template region
LBL: low blue light
LGL: low green light
LL: low light
OM: organic matter
PBP: phycobiliprotein
PBS: phycobilisome
PC: phycocyanin
PCB: phycocyanobilin
PE: phycoerythrin
PEB: phycoerythrobilin
PEC: phycoerythrocyanin
POM: particulate organic matter
PSI: type I photosystem
PSII: type II photosystem
PT: pigment type
PUB: phycourobilin
PVB: phycobiliviolin
RC: reaction center
TA: terminal acceptor
WT: wild type
Zea: zeaxanthin

Introduction

I. Photosynthesis and light harvesting

I.1. A bit of history

Oxygenic photosynthesis, which first appeared in ancestors of modern-day cyanobacteria (Adir, 2005; Adir et al., 2006), is one of the most important metabolic innovations in the history of Earth (Blankenship and Hartman, 1998; Fischer et al., 2016; Sánchez-Baracaldo and Cardona, 2020). On the one hand, this process has enabled multiple living beings to produce organic carbon from carbonic gas and water using solar energy, thus significantly increasing primary production. On the other hand, the resulting release of a large quantity of oxygen, particularly during the Great Oxidation Event (2.4 – 2.32 billion years ago) and the Neoproterozoic Oxidation Event (800 – 600 million years ago; Sánchez-Baracaldo and Cardona, 2020), irreversibly changed the redox state and composition of the atmosphere and oceans. This further led to a complete restructuration of ecosystems and to strong alterations of the main biogeochemical cycles (Fischer et al., 2016; Schirrmeister et al., 2016).

Photosynthesis is an ancient process and dating its appearance remains a challenge requiring the integration of a wide range of scientific disciplines (Fischer et al., 2016). Little is also known about the origin and evolutionary history of cyanobacteria, which form a monophyletic group of gram-negative bacteria that derived from ancestral heterotrophic bacteria (Melainabacteria and Sericytochromatia; Schirrmeister et al., 2016; Soo et al., 2017; Sánchez-Baracaldo and Cardona, 2020). However, their presence on Earth must be older than the Great Oxidation Event since they are widely recognized as being responsible for it (Fig. 1).

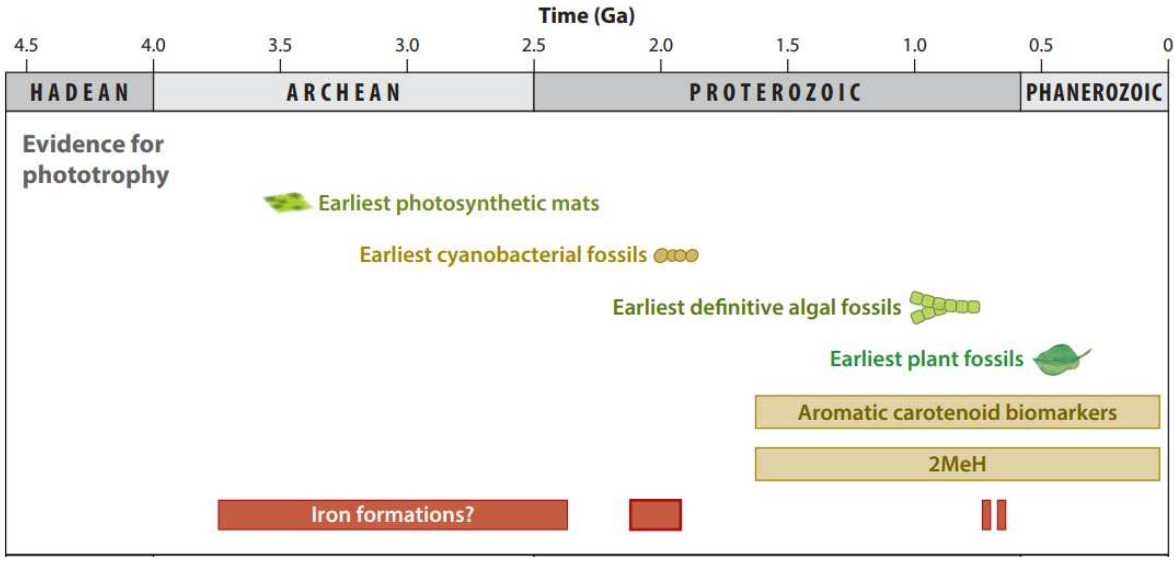

Figure 1: Oxygen enrichment of the atmosphere and evolution of phototrophy over geological times. The first forms of life on Earth were most probably non-photosynthetic. The appearance of anoxygenic phototrophy is dated to 3.5 billion years ago in fossilized microbial mats. The oldest unambiguous evidence of cyanobacteria fossils, and thus of oxygenic photosynthesis, dates back to 1.9 billion years (Fischer et al., 2016).

Besides being responsible for a major environmental transition, the ancestors of present-day cyanobacteria have played an important role in the evolutionary history of plants and animals. The progressive dioxygen enrichment of the atmosphere and oceans indeed allowed the appearance of more complex multicellular life forms capable of aerobic respiration (Adir, 2005; Schirrmeister et al., 2016; Soo et al., 2017; Sánchez-Baracaldo and Cardona, 2020). In addition, cyanobacteria are recognized as the ancestors of chloroplasts. Higher plants and algae have therefore acquired their photosynthetic capacities by endosymbiosis of an ancestral cyanobacterium (Sagan, 1967).

I.2. Photosynthesis in the tree of life

The tree of life has been divided into three domains (Archaea, Bacteria and Eukarya) based on the comparison of the gene sequences of small ribosomal subunits (16S and 18S rDNA) from many organisms. Photosynthesis, which can globally be defined as the process allowing an organism to capture, store and use light energy, is present within two of the three domains of life, being totally absent from Archaea (Fig. 2; Blankenship, 2014). The forms of photosynthesis are diverse and varied. Still, the most common form involves

chlorophyll type pigments bound to photosystems. In Bacteria, six major groups are able to carry out chlorophyll-based photosynthesis: (i) chloroacidobacteria, green sulfur bacteria and heliobacteria, which have type I photosystems; (ii) filamentous anoxygenic phototrophs (FAPs) and purple bacteria, which are characterized by type II photosystems; and finally (iii) cyanobacteria. While the first five groups are anoxygenic, cyanobacteria belong to oxygenic organisms. They are the only bacteria to have the two types of photosystems and to produce molecular oxygen as a by-product during photosynthesis (Blankenship, 2014; Sánchez-Baracaldo and Cardona, 2020).

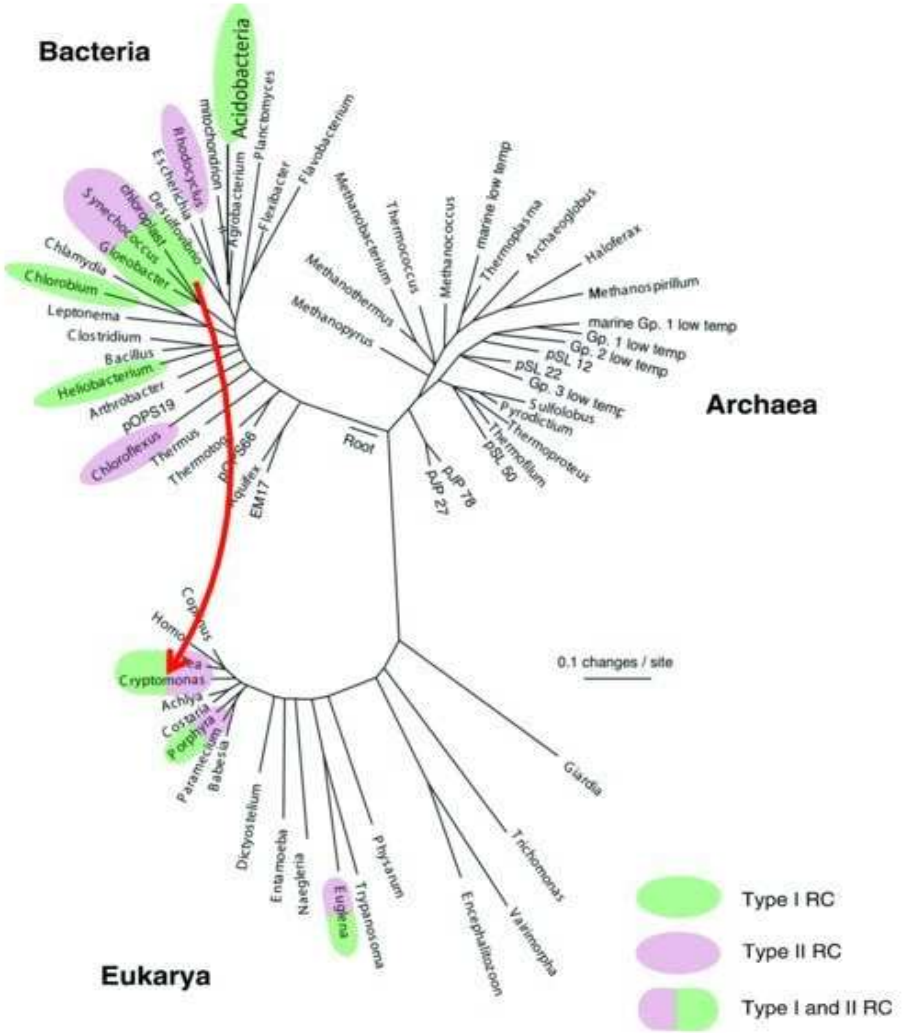

<u>Figure 2:</u> Distribution within the three domains of life (Archaea, Bacteria and Eukarya) of chlorophyll-based photosynthesis. The phylogeny presented here is the result of the comparison of numerous sequences of 16S rRNA (Archaea and Bacteria) and 18S rRNA (Eukarya). The taxa highlighted include photosynthetic organisms and colors correspond to the different types of reaction centers (RC). The red arrow indicates the primary endosymbiosis event at the origin of chloroplasts (Blankenship, 2014).

Reflecting the great diversity of organisms practicing photosynthesis, different types of photosynthetic apparatus associated with bilayer lipid membranes exist (Fig. 3). While the reaction centers are relatively well preserved from a functional and structural point of view, light-harvesting antennae (chlorosome, LH1/2, LHCI/II, phycobilisome, etc.) and the pigment content of the photosynthetic apparatus (bacteriochlorophylls, bilins, carotenoids, chlorophylls, xanthophylls, etc.) are highly variable between (and sometimes even within) bacterial groups (Ong and Glazer, 1991; Adir, 2005; Adir et al., 2006; Blankenship, 2014; Singh et al., 2015). This suggests that antennae have appeared several times during evolution to allow adaption to different photic environments. In fact, the type, size and number of antennae seemingly reflect the light niches in which the organisms preferentially thrive (smaller and fewer antennae complexes in environments characterized by high light intensities, and vice versa; Grossman et al., 1993; Anderson and Toole, 1998; Blankenship, 2014).

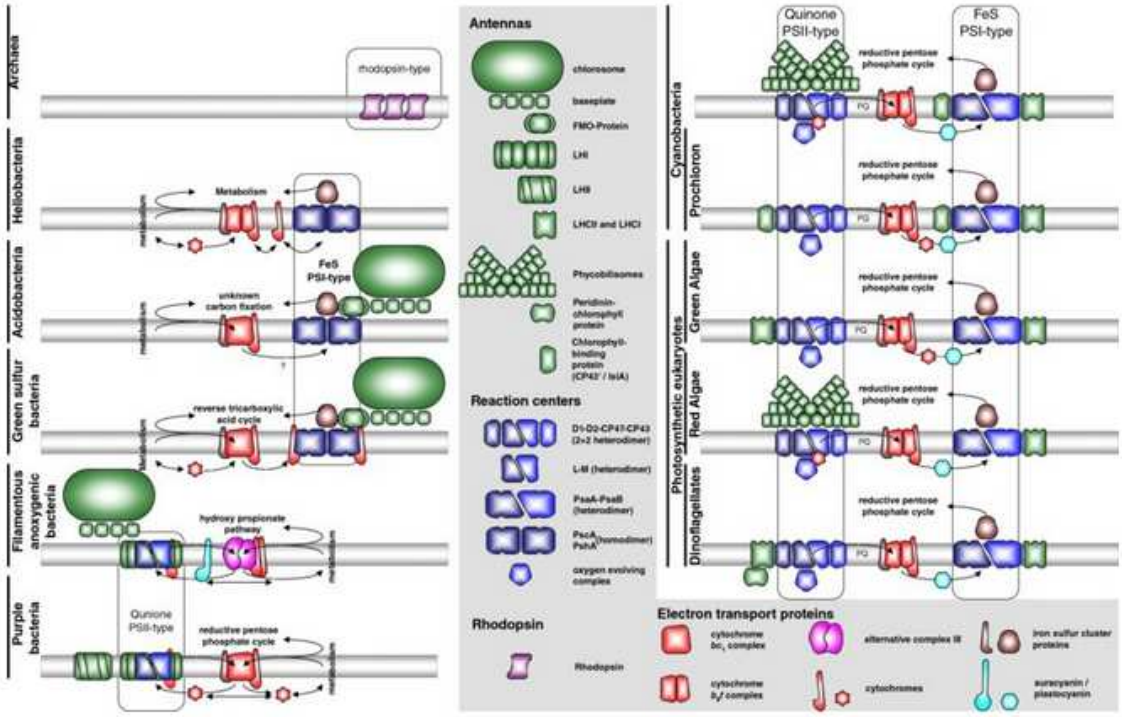

Figure 3: Schematic representation of the wide diversity of photosynthetic apparatuses found in anoxygenic bacteria, cyanobacteria and photosynthetic eukaryotes, as compared to the mere archaerhodopsin-type proton pump found in some archaea (phototrophy). While photosynthetic reaction centers are fairly well conserved, antenna complexes are very variable in terms of type, number, size, pigmentation and association with the membrane (membrane integral, extrinsic but strongly associated with the reaction centers, peripheral, etc.; Blankenship, 2014).

The cellular localization of photosynthetic apparatuses also strongly varies depending on organisms. In eukaryotes, photosynthesis occurs in chloroplasts that are cell organelles derived from the primary endosymbiosis event. Chloroplasts contain thylakoids that form a large membrane system. This comprise many photosynthetic complexes binding chlorophyll *a* and several accessory pigments necessary for harvesting and transferring photons to reaction centers. The specificity of higher plants, compared to the majority of algae, relies in the association of thylakoids in grana linked by stromatic lamellae (Fig. 4; Blankenship, 2014).

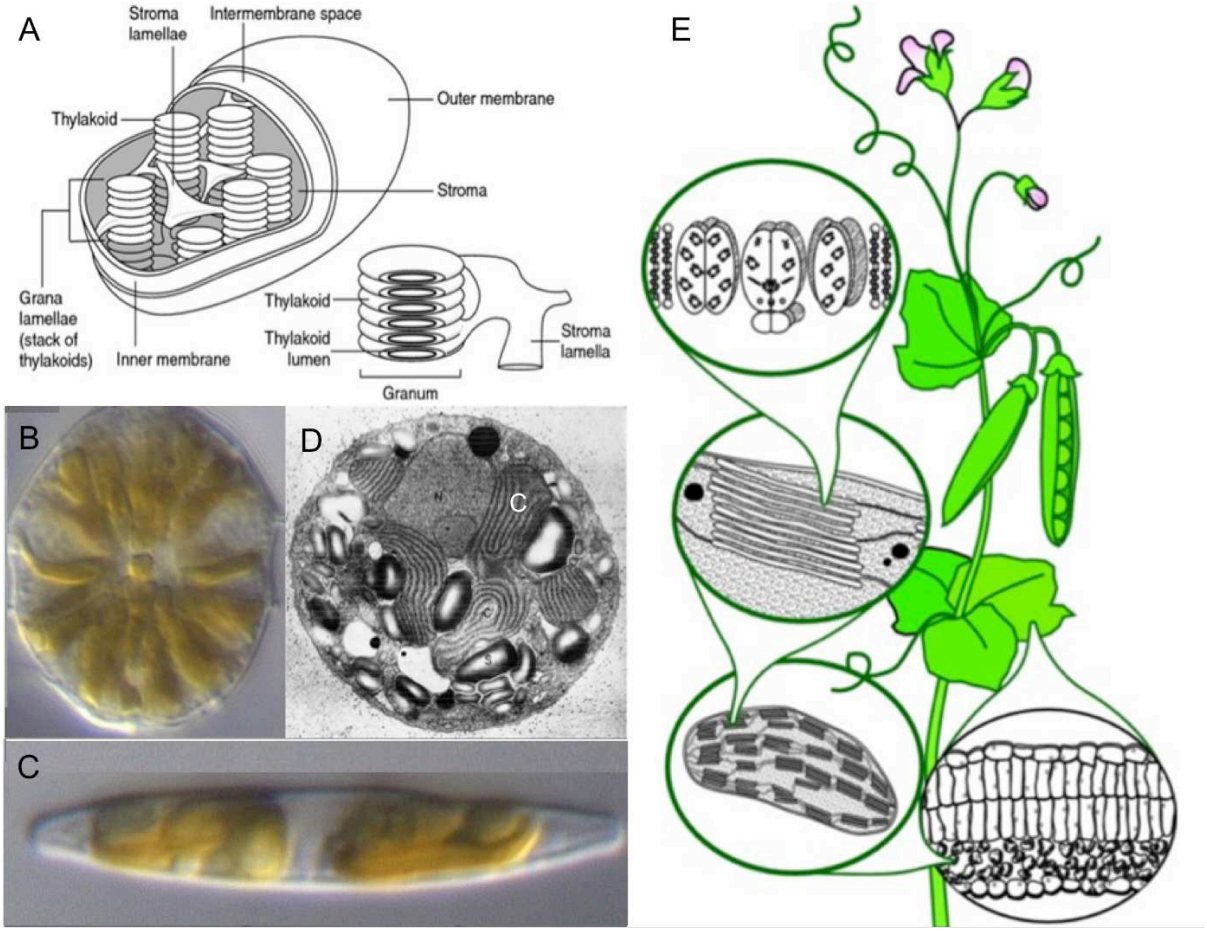

Figure 4: Location of photosynthetic apparatus in eukaryotes. (A) Schematic representation of a chloroplast (Blankenship, 2014). (B) Image of a dinoflagellate (*Alexandrium minutum*, RCC2330, Roscoff Culture Collection). Chloroplasts are the greenish-brown aggregates. (C) Image of a diatom (*Nitzschia. sp*, RCC2276, Roscoff Culture Collection). (D) Image of a section of the red alga *Porphyridium cruentum* (Gantt and Conti, 1966). C, chloroplast. (E) Schematic representation of the photosynthetic apparatus in higher plants. In the bubbles are successively represented: a leaf cross section, a chloroplast, thylakoids assembled in grana, a thylakoid membrane containing a reaction center and its antenna (Blankenship, 2014).

In prokaryotes, the photosynthetic process takes place in the cytoplasm and more precisely in specialized intracellular membranes that form a dense network of cylindrical layers, the thylakoids. In a large number of cyanobacteria, these are parallel to one another and to the cytoplasmic membrane (Fig. 5; Stanier and Cohen-Bazire, 1977; Johnson and Sieburth, 1979; Chisholm et al., 1988; Blankenship, 2014). Their number varies according to strains and growth conditions.

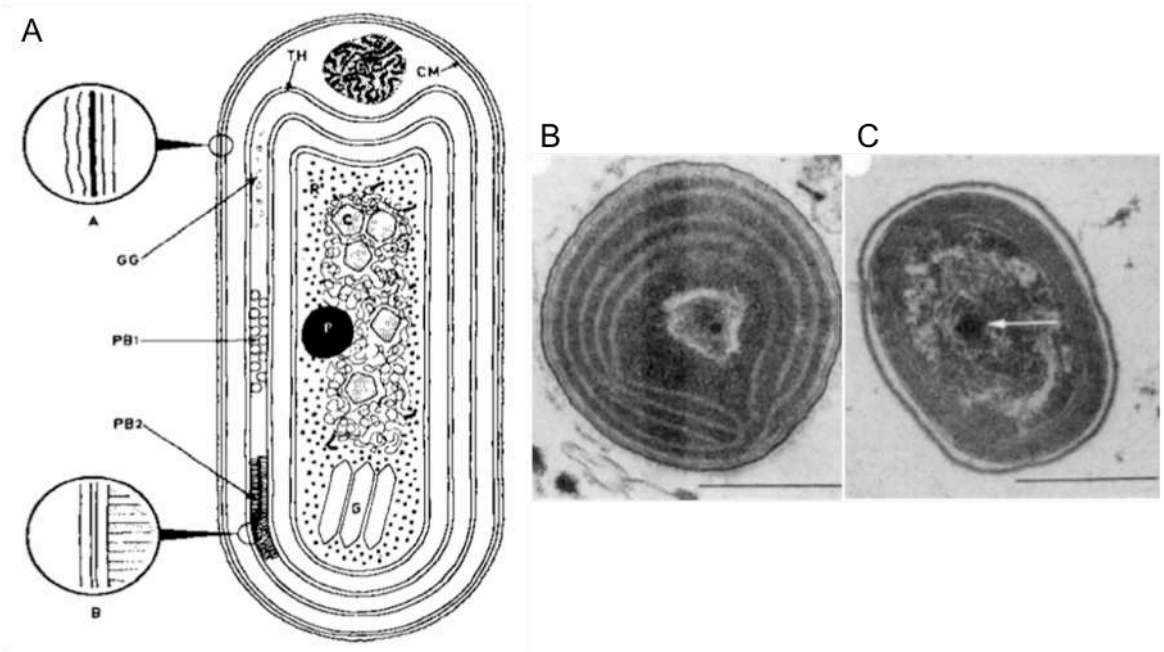

Figure 5: Location of photosynthetic apparatus in cyanobacteria. (A) Schematic representation of a cyanobacterial cell (Stanier and Cohen-Bazire, 1977). CM, cell membrane; TH, thylakoid; PB1 and PB2, phycobilisomes; GG, glycogen granules; CY, cyanophycin granule; P, polyphosphate granule; R, 70S ribosomes; C, carboxysome; G, gas vesicle. (B) and (C) Images of *Synechococcus* and *Prochlorococcus* cells taken by transmission electron microscopy (Chisholm et al., 1988). The scale bar is 0.5 µm for each image. The concentric thylakoids are parallel to the plasma membrane. They are widely interspaced from each other in *Synechococcus* (40 – 50 nm) and closely appressed in *Prochlorococcus*.

In addition of being the site of light energy absorption in eukaryotes and prokaryotes, thylakoid membranes are involved in the first stages of the transformation of photon energy into chemical energy, as well as the conveying of electrons through the electron transport chain (Blankenship, 2014).

I.3. Molecular mechanisms in oxygenic photosynthesis

Photosynthetic organisms are photoautrophs since they use light energy from the sun and mineral electron donors, most often carbon dioxide (CO_2) or water (H_2O), to synthesize their own carbonaceous organic matter (Blankenship, 2014; Fischer et al., 2016). The global equation of oxygenic photosynthesis is as follows:

$$nCO_2 + H_2O \rightarrow (CH_20)_n + O_2$$

Yet this process is divided into two decoupled phases, often called the 'light reactions' and the 'dark reactions'. The four transmembrane multiprotein complexes involved in the light reactions, i.e. the highly conserved photosystems I and II, cytochrome b_6f and ATP synthase, are located in the thylakoid membrane (Fig. 6; Ke, 2001; Blankenship, 2014; Fischer et al., 2016).

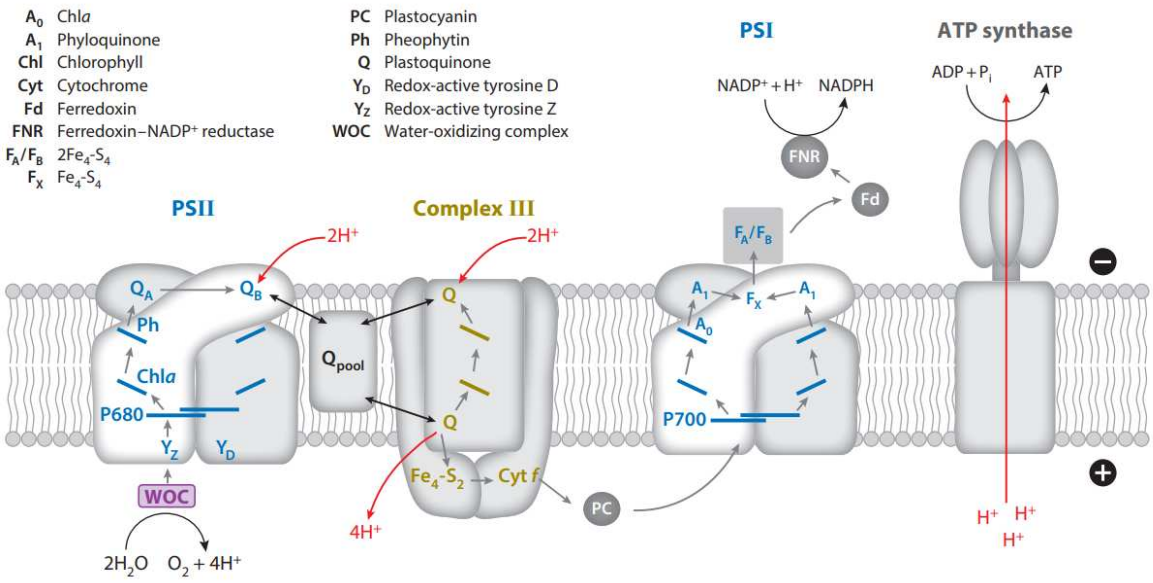

Figure 6: Schematic representation of electron and proton transports during the light phase of oxygenic photosynthesis in the thylakoid membrane. Grey arrows indicate the path taken by electrons; red ones represent the translocation of protons. PSII light absorption leads to charge separation. Electrons are transferred to the PSI via the cytochrome b_6f (here complex III). The pair of oxidized chlorophylls ($P680^+$) recovers electrons via the action of the Oxygen Evolving Complex (here WOC). The proton transmembrane electrochemical gradient, created by electrons transport, is dissipated by the ATP synthase that produces ATP (Fischer et al., 2016).

During the light phase in cyanobacteria, the photon energy harvested by antenna pigments is transmitted to a special pair of chlorophylls *a*, P680 (λ_{max} = 680 nm), located in the reaction center (RC) of photosystem II (PSII), itself consisting of a protein dimer (D1 and D2). After excitation, the chlorophyll pair reaches an oxidized state, $P680^+$, and rapidly releases an electron to a primary acceptor called pheophytin. Following this photoinduced charge separation, the $P680^+$ recovers an electron from a primary donor, the tyrosine Z residue of the D1 protein, in order to return to its fundamental state. In organisms performing oxygenic photosynthesis, this electron comes from the water photolysis occurring at the level of the Oxygen Evolving Complex. The dissociation of two water molecules by four successive photo-oxidation reactions is catalyzed by a cluster of manganese and calcium (Mn_3CaCO_4) and results in the release of one dioxygen molecule, 4 protons and 4 electrons (Fig. 6; Ke, 2001; Blankenship, 2014; Fischer et al., 2016).

Photoinduced charge separation results in electron transfer within the thylakoid membrane via successive oxidation-reduction reactions. Besides pheophytin, this transport involves plastoquinones A and B, cytochrome b_6f, plastocyanin and then photosystem I (PSI). The energy transfer within PSI is similar to what has been described for PSII. Light energy is transmitted to a special pair of chlorophyll *a*, P700 (λ_{max} = 700 nm), located in the RC of PSI, itself composed of the proteins PsaA and PsaB. The $P700^+$ yields an electron to the powerful reducer A_0, which is transmitted to different cofactors (A_1, iron-sulfur proteins, ferredoxin) up to a final acceptor, the ferredoxin-NADPH oxidoreductase. This uses electrons to reduce $NADP^+$ to NADPH, which serves as a reducing agent in many cellular processes. These redox reactions between the two photosystems constitute the non-cyclic transport of electrons (Fig. 7; Ke, 2001; Blankenship, 2014; Fischer et al., 2016).

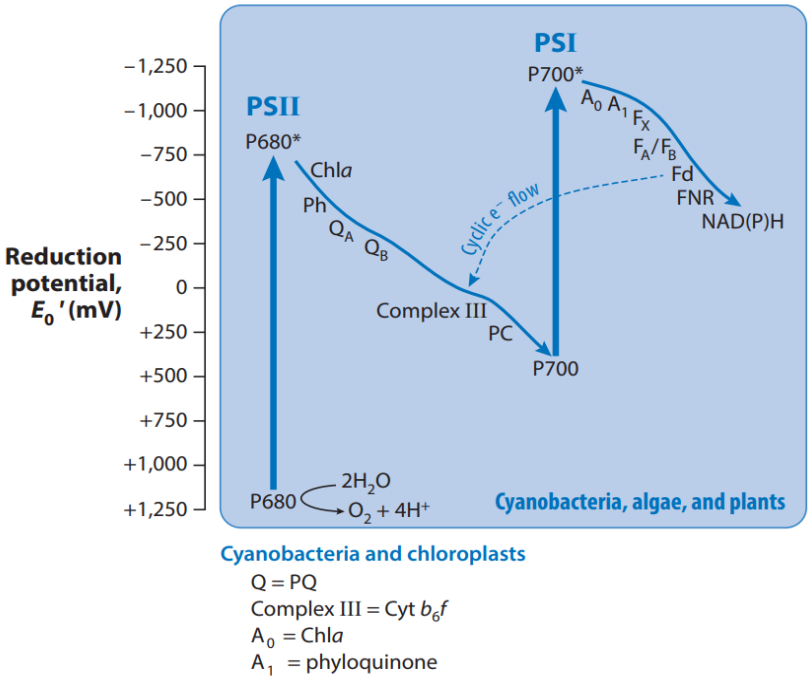

Figure 7: Schematic representation of the cyclic and non-cyclic transport of electrons during oxygenic photosynthesis. P680, pair of chlorophyll *a* from the photosystem II (PSII) reaction center; Ph, pheophytin; Q_A/Q_B, plastoquinones; complex III, cytochrome b_6f; PC, plastocyanin; P700, pair of chlorophyll *a* from the PSI reaction center; A_0/A_1, electron carriers; F_X/F_A, iron-sulfur proteins; F_d, ferredoxin; FNR, ferredoxin-$NADP^+$ oxidoreductase; NADPH, nicotinamide adenine dinucleotide phosphate reduced (Fischer et al., 2016).

In some cases, a cyclic electron transport may be established to control the transmembrane electrochemical gradient and the production of NADPH. During the transfer of electrons from the primary to the terminal acceptor, the cytochrome *b_6f* uses a part of the excitation energy to pump protons through the thylakoid membrane, creating an electrochemical gradient (Fig. 6). Cyclic transport involves the transfer of electrons from ferredoxin back to cytochrome *b_6f*, which transfers additional protons through the membrane (Fig. 7; Ke, 2001; Blankenship, 2014; Fischer et al., 2016).

It is the adenosine triphosphate (ATP) synthase, the fourth complex of thylakoid membranes (Fig. 6), which dissipates and transforms the generated electrochemical gradient into chemical energy via the phosphorylation of adenosine diphosphate (ADP) into ATP. The ATP and NADPH molecules produced by this process are then used during the dark (light-independent) phase of photosynthesis to fix CO_2 and incorporate it into sugars during the

Calvin-Benson cycle. These organic molecules are then included in many biomolecules (DNA, RNA, proteins; for more details, see Blankenship, 2014).

I.4. The phycobilisome, the light-harvesting antennae of most cyanobacteria

I.4.a. Overview

Most cyanobacteria and all red algae are characterized by the presence of huge membrane-extrinsic antenna complexes called phycobilisomes (PBS). The first PBS components were discovered by Von Esenbeck (1836). He described “saprocyanin”, a water-soluble blue pigment fluorescing in red, in the freshwater cyanobacterium *Oscillaria* sp. This pigment was renamed “phykokan” by Kützing (1843), who isolated a water-soluble red pigment with similar properties from red algae, which he called “phykoerythrin”. The first crystals of those two molecules were obtained at the end of the 19th century (Cramer, 1862; Möllisch, 1894, 1895) and allowed Kylin (1910, 1912) to demonstrate that both were in fact made up of an apoprotein similar to hemoglobin and a pigment (see Tandeau de Marsac, 2003 for more information).

The structure and uniform distribution of granules associated with the thylakoid membrane in the red algae *Porphyridium cruentum* were first observed in the 1950s, thanks to the spectacular advances made at that time in the field of electron microscopy (Fig. 8; Gantt and Conti, 1965, 1966). Gantt and Conti suggested that these granules contained accessory pigments involved in photosynthesis and gave them the name ‘phycobilisomes’ after successfully isolating them.

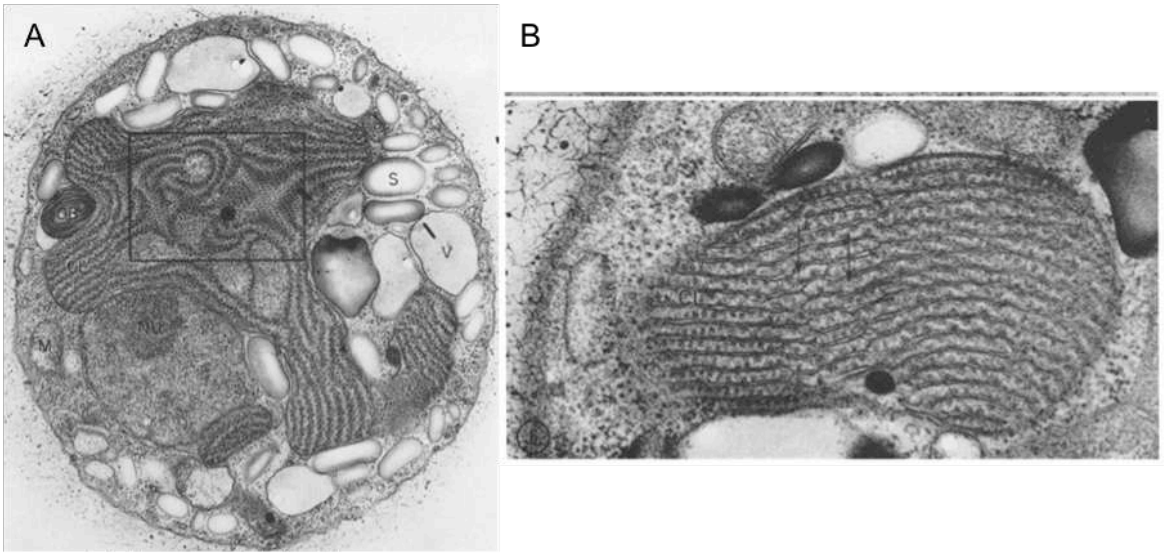

Figure 8: Electron microscopy images of cells of the red algae *Porphyridium cruentum*. (A) Section of a cell (x27 000). The granules (phycobilisomes) are regularly ordered at the surface of the chloroplasts. NU, nucleus; CL, chloroplast lamellae. (B) Zoom on the chloroplast lamellae (x50 000; (Gantt and Conti, 1965).

Beyond the study of the PBS complex as a whole, many researchers have been interested in the characterization of its components (proteins and pigments). After numerous attempts to separate the PBS subunits, the structural and spectral properties of the pigments, as well as their mode of interaction with the proteins, were determined in the 1960s. The physico-chemical properties of the latter were studied in the 1970 – 1980s using electron microscopy and X-ray diffraction techniques (Adir et al., 2020). All these advances enabled Bryant and collaborators (1979) to produce the first description of the 3D structure of PBS, which subsequently served as a basis for many works (for more details see Tandeau de Marsac, 2003). At the same time, fluorescence polarization analyses helped scientists to better understand how energy is transferred within PBS. A detailed description of the mechanism was published by Glazer (1989), almost a hundred years after Engelmann (1881 – 1884) first demonstrated the involvement of phycocyanin and phycoerythrin in the harvesting of light energy.

Since the description of *P. cruentum* PBS, electron microscopy and isolation techniques have been improved and used to study the ultrastructure of the light-harvesting complexes of many cyanobacteria and red algae.

I.4.b. General structure

The presence of PBS, which are huge macro-complexes located on top of photosynthetic membranes and associated with photosystems, differentiates the photosynthetic apparatus of most cyanobacteria and red algae from the intra-membrane light-harvesting complexes of green algae and higher plants (Anderson and Toole, 1998). Although their localization within the cell is different from other antenna complexes, PBS also act as light energy collectors. Their peculiar pigmentation allows cyanobacterial cells to exploit the visible light spectrum between 450 and 665 nm, thus, considerably expending the spectral range of chlorophyll *a* that collects blue and red light (430 nm and 680 nm; Gantt, 1981; Glazer, 1989; Grossman et al., 1993; Sidler, 1994; MacColl, 1998; Scheer and Zhao, 2008; Singh et al., 2015; Adir et al., 2020, 2020).

PBS are large hydrophilic complexes (7 000 to 15 000 kDa; Glazer, 1985, 1989; Ong and Glazer, 1991; Grossman et al., 1993; Singh et al., 2015) composed of a pyramid-shaped core and several peripheral rods (Fig. 9). The number of cylinders constituting the core (2 to 5) and the rods (2 to 6), as well as the number of rods (6 to 8), varies between species and strains (Gantt, 1981; Glazer, 1985, 1989; Sidler, 1994; Adir, 2005; Six et al., 2005; Adir et al., 2006; Arteni et al., 2009). Both PBS core and rods are made of chromophorylated proteins called phycobiliproteins (PBPs) and maintained together by protein linkers, representing 85% and 15% of the total PBS mass, respectively (Gantt, 1981; Glazer, 1985; Grossman et al., 1993; Wilbanks and Glazer, 1993; Sidler, 1994; MacColl, 1998; Adir et al., 2006).

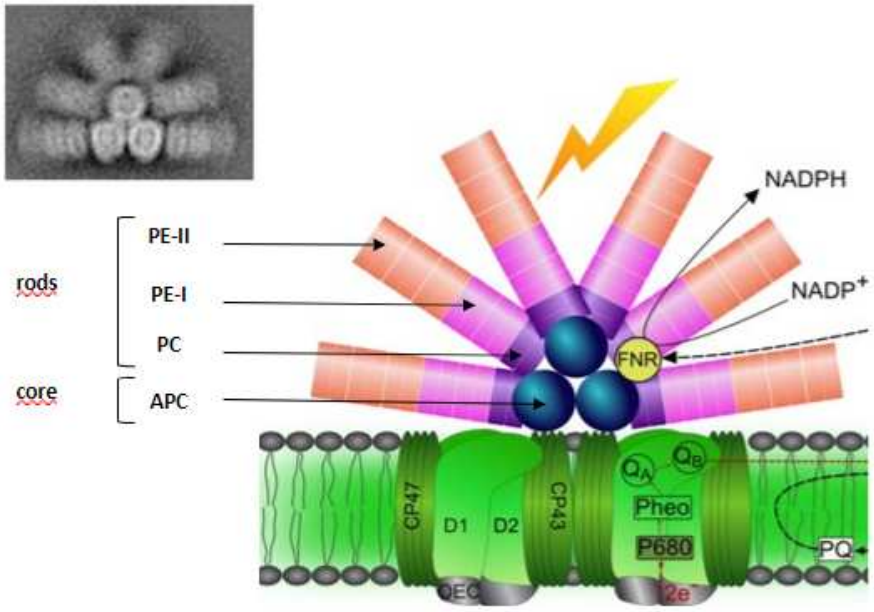

Figure 9: Scheme of a phycobilisome and its association with the thylakoid membrane (cytoplasm side). The PBS core is located in close contact with the thylakoid membrane in order to associate with the reaction center of the photosystem (Grébert, 2017). Insert: Image taken by electron microscopy showing an isolated PBS from *Synechocystis* sp. PCC6803 (Arteni et al., 2009).

The PBS core is located close to the thylakoid membrane so that it can associate physically and energetically with the reaction center of PSII and, more occasionally PSI (Anderson and Toole, 1998; Adir et al., 2020). While the structure of some isolated components has been determined (Adir, 2005; Chang et al., 2015), the structure of the entire complex and its mode of association with photosystems are less well documented. Few PBS associated with a photosystem have indeed been isolated and characterized by electron microscopy so far, probably due to the increasing flexibility and instability of the rods towards their extremities (Arteni et al., 2009; Chang et al., 2015).

The morphology of phycobilisomes is variable. Various models (hemiellipsoidal, hemiellidiscoidal, 'bundle-shaped', 'block-shaped'; Glazer, 1989; Sidler, 1994; MacColl, 1998; Arteni et al., 2009; Singh et al., 2015) have been proposed. Still, the most popular is probably the 'hemi-discoidal', i.e. non-parallel rods emanating from the core and radiating at approximately equal distances from each other (Fig. 9; Glazer, 1985; MacColl, 1998; Adir, 2005; Adir et al., 2006). PBS with such a structure are divided into three subgroups according to the number of cylinders that make up the core (2, 3 or 5; Fig. 10; Sidler, 1994; MacColl,

1998; Arteni et al., 2009; Singh et al., 2015). Complexes with tricylindrical cores (Fig. 10B) are the most common in cyanobacteria.

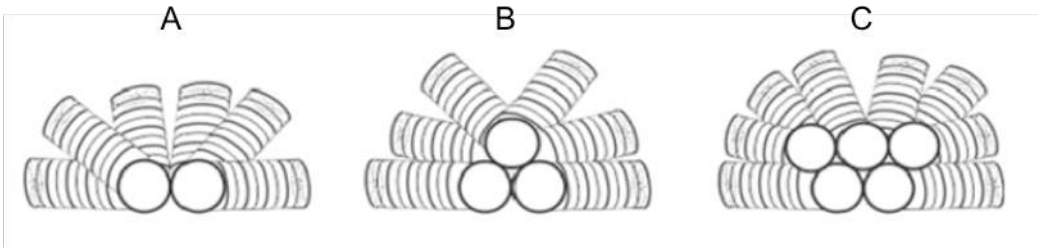

Figure 10: Schematic representation of the three subgroups of hemi-discoidal phycobilisomes. The core of the complex can be composed of: (A) 2 cylinders; (B) 3 cylinders, as the majority of cyanobacteria; (C) 5 cylinders (Singh et al., 2015).

Recently, Domínguez-Martín and co-workers (2022) found in *Synechocystis* sp. PCC 6803 that two of the PBS rods are mobile and can switch position within the antenna. The fact that PBS have several conformational states could constitute a new mode of regulation of light-harvesting, allowing cyanobacteria to optimize energy collection and transfer to reaction centers in different environmental conditions.

I.4.c. Phycobiliproteins

I.4.c.i. Generalities

In cyanobacteria, the monophyletic family of phycobiliproteins (PBPs) is divided into four classes on the basis of their absorption properties: (i) allophycocyanin (APC, λ_{max} = 652 nm) constituting the PBS core (Fig. 9); (ii) phycocyanin (PC, λ_{max} = 620 nm) constituting either the whole PBS rods or only their core proximal; (iii) one or two types of phycoerythrin (PE, λ_{max} = 560 nm) or more rarely (iv) phycoerythrocyanin (PEC, λ_{max} = 575 nm) constituting the distal part of PBS rods (Gantt, 1981; Glazer, 1985; Ong and Glazer, 1991; Grossman et al., 1993; Sidler, 1994; Adir, 2005; Adir et al., 2006, 2020). The phycobiliproteins composing the rods are always heterodimeric, i.e. composed of two subunits (α and β), while the APC core comprises two major (α-APC and β-APC) and two minor subunits (α-APB and β-AP18; in the latter case, the number indicates the molecular mass of the subunit and may vary depending on strains; Sidler, 1994). These different phycobiliproteins differ by the number of pigment

binding sites, which are more numerous in peripheral PBPs, impacting their tertiary structures (Adir, 2005).

I.4.c.ii. Evolutionary history of phycobiliproteins

The high degree of homology between the subunits composing the different phycobiliproteins led Glazer and collaborators (1976) to hypothesize that they evolved from an ancestral protein via multiple duplication events. An evolutionary scenario was subsequently published by Apt and co-workers (1995) based on the study of the level of conservation of the amino acid sequences of APC, PC, PE and PEC. This scenario proposed a progressive expansion of the PBP family from a common protein ancestor that already possessed a chromophore, as well as all residues necessary to form dimers, trimers or hexamers, and that interacted with the plasmid membrane. This ancestor likely had a 3-D structure similar to modern phycobiliproteins. Apt and collaborators (1995) suggested that a first duplication event gave rise to a tandem of genes that co-evolved into two subunits α and β (Fig. 11). The subsequent duplication of this pair led to the advent of two lineages, i.e. “core” and “rod” phycobiliproteins (Fig. 11). Then, other duplication events resulted in the emergence of α and β subunits of APC, PC, PE and PEC (for more details, see Apt et al., 1995). Beyond these events, the evolutionary history of PBS rods seems to have been influenced by horizontal gene transfer and gene losses (Six et al., 2007b; Everroad and Wood, 2012; Sánchez-Baracaldo et al., 2019; Grébert et al., 2022). It is for this reason that phylogenies based on phycobiliproteins and other genes involved in the synthesis of the PBS rods do not correspond to phylogenies based on ribosomal loci (Six et al., 2007b; Dufresne et al., 2008; Haverkamp et al., 2008, 2009; Everroad and Wood, 2012; Humily et al., 2013, 2014; Grébert et al., 2018). In contrast, trees made with allophycocyanin protein sequences are congruent with phylogenies based on ribosomal loci, indicating that the PBS core has probably evolved together with the core genome (Six et al., 2007b).

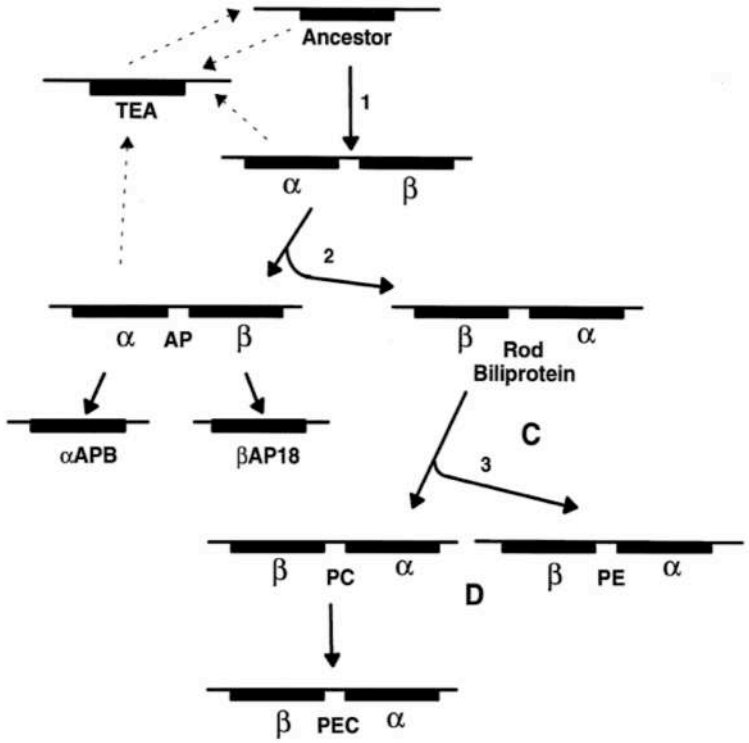

Figure 11: Evolution of the genes encoding the different phycobiliproteins in phycobilisomes. The arrows correspond to the duplication events. TEA, terminal energy acceptor; AP, allophycocyanin; PC, phycocyanin; PE, phycoerythrin; PEC, phycoerythrocyanin (Apt et al., 1995).

The marine *Synechococcus* group displays by far the largest variability of PBS structure of all cyanobacteria. Moreover, the degree of PBS complexity seems to have increased over the course of the evolution (from simple PBS rods made of PC only to complex PBS rods containing PC, PE-I and PE-II). This diversification, associated with an increase in the number of pigments bound per PBP, made it possible the colonization of very diverse environments in terms of light quality and quantity (Wood, 1985; Apt et al., 1995; Six et al., 2005, 2007b; Everroad and Wood, 2012; Humily et al., 2013; Singh et al., 2015), notably the open ocean where blue wavelengths predominate.

I.4.d. Phycobilins

I.4.d.i. Generalities

Phycobilins are linear tetrapyrrole pigments specialized in the absorption of yellow, orange and green wavelengths, while chlorophylls mainly absorb blue and red (Glazer, 1989; MacColl, 1998; Adir et al., 2006; Scheer and Zhao, 2008; Śliwińska-Wilczewska et al., 2020). Four types of phycobilins can be found in cyanobacteria (Fig. 12): phycocyanobilin (PCB, λ_{max} = 650 nm, red-absorbing pigment), phycoerythrobilin (PEB, λ_{max} = 550 nm, green-absorbing pigment), phycourobilin (PUB, λ_{max} = 495 nm, blue-absorbing pigment) and phycobiliviolin (PVB, λ_{max} = 590 nm; Scheer, 1981; Glazer, 1985; Grossman et al., 1993; Sidler, 1994; MacColl, 1998; Adir, 2005). Despite their very close structure, these four chromophores have very different spectroscopic properties (Teale and Dale, 1970; Glazer, 1989; Grossman et al., 1993). The number and positioning of C:C double bonds indeed strongly influence phycobilins absorption maxima, as well as their emission peaks (MacColl, 1998; Adir et al., 2006).

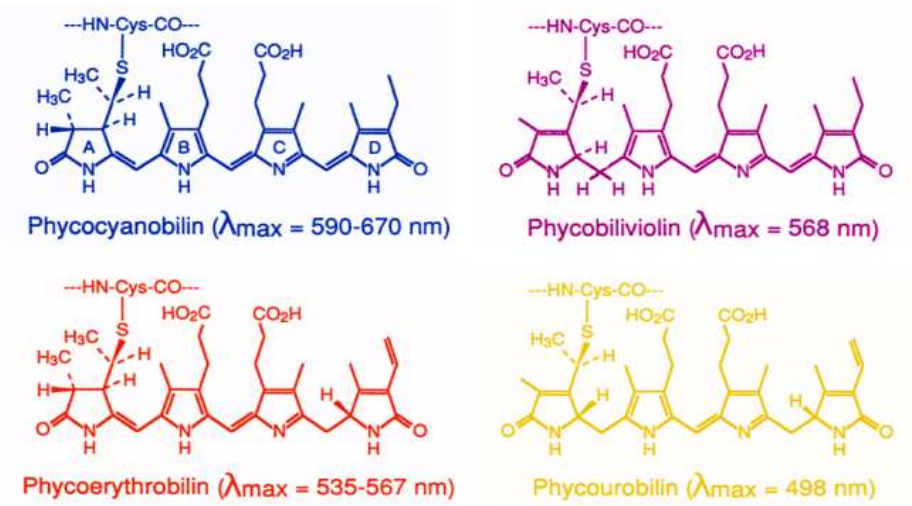

Figure 12: Different types of phycobilins present in red algae and cyanobacteria. The four pigments are stereoisomers and differ in the number and location of the C:C double bonds. Only phycocyanobilin, phycoerythrobilin and phycourobilin are found in marine *Synechococcus* (after Grossman et al., 1993; modified by Grébert, 2017).

It is the combination of chromophores associated with apoproteins that determines the color of phycobiliproteins (blue, green, pink, red) and therefore the color of cells, as well as

the region of the light spectrum used for light energy harvesting (Six et al., 2007b). To note, only five spectral niches (violet, blue, green, orange, red) delineated by the vibrational modes of water molecules have been recently demonstrated to be available for photosynthesis (Fig. 13; Holtrop et al., 2021).

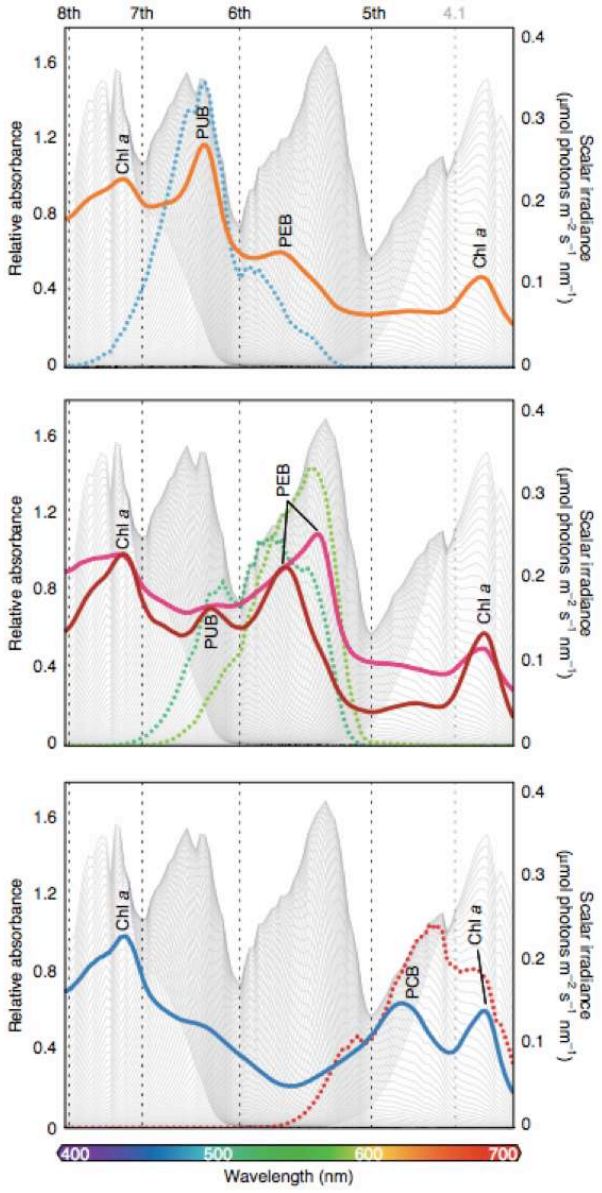

Figure 13: Spectral niches and absorption spectra of the main *Synechococcus* pigments. Colored lines represent light absorption spectra from a PUB-rich strain (orange), two PEB-rich strains (brown and magenta), and a PCB-rich strain (blue). Grey peaks and valleys in the background refer to simulated underwater irradiance spectra. Vertical dashed lines indicate harmonics of water molecules. Underwater irradiance spectra with the closest match with phycobilins absorption peaks are represented in colored dotted lines. Chl *a*, chlorophyll *a*; PCB, phycocyanobilin; PEB, phycoerythrobilin; PUB, phycourobilin (Holtrop et al., 2021).

I.4.d.ii. Phycobilin biosynthesis pathway

The phycobilin biosynthesis pathway is complex. It is identical to that of chlorophylls up to the synthesis of protoporphyrin IX (for more details, see Blankenship, 2014). Protoporphyrin IX is then converted into heme, which is successively ringopened by a heme oxygenase, generating biliverdin IXα (Fig. 14). This biosynthetic precursor is reduced to PCB and PEB by a family of enzymes called ferredoxin-dependent bilin reductases, which have been subdivided into different classes based on their substrate preference and double-bond regiospecificity. In cyanobacteria, PebA and PebB catalyze the conversion of biliverdin IXα to 3(E/Z)-PEB while PcyA reduces it to 3(E/Z)-PCB (Frankenberg et al., 2001; Ledermann et al., 2016). Interestingly, genes catalysing reduction of biliverdin IXα to PEB (*pebS*, *pcyX)* have been discovered in cyanophages.

Once produced, PCB and PEB are covalently bound to cysteine residues of phycobiliproteins' α and β subunits (see Introduction § I.4.f) by specific enzymes, called phycobilin lyases (Grossman et al., 1993; Frankenberg et al., 2001; Adir et al., 2006, 2020; Singh et al., 2015; Ledermann et al., 2016). Contrary to PCB and PEB, PUB and PVB are not directly synthesized by cyanobacteria but produced by bi-functional enzymes called phycobilin lyase-isomerases. Besides covalently binding PCB or PEB to PC or PE subunits, these enzymes also isomerize them into PVB or PUB, respectively (Zhao et al., 2002; Blot et al., 2009). This isomerization process allows the cells to collect shorter wavelengths and thus to adapt to a large range of light environments (Scheer and Zhao, 2008; Schluchter et al., 2010).

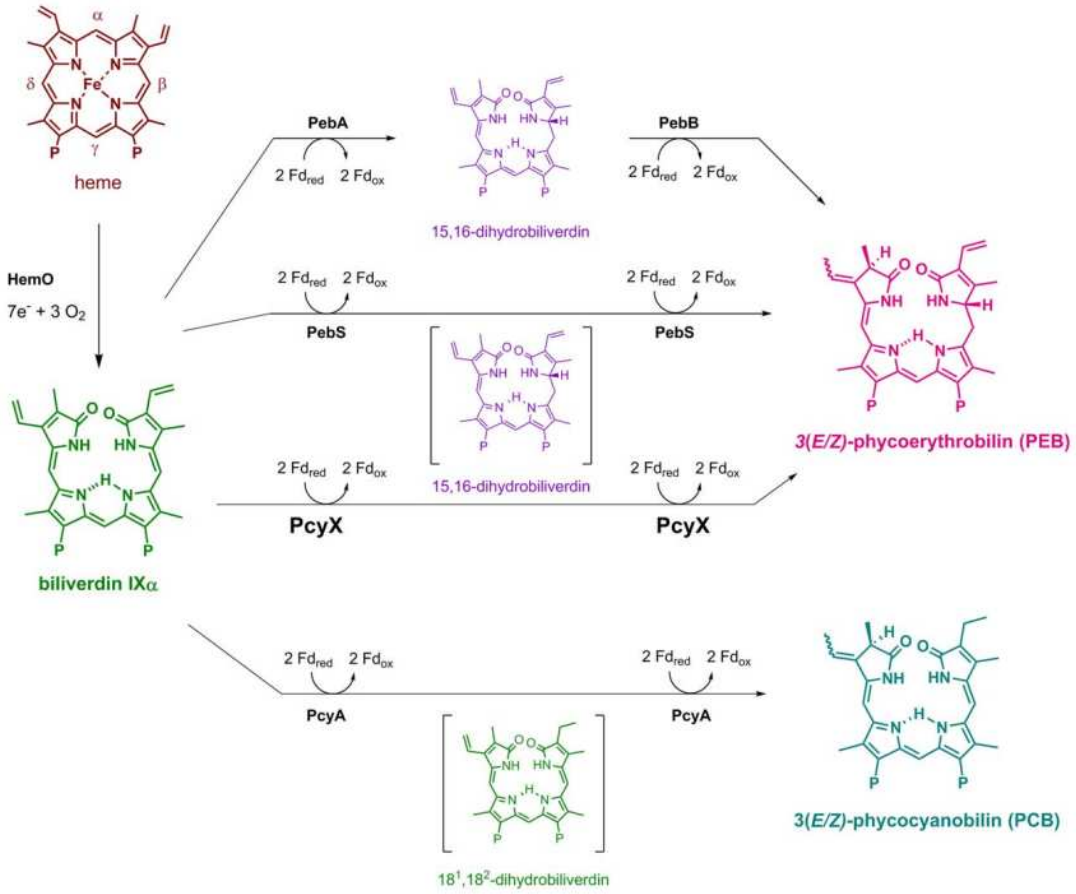

Figure 14: Schematic representation of the biosynthesis pathway of PCB and PEB from heme in cyanobacteria. The names of the enzymes involved in the process are shown in bold black (Ledermann et al., 2016).

Interestingly, phycobilins can also be bound to phycobiliproteins spontaneously *in vitro*. However, this process generally occurs with low fidelity and the resulting chromophorylated proteins are not found *in vivo* (with the exception of the core-membrane linker, L_{CM}; Liu et al., 2005). Thus, the major functions of phycobilin lyases are probably to ensure an appropriate stereochemistry and to avoid spontaneous attachment errors in a 'chaperone-like fashion' (Schluchter and Glazer, 1999; Zhao et al., 2007; Scheer and Zhao, 2008; Schluchter et al., 2010).

I.4.e. Linkers

Linkers are polypeptides of variable size necessary for the assembly and stability of individual phycobiliprotein hexamers and of the whole PBS complex, as well as its good interaction with photosynthetic membranes. They also modulate the spectral properties of PBPs to promote the unidirectional transfer of excitation energy from the periphery of the PBS to the core (Gantt, 1981; Glazer, 1985, 1989, 198; Grossman et al., 1993; Sidler, 1994; Apt et al., 1995; MacColl, 1998; Liu et al., 2005; Adir et al., 2006, 2020; Arteni et al., 2009; Singh et al., 2015). Four groups of linkers can be defined according to their position within the PBS (Fig. 15):

- L_C (core linker encoded by *apcC*) are small polypeptides that participate in the assembly of allophycocyanin (APC) cylinders into a core. They considerably improve the stability of the complex and the efficiency of energy transfer;

- L_{CM} (core-membrane linker encoded by *apcE*) are the longest linker polypeptides. They are essential for the proper functioning of phycobilisomes partly because of their central role in the assembly of the APC discs into cylinders and then into a core. They also promote the anchoring of the APC core to the thylakoid membrane. In addition, they appear to be among the main terminal excitation energy acceptors within the PBS, which they transmit to the PSII (Lundell et al., 1981; Capuano et al., 1991);

- L_R (rod linker encoded by *cpcCD* for PC, *cpeCD* for PE-I, *mpeCEFGH* for PE-II and *mpeD* for the PE-I/PE-II linkage; Six et al., 2005, 2007b; Grébert et al., 2022) are involved in the assembly and stabilization of the peripheral rods. In cyanobacteria, their number depends on the length of the rods;

- L_{RC} (rod-core linker encoded by *cpcG1*) ensure the attachment of the rods to the APC core as well as the optimal transmission of excitation energy at this junction.

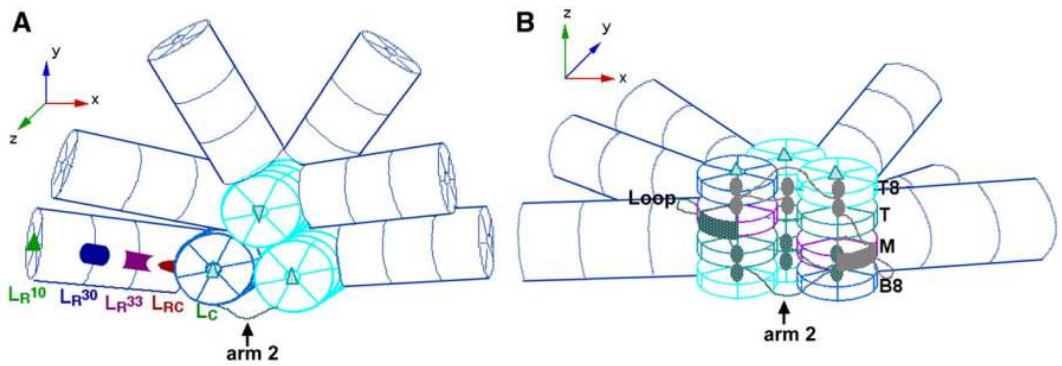

Figure 15: Representation of a hemi-discoidal phycobilisome seen from the side (A) and the bottom (B). The linkers shown in (A) are: L_C, core linker; L_{RC}, rod-core linker; L_R, rod linker. Figure (B) illustrates the different domains of the L_{CM}, core-membrane linker. As the homogeneous composition of the PBS rods in phycobiliproteins and linkers, as well as the non-overlapping of the linkers, have not been proven yet, other models cannot be excluded (Arteni et al., 2009).

Most linkers are not pigmented (Glazer, 1985; Sidler, 1994; Liu et al., 2005; Six et al., 2005; Scheer and Zhao, 2008; Adir et al., 2020) but there are exceptions in marine cyanobacteria including: (i) the L_{CM}, the amino-terminal part of which carries a cysteine residue capable of binding a red-shifted PCB (λ_{max} = 665 nm) involved in the transfer of energy from APC to the chlorophylls *a* of the reaction centers (Grossman et al., 1993); and (ii) the rod linkers associated with PE-II (called γ-linkers: MpeC, MpeD and MpeE), which in *Synechococcus* sp. WH8102 have been shown to be chromophorylated with PUB (Six et al., 2005). They appear to be widespread in marine *Synechococcus* strains and may be involved in the collection of light energy.

I.4.f. Assembly of the phycobilisome

The phycobilisomes of cyanobacteria are assembled progressively, in an orderly and controlled manner (Adir, 2005). Phycobiliproteins form the basic unit of the complex. They consist of two polypeptides α and β (Fig. 16), which differ in their molecular weights (15 to 22 kDa; Glazer, 1985; Grossman et al., 1993; MacColl, 1998; Adir et al., 2020), amino acid sequence (160 – 184 a.a.) and chromophore content, but have very similar tertiary structures (Gantt, 1981; Apt et al., 1995; Adir et al., 2006; Singh et al., 2015). Each subunit

consists of eight α helices. Six of them are assembled into a structure similar to that of globin. The two others are responsible for the strong and stable association of the subunits to form an αβ monomer (Fig.16). Monomers spontaneously self-assemble to form trimers $(\alpha\beta)_3$, which then aggregate face to face into hexamers $(\alpha\beta)_6$, also called discs. These hexamers stack up on top of each other using linkers and ultimately form the PBS rods (Gantt, 1981; Grossman et al., 1993; Sidler, 1994; Apt et al., 1995; Anderson and Toole, 1998; Adir, 2005; Adir et al., 2006, 2020; Arteni et al., 2009; Singh et al., 2015). The linker-PBPs association has not been fully elucidated. It is probably based on a combination of hydrophobic and multiple charged interactions (Gantt, 1981; Sidler, 1994; Liu et al., 2005).

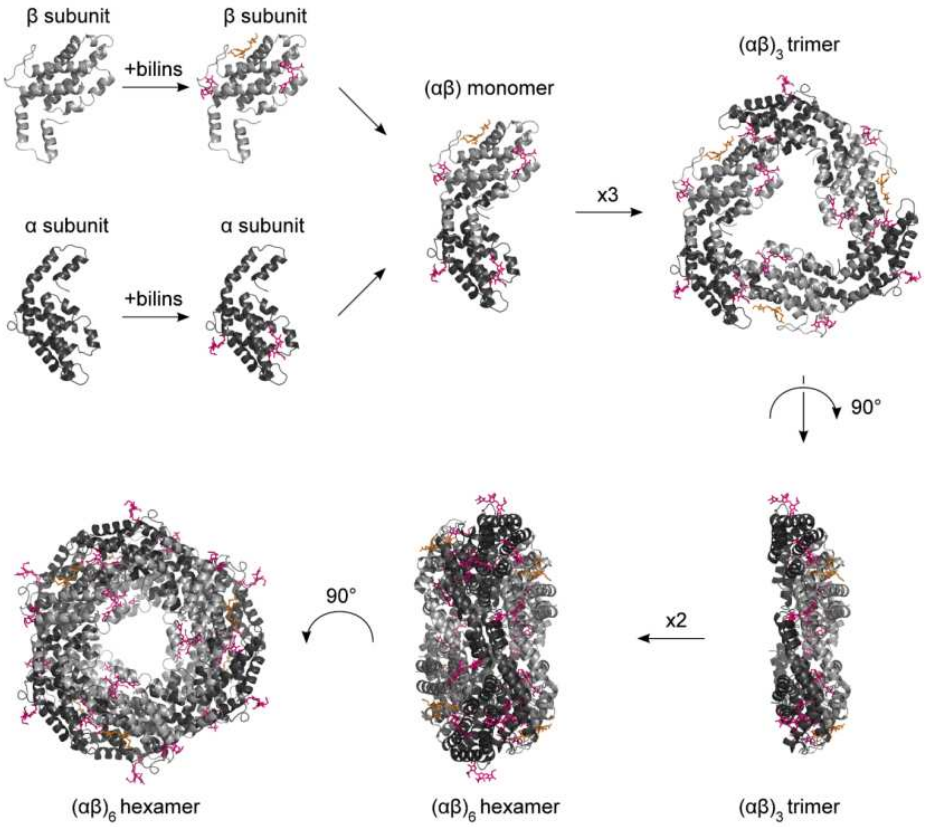

Figure 16: Schematic representation of the assembly of the rods of phycobilisomes. The monomer consists of a α and a β subunits to which the chromophores have previously been attached by phycobilin lyases. Monomers spontaneously assemble into trimers. With the help of linkers inserted in the central cavity, trimers aggregate into hexamers that form the rods (Grébert, 2017).

The length of PBS rods varies according to organisms, light conditions (intensity and/or quality) and nutrients availability (Gantt, 1981; Glazer, 1985). They consist of two to four hexamers stacked on top of each other using linkers.

Before the assembly of PBPs into monomers, chromophores are covalently bound by phycobilin lyases via thioether bonds at highly conserved residues of α and β subunits (Gantt, 1981; Glazer, 1985, 1989; Ong and Glazer, 1991; Grossman et al., 1993; Sidler, 1994; MacColl, 1998; Adir et al., 2006; Scheer and Zhao, 2008). One to three chromophores are attached to each subunit, with the number of pigments carried by each monomer increasing from APC (2 sites) to PE-II (6 sites; Fig. 17). While some sites always carry the same pigment, others bind different phycobilins depending on the strain, allowing organisms to adapt to their light environment (Scheer and Zhao, 2008). The family of phycoerythrins, which are adapted to absorb blue and green light (Six et al., 2007b; Everroad and Wood, 2012), shows the greatest variability.

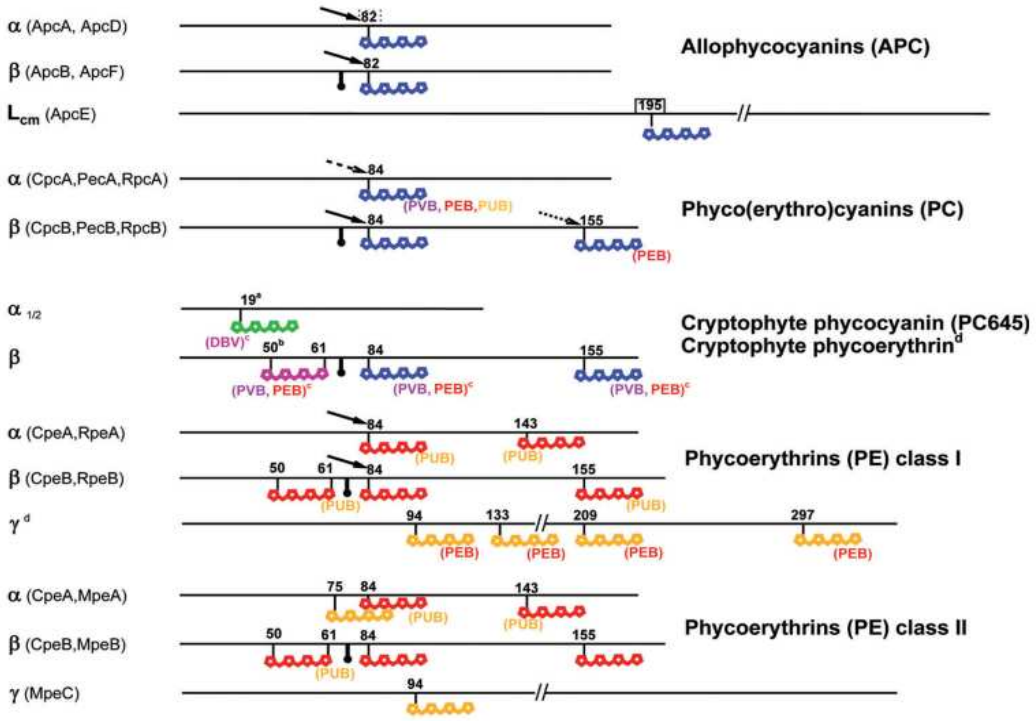

Figure 17: Chromophorylation of the different phycobiliproteins of marine *Synechococcus*. The number of chromophore binding sites increases from APC and PC to PE-II. Some sites always carry the same pigment while others bind different phycobilins depending on the strain. Phycoerythrins I and II have double-bounded chromophores at Cys-50/61 of the β subunit, which considerably affects their conformation and absorption properties. PCB, phycocyanobilin (in blue); PEB, phycoerythrobilin (in red); PUB, phycourobilin (in orange); PVB, phycobiliviolin (in purple; Scheer and Zhao, 2008).

I.4.g. Phycobilin lyases

Phycobilin lyases form a very diverse family of multi-domain enzymes, a number of which have been biochemically and genetically characterized on model strains (Scheer and Zhao, 2008; Schluchter et al., 2010; Bretaudeau et al., 2013). Three lyase clans have been identified to date (E/F clan, S/U clan, T clan), each grouping enzymes with similar 3D structures. In the nomenclature of phycobilin lyases and related proteins proposed on the Cyanolyase web site (http://cyanolyase.genouest.org/), clans are subdivided into sub-clans, superfamilies, families and sub-families.

I.4.g.i. E/F clan

The enzymes of E/F clan are characterized by a very high specificity (Scheer and Zhao, 2008). In other words, they act on a single cysteine residue of a given protein subunit. E/F clan is the only one to be divided into two sub-clans. While all enzymes in sub-clan 1 are heteroduplex (E/F or Y/Z) or fusion proteins (RpcG), members of sub-clan 2 appear to take the form of monomers or homodimers.

Sub-clan 1. The members of CpcE/RpcE and CpcF/RpcF families, which are found in C-PC containing strains, form heterodimers. It has been demonstrated that CpcE-I/CpcF-I heterodimer attaches PCB to Cys-84 of α-PC in *Synechococcus* sp. PCC7002 and suggested that RpcE/F, which is present in R-PC containing *Synechococcus* strains, links PEB to Cys-84 of α-PC-II (Fairchild et al., 1992; Zhou et al., 1992; Fairchild and Glazer, 1994; Six et al., 2007b; Scheer and Zhao, 2008; Schluchter et al., 2010). Within the E/F clan are also found bi-functional enzymes capable of isomerizing PCB into PVB and PEB into PUB during the covalent attachment of chromophores to proteins. These phycobilin lyase-isomerases allow the cells to collect shorter wavelengths and thus to adapt to a large variability of light environments. Members of the PecE and PecF families, which are found in PEC-containing stains, form a heterodimeric lyase-isomerase that binds PCB to Cys-84 of α-PEC and isomerizes it into PVB in *Mastigocladus laminosus* (Zhao et al., 2000; Storf et al., 2001; Scheer and Zhao, 2008). Finally, fusions proteins of the RpcG family, which is present in

some PE-II-containing marine strains, bind PEB to Cys-84 of α-PC and isomerize it into PUB in *Synechococcus* sp. WH8102 (Blot et al., 2009).

Sub-clan 2. CpeF was shown to be responsible for the double binding of PEB to Cys-48,59 of the β-PE in *Fremyella diplosiphon* (Kronfel et al., 2019). CpeF belongs to the same E/F lyase superfamily as three PE-II associated lyases: MpeU, MpeV and MpeX. To date, only MpeV, present in some type IV chromatic acclimaters (see Introduction § II.4), has been fully characterized and was found to be a lyase-isomerase that double bind PEB to Cys-50,61 of β-PE-I and β-PE-II and isomerize it into PUB in *Synechococcus* sp. RS9916 (Carrigee et al., 2022).

The phylogeny of a second lyase superfamily, CpeY-MpeQ-W-Y-Z, has also been recently elucidated (Grébert et al., 2021). CpeY, whose activity is enhanced by CpeZ, attaches PEB to Cys-82 of α-PE in *Fremyella diplosiphon* (Biswas et al., 2011). Both enzymes are present in all PE-containing cyanobacteria. The four other members of this superfamily (MpeQ, W, Y and Z), that all act on Cys-83 of α-PE-II, have been shown to play a key role in the two forms of type IV chromatic acclimation.

I.4.g.ii. S/U clan

Several members of the CpcS family have been biochemically characterized (CpcS-I from *Synechococcus* sp. PCC 7002 and CpcS-III from *Nostoc* sp. PCC7120). It has been shown that both enzymes bind *in vivo* PCB to Cys-82 (consensus numbering) of a large diversity of subunits (Saunée et al., 2008; Shen et al., 2008; Biswas et al., 2010; Schluchter et al., 2010). They seem to have a low specificity for the protein but a high one for the binding site (Scheer and Zhao, 2008). Lyases of the CpcS family can form both homodimers and heterodimers with the CpcU family. Two members of CpeS family have been characterized: CpeS_Pro-HL from *Prochlorococcus marinus* MED4, which was found to bind PEB to Cys-82 of β-PE-III (Wiethaus et al., 2010), and CpeS-I from *Fremyella diplosiphon* that binds PEB to Cys-80 of β-PE-I (Biswas et al., 2011). No enzyme was biochemically characterized in the CpeU family. Given the genomic context of *cpeU*, it is probable that this enzyme is a PEB:phycoerythrin lyase, but its site specificity is unknown yet.

I.4.g.iii. T clan

Enzymes belonging to T clan form homodimers and have, like CpcS, a moderate specificity but a high site specificity (Scheer and Zhao, 2008). The role of CpcT family was determined in *Synechococcus* sp. PCC 7002 and *Nostoc* sp. PCC 7120 as a lyase binding PCB to Cys-153 (consensus numbering) of β-PC (Shen et al., 2006; Zhao et al., 2007; Scheer and Zhao, 2008; Schluchter et al., 2010). Similarly, the CpeT from *P. marinus* MED4 cyanophage P-HM1 was biochemically characterized as attaching PEB to Cys-155 of β-PE-I (Gasper et al., 2017). CpeT has likely the same role in marine *Synechococcus*, in which it could also act on the homologous position of β-PE-II. No member of the RpcT family identified in marine *Synechococcus* has been formally characterized so far, but it has been suggested that these CpcT paralogs bind PEB to Cys-153 of β-PC (Blot et al., 2009).

I.4.g.iv. Yet uncharacterized phycobilin lyases

Although the function of many lyases or lyases-isomerases has been biochemically characterized in one or several cyanobacterial species, the chromophorylation mechanism of a few binding sites remains to be elucidated. This is notably the case in marine *Synechococcus* strains for the PEB or PUB chromophores bound at Cys-139 of α-PEI as well as Cys-75 and Cys-140 of α-PEII (Ong and Glazer, 1991). It is interesting to note in this context that small allelic variations could be sufficient to confer a new function to a lyase, as recently demonstrated for the different members of the MpeQ-W-X-Y family (Grébert et al., 2021; Kumarapperuma et al., 2022). Such variations could notably explain how such a fairly small set of candidate lyases can generate all observed chromophore combinations. An alternative explanation would be that some chromophores could be bound autocatalytically or by proteins different from known lyases.

I.4.h. Energy transfer within the phycobilisome

Light energy captured at the extremities of the PBS rods is transmitted according to the Förster model (1948) to the chlorophylls *a* of the reaction centers (RC). The arrangement of phycobiliproteins within the PBS (Fig. 18; low energy APC for the core, intermediate energy

PC and high energy PE for the proximal and distal part of the rods) is largely responsible for the excitation energy gradient that allows high photon transfer speed and efficiency (about 90 – 99% of the collected excitation energy reaches the RC where it is converted into chemical energy through charge separation; Gantt, 1981; Glazer, 1985, 1989; Ong and Glazer, 1991; Grossman et al., 1993; Sidler, 1994; MacColl, 1998; Adir, 2005; Adir et al., 2006).

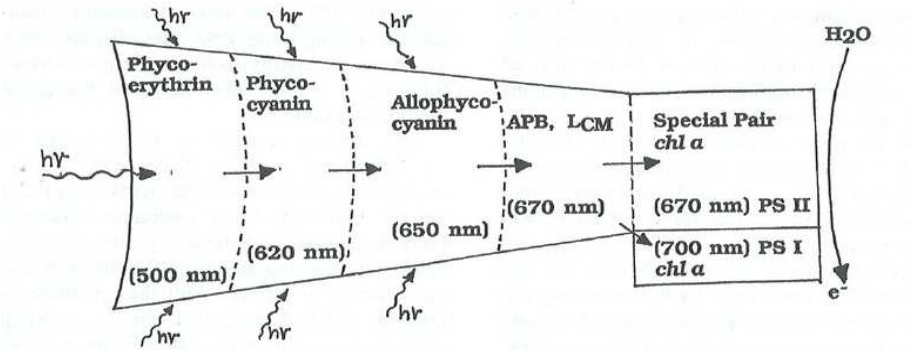

Figure 18: Schematic representation of energy transfer within a phycobilisome rod. Excitation energy transits from phycoerythrin, which absorbs short wavelengths, to the special pair of chlorophyll *a* of the photosystems (PSI/II). A maximum of five transfer steps are required for the energy collected at any point of the PBS to reach the terminal acceptor (Sidler, 1994).

Chromophores arrangement is also important for unidirectional transfer along the PBS rods (Sidler, 1994). Sensitive pigments at the periphery of the trimers, such as those bound to the cysteine residues α-84 and β-155 of PC (Fig. 19), harvest excitation energy which is rapidly transmitted to the fluorescent chromophores located in the central cavity of the hexamer (β-84). Excitation energy finally reaches the final acceptor and then the reaction centers (Glazer, 1985, 1989; Ong and Glazer, 1991; Grossman et al., 1993; Sidler, 1994). This configuration makes it possible to limit energy losses through heat dissipation or fluorescence. Finally, the protein environment and chromophore conformation play a crucial role in the optimization of energy collection and transfer, notably by influencing the spectral properties of PBPs as well as the time and amplitude of the excited state (Glazer, 1985, 1989; Grossman et al., 1993; Singh et al., 2015). Free bilins are indeed not very suitable as they do not absorb light well and their excitation time is too short (Scheer and Zhao, 2008).

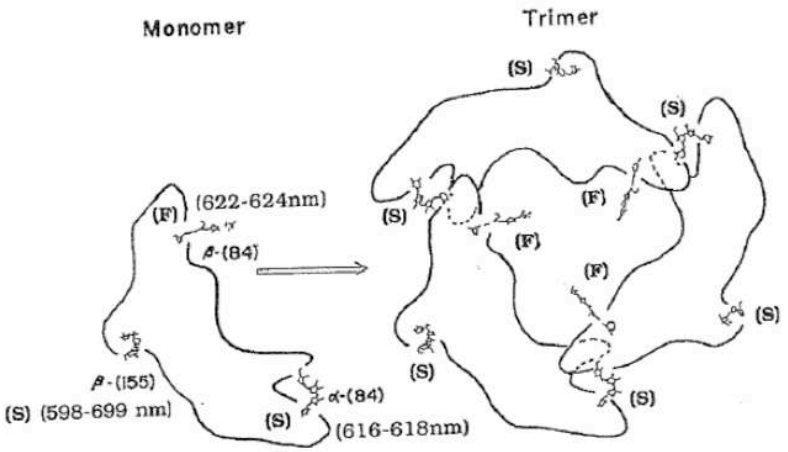

Figure 19: Arrangement of sensitive (α-84 and β-155) and fluorescent (β-84) chromophores at the level of a phycocyanin monomer and trimer. The pigments at the periphery absorb short wavelengths (high energy) and transfer energy to the central chromophores. Phycoerythrins carry two to three additional sensitive chromophores (Sidler, 1994).

Energy transfer is very fast within the light-harvesting complex. However, there are limiting steps such as the junctions between the rods and the core, as well as disc-to-disc steps (Glazer, 1985). According to the model of Arteni and collaborators (2009), phycobilisomes associated with neighboring photosystems could be in contact via certain rods. This arrangement could notably allow a redistribution of the excitation energy and finally an optimization of the light harvesting process.

I.5. The light-harvesting complex of cyanobacteria of the genus *Prochlorococcus*

Marine picocyanobacteria of the genus *Prochlorococcus* have the peculiarity to possess membrane-intrinsic light-harvesting complexes. These antennae consist of prochlorophyte chlorophyll-binding proteins (Pcb), which are associated with divinyl-chlorophyll *a* and *b* (Fig. 20; Chisholm et al., 1988; Roche et al., 1996; Hess et al., 1999; Ting et al., 2002; Coleman and Chisholm, 2007; Scanlan, 2012). Pcb-pigment complexes have a red-shifted absorption peak, compared to chl *a* and *b*, which enables them to collect more efficiently the blue light that penetrates deep into the water column. The replacement of PBS by this atypical antenna, less rich in nitrogen and iron, is probably the result of the oligotrophic lifestyle of

Prochlorococcus (Ting et al., 2002; Partensky and Garczarek, 2010). In their highly diluted environment, macro- and micronutrients are indeed less available.

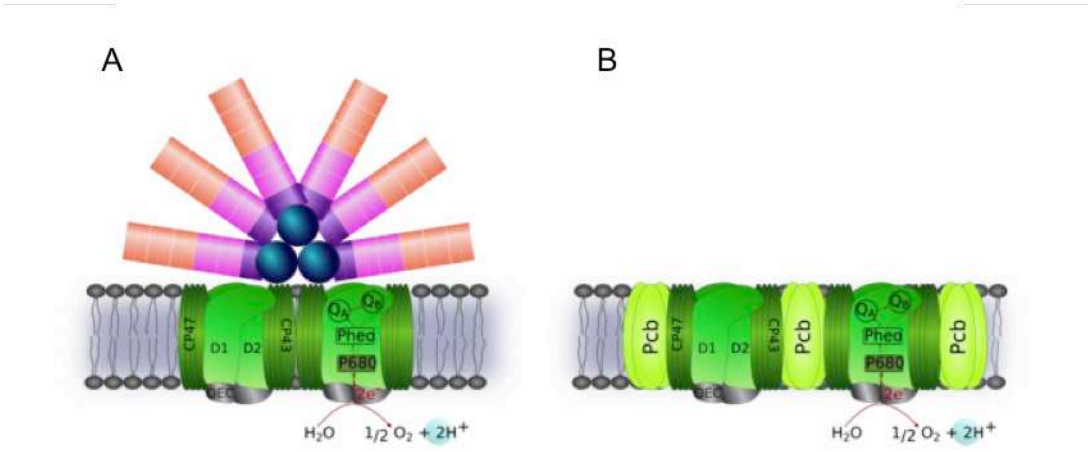

Figure 20: Schematic representation of the light harvesting antennae of the marine picocyanobacteria *Synechococcus* and *Prochlorococcus*. (A) *Synechococcus* cells have large extra-membrane PBS while (B) *Prochlorococcus* have intrinsic antennae made up of 'prochlorophyte chlorophyll *a/b* binding' proteins (Pcb). These are homologous to the iron-stress induced protein (IsiA). Several other atypical cyanobacteria including *Prochlorothrix*, *Prochloron* and *Acaryochloris* also possess Pcb-type antennae (Doré, 2017).

Interestingly, remnants of phycoerythrin can be found in all strains of *Prochlorococcus*, but seem to be active only in some low light-adapted strains, such as *P. marinus* SS120 (Hess et al., 1996, 1999). The function of this so-called PE-III is not well understood but possible roles in blue-green light-harvesting, light-sensing or nitrogen storage have been suggested (Hess et al., 1999; Lokstein et al., 1999; Partensky et al., 1999; Coleman and Chisholm, 2007; Scanlan, 2012). It is important to note that a complete set of PBS synthesis genes (including APC, PC, PE-I, PE-II and associated linkers) was recently found in single-amplified genomes (SAGs) obtained from natural *Prochlorococcus* cells thriving in anoxic marine zones (AMZ-II and III ecotypes located at the base of *Prochlorococcus* lineage; Ulloa et al., 2021). These SAGs seem to lack typical *pcb* genes, suggesting that the monophyletic *Prochlorococcus* lineage arose from a *Synechococcus*-like ancestor before transitioning from PBS to Pcb-type antennae.

I.6. Impact of environmental variations on the phycobilisome and response of marine cyanobacteria

Photosynthesis is an essential process for production of chemical energy and regulation of cellular metabolism in oxygenic phototrophs. However, its performance is heavily impacted by stresses caused by environmental changes. In particular, phycobilisomes, which are the most efficient light-harvesting structures known so far (Sidler, 1994; Hess et al., 1999), can be severely damaged by sudden changes. For example, it has been shown that nitrogen deficiency can lead to a degradation of phycobiliproteins (bleaching phenotype) allowing to reduce the input of energy in a context of slowed metabolism, and also because they constitute a potential source of macronutrients (Grossman et al., 1993; Collier and Grossman, 1994; Adir et al., 2006). Although the effect of micronutrient deficiencies is less well known, the lack of iron, an essential component of the photosynthetic apparatus (up to 50% of the intracellular iron pool; Behrenfeld and Milligan, 2013), also leads to a decrease in cell pigmentation and in the number of photosystems. This is particularly true for PSI, the most iron-rich structure of the photosynthetic apparatus, resulting in a decrease of the cellular PSI:PSII ratio (Sandström et al., 2002; Morrissey and Bowler, 2012).

Both light and temperature stresses can induce a shortening of PBS rods by disconnection of the proximal phycobiliproteins (more specifically between PE-I and PE-II) or even a complete dismantling of the photosynthetic apparatus (Li et al., 2001; Six et al., 2004; Pittera et al., 2017). Environmental stresses can also damage the reaction center of PSII and trigger the degradation of the D1 protein, leading to photoinhibition and potentially cell death (Nishiyama et al., 2006; Takahashi and Murata, 2008). Under UV or high light intensities, a decrease in the expression of genes encoding certain components of phycobilisomes (α- and β-subunits of all phycobiliproteins, linkers associated to PE) can also be observed (Six et al., 2007a). On the contrary, when light intensities are low, photosynthetic organisms increase their cellular content of PBS, phycobiliproteins and other photosynthetic pigments. Another strategy relies on the increase of the size of the PBS rods.

Thermal stresses also have an effect on the fluidity of the thylakoid membranes, where the electron transport chain is located, as well as on the molecular stability of

phycobiliproteins (Pittera et al., 2017, 2018). They can also impact the relative abundance of proteins coding for PBS and PSII.

Finally, any variations of environmental conditions causing a slow down of the cell metabolism increase the production of reactive oxygen species (ROS), which have deleterious effects on PSII (Nishiyama et al., 2006; Takahashi and Murata, 2008; Latifi et al., 2009; Blot et al., 2011).

Cyanobacteria have thus acquired various mechanisms for protection, repair and regulation of their PBS and PSII according to environmental conditions. Some of the most studied mechanisms are the: (i) D1 repair cycle that enables the continuous synthesis of new D1 proteins in order to maintain a constant photosynthetic activity (Aro et al., 1993; Nishiyama et al., 2006; Garczarek et al., 2008); (ii) nonphotochemical quenching of fluorescence to dissipate excess light energy in the form of photons (fluorescence) or vibrations (heat; ; (iii) state transitions that permit the equitable redistribution of energy between the two photosystems when one of them does not work efficiently (Mullineaux, 2014); (iv) use of 'high-light inducible proteins' to dissipate directly or indirectly excess light energy (Havaux et al., 2003), to transport free-chlorophylls released by the PSII repair cycle that could have phototoxic effects (Xu et al., 2004) and to eliminate ROS (He et al., 2001); (v) use of alternative ways of transporting (flavoproteins; Zhang et al., 2012) or eliminating electrons (catalase-peroxydase, superoxide dismutase; He et al., 2001).

All of these strategies allow cyanobacteria to acclimate more or less quickly to variations of environmental conditions, and by extension have enabled them to colonize successfully a large variety of niches. The process studied during this thesis, chromatic acclimation (see Introduction § II.4), which confers certain strains of marine *Synechococcus* the advantageous ability to reversibly modify their PBS pigmentation, is also part of regulation mechanisms. Indeed, laboratory studies have shown that photosynthetic performance and growth are greater when light is complementary to cell pigmentation (Stomp, 2008). These results have been supported by environmental studies suggesting that the pigment types most complementary to the water color predominate in the field (Olson et al., 1990; Wood et al., 1998; Haverkamp et al., 2008; Grébert et al., 2018).

II. The marine picocyanobacterium *Synechococcus*, an ecologically relevant model to study the response of phytoplankton to environmental variations

II.1. Phytoplankton

II.1.a. Diversity

Oceans cover 70% of the planet and are inhabited by a multitude of living beings. Most of them are microscopic eukaryotes or prokaryotes drifting along with the currents, and are collectively called 'the plankton'. Marine planktonic organisms display various shapes, sizes (pico- to mega-plankton; Fig. 21) and trophic modes (phototrophy, heterotrophy, mixotrophy, etc.). Those capable of oxygenic photosynthesis are called the phytoplankton (Brierley, 2017) and exhibit very diverse physiological and genetic characteristics (Caron et al., 2012; Worden et al., 2015). They mainly colonize the upper illuminated layer of the water column (euphotic zone), which can extend to a depth of 250 m when water transparency is high (South Pacific).

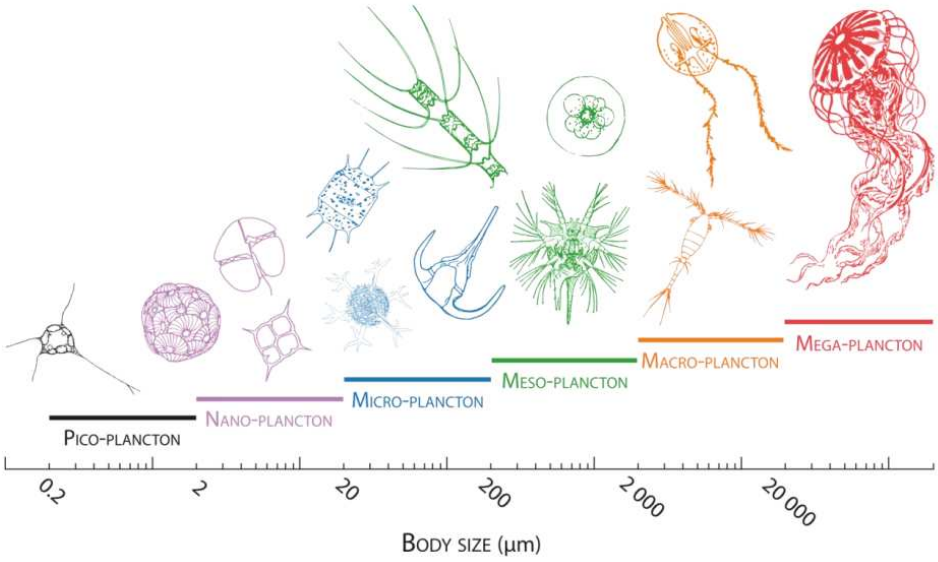

Figure 21: Different size classes of plankton. From (Biard, 2015).

Phytoplankton is divided into three size classes: (i) microphytoplankton (20 – 200 µm) which mainly comprises diatoms and dinoflagellates; (ii) nanophytoplankton (2 – 20 µm) which includes cryptophytes, some filamentous cyanobacteria and haptophytes; (iii)

picophytoplankton (0.8 – 2 μm) which includes picoeukaryotes (chlorophytes, haptophytes and heterokonts) as well as bacteria. While eukaryotic photosynthetic microalgae are highly diverse (Moon-van der Staay et al., 2001; Vaulot et al., 2008), the prokaryotic component of picophytoplankton is largely dominated by picocyanobacteria. Among these are the two most abundant phototrophic organisms in the oceans, *Prochlorococcus* and *Synechococcus*, which have an estimated global abundance of 2.9×10^{27} and 7×10^{26} cells, respectively (Partensky et al., 1999; Flombaum et al., 2013).

II.1.b. Role of phytoplankton in the marine ecosystem

Phytoplankton communities are located at the base of complex marine food webs and play a key role in major biogeochemical cycles (Caron et al., 2012; Worden et al., 2015; Brierley, 2017). They account for nearly 50% of global primary production while they constitute less than 1% of Earth's photosynthetic biomass (Field et al., 1998; Brierley, 2017). This efficiency can be explained by the high multiplication rate of these microorganisms as well as their high surface/volume ratio, which enable them to fix a large amount of carbon in a small volume (Partensky et al., 1999; Partensky and Garczarek, 2010).

Phytoplankton contributes significantly to the carbon cycle not only by fixing atmospheric CO_2, but also by producing organic carbon and more generally organic matter (OM; Richardson and Jackson, 2007). The fate of OM is variable (Fig. 22): (i) some is acquired through phytoplankton grazing by zooplankton and heterotrophic or mixotrophic protists, which are themselves predated by higher trophic levels, and thus forms the basis of a complex trophic food web; (ii) another part is excreted as dissolved organic matter (DOM; Becker et al., 2014; Worden et al., 2015; Guidi et al., 2016; Brierley, 2017). A fraction of the DOM forms aggregates with zooplankton fecal pellets and cellular debris, and constitutes the marine snow or particulate organic matter (POM). The latter sinks from the photic layer to the ocean floor and can be re-mineralized by archaea and bacteria, a process called 'the microbial loop' (Azam et al., 1983). This allows the release of inorganic matter (carbon dioxide, nitrogen, phosphorus) that becomes available for phytoplankton. The small non-remineralised fraction (2% of the fixed carbon) reaches the ocean floor and is buried in the

sediments, thus favoring carbon sequestration in the very long term (thousands of years; Guidi et al., 2016). DOM can also be produced by the action of viruses through lysis of phytoplanktonic cells (Suttle, 2007; Worden et al., 2015). The emission of membrane vesicles containing proteins and nucleic acids, a process observed in certain bacteria including *Prochlorococcus*, could also play a role in the transfer of OM to marine microbial communities and to sediments (Biller et al., 2014).

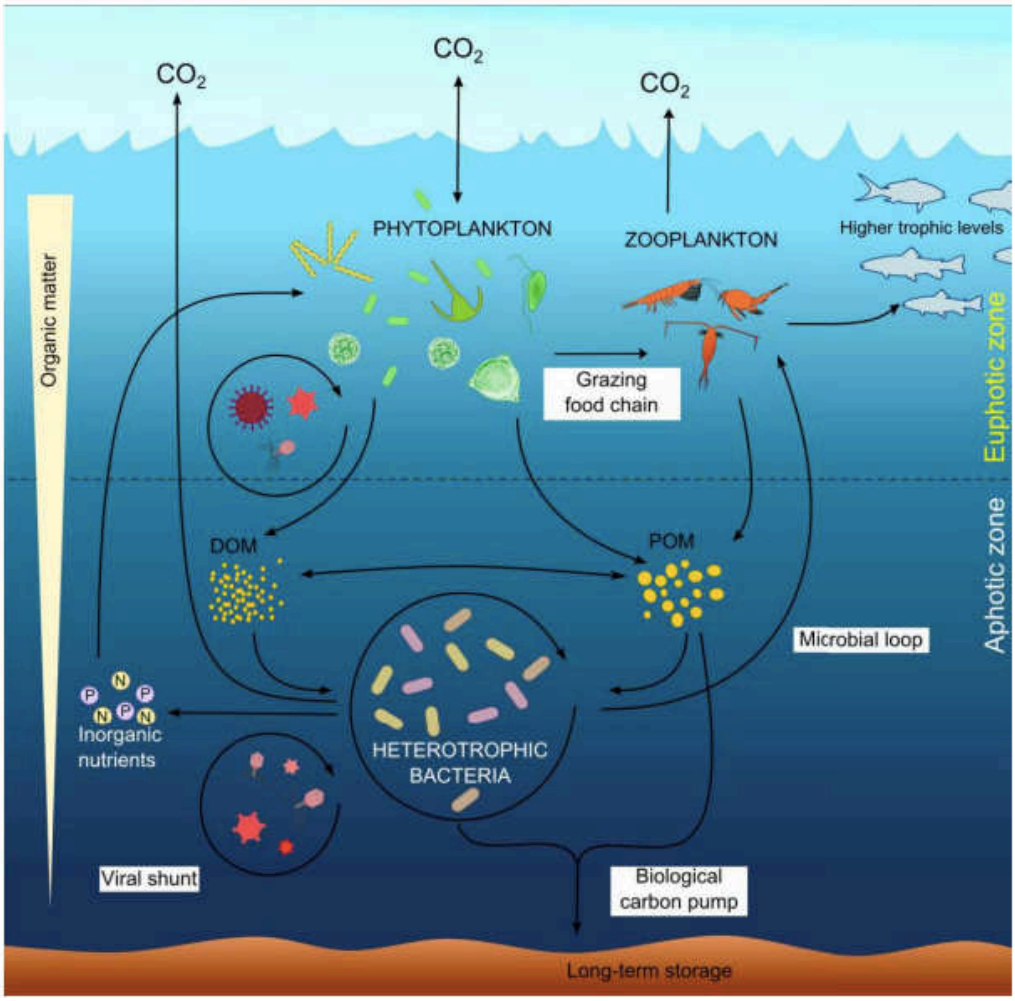

Figure 22: Cycle of organic matter produced by phytoplankton. DOM, dissolved organic matter; DOC/DON/DOP, dissolved organic carbon/nitrogen/phosphorus; POM, particulate organic matter; POC/PON/POP, particulate organic carbon/nitrogen/phosphorus (after Buchan et al., 2014; modified by Grébert, 2017).

II.2. Marine picocyanobacteria

II.2.a. Discovery of *Prochlorococcus* and *Synechococcus*

Cyanobacteria were initially called “blue-green algae” because of their resemblance to plants (ability to carry out oxygenic photosynthesis, presence of chlorophyll *a* and β-carotene). The “blue-green algae” designation was abandoned in the 1960s, when the differences in cellular organization between eukaryotes and prokaryotes were clarified (Stanier et al., 1971; Stanier and Cohen-Bazire, 1977). The first Chroococcales discovered and cultivated were mostly freshwater and coastal strains. The detection of unicellular marine picocyanobacteria came only at the end of the 70’s, due to their small size. It was Johnson and Sieburth (1979) who first revealed their omnipresence in the open ocean, as well as their abundance and diversity (Fig. 23).

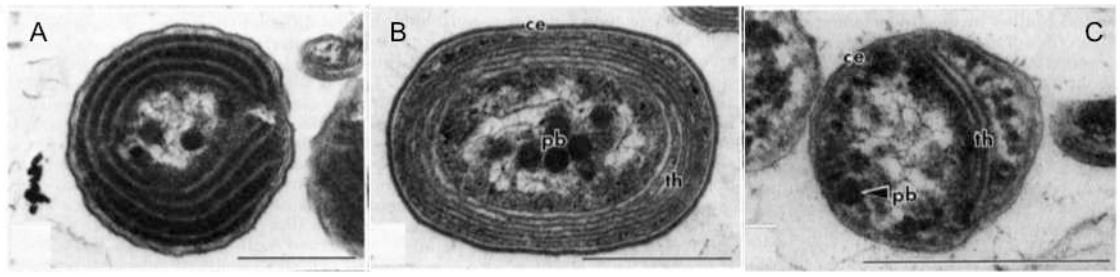

Figure 23: Images of marine chrococcoid cyanobacteria (A) type I, (B) type II and (C) type III. The scale bar is 0.5 µm for all three photographs (Johnson and Sieburth, 1979).

Advances in the field of epifluorescence microscopy subsequently enabled Waterbury and collaborators (1979) to reveal small unicellular (0.9 – 2.2 µm) orange autofluorescent chrococcoid cells in several samples from the open ocean. These phycoerythrin-rich cyanobacteria, morphologically similar to the type I cells (Fig. 23) described by Johnson and Sieburth (1979), were classified in the genus *Synechococcus* on the basis of their resemblance to freshwater strains.

The application of flow cytometry to oceanography in the 1980’s enabled (Chisholm and co-workers (1988) to discover, in the lower euphotic zone, cells smaller than those of *Synechococcus* (less than 0.8 µm) and red autofluorescent. These ubiquitous and very

abundant cells, difficult to detect by epifluorescence microscopy, resembled the type II cyanobacteria (Fig. 23) identified by Johnson and Sieburth (1979). Chisholm and collaborators (1988) were thus able to describe, for the first time, the abundance, distribution and pigment content of the smallest photosynthetic organism known to date. It was given the name *Prochlorococcus marinus* a few years later on the basis of its resemblance to prochlorophytes of the genera *Prochlorothrix* and *Prochloron* (Chisholm et al., 1992).

II.2.b. Phylogeny

Prochlorococcus and *Synechococcus*, usually called 'marine picocyanobacteria', form a well-differentiated monophyletic cluster within the Cyanobacteria radiation, called 'cluster 5' (Urbach et al., 1998). Members of this branch are also called 'α-cyanobacteria', as they possess a IA form of the ribulose-1,5-bisphosphate carboxylase/oxygenase (RuBisCO) more closely related to the one found in some *Thiobacillus* species than to the IB form of all other 'β-cyanobacteria' (Badger and Price, 2003; Cabello-Yeves et al., 2022b).

Marine *Synechococcus* have initially been separated into three clusters (MC-A to C) based on various criteria: pigment content, swimming motility, salt requirement, structure and development, %GC (Waterbury, 1989). This classification has been subsequently abandoned and marine picocyanobacteria are now grouped together within the cluster 5 (Herdman, 2001; Fuller et al., 2003; Scanlan, 2012), which has been subdivided into three distinct phylogenetic groups on the basis of 16S rRNA (Fig. 24; Dufresne et al., 2008). Subcluster 5.1 is composed almost exclusively of obligate marine strains (except for clade VIII) and appears to be the most abundant and diverse in the open ocean (Farrant et al., 2016). Subcluster 5.2 is mainly composed of freshwater or halotolerant strains thriving in estuarine areas and high-latitude marine waters (Chen et al., 2006; Cai et al., 2010; Huang et al., 2012; Larsson et al., 2014; Cabello-Yeves et al., 2022a). Finally, the less well-studied subcluster 5.3 includes both strictly marine and lacustrine strains, respectively (Huang et al., 2012; Cabello-Yeves et al., 2017, 2022a). Concerning *Prochlorococcus*, it forms a monophyletic group sister to subcluster 5.1 (Fig. 24; Partensky and Garczarek, 2010). While the date of divergence of these two closely related genera remains elusive, most models agree on an origin of marine

picocyanobacteria in the Neoproterozoic, i.e. between 500 and 1,000 Million years (Dvořák et al., 2014; Sánchez-Baracaldo, 2015; Fournier et al., 2021).

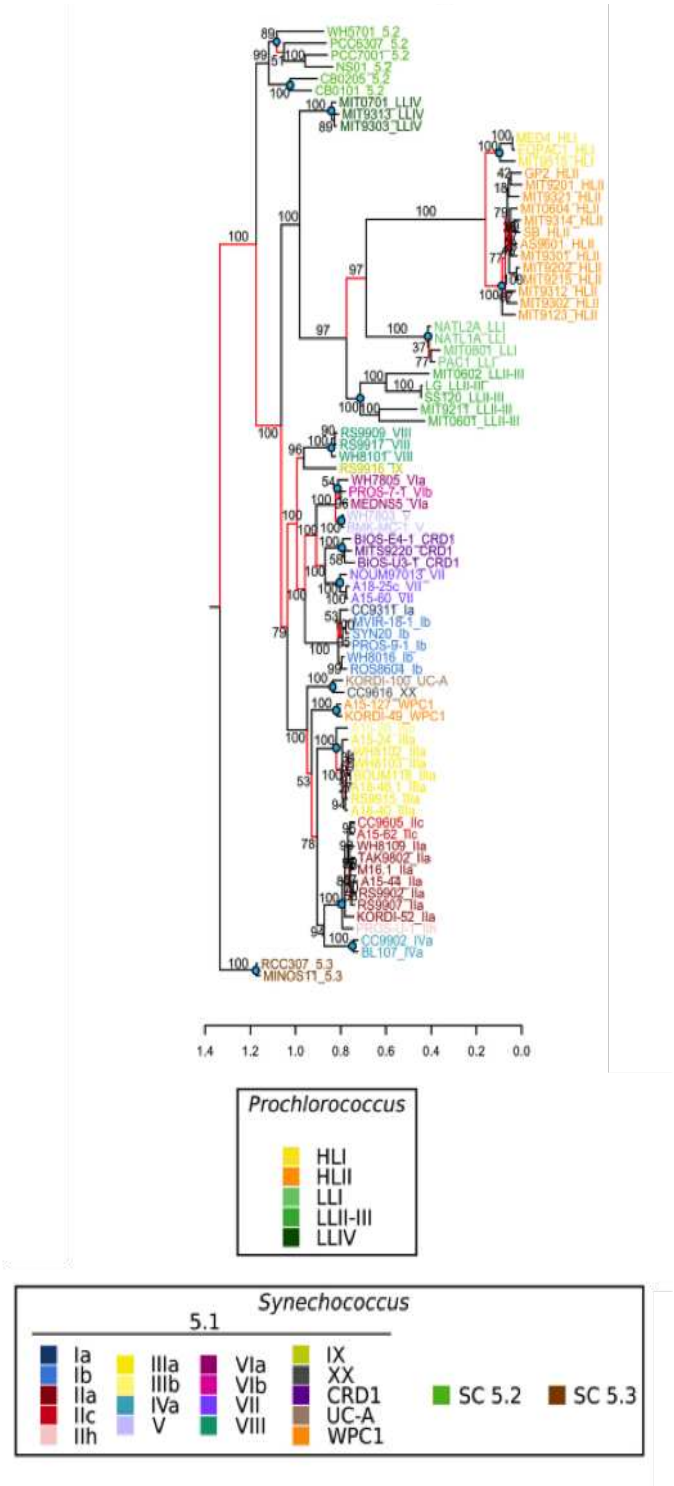

Figure 24: Phylogenetic tree of α-picocyanobacteria. The phylogeny is based on core protein sequences. The tree was built using a 'Maximum Likelihood' algorithm based on the alignment of 821 concatenated core proteins. Colors refer to the strains sub-clades (Doré et al., 2020).

A large number of clades have been highlighted in *Prochlorococcus* and *Synechococcus*. Their phylogenetic relationships are becoming clearer but are largely influenced by the genetic marker used (16S rRNA, ITS region, *ntcA*, *rpoC1*, *petB*, etc.). The current classification based on *petB* gene includes 15 phylogenetic clades and about 30 sub-clades in *Synechococcus* (Mazard et al., 2012).

II.2.c. Ecology of marine picocyanobacteria

II.2.c.i. Variability of environmental conditions in the ocean

The marine environment, and more particularly the euphotic layer, is subjected to significant variations in many abiotic (nutrients availability, light intensity and spectral quality, temperature, salinity, etc.) and biotic parameters (grazing, viral infections, toxins, competition, etc.). These changes take place at different scales of space and time, and can be either regular (daily or seasonal) or not (Meyers and Bull, 2002; Brierley, 2017).

Nutrients. The availability of nutrients varies significantly on a global scale. Some areas such as the coasts receive various nutrient-rich river or wind-transported inputs, while offshore regions can be very depleted in nitrogen, phosphate or iron, or even co-limited by several nutrients (Fig. 25; Moore et al., 2013). The organisms colonizing such environments experience waters in which essential micro- (trace metals) and macronutrients are little concentrated (picomolar to nanomolar).

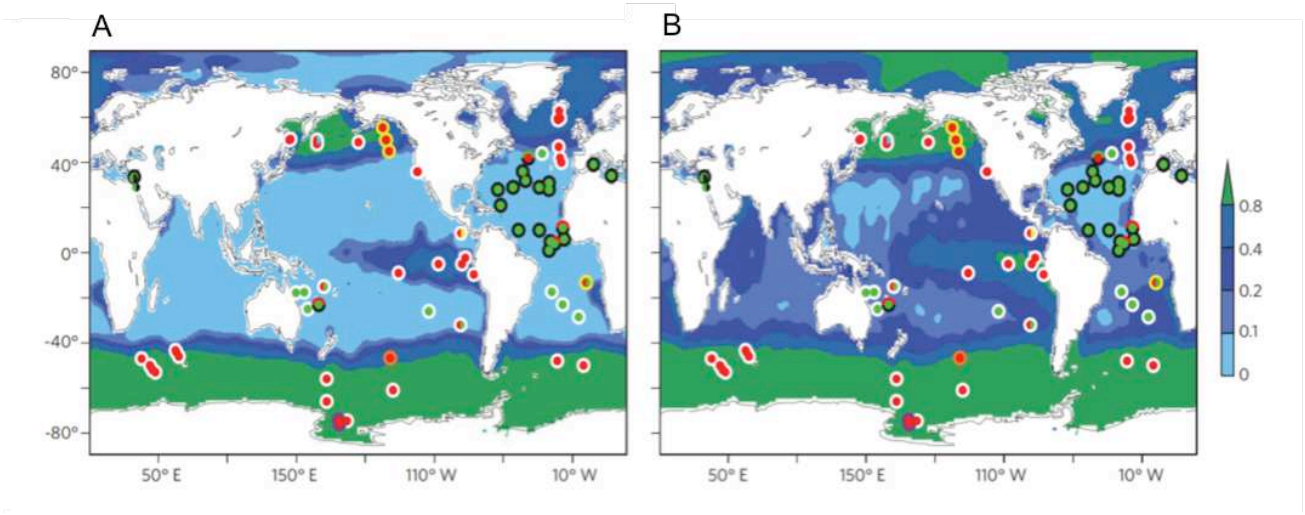

Figure 25: Annual average surface concentrations (µmol kg^{-1}) of (A) nitrate and (B) phosphate at the level of the global ocean. A certain number of oceanic zones are limited or co-limited by nitrate and phosphate. Symbols indicate the primary (central circles) and secondary (outer circles) limiting nutrients as inferred from chlorophyll and/or primary productivity increases following artificial amendment of: N (green), P (black), Fe (red), Si (orange), Co (yellow), Zn (cyan) and vitamin B12 (purple). Divided circles indicate potentially co-limiting elements. White outer circles indicate that no secondary limiting nutrient was identified (Moore et al., 2013).

The accessibility of nutrients also depends on the oceanic regime (stratified or not), which itself varies geographically and seasonally. During summer in tropical or temperate areas, the increase in surface water temperature leads to stratification of the water column. This process creates a physical barrier hindering nutrient supply from the deep waters and hence causes a limitation of phytoplankton growth in the upper mixed layer when nutrients stocks have been consumed (Fig. 26). During winter in temperate zones, the cooling of surface waters and the mixing events (storms for example) tend to homogenize the water column, disrupting the stratification and enriching the surface with nutrients. This enrichment creates good conditions for the formation of phytoplankton blooms in spring when the temperature becomes high enough to promote positive net growth (Lindell and Post, 1995; Hunter-Cevera et al., 2016a). In intertropical areas, local upwelling or storms only occasionally disrupt the stratification of the water column.

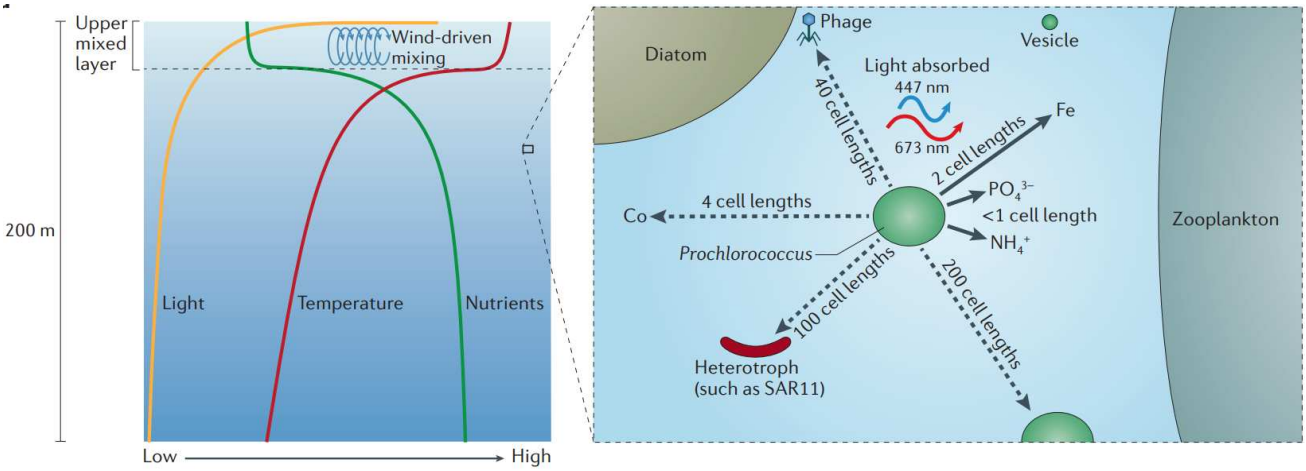

Figure 26: Variations of light, temperature and nutrients in the euphotic layer. The water column is characterized by macroscale gradients of these three abiotic parameters. In the upper mixed layer, nutrients and temperature do not vary much whereas light attenuates very quickly with depth. In deeper waters, both temperature and light continue to decrease, while nutrient concentration gradually increases (Biller et al., 2015).

Light. Fluctuations of light intensity can occur at very high frequency and magnitude. For example, 100-fold variations in surface irradiance can be observed in a matter of seconds when clouds pass (Adir et al., 2020). The photon flux also decreases exponentially with depth until it is no longer available to photosynthetic organisms (Fig. 26). The depth of the aphotic zone fluctuates according to the oceanic region. For instance, oligotrophic zones, where the quantity of suspended particles and large phytoplankton cells is low, are characterized by transparent waters where the light penetrates deeply.

Beside variations in light intensity, the oceanic environment is also characterized by strong variations in light quality. The atmosphere acts as a filter (notably for UV light), so the light quality arriving at the surface of the oceans fluctuates with cloud cover, wind, time of the day and the year, etc. (Kirk, 1992). The water column also acts as a color filter, with red light being preferentially absorbed by the water molecules and thus disappearing quickly with depth. On the contrary, blue light is scattered by water molecules but absorbed by DOM and POM. Interestingly, phytoplankton itself can be a major contributor to light absorption in productive areas (Kirk, 1994; Stomp, 2008; Holtrop et al., 2021).

Light quality also changes horizontally, and more specifically along coast-offshore gradients. In brackish and/or turbid environments, red light (600 – 650 nm) predominates

(Fig. 27), other wavelengths being quickly absorbed in the first meters by OM. In coastal areas, it is the green light that penetrates the deepest (20 m), the high concentrations of chlorophyll and organic matter absorbing red and blue wavelengths. In open ocean waters, and especially in oligotrophic environments such as gyres, blue light (450 – 500 nm) is scattered by water molecules and thus penetrates deeply into the water column (Pick, 1991; Wood et al., 1998; Stomp, 2008; Haverkamp et al., 2009; Holtrop et al., 2021).

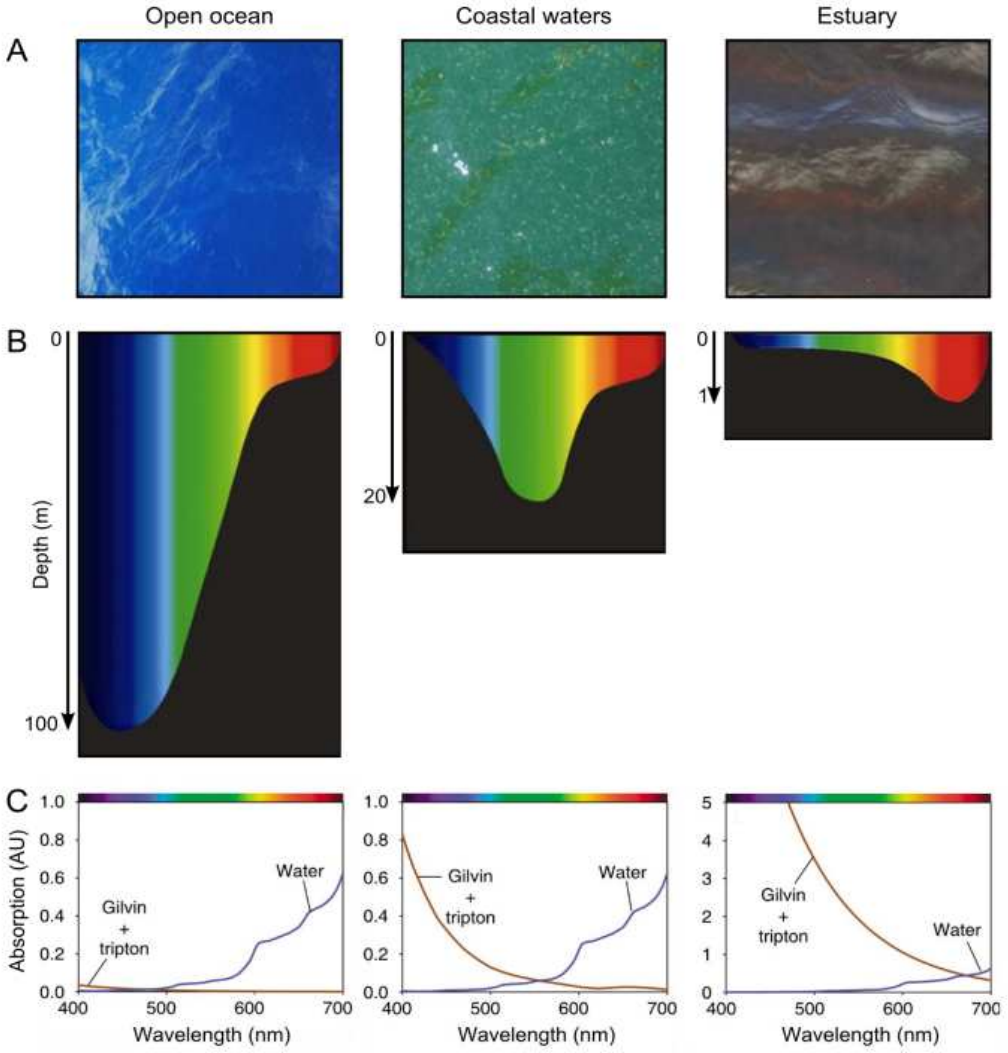

Figure 27: Light quality in different aquatic environments. (A) Visual aspect of the water quality in the open ocean, coastal areas and estuaries. (B) Availability of different light wavelengths according to depth. (C) Light absorption of 'gilvin + tripton' (brown line) and water (blue line) in the corresponding aquatic environments (after Stomp 2008; modified by Grébert, 2017).

Temperature. Temperature varies not only with seasons, but also over a latitudinal gradient, the average temperature decreasing by about 0.4°C per degree of latitude from the equator (30°C) to the poles (2°C to -1.8°C; Fig. 28; Greenwood and Wing, 1995). It should also be noted that temperature gradient anomalies exist in the oceans, notably at the level of upwellings, which are characterized by ascendant cold waters, or gyres. The temperature also decreases significantly from surface to depth (Fig. 26).

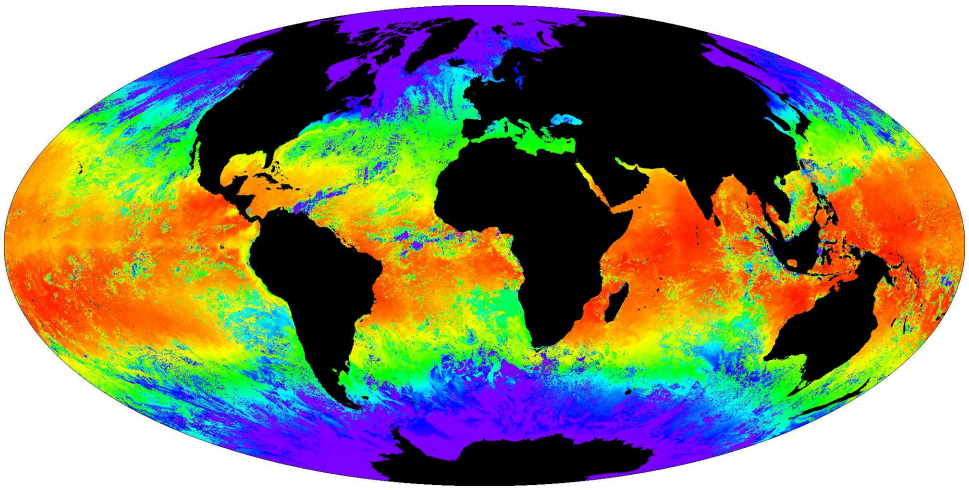

Figure 28: Global sea surface temperature. The global ocean is characterized by a latitudinal temperature gradient. Temperatures decrease by about 0.4°C per degree of latitude from the equator to the poles (MODIS Ocean Science Team, 2000). Scale: -2°C (purple) to 35°C (red).

II.2.c.ii. Genus *Prochlorococcus*

With a global population estimated to 2.9 x 10^{27} cells, *Prochlorococcus* is globally the most abundant cyanobacterium on Earth. Members of this genus are distributed between 50°N and 40°S (Fig. 29) and appear to be well adapted to warm, stratified and oligotrophic waters where they can reach high concentrations (Partensky et al., 1999; Johnson et al., 2006; Coleman and Chisholm, 2007; Zwirglmaier et al., 2007, 2008; Scanlan, 2012; Flombaum et al., 2013). Their density decreases in nutrient-rich waters from which they are often excluded by more competitive organisms, or by grazing. Besides temperature and nutrient availability, light is also one of the main environmental factors influencing the vertical and horizontal distribution of *Prochlorococcus* populations. Cells are indeed capable

to spread over several orders of magnitude of light intensity. Their concentration increases along the water column to reach a maximum at 50 – 100 m, and then decreases down to 200 – 250 m (Fig. 29; Partensky et al., 1999; Johnson et al., 2006; Coleman and Chisholm, 2007). The colonization of the entire euphotic layer is a specific feature of *Prochlorococcus* due to the specialization of physiologically and genetically distinct populations to specific light intensity ranges (a process called photoadaptation). Early flow cytometry studies have made it possible to highlight a surface 'dim' population with low red autofluorescence, and a deep 'bright' population with high red fluorescence. Strains representative of these two populations were shown to differ both genetically and physiologically, notably by their growth irradiance optima and divinyl-chlorophyll *b/a* ratio (Moore et al., 1998). They were therefore renamed HL (High Light) and LL (Low Light) ecotypes, respectively.

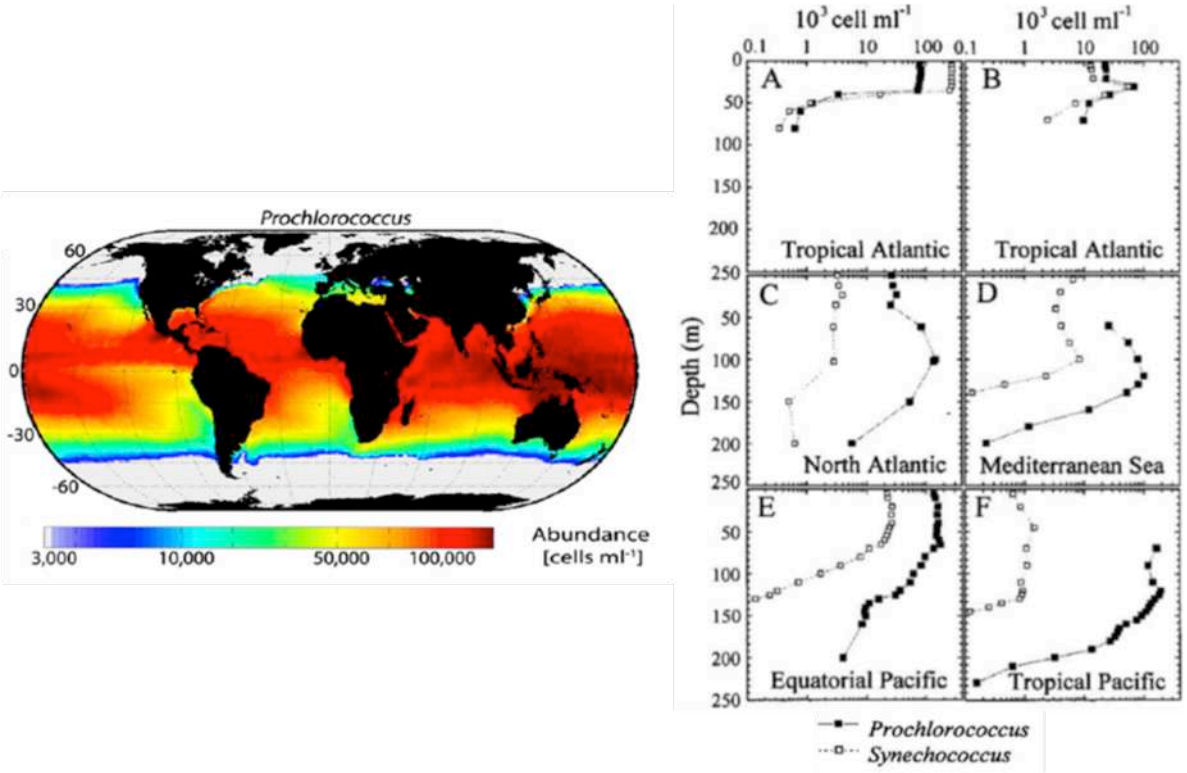

Figure 29: Horizontal and vertical distribution of *Prochlorococcus*. The left figure illustrates a global distribution model of the genus (Flombaum et al., 2013). The figure on the right illustrates the vertical distribution of *Prochlorococcus* cells in different marine environments (Partensky et al., 1999).

II.2.c.iii. Genus *Synechococcus*

The polyphyletic genus *Synechococcus*, which includes freshwater, halotolerant and marine strains, is globally widespread. It is found from the equator to the subpolar circles (60°N to 50°S, with some reports at 80°N; Paulsen et al., 2016), and from nutrient-rich estuarine to oligotrophic areas (Fig. 30; Zwirglmaier et al., 2007, 2008; Scanlan, 2012; Flombaum et al., 2013). *Synechococcus* dominates the picocyanobacterial communities in coastal and mesotrophic open ocean waters (Partensky et al., 1999; Huang et al., 2012). However, this genus is often one or two orders less abundant than *Prochlorococcus*, even if it can reach seasonally or permanently higher densities. This is notably the case of nutrient-rich zones such as the Costa Rica upwelling dome, where record concentrations of 3.6 x 10^6 cells mL^{-1} have been reported (Saito et al., 2005).

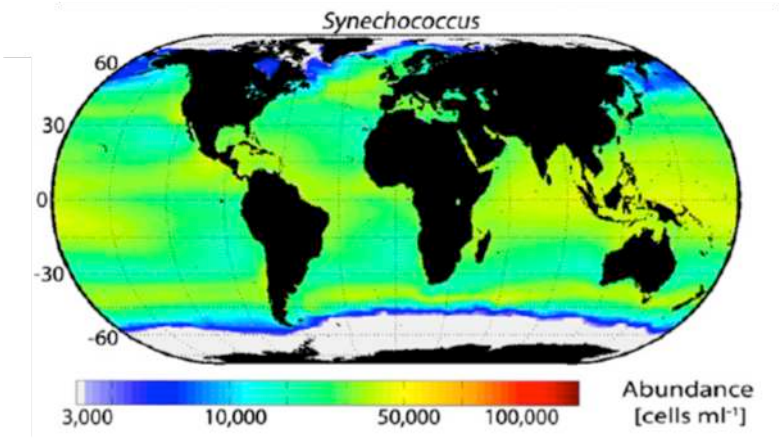

Figure 30: Horizontal distribution of *Synechococcus*. The figure comes from a global distribution model of the genus (Flombaum et al., 2013).

The main factors influencing the global distribution of these picocyanobacteria are nutrient availability (nitrogen, phosphorus, iron), temperature and salinity (Sohm et al., 2015; Farrant et al., 2016). *Synechococcus* is more abundant in nutrient-rich regions (upwelling or coastal areas) and tolerates temperature ranges from 10 to 30°C (Scanlan, 2012). Concerning the light intensity, it seems that, contrary to *Prochlorococcus*, this parameter has relatively little effect on the structure of *Synechococcus* populations. Maximum cell concentrations are generally found either in the upper mixed layer or at

nitracline level, then decline rapidly with depth. Consequently, *Synechococcus* cells are rarely detected below 100 – 150 m (Figure 29; Partensky et al., 1999; Scanlan, 2012), except for a few cells transported down the water column during productive seasons by attachment to large particles such as microphytoplankton (Sohrin et al., 2011).

The scientific community has long believed that only four clades predominated *in situ* within subclade 5.1: (i) clades I and IV in coastal and oceanic areas characterized by cold/temperate and nutrient-rich waters at high latitudes (above 30°N); (ii) clade II in warm tropical and subtropical environments, corresponding to iron-replete oligotrophic or mesotrophic waters; and (iii) clades II and III in warm coastal and/or oligotrophic waters (Zwirglmaier et al., 2007, 2008; Ahlgren and Rocap, 2012; Huang et al., 2012; Mazard et al., 2012). More recent studies using high-resolution genetic markers actually showed that clade II is by far the dominant ecotype in (sub)tropical nitrogen-limited waters, while clade III preferentially thrives in warm and temperate phosphorus-deprived areas. These studies also revealed the ecological importance of the CRD1 clade, initially described in the Costa Rica Dome (Saito et al., 2005), in iron-depleted waters of the Pacific Ocean (Sohm et al., 2015; Farrant et al., 2016; Doré et al., 2023). By defining Ecologically Significant Taxonomic Units (ESTUs, i.e. genetically related subgroups within clades that co-occur in the field), Farrant and collaborators (2016) also highlighted the large microdiversity existing within the major clades and showed that these encompass several ESTUs, occupying distinct ecological niches *in situ*.

II.3. Pigment diversity of *Synechococcus* picocyanobacteria

II.3.a. Pigment types and subtypes

The large pigment diversity of marine *Synechococcus* strains has been attributed to the variable composition of PBS in phycobiliproteins and chromophores (Six et al., 2007b; Haverkamp et al., 2008; Humily et al., 2013; Grébert et al., 2022). Three pigment types occupying different ecological niches have been defined: (i) pigment type 1 (PT 1, blue-green strains) whose rods are composed exclusively of PC binding PCB; (ii) PT 2 (pink strains) whose rods are made up of PC and PE-I binding PCB and PEB; (iii) PT 3, specific to marine

Synechococcus whose rods are made up of PC, PE-I and PE-II binding PCB, PEB and PUB (Fig. 31; Six et al., 2007b).

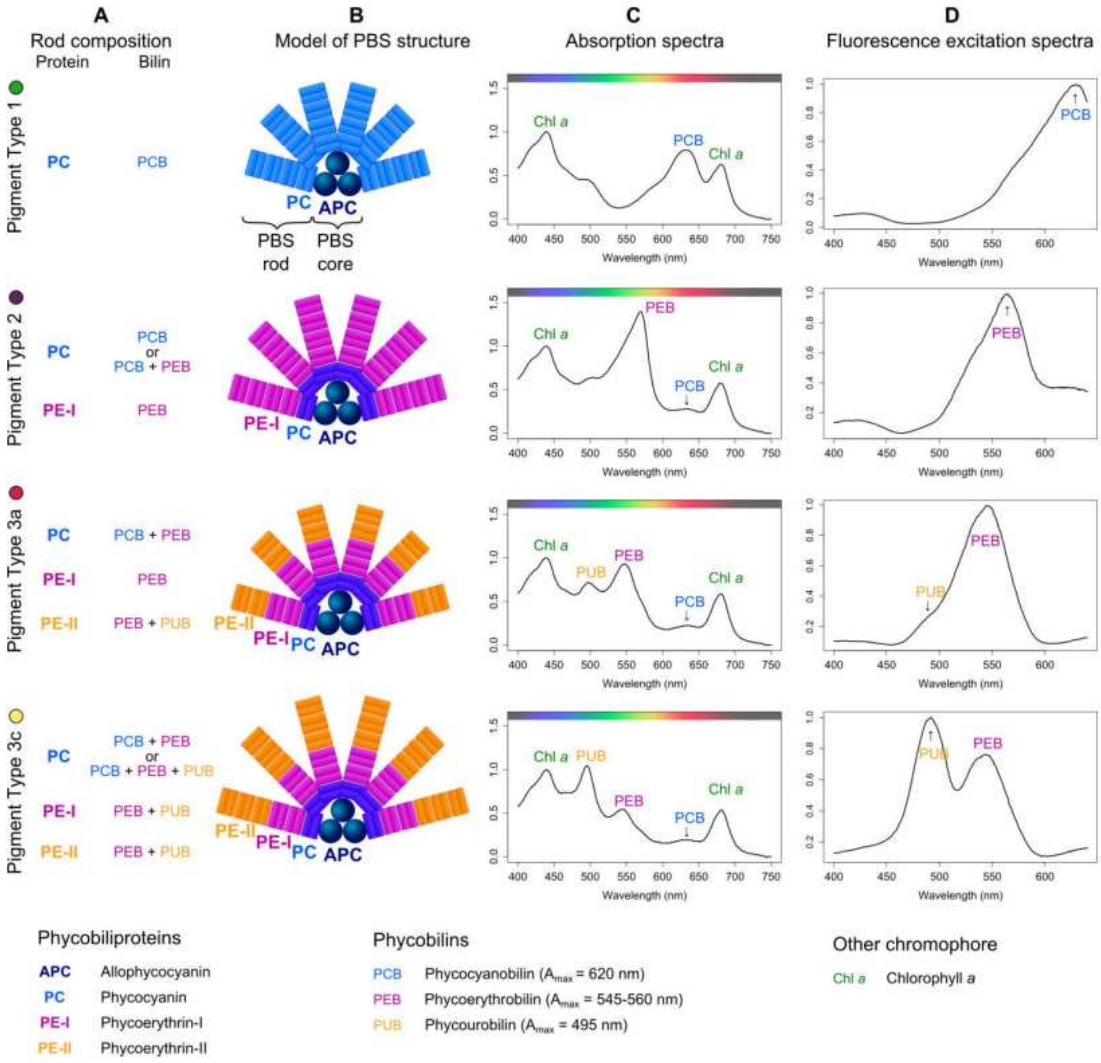

Figure 31: Composition and spectral properties of the phycobilisomes specific of the three pigment types of marine *Synechococcus*. (A) Phycobiliproteins and chromophores composition of the rods. (B) Structure of the different PBS. (C) Absorption spectra of the cells representatives of each pigment type. (D) Excitation spectra of the same cells (Grébert, 2017).

Six and collaborators (2007b) further subdivided PT 3 into several subtypes, based on the variable PBS content in PEB and PUB (Palenik, 2001; Everroad et al., 2006; Everroad and Wood, 2012; Humily et al., 2013; Sanfilippo et al., 2019a). The PUB:PEB ratio of a strain (as estimated from the fluorescence ratio at 495 nm and 545 nm with an emission fixed at 580

nm) can be: low ($Ex_{495:545} < 0.5$) in subtype PT 3a, high ($1.6 \leq Ex_{495:545}$) in PT 3c, variable (0.6 – 0.7 in green light and 1.6 – 1.7 in blue light) in PT 3d (Everroad et al., 2006; Six et al., 2007b; Everroad and Wood, 2012; Humily et al., 2013). While strains belonging to PTs 3a, 3b and 3c have fixed pigmentations that enable them to absorb green or blue light efficiently, PT 3d strains are type IV chromatic acclimaters. In other words, they are capable of reversibly modifying their pigmentation according to the color of the incident light in order to collect the most abundant wavelengths. PT 3d cells have a phenotype similar to PT 3a in green and white light (low PUB:PEB ratio), and equivalent to PT 3c in blue light (high PUB:PEB ratio). To note, two genetically distinct types of type IV chromatic acclimaters have been reported and called PTs 3dA and 3dB (see Introduction § II.4; Humily et al., 2013).

Interestingly, several other scarcer pigment types have been reported in the literature:

- PT 3b strains are characterized by an intermediate ($0.6 < Ex_{495:545} < 1.6$) PUB:PEB ratio. In all cases, these strains are phylogenetically identical to either PTs 3dA or 3dB but are stuck between GL and BL phenotypes, probably due to a mutation or disruption of the Type 4 chromatic acclimation (CA4) regulatory machinery;
- PT 3e cells display a low amplitude of variation of the $Ex_{495:545}$ during a shift from GL to BL (Humily et al., 2013), likely due to a misfunctioning of the CA4 process;
- Finally, Xia and collaborators (2017) have described a new pigment type, PT 3f, which is phenotypically similar but genetically distinct from PT 3c. Only two cultures strains have been reported to display PT 3f so far (KORDI-100 and CC9616), but a recent study has found that this PT could be quite abundant at some stations in the eastern Indian Ocean (Zhang et al., 2022).

II.3.b. The PBS region

Genes encoding the proteins, enzymes and regulators involved in photosynthesis are often dispersed in the genome (Blankenship, 2014). However, the genes necessary for the biosynthesis and regulation of phycobilisomes in α-cyanobacteria are an exception, since they are grouped into clusters and co-transcribed operons (Grossman et al., 1993; Anderson and Toole, 1998; Six et al., 2007b). Thus, most genes encoding components of PBS rods are

found in a large (up to 32 kb) genomic region named the 'PBS region' (Fig. 32; Wilbanks and Glazer, 1993; Six et al., 2005, 2007b; Humily et al., 2013).

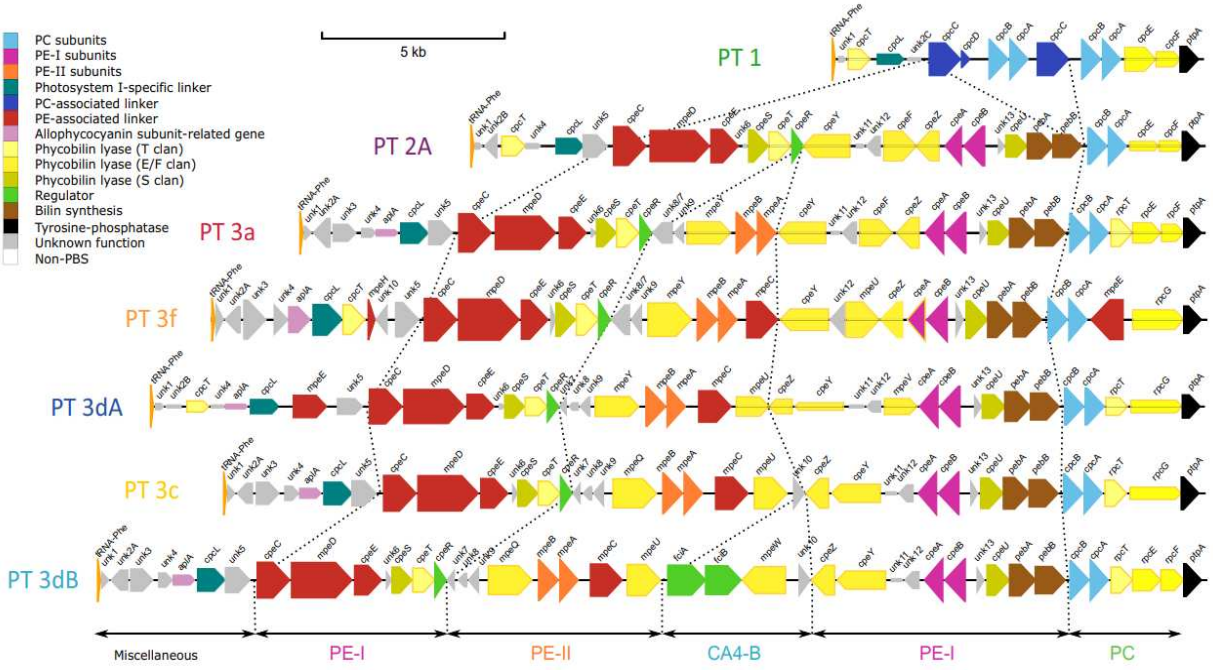

<u>Figure 32:</u> Organization of the PBS regions in different pigment types of marine *Synechococcus*. This genomic region is increasingly more complex from PT 1 to PT 3dB. Colors refer to the gene functions, as indicated in the inset (Grébert et al., 2022).

The size, organization and gene content of this region vary significantly between PTs, but is remarkably conserved among cultured and field representatives of a given PT (Six et al., 2007b; Humily et al., 2013; Grébert et al., 2018, 2022). PBS regions comprise genes encoding PBP α- and β-subunits, linkers and enzymes necessary for biosynthesis, chromophore attachment and regulation of PBS, as well as a number of yet uncharacterized genes called unknowns (Grossman et al., 1993; Anderson and Toole, 1998; Six et al., 2005, 2007b; Adir et al., 2006; Grébert et al., 2022). The names of PBS-related genes have a prefix that generally designates the corresponding phycobiliprotein, namely *apc* for allophycocyanin, *cpc*/*rpc* for phycocyanin, *cpe* for PE-I, *mpe* for PE-II (although some may have multiple substrates, e.g. PE-I and PE-II). PT1 strains have the smallest and simplest PBS rod region, consisting of the

cpc cluster only. This notably includes one to four copies of the *cpcBA* operon encoding α and β-PC subunits, two to four rod linker genes, three phycobilin lyase genes (*cpcT*, *cpcE* and *cpcF*), as well as two uncharacterized genes; Fig. 32). PT 2 strains have replaced all but one copy of the *cpcBA* operons by a set of sixteen to eighteen genes necessary to synthesize and regulate PE-I. These include three linkers, six lyases and two enzymes involved in PEB synthesis, *pebA* and *pebB* (Frankenberg et al., 2001). PT 3 strains have the most complex PBS region, with the *mpe* cluster (containing the fusion *unk8/7*gene, *unk9*, *mpeY* and the *mpeBA* operon) interrupting the *cpe* cluster between *cpeR* and *cpeY* (Six et al., 2007b).

Interestingly, genomic differences exist between PT 3 subtypes (Fig. 32). For example, all other subtypes than PT 3a possess the *mpeC* gene that encodes a PUB-binding PE-II associated linker (Six et al., 2005), as well as *mpeU* that encodes a partially characterized lyase-isomerase (Wilbanks and Glazer, 1993; Mahmoud et al., 2017). In PTs 3c and 3dB, the PEB lyase gene *mpeY* is replaced by *mpeQ*, which encodes a lyase-isomerase (Grébert et al., 2021, 2022). Moreover, *unk10* is present in the middle of the PBS region of PTs 3c and 3dB, and outside in PT 3dA. Finally, PT 3dB differ from other PT 3 subtypes by the insertion of a small genomic island (CA4-B island) between *mpeU* and *cpeZ* genes.

It is important to note that, although the genomic organization of the PBS rod region is globally conserved among representatives of a given pigment type, the allelic diversity of the genes gathered in the region can be important for linkers, phycobilin lyases or uncharacterized conserved proteins (Grébert et al., 2022).

II.3.c. Evolution of the PBS region

The pigment diversity of marine *Synechococcus* is not directly correlated with the core genome phylogeny of the strains (Toledo et al., 1999; Six et al., 2007b; Dufresne et al., 2008; Everroad and Wood, 2012; Humily et al., 2014; Grébert et al., 2018, 2022). Indeed, closely related strains may have different PTs while phylogenetically distant strains may have the same (Fig. 33). The PBS region is therefore assumed to have played an important role in the adaptation to the various light niches colonized by marine *Synechococcus*.

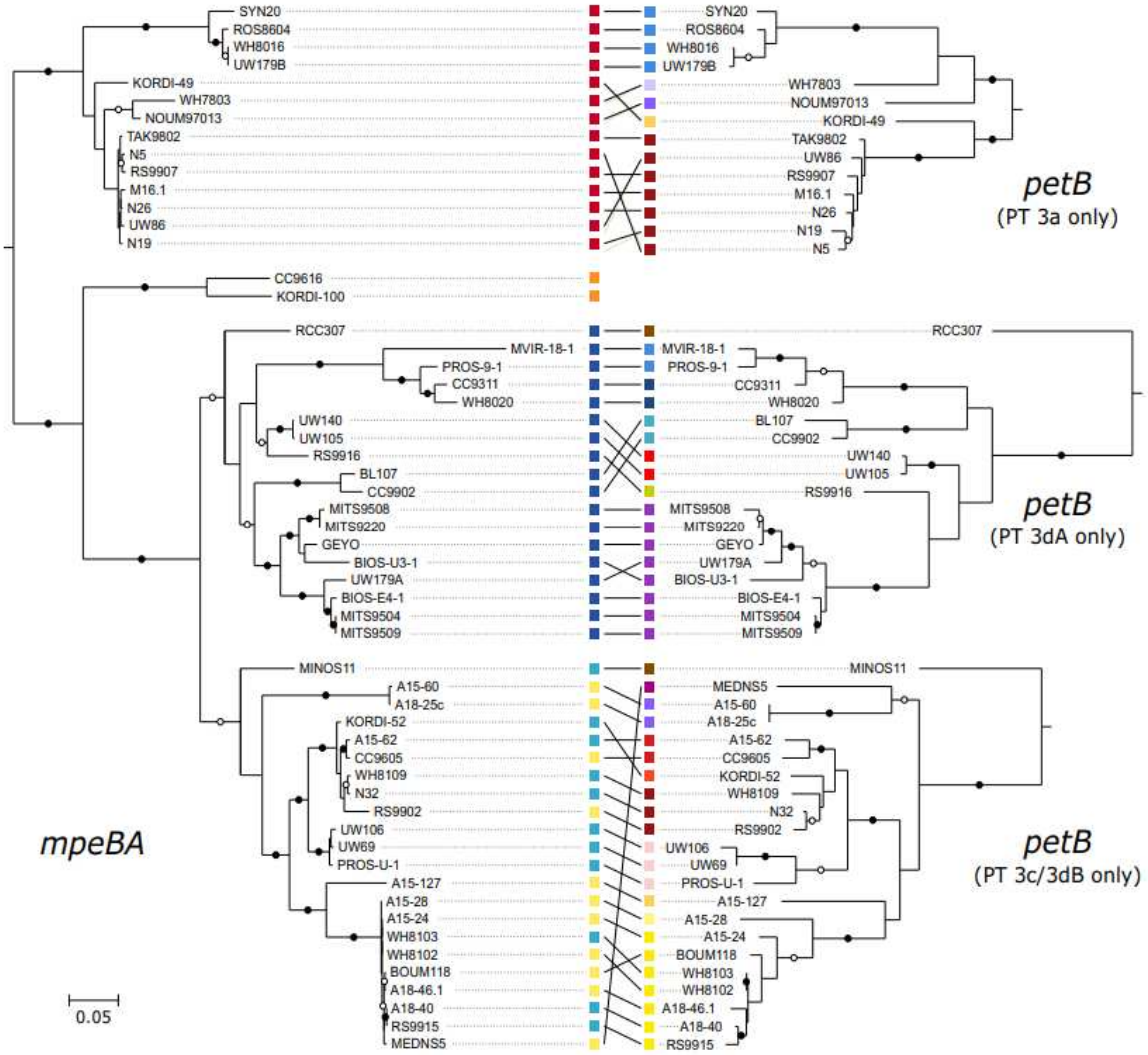

<u>Figure 33:</u> Phylogenetic tree of *Synechococcus* radiation representing the major clades and pigment types. Phylogenies of the *mpeBA* operon and the marker gene *petB* do not fully correspond. Pigment types are indicated by a colored square in the *mpeBA* phylogeny (Grébert et al., 2022).

By exploring the long evolutionary history of PBS genes, Grébert and collaborators (2022) demonstrated that the rod region experienced significantly more transfers and losses than other genes. Furthermore, it was shown that recombination events are more frequent between, than within clades. The mechanisms proposed in this study for the variable gene content and organization of the PBS rod region are: (i) lateral transfer via tycheposons, a type of mobile genetic element discovered in *Prochlororoccus* (Hackl et al., 2023), and transposition into the PBS rod region; (ii) gene transfer and loss, a phenomenon called

'incomplete lineage sorting'; and finally (iii) duplication and/or divergence of ancestral pre-existing genes.

II.4. Chromatic acclimation

Unlike adaptation, a long-term evolutionary process involving changes in the genetic composition of an organism, chromatic acclimation refers to the expression of different phenotypes according to environmental conditions (Kehoe and Gutu, 2006; Sanfilippo et al., 2019a). Engelmann (1902) and Gaidukov (1903) first used the term "chromatic adaptation" when observing filamentous cyanobacteria isolated from a lake change color in response to ambient light quality. The understanding of the process progressed from 1950 thanks to studies using model organisms (*Calothrix* sp. PCC7601, *Fremyella diplosiphon*, *Synechocystis* sp. PCC 6701; Kehoe and Gutu, 2006). Since then, six types of chromatic acclimation (with different sensors, regulatory networks and outcomes) have been described in the Cyanobacteria phylum. Those involve changes in: (i) rod-core linkers (CA1); (ii) phycobiliprotein and chromophore composition (CA2 and CA3); (iii) PBS chromophorylation (CA4); (iv) phycobiliprotein abundance (CA5); (v) PBS and photosynthetic apparatus biosynthesis (CA6; Sanfilippo et al., 2019a). The aim of all these processes is to maximize the absorbance of the predominant wavelengths, and thus energy collection for photosynthesis. CA1, CA2 and CA3 are specific to freshwater organisms and are useful in niches where red and green light predominates. CA4 is associated to the marine environment where natural gradients of blue and green light occur. Concerning CA5 and CA6, both concern red/far-red acclimation found in terrestrial organisms (for more information, see, 2019a).

Type IV chromatic acclimation (CA4) is specific to marine *Synechococcus* and widely distributed within the cluster 5 radiation (Humily et al., 2013). It was first reported by Palenik (2001) who observed light color-induced changes in fluorescence excitation spectra in several *Synechococcus* strains. Later studies have shown that this process involves chromophore variations at three residues (Cys-139 of α-PE-I, Cys-83 and Cys-140 of α-PE-II), with PUB attached in BL and PEB in GL (Everroad et al., 2006; Shukla et al., 2012; Sanfilippo et al., 2016). It is most likely that the CA4 process does not imply any degradation or change

in the pigmentation of pre-existing PBS, the accessibility of phycobilin lyases to chromophores being too limited (Bennett and Bogorad, 1973; Adir, 2005). Instead, CA4 probably occurs via the synthesis of new PBS complexes with a chromophorylation matching the new light color, as well as a progressive dilution of the previously existing PBS (Everroad et al., 2006; Singh et al., 2015; Sanfilippo et al., 2019a). Such a neosynthesis is consistent with the duration necessary for the cells to acclimate to the new light quality conditions (about six generations; Everroad et al., 2006; Humily et al., 2013). To date, no light-sensing molecule involved in CA4 has been identified (Sanfilippo et al., 2016, 2019a).

Comparative genomics analyses have shown that the CA4 process is correlated with the presence of a small genomic island (4 to 6 Kbp), which occurs under two structurally close but genetically distinct configurations: CA4-A and CA4-B (Fig. 34; Humily et al., 2013). Each is specific of PTs 3dA and 3dB, respectively, and is located either in the middle of the PBS region (CA4-B) or outside the PBS region (CA4-A).

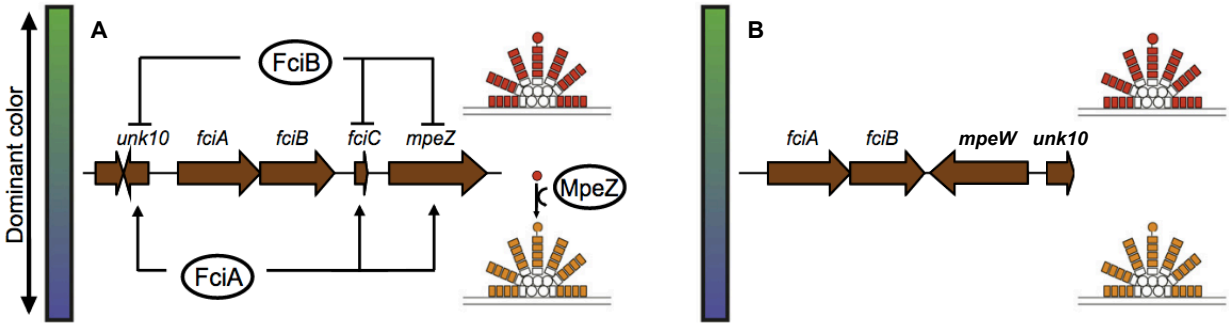

Figure 34: Representation of (A) CA4-A and (B) CA4-B genomic islands. The differential expression of the genes as a function of light color (blue or green) as well as the composition of the phycobilisomes are shown (modified from Sanfilippo et al., 2016).

Several of the genes included in the CA4-A island have been characterized in the model PT 3dA strain *Synechococcus* sp. RS9916 (Fig. 34A): *fciA* and *fciB* genes encoding two master regulators of the CA4 process (activator in BL and repressor in GL respectively; Sanfilippo et al., 2016), and *mpeZ* that encodes a phycobilin lyase-isomerase overexpressed in BL and responsible for the attachment of PUB to a specific cysteine residue (Cys-83) of α-PE-II

(Shukla et al., 2012). In contrast, the functions of *fciC*, *unk10* and *unk14* (the latter gene being only present in a subset of PT 3dA strains) are unknown. It must be stressed that MpeZ has been found to 'compete' with MpeY that is not light-regulated and is encoded in the PBS region (Sanfilippo et al., 2019b). This enzyme is involved in the binding of PEB to the same cysteine residue as MpeZ in GL. It has been suggested that it is the changes in the relative MpeZ/MpeY abundance ratios that determines which chromophore is attached.

While the molecular bases of the CA4-A process have been partially characterized, the function of *fciA*, *fciB* and *unk10* genes included in the CA4-B island (Fig. 34B) is unknown yet. As concerns *mpeW*, it is only very recently that Grébert and collaborators (2021, a study to which I have participated) have characterized its function in the *Synechococcus* PT 3dB model strain A15-62.

II.5. Pigment types distribution in the environment

The large pigment diversity observed in marine *Synechococcus* is responsible for the adaptation of this genus to a wide variety of light niches, from particle-rich estuaries to the clear waters of the open ocean (Campbell and Iturriaga, 1988; Olson et al., 1988; Lantoine and Neveux, 1997; Campbell et al., 1998; Wood et al., 1998; Michelle Wood et al., 1999; Neveux et al., 1999; Sherry and Michelle Wood, 2001; Haverkamp et al., 2008; Larsson et al., 2014; Liu et al., 2014; Hunter-Cevera et al., 2016a; Xia et al., 2017; Grébert et al., 2018). Pigment type 1 (blue-green strains) dominates in estuaries and coastal/saline waters characterized by low salinity and high turbidity (Fig. 27). Because blue light is strongly absorbed by suspended matter in the first few meters of water, these cells specialized in absorbing red light (λ_{max} = 600 – 660 nm) are favoured. PT 2 (pink-colored strains) is found in coastal eutrophic waters and in transition zones between brackish and marine environments, where green light penetrates the deepest. Coexistence of PTs 1 and 2 can be observed in coastal areas, estuaries and freshwater lakes where waters are of intermediate coloration. Concerning PT 3 (red to orange strains), it is apparently restricted to marine environments, with green light specialists (PT 3a) being more numerous in mesotrophic

waters (regional seas and ocean margins) and blue light specialists (PT 3c) dominating transparent, oligotrophic waters where blue light predominates.

For a long time, studies on the distribution of *Synechococcus* pigment types in the field used fluorescence-based techniques, namely epifluorescence microscopy, spectrofluorimetry or flow cytometry (Campbell and Iturriaga, 1988; Olson et al., 1988; Lantoine and Neveux, 1997; Campbell et al., 1998; Wood et al., 1998; Michelle Wood et al., 1999; Neveux et al., 1999; Sherry and Michelle Wood, 2001; Haverkamp et al., 2008), with which it was impossible to distinguish chromatic acclimaters acclimated to GL and BL from their fixed-pigmentation counterparts (PTs 3a and 3c, respectively). More recently, genetic analyses based on a single PBS gene marker (*cpeBA* that encodes PE-I subunits) allowed some advances on this topic. With this approach, it was indeed found that PT 3dA was dominant in subpolar waters. Yet, the use of a single marker did not enable differentiating all the different subtypes within PT 3. More recently, Grébert and collaborators (2018) identified three genes involved in the biosynthesis of PBS, which proved necessary and sufficient to discriminate all the PTs and subtypes of marine *Synechococcus* (Fig. 35). Those genes are: (i) *cpcBA*, which encodes PC and allows discrimination of PTs 1, 2 and 3; (ii) *mpeBA*, which encodes PE-II and discriminates all PT 3 subtypes, except PTs 3c and 3dB that are phylogenetically indistinguishable; (iii) *mpeW*, which encodes a phycobilin lyase specifically targeting PT 3dB and, by subtraction, allows enumeration of PT 3c cells.

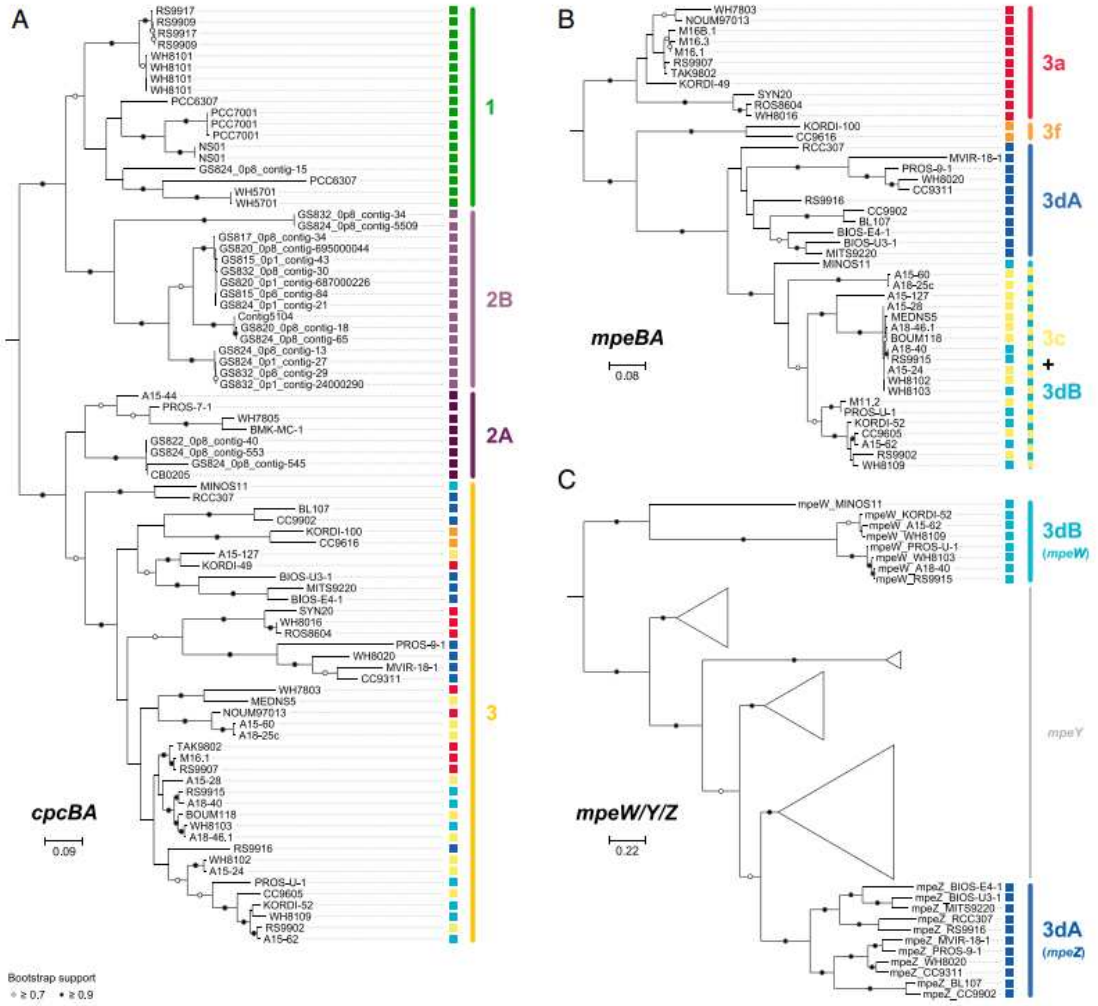

Figure 35: Phylogenetic tree based on (A) *cpcBA*, (B) *mpeBA*, (C) *mpeW/Y/Z*. These three markers are necessary and sufficient to highlight all pigment types and subtypes in marine *Synechococcus* (Grébert et al., 2018).

Using these three molecular markers to recruit reads from *Tara* Oceans metagenomics dataset, Grébert and co-workers (2018) showed that only four PTs dominate in the environment, altogether totalling 95% of the marine *Synechococcus* population: (i) PT 3a, which account for 20% of the global population and colonizes warm and green equatorial particle-rich waters (Arabian Sea, Red Sea, Gulf of Mexico/Panama area; Fig. 36); (ii) PT 3c, which make up 33% of the population and is particularly abundant in the warm, transparent, oligotrophic, iron-enriched areas (Mediterranean Sea, South Atlantic, Indian Ocean gyres, Marquesas Islands); and (iii) chromatic acclimaters which are globally the most abundant PT. Together, PTs 3dA and 3dB indeed constitute 42% of the *Synechococcus* population.

Moreover, the study revealed that the two types of chromatic acclimaters are equally abundant and are distributed in complementary niches. PT 3dA strains seem to prefer cold, nutrient-rich and highly productive waters. They represent up to 100% of the *Synechococcus* population at high latitudes in the northern hemisphere, and can also be dominant in other vertically mixed waters (Chilean upwelling, Agulhas current). PT 3dB cells are mostly found in warm iron-replete waters and appear to be more abundant at depth. However, the latter result remains to be confirmed since the *Tara Oceans* dataset used for this study comprises only two sampling depths, with the deep chlorophyll maximum (DCM) depth being available only for a subset of stations (Grébert et al., 2018).

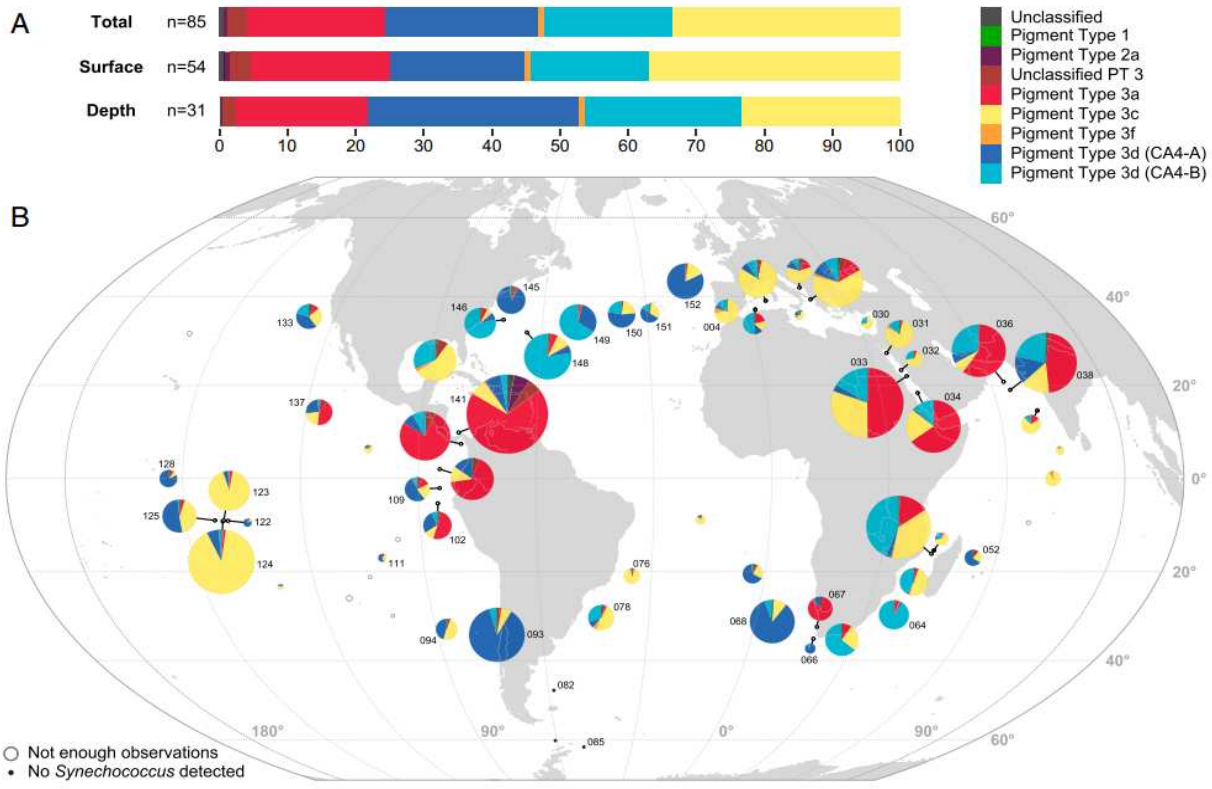

Figure 36: Global distribution of the different pigment types of *Synechococcus*. (A) Relative abundance of each pigment type in the dataset at two depths. (B) Map illustrating the distribution of the different PTs in surface along the *Tara* Oceans transect. The size of the pie charts is proportional to the number of *cpcBA* reads normalized by the sequencing effort (Grébert et al., 2018).

Beyond the horizontal coast-offshore gradient, it appears that in some eutrophic and mesotrophic areas the proportion of cells with a high PUB:PEB ratio increases along the water column (Olson et al., 1990; Lantoine and Neveux, 1997; Michelle Wood et al., 1999). The predominance of these populations at depth could be explained by the prevalence of blue wavelengths that are very little absorbed by water molecules along the water column. At other locations, such as oligotrophic regions, the cells pigment content does not seem to vary vertically (Campbell and Iturriaga, 1988; Neveux et al., 1999; Katano and Nakano, 2006; Yona et al., 2014), suggesting an important role of the oceanic regime and environmental parameters on this phenotypic trait.

Objectives

Although they were long undetected in the field by lack of suitable techniques or genetic markers, *Synechococcus* cells capable of type IV chromatic acclimation (PT 3d) were recently shown to represent more than 40% of the global population of this genus (Grébert et al., 2018). Thus, this process may confer an important adaptive advantage to cells displaying PT 3d with regard to the ones with a fixed pigmentation. In the same study, Grébert and collaborators (2018) also showed that the two genetically distinct types of chromatic acclimaters (PTs 3dA and 3dB; Humily et al., 2013) are equally abundant and occupy complementary niches in the field. However, the reasons for the prevalence of CA4 process in natural populations of *Synechococcus* remain obscure. In this context, the objective of this work performed in the framework of the ANR project EFFICACY, has been to better characterize chromatic acclimaters (and particularly PT 3dB) at three different organization scales (gene, cell and population), corresponding to the three following axes.

First axis: Molecular characterization of the function of the CA4-B genomic island genes. The capacity of *Synechococcus* cells to perform CA4 is clearly associated with the presence of a small genomic island, which exists in two configurations: CA4-A and CA4-B (Humily et al., 2013). While CA4-A has been well studied in the PT 3dA model strain RS9916 (Shukla et al., 2012; Sanfilippo et al., 2016, 2019b), the difference between the two types of CA4, notably at the regulation level, is still unclear. The main goal of this first part was thus to determine, using a mutagenesis approach, the function of the yet-uncharacterized genes of the CA4-B genomic island in order to better understand what differentiates the two CA4 types from a functional point of view.

Second axis: Comparative analysis of the fitness of different marine Synechococcus pigment types. The two types of chromatic acclimaters (PTs 3dA and 3dB) have so far been considered as phenotypically equivalent (Humily et al., 2013). In order to unveil possible subtle differences between the two CA4 processes, comparative physiology experiments were performed with several representatives of both PTs in various conditions of light quantity and quality, as well as temperature. Furthermore, only a couple of studies have so

far focused on the adaptive value of chromatic acclimation, and this only in freshwater strains displaying CA3, a process that consists in adjusting the phycobiliprotein composition of PBS rods between red and green light (Stomp et al., 2004, 2008; Luimstra et al., 2020). To tackle this question, mono- and co-cultures of the three major *Synechococcus* PTs in the global ocean (3a, 3c and 3d) were conducted in order to: (i) assess their respective fitness according to the ambient light quality (blue vs. green) and quantity (low vs. high); and (ii) determine whether CA4 confers a fitness advantage over fixed pigmentation, and under which light conditions.

***Third axis: Study of the temporal and spatial dynamics of different pigment types of marine* Synechococcus.** Analysis of the metagenomic data from the *Tara* Oceans expedition has provided crucial knowledge on the spatial distribution and relative abundance of the different PTs of marine *Synechococcus* at a global scale (Grébert et al., 2018). However, their temporal variability has not been studied so far. The objective of this third axis has therefore been to study the seasonal variations of the different PTs of marine *Synechococcus* over two successive years at two stations with contrasting oceanic regimes: BOUSSOLE (Mediterranean Sea) and SOMLIT-Astan (English Channel). Metagenomic analyses and water color measurements have been performed in addition to more classical physico-chemical parameters in order to: (i) identify the seasonal cycles of the different genotypes and PTs; and (ii) highlight the abiotic factors driving the variations in relative abundance of the different PTs at both long-term stations.

Chapter 1:

Molecular approaches to better characterize type IV chromatic acclimation

I. Context of the work

Type IV chromatic acclimation (CA4) was shown to be correlated with the presence of a small genomic island encountered in two genetically distinct configurations (CA4-A and B; Humily et al., 2013). At the beginning of my thesis, three out of five genes of the CA4-A island were characterized in the PT 3dA model strain *Synechococcus* sp. RS9916. These included the lyase-isomerase gene *mpeZ* (Shukla et al., 2012) and the two regulatory genes *fciA and fciB* (Sanfilippo et al., 2016, 2019b). Another putative viral-like regulator (*fciC*) and a short gene encoding an unknown protein (*unk10*) remained to be characterized. In contrast, very little was known about the CA4-B version of this island. In this context, the main objective of this chapter was to characterize the function of the four genes of the CA4-B genomic island (*fciA*, *fciB*, *unk10* and *mpeW*) with the goal to better understand the functional differences between the two types of type IV chromatic acclimaters.

II. Summary and contribution to studies on the characterization of PBS genes

At the very beginning of my thesis, I had the chance to be involved in the completion of a study by Grébert and co-workers (2021). This study aimed to characterize the function of two genes involved in the CA4-B process in *Synechococcus* PT 3dB strain A15-62: *mpeW,* present in the CA4-B island and encoding a PEB-lyase, and *mpeQ,* present in the main PBS rod region and encoding a lyase-isomerase. The two enzymes were shown to compete for binding either a PEB or a PUB at Cys-83 of the PE-II α-subunit in green and blue light, respectively (see Chapter 1 § III). More precisely, my contribution to this paper has been, first, to prepare large volumes (10 L) of *Synechococcus* sp. strain WH7803, then extract its phycobilisomes for further HPLC separation of PE-II subunits at the University of New Orleans followed by mass spectrometry analysis at the Indiana University. The goal here was to determine which chromophores were bound to the PE-II α-subunit. I also investigated the differential expression of *mpeW* and *mpeQ* genes in A15-62 cultures acclimated to blue and green light by real time RT-PCR.

As concerns the functional characterization of *fciA*, *fciB* and *unk10* genes, I used a CRISPR-Cpf1 genome editing system to tentatively generate single (*fciA*$^-$ and *unk10*$^-$) and double

(*fciAB*$^-$) mutants of A15-62 (see Chapter 1 § IV). This technique was developed for marine *Synechococcus* by Prof. David Kehoe (unpublished data) and then successfully applied by Morgane Ratin (research engineer in our team) to generate a *fciB*$^-$ mutant in A15-62 prior to the start of my PhD thesis. I participated in the preliminary characterization of this mutant, as well as designed and produced constructs to knock out *fciA*, *fciAB* or *unk10* genes with Morgane Ratin's help. Following this step, I used the constructs to transform *E. coli* MC1061, performed the conjugation between *E. coli* competent cells and *Synechococcus* A15-62, picked individual colonies and finally tested them for the presence of potential mutants. Unfortunately, despite repeated attempts, we could not get any additional mutants before the submission of the present thesis manuscript.

Finally, I also contributed to a study on the functional characterization of another PBS gene led by Lyndsay A. Carrigee (Carrigee et al., 2022; see Annex 1). This study specifically dealt with the characterization of the enzymatic activity of the E/F-type lyase MpeV in *Synechococcus* sp. WH8020. Indeed, a previous study from this group (Carrigee et al., 2021) had shown that, in the model PT 3dA strain RS9916, MpeV was acting as a lyase-isomerase that doubly linked PUB at Cys-50,61 of the β-subunits of both PE-I (CpeB) and PE-II (MpeB). However, this result was at odds with a previous study on another PT 3dA strain (WH8020; Ong and Glazer, 1991), since these authors had shown that the chromophore bound at Cys-50,61 of WH8020 CpeB was a PEB, and not a PUB. In the 2022 study, we confirmed Ong and Glazer's finding in WH8020 and demonstrated that the isomerase activity of MpeV was hindered by the presence of a histidine at CpeB-141 in WH8020, instead of a leucine at the same position in RS9916. Yet, MpeV was still acting as a lyase-isomerase on WH8020 MpeB, which like RS9916 MpeB possesses a leucine at position 141 and has a PUB attached at Cys-50,61. A mechanism for the role of H141 in blocking isomerization due to steric hindrance was proposed using a structural model. My contribution to this work was to acclimate the WH8020 strain to blue and green light in large volume (10 L), then to extract the PBS for further HPLC separation of PE subunits and mass spectrometry analysis, as described above.

III. Functional characterization of the MpeW/MpeQ dual enzyme system involved in the CA4-B process (Grébert et al., 2021)

Molecular bases of an alternative dual-enzyme system for light color acclimation of marine *Synechococcus* cyanobacteria

Théophile Grébert[a,1,2], Adam A. Nguyen[b,c,1], Suman Pokhrel[b], Kes Lynn Joseph[b], Morgane Ratin[a], Louison Dufour[a], Bo Chen[d], Allissa M. Haney[d], Jonathan A. Karty[e], Jonathan C. Trinidad[e], Laurence Garczarek[a], Wendy M. Schluchter[b], David M. Kehoe[d], and Frédéric Partensky[a,3]

[a]Ecology of Marine Plankton Team, UMR 7144 Adaptation and Diversity in the Marine Environment, Station Biologique, Sorbonne Université, CNRS, 29680 Roscoff, France; [b]Department of Biological Sciences, University of New Orleans, New Orleans, LA 70148; [c]Department of Chemistry, University of New Orleans, New Orleans, LA 70148; [d]Department of Biology, Indiana University, Bloomington, IN 47405; and [e]Department of Chemistry, Indiana University, Bloomington, IN 47405

Edited by Edward F. DeLong, University of Hawaii at Manoa, Honolulu, HI, and approved January 11, 2021 (received for review September 20, 2020)

Marine *Synechococcus* cyanobacteria owe their ubiquity in part to the wide pigment diversity of their light-harvesting complexes. In open ocean waters, cells predominantly possess sophisticated antennae with rods composed of phycocyanin and two types of phycoerythrins (PEI and PEII). Some strains are specialized for harvesting either green or blue light, while others can dynamically modify their light absorption spectrum to match the dominant ambient color. This process, called type IV chromatic acclimation (CA4), has been linked to the presence of a small genomic island occurring in two configurations (CA4-A and CA4-B). While the CA4-A process has been partially characterized, the CA4-B process has remained an enigma. Here we characterize the function of two members of the phycobilin lyase E/F clan, MpeW and MpeQ, in *Synechococcus* sp. strain A15-62 and demonstrate their critical role in CA4-B. While MpeW, encoded in the CA4-B island and up-regulated in green light, attaches the green light-absorbing chromophore phycoerythrobilin to cysteine-83 of the PEII α-subunit in green light, MpeQ binds phycoerythrobilin and isomerizes it into the blue light-absorbing phycourobilin at the same site in blue light, reversing the relationship of MpeZ and MpeY in the CA4-A strain RS9916. Our data thus reveal key molecular differences between the two types of chromatic acclimaters, both highly abundant but occupying distinct complementary ecological niches in the ocean. They also support an evolutionary scenario whereby CA4-B island acquisition allowed former blue light specialists to become chromatic acclimaters, while former green light specialists would have acquired this capacity by gaining a CA4-A island.

light regulation | marine cyanobacteria | photosynthesis | phycobilin lyase | phycoerythrin

Marine *Synechococcus* are the second most abundant phototrophs in the oceans, significantly contributing to oceanic primary production and carbon cycling (1, 2). These picocyanobacteria occupy the upper sunlit layer of marine waters from the equator up to 80 °N (3, 4) and exhibit a broad range of photosynthetic pigments, allowing them to optimally exploit a large variety of light environments, from particle-loaded estuaries to the optically clear open ocean waters (5). This pigment diversity arises from a large flexibility in the composition of their light-harvesting antennae, called phycobilisomes (PBS). Structurally, these complexes comprise a central core from which radiate six or eight rods made of α/β heterodimers of phycobiliproteins that first assemble into $(\alpha\beta)_6$ hexamers and then stack into rods with the assistance of linker proteins (6). In the open ocean, virtually all *Synechococcus* cells belong to pigment type 3 (PT 3), in which PBS rods are made of the three phycobiliproteins, phycocyanin (PC), phycoerythrin-I (PEI), and phycoerythrin-II (PEII), which can covalently bind three chromophore types: the red light-absorbing phycocyanobilin (A_{max} = 650 nm), the green light (GL)-absorbing phycoerythrobilin (PEB; A_{max} = 550 nm), and the blue light (BL)-absorbing phycourobilin [PUB; A_{max} = 495 nm (7, 8)]. Different pigment subtypes have been defined within PT 3, based on the relative ratio of fluorescence excitation at 495 and 545 nm with emission at 580 nm ($Exc_{495:545}$), a proxy for their molar PUB:PEB ratio. This ratio is constitutively low ($Exc_{495:545} < 0.6$), intermediate ($0.6 \leq Exc_{495:545} < 1.6$), or high ($Exc_{495:545} \geq 1.6$) in PT 3a, 3b, and 3c, respectively (5, 9). Furthermore, in PT 3d strains, which appear to make up nearly half of the PT 3 population globally (9), the PUB:PEB ratio can reversibly vary with ambient light color, a process called type IV chromatic acclimation (CA4) that allows cells to optimally absorb either GL or BL, depending on the ambient ratio of these light colors (10, 11). While most genes coding for PBS rod components are localized in a large genomic region, called the PBS region (5), strains capable of CA4 additionally possess a small genomic island existing in one of two distinct configurations

Significance

Of all cyanobacteria on Earth, marine *Synechococcus* are those displaying the greatest pigment diversity. The most sophisticated pigment type is cells able to reversibly modify their color by a phenomenon called type IV chromatic acclimation or CA4. Two genetically distinct CA4 types (CA4-A and CA4-B) have evolved in different lineages. Together, they represent almost half of all *Synechococcus* cells in oceanic areas and are equally abundant but occupy complementary ecological niches. While the molecular mechanism of CA4-A has recently started to be deciphered, the CA4-B mechanism was so far uncharacterized. Here, by unveiling this mechanism and demonstrating its singularity relative to CA4-A, we provide highlights on the evolutionary history of *Synechococcus* acclimation to light color in the oceans.

Author contributions: T.G., L.G., W.M.S., D.M.K., and F.P. designed research; T.G., A.A.N., S.P., K.L.J., M.R., L.D., B.C., J.A.K., and J.C.T. performed research; S.P., A.M.H., J.C.T., and D.M.K. contributed new reagents/analytic tools; T.G., A.A.N., S.P., K.L.J., M.R., L.D., J.A.K., J.C.T., L.G., W.M.S., and F.P. analyzed data; and T.G., J.A.K., L.G., W.M.S., D.M.K., and F.P. wrote the paper.

The authors declare no competing interest.

This article is a PNAS Direct Submission.

[1]T.G. and A.A.N. contributed equally to this work.

[2]Present address: Synthetic Biology Group, Department of Microbiology, Pasteur Institute, 75015 Paris, France.

[3]To whom correspondence may be addressed. Email: frederic.partensky@sb-roscoff.fr.

This article contains supporting information online at https://www.pnas.org/lookup/suppl/doi:10.1073/pnas.2019715118/-/DCSupplemental.

Published February 24, 2021.

(12). Each contains the two regulators encoded by *fciA* and *fciB* (13) and one gene coding for a putative phycobilin lyase family member, which can be either *mpeZ* or *mpeW*, defining the two distinct genotypes CA4-A and CA4-B [the corresponding PTs are named 3dA and 3dB, respectively (12)]. Phycobilin lyases are enzymes responsible for the covalent attachment of chromophores at specific cysteine residues of phycobiliprotein subunits and are thus key players in *Synechococcus* pigmentation. Indeed, chromophore ligation takes place prior to phycobiliprotein subunit assembly, and proper phycobilin arrangement is crucial for efficient energy transfer along the rods (14). However, among the dozen (putative) phycobilin lyases encoded in marine *Synechococcus* genomes (5), only a few have been biochemically characterized. RpcG from *Synechococcus* sp. WH8102 (PT 3c) was shown to attach PEB to cysteine-84 (C84) of the α-subunit of PC and to isomerize it to PUB (15). Such dual-function enzymes are called phycobilin lyase-isomerases. More recently, the biochemical characterization of the CA4-A strain *Synechococcus* sp. RS9916 (clade IX) revealed the specific chromophore changes that occur during CA4; namely, one out of five chromophore-binding sites on PEI and two of the six sites of PEII change from PEB in GL to PUB in BL. Two enzymes implicated in CA4-A and belonging to the E/F structural clan (16) have been characterized: MpeZ is the lyase-isomerase adding PUB at C83 of the PEII α-subunit (MpeA) in BL (17), whereas its paralog MpeY is the PEB lyase acting on the same site in GL (18). While *mpeZ* was found to be expressed more highly under BL (12, 13, 17), *mpeY* is constitutively expressed whatever the ambient light color. This led to the suggestion that the cellular MpeZ:MpeY protein ratio ultimately controls the chromophore bound at MpeA-C83 (18). By contrast, the identity and function of the corresponding enzymes in CA4-B strains were so far unknown.

Here we characterize the *mpeW* gene located in the CA4 genomic island of the CA4-B strain *Synechococcus* sp. A15-62 (subclade IIc). We show that it encodes a phycobilin lyase acting on MpeA-C83 in GL that vies with a previously unidentified lyase-isomerase (MpeQ) acting on the same cysteine position in BL. Our results highlight the key role of the diversification of the MpeY enzyme family in the adaptation of marine *Synechococcus* to different light color niches and provide insights to explain the occurrence of two mutually exclusive CA4 systems in marine *Synechococcus*.

Results

The MpeY Phycobilin Lyase Family Is Polyphyletic. Based on its conserved genomic position in the PEII-specific subregion of the PBS region (Fig. 1*A*) and on sequence similarity, the gene located immediately upstream of the *mpeBA* operon (encoding the two subunits of PEII) was previously named *mpeY* in all *Synechococcus* strains containing PEII (5, 9, 18). However, the phylogenetic analysis of the different members of this family revealed that *mpeY* is in fact polyphyletic, with three distinct clusters, each corresponding to a different pigment subtype (Fig. 1*C*). PT 3a strains (i.e., GL specialists) possess the MpeY^{3a} variant encoded by the PT 3a-specific *mpeY* allele, and PT 3dA strains contain the MpeY^{3dA} variant recently characterized in the PT 3dA strain *Synechococcus* sp. RS9916 as a PEB lyase acting on C83 of the α-PEII subunit (MpeA) (18), while a third variant is found in PT 3c (i.e., BL specialists) and 3dB strains. Strikingly, sequences from the latter two pigment subtypes were intermingled in the phylogenetic tree, as was previously observed for *mpeBA* or *cpeBA* phylogenies, indicating that PBS genes of these pigment subtypes are phylogenetically too close to be distinguishable (9, 12). Tandem mass spectrometry (MS/MS) analysis of the chromophorylation of MpeA from the PT 3a strain *Synechococcus* sp. WH7803 revealed that MpeA-C83 binds a PEB, while PUB is bound to both MpeA-C75 and 140 (*SI Appendix*, Fig. S1). This suggests that MpeY^{3a} must have a PEB lyase function, like MpeY^{3dA}. In contrast, as demonstrated below, the function of the MpeY-like protein found in PT 3c and 3dB differs from that of both MpeY^{3a} and MpeY^{3dA}, and we therefore renamed it "MpeQ" in the tree (Fig. 1*C*) and in the text hereafter. The protein sequences of MpeW, MpeZ, MpeQ, MpeY^{3a}, and MpeY^{3dA} have on average 34 to 58% amino acid identity over their whole length, compared to an average of 70 to 82% identity among members of each of these subfamilies (Fig. 1*B* and Dataset S1).

Chromophore Changes Occurring during CA4-B Are the Same as Those Occurring in the CA4-A Process. Although the Exc$_{495:545}$ ratios of CA4-A and CA4-B strains have previously been shown to be similar in both BL (1.6 to 1.7) and GL (0.6 to 0.7) (12), it was unclear what specific changes in chromophorylation were taking place during the CA4 process in CA4-B strains. To investigate this, PBS from wild-type (WT) *Synechococcus* sp. A15-62 grown under BL or GL were purified, and PEI and PEII subunits were separated by high performance liquid chromatography (HPLC). Absorption spectra of individual subunits (Fig. 2 and *SI Appendix*, Fig. S2) suggested that the PUB:PEB molar ratio changed between GL and BL from 0:2 to 1:1 for the α-PEI subunit (CpeA) and from 1:2 to 3:0 for the α-PEII subunit (MpeA), while the chromophorylation of β-PEI (CpeB) and β-PEII (MpeB) subunits did not vary with light color (1:2 in both conditions; Table 1). The chromophorylation of the two α-subunits was further characterized by MS/MS, confirming the above-mentioned molar ratios and demonstrating that the three cysteine positions that change chromophorylation (from PEB in GL to PUB in BL) are MpeA-C83 and C140 and CpeA-C139 (Table 1, Dataset S2, and *SI Appendix*, Figs. S3–S5), i.e., the same chromophores and positions as in the CA4-A strain RS9916 (17).

MpeW and MpeQ Are Required for PEB and PUB Attachment on MpeA, Respectively. Since the biochemical characterization of MpeZ and MpeY^{3dA} in RS9916 showed that they were a PEB lyase-isomerase and a PEB lyase, respectively, both acting on MpeA-C83 (17, 18), we hypothesized that the corresponding enzymes in CA4-B strains, MpeW and MpeQ (Fig. 1*A*), could be a PEB lyase and PEB lyase-isomerase, respectively, both also acting on MpeA. To test this hypothesis, we created *mpeW*$^-$ and *mpeQ*$^-$ insertion mutants in the CA4-B strain A15-62. Comparison of fluorescence excitation spectra revealed that for GL-grown cultures, Exc$_{495:545}$ was increased in the *mpeW*$^-$ mutant compared to the WT, whereas no difference was observed under BL (Fig. 3 *A* and *B*). Conversely, no difference could be seen between Exc$_{495:545}$ of *mpeQ*$^-$ mutants and WT under GL, while the Exc$_{495:545}$ ratio dramatically decreased in BL-grown *mpeQ*$^-$ mutants compared to WT (Fig. 3 *C* and *D*). Both mutants still exhibited some levels of chromatic acclimation since the Exc$_{495:545}$ ratio changed from 1.17 ± 0.01 in GL to 1.68 ± 0.07 in BL for *mpeW*$^-$ and from 0.74 ± 0.02 in GL to 0.91 ± 0.01 in BL for *mpeQ*$^-$, as compared to 0.74 ± 0.01 in GL and 1.72 ± 0.09 in BL for WT cells (all data are average ± SE; $n = 2$). Based on these results, we hypothesized that 1) MpeW is required for PEB attachment, while MpeQ is required for PEB attachment and isomerization to PUB, and 2) both are acting on one or possibly two chromophore binding cysteine(s) but seemingly not all three sites that change chromophorylation during the CA4 process. The CA4 phenotype of both mutants could be restored with the reintroduction of WT *mpeW* or *mpeQ* genes in *trans* (Fig. 3 and *SI Appendix*, Fig. S6).

Since in the CA4-A strain RS9916, the transcript levels of the lyase-isomerase *mpeZ* were found to be about 32-fold higher in BL than GL (12, 13), while the *mpeY* lyase levels were similar in both colors (18), we also checked the light color response of the counterparts *mpeQ* and *mpeW* genes in the CA4-B strain A15-62. Real-time PCR expression data showed that while *mpeQ* is not

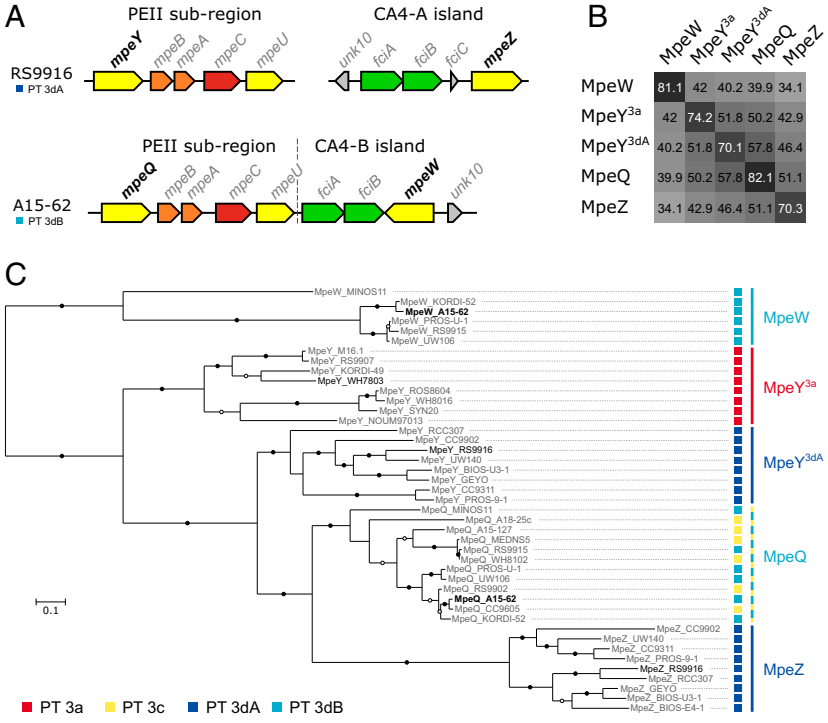

Fig. 1. Phylogeny and similarity of the different members of the MpeQWYZ phycobilin lyase enzyme family and genomic organization of the corresponding genes. (*A*) Comparison of the genomic regions involved in CA4-A and CA4-B processes. The CA4-A genomic island and the PEII subregion of the PBS genomic region are located at two different loci on the chromosome of *Synechococcus* strain RS9916 (*Top*), whereas in strain A15-62 the CA4-B genomic island is located in the middle of the PBS genomic region, immediately downstream the PEII subregion (*Bottom*). The two genes characterized in the present study (*mpeW* and *mpeQ*) are shown as underlined black bold letters, their functional homologs in the CA4-A strain RS9916 (*mpeY* and *mpeZ*) in black bold letters, and other genes in gray. (*B*) Mean pairwise percentage of identity between the protein sequences of MpeW, MpeQ, MpeZ, and MpeY^{3a} and MpeY^{3dA} (encoded by the two *mpeY* alleles), calculated based on full-length alignments. (*C*) Maximum likelihood phylogeny (protein sequences, LG + I + G + F model) of the MpeQWYZ enzyme family. CpeY sequences were used as outgroup to root the tree. Nodes with bootstrap support >70 and >90% are indicated by empty and filled black dots, respectively. Sequences of A15-62 used in this study are highlighted in bold black letters, and other sequences discussed in the text are shown in black, while all other sequences are shown in gray.

significantly differentially regulated between GL and BL, *mpeW* is 44.26 ± 1.34-fold (average ± SD; $n = 3$) more highly expressed in GL than BL (*SI Appendix*, Fig. S7).

***mpeW*$^-$ and *mpeQ*$^-$ Mutants Differ from the WT by the Chromophore Attached to MpeA-C83 in GL and BL, Respectively.** To identify the biochemical changes responsible for the differences in whole-cell fluorescence, PBS were purified from the *mpeW*$^-$ and *mpeQ*$^-$ mutants and PEI and PEII subunits separated by HPLC. Absorption spectra only differed between WT and mutants for MpeA (Fig. 2 and *SI Appendix*, Fig. S2). Indeed, compared to the WT, MpeA from the *mpeW*$^-$ mutant had a lower PEB absorption peak at 550 nm in GL (Fig. 2*A*), whereas MpeA from the *mpeQ*$^-$ mutant exhibited a PEB peak at 550 nm in BL not seen in WT cells (Fig. 2*D*). This confirmed that both MpeW and MpeQ are involved in MpeA chromophorylation, with MpeW being responsible for PEB attachment and MpeQ for PEB attachment and simultaneous isomerization to PUB. MS/MS of CpeA and MpeA, the two PE subunits that change chromophorylation during CA4 (see above), further showed that the *mpeW*$^-$ mutant mainly differed from the WT by having a PUB instead of a PEB at MpeA-C83 in GL, whereas the *mpeQ*$^-$ mutant differed from the WT by having a PEB instead of a PUB at MpeA-C83 in BL (Table 1 and *SI Appendix*, Figs. S8 and S9). Surprisingly, both WT and mutants displayed a mixed chromophorylation at MpeA-C140 in GL. The slightly higher proportion of PUB in mutants compared to the WT (35 and 15%, respectively; Table 1) could suggest that MpeQ and MpeW might also have a role in the chromophorylation changes occurring during CA4 at this position. If true, this effect is likely non-physiological since no chromophorylation of MpeA-C140 could be detected in our recombinant assays (see below).

Recombinant MpeW and MpeQ Are Both Acting on MpeA-C83. Activities of MpeW and MpeQ were tested using a heterologous plasmid coexpression system in *Escherichia coli*. Four different hexahistidine-tagged (HT-) versions of recombinant MpeA were used as substrates in the coexpressions: A15-62 and RS9916 HT-MpeA; a mutant RS9916 MpeA with C83 replaced by alanine, RS9916 HT-MpeA(C83A); and a mutant RS9916 MpeA with C75 and C140 each replaced with alanine, RS9916 HT-MpeA(C75A, C140A). RS9916 HT-MpeB and RS9916 HT-CpeA were also used to further test the substrate preference. These phycobiliprotein subunits were coexpressed with PEB synthesis enzymes and with either MpeW or MpeQ and purified, and their spectral properties were analyzed. The negative control (A15-62 HT-MpeA expressed with PEB synthesis enzymes but without any lyase) showed no detectable fluorescence (Fig. 4 *A* and *C*). The coexpressions of MpeA (either from A15-62 or RS9916) and either MpeW or MpeQ confirmed that the former attached PEB while the latter attached PUB to both versions of MpeA (Fig. 4 *A*–*D*), while coexpressions of MpeW or MpeQ and either MpeB or CpeA demonstrated that neither had lyase activity on these two proteins. Coexpressions of MpeW and mutants RS9916 MpeA, in which cysteine residues are replaced by alanine [RS9916 MpeA (C83A) or (C75A and C140A)], further

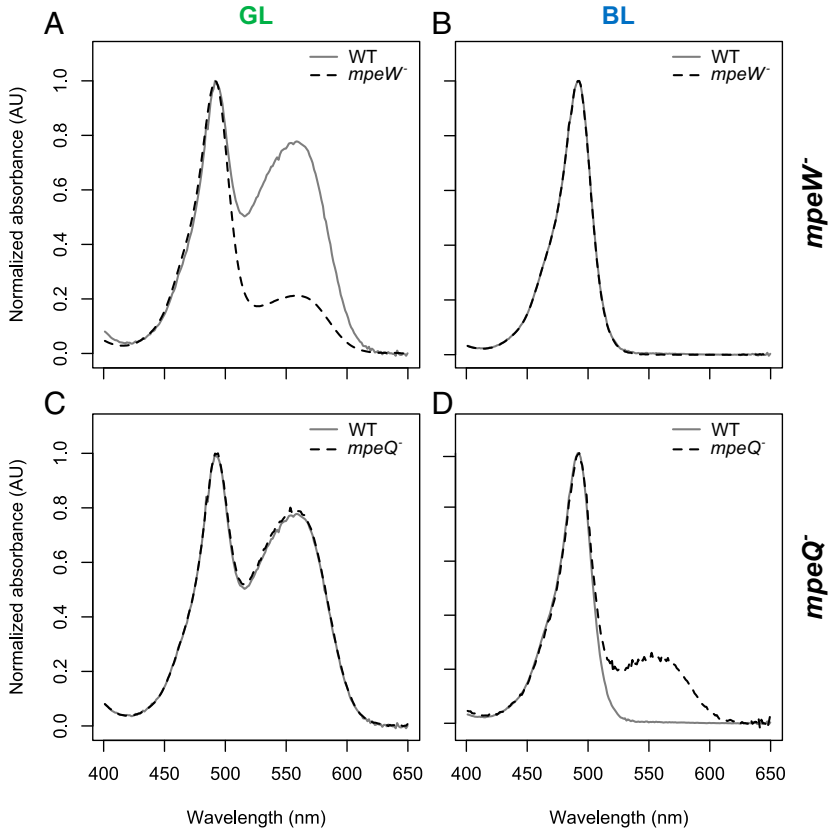

Fig. 2. Absorbance spectra of HPLC-purified phycoerythrin II α-subunit (MpeA) for WT *Synechococcus* sp. A15-62, *mpeW* inactivation mutant (*mpeW*$^{-}$), and *mpeQ* inactivation mutant (*mpeQ*$^{-}$) grown under GL or BL. (*A* and *C*) WT or mutant cells grown in GL. (*B* and *D*) WT or mutant cells grown in BL. See *SI Appendix*, Fig. S2, for absorbance spectra of the other PEI and PEII subunits.

showed that PEB was covalently bound to MpeA-C83 (Fig. 4 *A* and *B*). The same system was used to demonstrate that MpeQ also acted specifically on MpeA-C83 by ligating PEB and isomerizing it to PUB (Fig. 4 *C* and *D*). The minor fluorescence emission peak at ∼600 nm in the *mpeW* system (Fig. 4*A*) is likely coming from PEB that is not held in a stretched conformation.

Collectively, these results indicate that in the CA4-B process, MpeW is the lyase responsible for the attachment of PEB to MpeA-C83 in GL while MpeQ is the lyase-isomerase responsible for the attachment of PEB and its isomerization to PUB at MpeA-C83 in BL.

Discussion

With six phycobilin binding sites per α−β monomer, PEII is the most pigmented phycobiliprotein known so far in the *Cyanobacteria* phylum (7, 19), and the ecological success of marine *Synechococcus* spp. is likely tied with this biological innovation, as evidenced by the large predominance of PEII-containing cells (so-called PT 3) in open waters of the world ocean (9). Gain of PEII, which is thought to have occurred by duplication and divergence from the corresponding PEI encoding genes (20), also implied the concomitant acquisition of enzymes necessary for its proper chromophorylation (5). In this context, the diversification of the MpeQWYZ enzyme family, which belongs to the E/F structural clan (16) and likely derived by duplication and divergence from a *cpeY*-like gene ancestor (Fig. 1) (21, 22), has been pivotal for the development of CA4, the only example among the six chromatic acclimation forms known so far in *Cyanobacteria* to involve color-induced changes only in chromophore content (23). The fact that CA4 seemingly appeared twice during the evolution of marine *Synechococcus*, with CA4-A and CA4-B occurring in most cases in phylogenetically distant lineages and colonizing different light niches (Fig. 1) (9, 12), is particularly intriguing. Although the molecular mechanism underpinning CA4-A is starting to be understood (13, 17, 18), CA4-B was thus far biochemically uncharacterized, and the differences between the two CA4 systems remained unclear. Here we show that CA4-B is mechanistically similar to CA4-A since it also involves two enzymes that vie for the same binding site on α-PEII subunit (MpeA) and whose gene expressions are differentially regulated by the ambient light color (*SI Appendix*, Fig. S10). We demonstrate that MpeW is a phycobilin lyase attaching PEB at MpeA-C83 in GL, whereas MpeQ is a phycobilin lyase-isomerase binding PUB at the same position in BL. Intriguingly, the CA4-B-specific lyase/lyase-isomerase MpeW/Q pair exhibits a reversed activity compared to its counterpart pair MpeZ/Y in the CA4-A strain RS9916 (*SI Appendix*, Fig. S10). Indeed, the lyase-isomerase *mpeZ* was found to be up-regulated under BL, while in the CA4-B process the lyase *mpeW* is up-regulated under GL. In both cases, expression of the gene coding for the second enzyme of the couple is not differentially expressed between GL and BL (12, 13, 17). Our data therefore shed light on a fascinating dual-enzyme coevolution process that explains the cooccurrence of two mutually exclusive CA4 types in the marine *Synechococcus* radiation. Our data provide strong evidence for the previously proposed hypothesis (23, 24) that the basal state for CA4-A strains (i.e., in absence of CA4) corresponds to a GL specialist phenotype (low PUB:PEB ratio) and that CA4 confers

Table 1. Percentage of PUB chromophores, expressed as a PUB/(PEB+PUB) ratio, found at the different cysteinyl sites of the PEI and PEII α- (CpeA and MpeA) and β-subunits (CpeB and MpeB) in *Synechococcus* sp. A15-62 WT cells and *mpeW*⁻ and *mpeQ*⁻ mutants grown under GL and BL

PBP	Subunit	Cysteine position	%PUB attached in GL			%PUB attached in BL		
			WT	*mpeW*⁻	*mpeQ*⁻	WT	*mpeW*⁻	*mpeQ*⁻
PEII	MpeA	75	100	100	100	100	100	100
		83	**9**	**99**	**2**	**100**	**99**	**14**
		140	**15**	**35**	**36**	**93**	**99**	**99**
PEII	MpeB	50, 61	100	ND	ND	100	ND	ND
		82	0	ND	ND	0	ND	ND
		165	0	ND	ND	0	ND	ND
PEI	CpeA	82	0	0	0	0	0	0
		139	**0**	**100**	**21**	**100**	**98**	**43**
PEI	CpeB	50, 61	100	ND	ND	100	ND	ND
		82	0	ND	ND	0	ND	ND
		159	0	ND	ND	0	ND	ND

Underlined values indicate that the chromophorylation was confirmed by LC-MS/MS. Bold indicates that the chromophore is expected to change during the CA4 process. At some sites, the mass spectrometry analysis detected a mix of PUB and PEB, and the percentage of PUB (%PUB) is indicated. ND, not determined; PBP, phycobiliprotein.

these cells the ability to change their spectral properties upon BL illumination, by inducing the expression of the phycobilin lyase-isomerase MpeZ. Conversely, the basal state for CA4-B strains would correspond to a BL specialist phenotype (high PUB:PEB ratio), CA4 providing these cells the ability to acclimate to GL by inducing the synthesis of the PEB lyase MpeW. Thus, in both cases, CA4 appears to be a plug-and-play mechanism that adds on top of the existing basal chromophorylation. This view is further supported by the gathering into a small dedicated genomic island of genes necessary for CA4, including the regulators *fciA* and *fciB* and one phycobilin lyase (either *mpeZ* or *mpeW*; Fig. 1*A*). Furthermore, the absence of any allelic difference between PBS genes of PT 3c and 3dB strains (Fig. 1*C*; see also ref. 9) might suggest that the CA4-B island is more readily transferred between *Synechococcus* strains through horizontal gene transfer than is the CA4-A island. Surprisingly, however, the latter displays several typical genomic island features, including a biased GC content compared to the surrounding genomic context and presence in the vicinity of the island of hotspots for DNA recombination such as tRNA or *psbA* genes, which are absent in the case of the CA4-B island (12, 17). So, the mechanism by which a CA4-B island could be transferred from a PT 3dB strain to a BL specialist (PT 3c) and the frequency of such transfers remain unclear.

It is also interesting to note that as previously observed for *mpeZ*⁻ and *mpeY*$^{3dA-}$ mutants in the CA4-A strain RS9916 (17, 18), both *mpeW*⁻ and *mpeQ*⁻ CA4-B mutants still showed some degree of chromatic acclimation, variations of the $Exc_{495:545}$ ratio observed in the *mpeW*⁻ and *mpeQ*⁻ mutants representing about 51 and 18% of that occurring in the WT, respectively (Fig. 2 *C* and *D*). In both lyase-isomerase mutants (*mpeZ*⁻ and *mpeQ*⁻), $Exc_{495:545}$ is strongly decreased in BL (about 0.8) compared to the WT (1.5 to 1.6) but higher than in GL (0.6 to 0.7 for both mutants and WT; Fig. 2 *C* and *D* and ref. 17). Similarly, both lyase mutants (*mpeY*⁻ and *mpeW*⁻) had an increased $Exc_{495:545}$ in GL relative to the WT (about 1.1 vs. 0.6) but still lower than in BL (1.5 to 1.6 for both; Fig. 2 *A* and *B* and ref. 18). This suggests that other genes are involved in CA4. In the absence of any obvious other CA4-specific phycobilin lyase, an interesting candidate could be the conserved hypothetical gene *unk10*, which is present in both versions of the CA4 genomic island and strongly overexpressed in BL in the CA4-A strain RS9916 (12, 13, 17, 23). Future characterization of this unknown gene as well as the putative regulator *fciC*, present in CA4-A but not CA4-B islands (Fig. 1*A* and *SI Appendix*, Fig. S10), will help unravel the different regulatory mechanisms behind this remarkable dual light color acclimation process, which strongly impact the ecology and photophysiology of a key component of marine phytoplankton communities.

Materials and Methods

Phylogenetic Analyses. Sequences used in this study (MpeQ, W, Y, and Z) can be found in Dataset S1. Briefly, MpeQ, W, Y, and Z protein sequences were aligned using the multiple sequence alignment program MAFFT 7.299b L-INS-I (25). Pairwise identity between sequences was computed from this alignment using BioPython. Best model for phylogenetic reconstruction corresponded to LG aa substitution model with empirical base frequencies (F), gamma model of rate heterogeneity (G), and invariable sites (I) as selected with ProtTest 3.4.1 (26). Tree search was conducted using RAxML (Randomized Axelerated Maximum Likelihood) 8.2.9 (27) without the rapid hill-climbing heuristic (-f o). One hundred tree searches were conducted starting from randomized maximum parsimony tree (default), and 100 searches were conducted starting from fully random trees (-d). Best tree was selected, and 250 bootstraps performed. Tree was plotted using ETE3 (28). The same procedure was used to generate a tree with CpeY sequences to root the tree represented in Fig. 1*C*.

Strains and Growth Conditions. *Synechococcus* strain A15-62 was obtained from the Roscoff Culture Collection (http://roscoff-culture-collection.org; RCC strain 2374). It was originally isolated near Cape Verde (Atlantic Ocean) from 30 m depth (29). Both WT and mutant strains were routinely grown at 22 °C in PCR-S11 (30) in polystyrene flasks (CytoOne, StarLab) at ca. 25 μmol quanta m^{-2} s^{-1} white light. A15-62 mutants were maintained with 50 μg mL^{-1} kanamycin. Prior to whole-cell absorption and fluorescence measurements as well as to PBS isolation and separation of phycobiliproteins, WT and mutant strains were acclimated for at least two weeks at 20 μE m^{-2} s^{-1} BL or GL provided by LED ramps (Luxeon Rebel LED LXML-PB01-0040 and LXML-PM01-0100, respectively; Alpheus).

Fluorescence Measurements. Spectral properties of WT and mutant strains were measured using a LS-50B spectrofluorimeter (Perkin-Elmer). Fluorescence excitation was monitored from 420 to 560 nm (0.5-nm steps) with emission monitored at 580 nm.

Quantitative PCR Analysis of *mpeW* and *mpeQ* Gene Expression. The expression levels of *mpeQ* and *mpeW* genes were monitored by real-time qPCR, as previously described (12). Briefly, triplicate cultures of *Synechococcus* sp. strain A15-62 were acclimated at 20 μmol photons m^{-2} s^{-1} BL or GL, then cells were harvested and RNA was extracted. For *mpeW* and the control *rnpB* gene, encoding the RNA component of ribonuclease P, we used previously designed primers (12), while for *mpeQ*, gene-specific primers were designed using Primer Blast (National Center for Biotechnology Information; Dataset S3). After optimization steps, reverse transcription and qPCR analyses were performed according to ref. 12. The $2^{-\Delta\Delta CT}$ method (31) was finally used to quantify the relative fold change in mRNA levels using *rnpB* as a reference gene to normalize the relative transcript levels.

Plasmid Construction for *mpeW* and *mpeQ* Disruption and Complementation and Construction of Expression Plasmids. Primers are listed in Dataset S3, and plasmids are listed in Dataset S4. The pMUT100-A15-62-mpeW and pMUT100-A15-62-mpeQ constructs were made by PCR amplification of an 820 to 885 bp internal fragment of A15-62 *mpeW* and A15-62 *mpeQ* using the primers pairs Syn_A15-62_mpeW_126F_BamHI/999R_SphI and Syn_A15-62_mpeQ_123F_EcoRI/983R_SphI (*SI Appendix*, Fig. S11). The pMUT100 backbone was PCR-amplified using the primer pair pMUT100_1291F_SphI/5535R_BamHI (pMUT100-A15-62-mpeW) or pMUT100_1291F_SphI/5535R_EcoRI (pMUT100-A15-62-mpeQ). Vector and inserts were digested with SphI and either EcoRI or BamHI (NEB) and ligated. Conjugation between *E. coli* MC1061 containing either pMUT100-A15-62-mpeW or pMUT100-A15-62-mpeQ and *Synechococcus* A15-62 was performed as previously described (17, 32). Individual colonies were picked and tested for *mpeW* or *mpeQ* disruption by PCR amplification. For complementation, a derivative of the plasmid pRL153 (autonomously replicating in marine *Synechococcus*) was first constructed by cloning a lacZ cassette (pBClacZ) into the BamHI/EagI cloning site of pJS1 for convenient screening of *E. coli* colonies (*SI Appendix*, Fig. S11).

MICROBIOLOGY

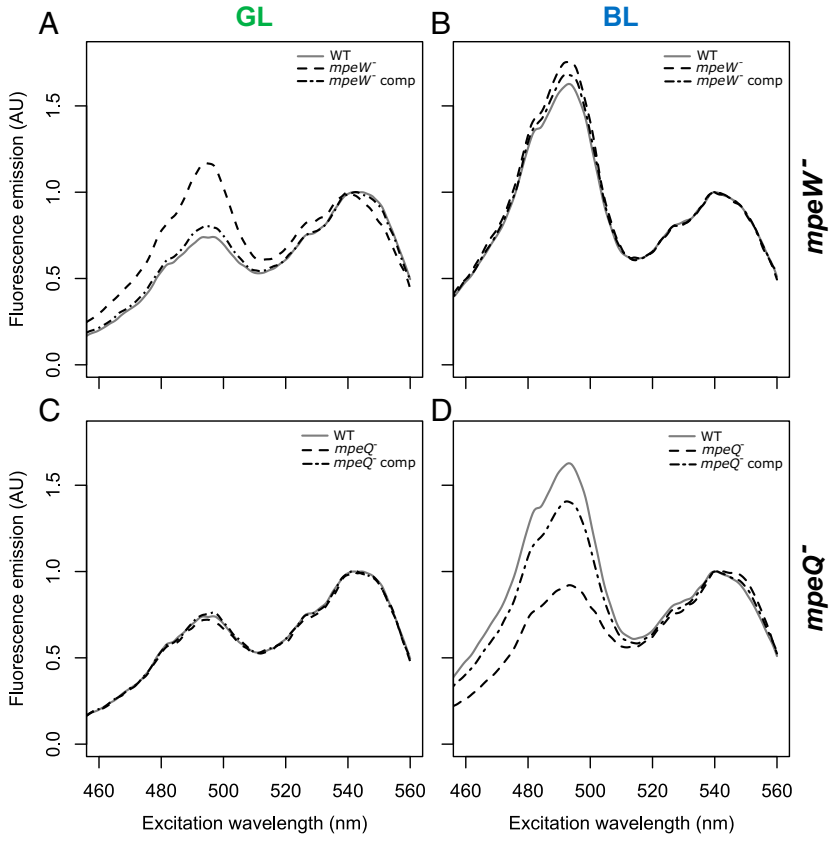

Fig. 3. Whole-cell fluorescence excitation spectra for WT *Synechococcus* sp. A15-62 and mutant strains. WT, *mpeW*⁻ mutant, and *mpeW*⁻ complemented strains grown either in (*A*) GL or (*B*) BL. WT, *mpeQ*⁻, and *mpeQ*⁻ complemented strains grown either in (*C*) GL or (*D*) BL. Fluorescence emission spectra are normalized at 545 nm. Emission was set at 580 nm. Measurements shown here were repeated twice (biological replicates). See *SI Appendix*, Fig. S6, for complementation control.

The pBClacZ-A15-62-mpeW and pBClacZ-A15-62-mpeQ constructs were made by PCR amplification of the promoter and ribosome-binding site of *mpeW* and *mpeQ*, using the primer pairs Syn_A15-62_unk10_38R_BamHI/Syn_A15-62_fciB_892F_EagI and Syn_A15-62_unk9_13R_ApaI/Syn_A15-62_mpeB_56R, respectively (*SI Appendix*, Fig. S11). PCR fragments were digested with EagI and either BamHI (*mpeW*) or ApaI (*mpeQ*) and ligated into similarly digested pBClacZ. Conjugation between *E. coli* MC1061 containing either pBClacZ-A15-62-mpeW or pBClacZ-A15-62-mpeQ and *Synechococcus* A15-62 *mpeW*⁻ or *mpeQ*⁻ was performed as previously described (17, 32). Individual colonies were picked and tested for *mpeW* or *mpeQ* complementation by PCR amplification (*SI Appendix*, Fig. S11).

PBS Isolation and Separation of Phycobiliproteins. PBS were purified as previously described (33), starting from 10 L of cultures. All steps were performed at room temperature unless specified. Briefly, cells were harvested by centrifugation, washed twice and resuspended in 0.65M phosphate buffer, and lysed twice using a French press system. Membranes and hydrophobic pigments were removed by 1 h incubation with 5% wt/vol Triton X-100 and centrifugation. The red aqueous layer was loaded onto 0.25 to 1.0 M discontinuous sucrose gradient in phosphate buffer and centrifuged overnight at 22,500 rpm (range: 42,500 to 91,300 × *g*) in a SW28 rotor (Beckman Coulter) at 22 °C, or 2 to 3 h at 49,000 rpm (198,000 × *g*) in a VTi 50 rotor (Beckman Coulter). Colored bands were collected and frozen at −20 °C until analysis (see figure 4 in ref. 34 for illustration).

Purified PBS were dialyzed in 5 mM sodium phosphate buffer, pH 7.0, with 5 mM 2-mercaptoethanol (β-Me) and then concentrated by ultrafiltration using Amicon Ultra-15 centrifugal filters (Millipore). A sample containing 500 μL of a 1:3 ratio of sample to 9 M urea (pH brought to 2.0 with HCl) was prepared prior to HPLC separation. A Waters E2695 pump (Waters Corporation) was used in conjunction with a Waters 2996 photodiode array and a Thermo-scientific BioBasic-4 HPLC column (Thermo-Scientific; 250 mm × 4.6 mm, 5 μm particle size) to separate each phycobiliprotein. The program used a flow rate of 1.5 mL min^{-1} with a gradient program starting at a 65:35 ratio of Buffer A (0.1% trifluoroacetic acid solution with 0.001 M sodium azide) to Buffer B (2:1 acetonitrile:isopropanol in 0.1% TFA with 0.001 M sodium azide). The starting conditions are 65% A:35% B. After the sample was injected, after holding for 2 min, buffer conditions were ramped to 100% B over 45 min. The samples were monitored at 280, 490, and 550 nm. Separated samples were concentrated using a vacuum centrifuge and stored in the freezer at −20 °C until ready for digestion by trypsin.

Heterologous Expression and Purification of Recombinant Proteins. For recombinant protein expression, each gene was amplified by PCR from *Synechococcus* RS9916 or A15-62 chromosomal DNA using the primers listed in Dataset S3 and cloned into plasmids as described in Dataset S4. Recombinant proteins were expressed and purified from *E. coli* BL21 (DE3) competent cells (Novagen/EMD Millipore Corp.) as previously described (35). Once at OD_{600nm}= 0.6, cultures were induced with 1 mM isopropyl 1-thio-β-D-galactopyranoside (IPTG), after which the cells were allowed to grow at 18 °C for an additional 24 h before being harvested by centrifugation. HT proteins were purified as described (36).

Protein and Bilin Analysis by Spectroscopy and Gel-Electrophoresis. Fluorescence emission and absorbance spectra were acquired on a Perkin-Elmer LS55 fluorescence spectrometer and a Lambda 35, dual-beam UV/Vis spectrometer (Perkin-Elmer) as previously described (37). Polyacrylamide gel electrophoresis (PAGE, 15% wt/vol) with sodium dodecyl sulfate (SDS) was used to analyze polypeptide samples acquired after purification of proteins as previously described (17). Zn-enhanced fluorescence of covalently attached bilins was visualized using an imaging system (Bio-Rad MP) with excitation at 460 nm (PUB detection) or 540 nm (PEB detection). Proteins in the gels were then stained by incubation in Coomassie brilliant blue G-250 overnight and destained in 10% methanol and 10% acetic acid and visualized with trans-white light (Bio-Rad MP).

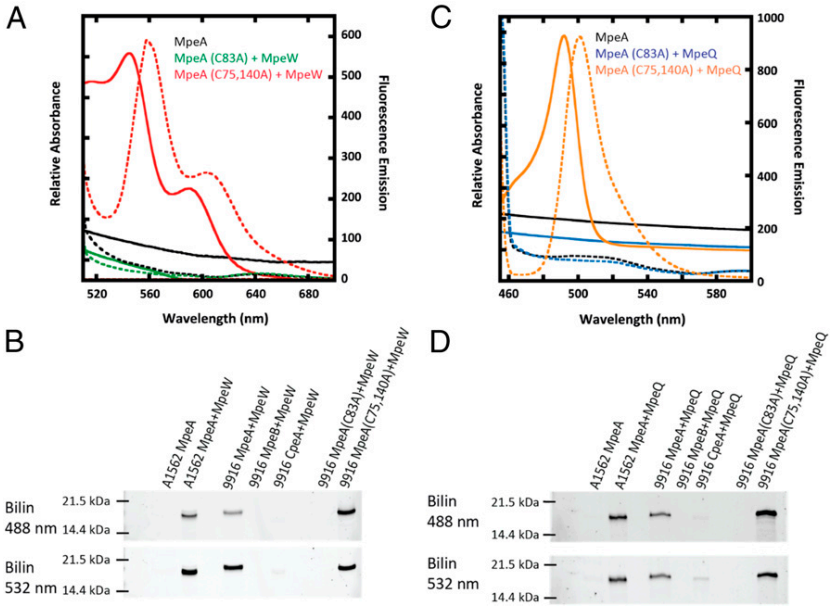

Fig. 4. Determination of the phycobiliprotein subunit and binding site specificities of the MpeW and MpeQ enzymes. Recombinant PEII α-subunit (MpeA) from *Synechococcus* sp. A15-62, PEII α- and β-subunits (MpeA and MpeB), and PEI α-subunit (CpeA) from RS9916, as well as site-mutated RS9916 MpeA in which either Cys-83 only or both Cys-75 and Cys-140 were replaced by an alanine [so-called MpeA (C83A) and MpeA (C75A and C140A), respectively], were coexpressed with either MpeQ (*A, B*) or MpeW (*C, D*) from A15-62 along with genes necessary for PEB synthesis. (*A* and *C*) Absorbance (solid lines) and fluorescence emission (dotted lines) spectra of PEB (*A*; excitation set at 490 nm) or PUB (*C*; excitation set at 440 nm) of purified recombinant WT and site-mutated MpeA from RS9916. The secondary emission peak at 610 nm in *A* likely corresponds to PEB at C83 (see text). (*B* and *D*) Zinc-enhanced fluorescence of SDS-PAGE gel showing relative PEB or PUB covalently bound to different recombinant phycoerythrin subunits under various coexpression conditions (indicated on top) for MpeW (*B*) or MpeQ (*D*). Data shown here are representative of three technical replicates.

Tryptic Digestion and Mass Spectrometry. Tryptic digestion of proteins was conducted as previously described (38). Tryptic-digested samples were analyzed using liquid chromatography (LC)-MS/MS on an Orbitrap Lumos Fusion mass spectrometer (Thermo Fisher) with an Agilent 1100 Capillary HPLC as its inlet. LC-MS/MS analysis was performed as previously described with a few modifications (13, 17). Alternatively, some samples were reanalyzed using a Thermo Easy-nLC 1000 capillary LC with the following conditions: Buffer A = 0.1% vol/vol aqueous formic acid; Buffer B = 80% vol/vol acetonitrile, 0.1% vol/vol formic acid in water. Load 2 μL with 0% B onto a 5 mm long, 0.1 mm i.d. C18 trapping column. A 0.075 mm i.d. × 150 mm long C18 analytical column led directly into the nanospray needle. The gradient was 2% B at 0 min, ramp to 7% B at 0.5 min, ramp to 50% B at 20 min, ramp to 100% B at 21 min, hold 100% B for 9 min. The trap column was reequilibrated with 12 μL of Buffer A and the analytical column with 10 μL of 2% B between each injection. Mass spectra were recorded continuously at 120,000 resolving power. Data-dependent tandem mass spectra were recorded at 30,000 resolving power with 3 s between MS1 spectra. The tandem mass spectra were processed using Thermo Proteome Discover 2.1 software, a simplified protein database consisting of only the 40 proteins expected to be part of the PBS was used to speed up the analysis. Bilin-containing peptides were confirmed by manual inspection of their associated MS1, MS2, and UV-VIS spectra. Extracted ion chromatograms for each of the bilin-containing peptides were generated using XCalibur 4.0 software (Thermo Fisher). Briefly, intensities for a 20-ppm window around the masses indicated were extracted, and the resulting chromatograms were smoothed with a five-point boxcar algorithm. Areas were computed using the default Genesis algorithm in XCalibur; a combination of UV-VIS spectra confirmation, retention time, and tandem MS/MS data were used to differentiate between the PUB and PEB isomers. The ionizability of PEB and PUB modified versions of the same peptide were considered to be identical for comparisons. The areas of multiple peaks corresponding to the same bilin isomer were added together (oxidized versions of PEB-containing peptides sometimes split into more than one peak with nearly identical tandem mass spectra). The PUB fraction was computed by summing the area of all PUB-containing features for a single modified cysteine and dividing it by the total of both PUB and PEB modified versions of features containing the same cysteine.

Data Availability. All study data are included in the article and *SI Appendix*.

ACKNOWLEDGMENTS. This research was supported by the French National Agency for Research (ANR) programs CINNAMON (ANR-17-CE2-0014) and EFFICACY (ANR-19-CE02-0019) as well as the European Union program Assemble+ for F.P and L.G., by National Science Foundation grants to W.M.S. (MCB-1244339 and MCB- 2017171) and to D.M.K. (MCB-1818187 and MCB-2017171), and by a Fulbright Fellowship to T.G. This work was also supported by the European Marine Biological Resource Centre (EMBRC-France), managed by the ANR in the "Investments for the Future" program under the reference ANR-10-INSB-02. We also acknowledge the Ecology and Environment Institute of the French National Center for Research for facilitating exchanges between the different partner laboratories through the International Project of Scientific Collaboration program ChromaCya (2016-19). The Orbitrap Fusion Lumos was purchased with funds from the Indiana University Precision Health Initiative. The Genomer platform (Biogenouest) is warmly thanked for help with sequencing.

1. P. Flombaum *et al.*, Present and future global distributions of the marine Cyanobacteria *Prochlorococcus* and *Synechococcus*. *Proc. Natl. Acad. Sci. U.S.A.* **110**, 9824–9829 (2013).
2. L. Guidi *et al.*; Tara Oceans coordinators, Plankton networks driving carbon export in the oligotrophic ocean. *Nature* **532**, 465–470 (2016).
3. M. L. Paulsen *et al.*, *Synechococcus* in the Atlantic Gateway to the Arctic Ocean. *Front. Mar. Sci.* **3**, 191 (2016).
4. K. Zwirglmaier *et al.*, Global phylogeography of marine *Synechococcus* and *Prochlorococcus* reveals a distinct partitioning of lineages among oceanic biomes. *Environ. Microbiol.* **10**, 147–161 (2008).
5. C. Six *et al.*, Diversity and evolution of phycobilisomes in marine *Synechococcus* spp.: A comparative genomics study. *Genome Biol.* **8**, R259 (2007).
6. W. A. Sidler, "Phycobilisome and phycobiliprotein structure" in *The Molecular Biology of Cyanobacteria*, D. A. Bryant, Ed. (Kluwer Academic Publishers, 1994), pp. 139–216.
7. L. J. Ong, A. N. Glazer, Phycoerythrins of marine unicellular cyanobacteria. I. Bilin types and locations and energy transfer pathways in Synechococcus spp. phycoerythrins. *J. Biol. Chem.* **266**, 9515–9527 (1991).
8. L. J. Ong, A. N. Glazer, J. B. Waterbury, An unusual phycoerythrin from a marine cyanobacterium. *Science* **224**, 80–83 (1984).

9. T. Grébert *et al*., Light color acclimation is a key process in the global ocean distribution of *Synechococcus cyanobacteria*. *Proc. Natl. Acad. Sci. U.S.A.* **115**, E2010–E2019 (2018).
10. B. Palenik, Chromatic adaptation in marine *Synechococcus* strains. *Appl. Environ. Microbiol.* **67**, 991–994 (2001).
11. C. Everroad *et al*., Biochemical bases of type IV chromatic adaptation in marine *Synechococcus* spp. *J. Bacteriol.* **188**, 3345–3356 (2006).
12. F. Humily *et al*., A gene island with two possible configurations is involved in chromatic acclimation in marine *Synechococcus*. *PLoS One* **8**, e84459 (2013).
13. J. E. Sanfilippo *et al*., Self-regulating genomic island encoding tandem regulators confers chromatic acclimation to marine *Synechococcus*. *Proc. Natl. Acad. Sci. U.S.A.* **113**, 6077–6082 (2016).
14. A. N. Glazer, Light guides. Directional energy transfer in a photosynthetic antenna. *J. Biol. Chem.* **264**, 1–4 (1989).
15. N. Blot *et al*., Phycourobilin in trichromatic phycocyanin from oceanic cyanobacteria is formed post-translationally by a phycoerythrobilin lyase-isomerase. *J. Biol. Chem.* **284**, 9290–9298 (2009).
16. A. Bretaudeau *et al*., CyanoLyase: A database of phycobilin lyase sequences, motifs and functions. *Nucleic Acids Res.* **41**, D396–D401 (2013).
17. A. Shukla *et al*., Phycoerythrin-specific bilin lyase-isomerase controls blue-green chromatic acclimation in marine *Synechococcus*. *Proc. Natl. Acad. Sci. U.S.A.* **109**, 20136–20141 (2012).
18. J. E. Sanfilippo *et al*., Interplay between differentially expressed enzymes contributes to light color acclimation in marine *Synechococcus*. *Proc. Natl. Acad. Sci. U.S.A.* **116**, 6457–6462 (2019).
19. S. M. Wilbanks, A. N. Glazer, Rod structure of a phycoerythrin II-containing phycobilisome. I. Organization and sequence of the gene cluster encoding the major phycobiliprotein rod components in the genome of marine *Synechococcus* sp. WH8020. *J. Biol. Chem.* **268**, 1226–1235 (1993).
20. R. C. Everroad, A. M. Wood, Phycoerythrin evolution and diversification of spectral phenotype in marine *Synechococcus* and related picocyanobacteria. *Mol. Phylogenet. Evol.* **64**, 381–392 (2012).
21. L. A. Carrigee *et al*., CpeY is a phycoerythrobilin lyase for cysteine 82 of the phycoerythrin I α-subunit in marine *Synechococcus*. *Biochim. Biophys. Acta Bioenerg.* **1861**, 148215 (2020).
22. A. Biswas *et al*., Biosynthesis of cyanobacterial phycobiliproteins in *Escherichia coli*: Chromophorylation efficiency and specificity of all bilin lyases from *Synechococcus* sp. strain PCC 7002. *Appl. Environ. Microbiol.* **76**, 2729–2739 (2010).
23. J. E. Sanfilippo, L. Garczarek, F. Partensky, D. M. Kehoe, Chromatic acclimation in cyanobacteria: A diverse and widespread process for optimizing photosynthesis. *Annu. Rev. Microbiol.* **73**, 407–433 (2019).
24. T. Grébert, "Pigment diversity in marine *Synechococcus* sp.: Molecular basis, evolution and ecological role," PhD thesis, Université Pierre et Marie Curie–Paris VI, Paris, France (2017). https://tel.archives-ouvertes.fr/tel-02422222.
25. K. Katoh, D. M. Standley, MAFFT multiple sequence alignment software version 7: Improvements in performance and usability. *Mol. Biol. Evol.* **30**, 772–780 (2013).
26. D. Darriba, G. L. Taboada, R. Doallo, D. Posada, ProtTest 3: Fast selection of best-fit models of protein evolution. *Bioinformatics* **27**, 1164–1165 (2011).
27. A. Stamatakis, RAxML version 8: A tool for phylogenetic analysis and post-analysis of large phylogenies. *Bioinformatics* **30**, 1312–1313 (2014).
28. J. Huerta-Cepas, F. Serra, P. Bork, ETE 3: Reconstruction, analysis, and visualization of phylogenomic data. *Mol. Biol. Evol.* **33**, 1635–1638 (2016).
29. S. Mazard, M. Ostrowski, F. Partensky, D. J. Scanlan, Multi-locus sequence analysis, taxonomic resolution and biogeography of marine *Synechococcus*. *Environ. Microbiol.* **14**, 372–386 (2012).
30. R. Rippka *et al*., *Prochlorococcus marinus* Chisholm et al. 1992 subsp. pastoris subsp. nov. strain PCC 9511, the first axenic chlorophyll a_2/b_2-containing cyanobacterium (Oxyphotobacteria). *Int. J. Syst. Evol. Microbiol.* **50**, 1833–1847 (2000).
31. T. D. Schmittgen, K. J. Livak, Analyzing real-time PCR data by the comparative C(T) method. *Nat. Protoc.* **3**, 1101–1108 (2008).
32. B. Brahamsha, A genetic manipulation system for oceanic cyanobacteria of the genus *Synechococcus*. *Appl. Environ. Microbiol.* **62**, 1747–1751 (1996).
33. C. Six, L. Joubin, F. Partensky, J. Holtzendorff, L. Garczarek, UV-induced phycobilisome dismantling in the marine picocyanobacterium *Synechococcus* sp. WH8102. *Photosynth. Res.* **92**, 75–86 (2007).
34. R. M. Mahmoud *et al*., Adaptation to blue light in marine *Synechococcus* requires MpeU, an enzyme with similarity to phycoerythrobilin lyase isomerases. *Front. Microbiol.* **8**, 243 (2017).
35. A. Biswas *et al*., Characterization of the activities of the CpeY, CpeZ, and CpeS bilin lyases in phycoerythrin biosynthesis in *Fremyella diplosiphon* strain UTEX 481. *J. Biol. Chem.* **286**, 35509–35521 (2011).
36. N. A. Saunée, S. R. Williams, D. A. Bryant, W. M. Schluchter, Biogenesis of phycobiliproteins: II. CpcS-I and CpcU comprise the heterodimeric bilin lyase that attaches phycocyanobilin to CYS-82 OF beta-phycocyanin and CYS-81 of allophycocyanin subunits in *Synechococcus* sp. PCC 7002. *J. Biol. Chem.* **283**, 7513–7522 (2008).
37. C. M. Kronfel *et al*., Structural and biochemical characterization of the bilin lyase CpcS from *Thermosynechococcus elongatus*. *Biochemistry* **52**, 8663–8676 (2013).
38. D. M. Arciero, D. A. Bryant, A. N. Glazer, In vitro attachment of bilins to apophycocyanin. I. Specific covalent adduct formation at cysteinyl residues involved in phycocyanobilin binding in C-phycocyanin. *J. Biol. Chem.* **263**, 18343–18349 (1988).

IV. Functional characterization of other genes involved in the CA4-B process

IV.1. Materials and Methods

The CRISPR editing plasmid pJU87 vector was kindly provided by Prof. David Kehoe. This carries: (i) *Francisella novicida*'s native CRISPR array; (ii) a kanamycin resistance gene; and (iii) *cpf1*, which encodes an alternative nuclease that is non-toxic to cyanobacteria and has been proved efficient in three cyanobacterial models (*Synechococcus*, *Synechocystis* and *Anabaena;* Ungerer and Pakrasi, 2016; Walker, 2022). For each targeted gene (*fciA*, *fciB* and *unk10*), as well as for the whole *fciAB* operon, specific guide RNA (gRNA) and homologous template regions (HTR) were produced by PCR amplification of *Synechococcus* sp. A15-62 genome fragments using high-fidelity polymerase (Fidelio, Ozyme) and primers designed for this purpose (Geneious® version 11.0.5; see Chapter 1 § V, Supplementary Table 1).

Following this step, the pJU87 vectors (Fig. 1) were digested using AarI and KpnI restriction enzymes (NEB), ligated with the corresponding gRNA and HTR (T4 DNA ligase and NEBuilder® HiFi DNA Assembly Master mix, NEB) and transformed into Top10 competent *E. coli* cells (ThermoFisher Scientific). Resulting colonies were picked, PCR tested and sequenced before proceeding to the next steps. The plasmids containing all elements necessary for genome editing were then transferred into MC1061 competent *E. coli* cells (Casadaban and Cohen, 1980), containing the conjugative plasmid pRK24 (Meyer et al., 1977) and the helper plasmid pRL528 (Elhai and Wolk, 1988). Conjugation with wild-type *Synechococcus* A15-62 was performed as previously described (Brahamsha, 1996; Shukla et al., 2012). Individual colonies were picked and tested for *fciA*, *fciB, fciAB* and *unk10* disruption by PCR amplification and sequencing.

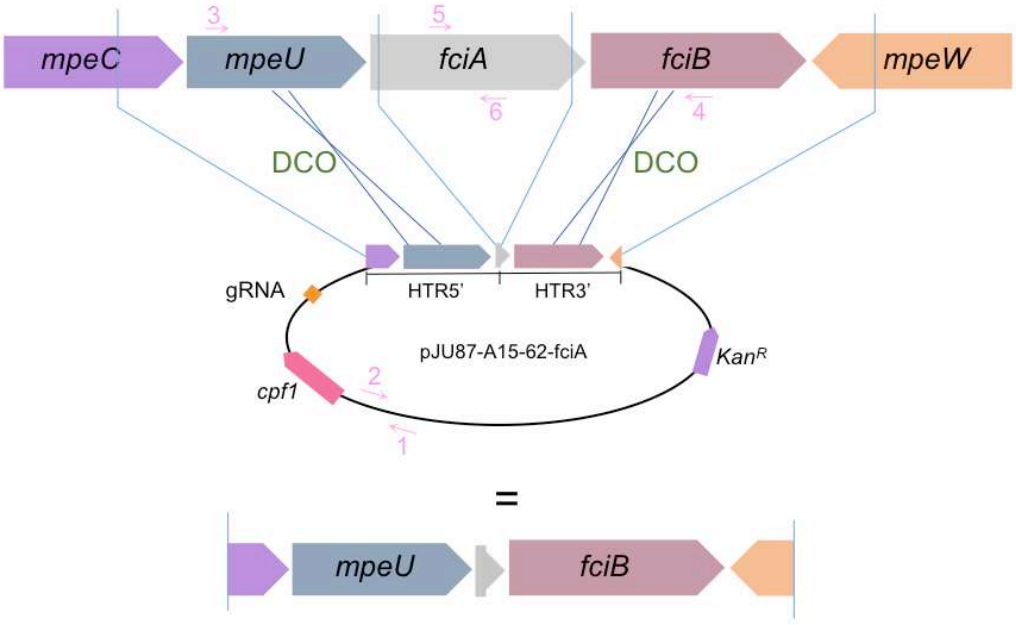

Figure 1: Example of the CRISPR construct designed and produced to knock out *fciA* gene in *Synechococcus* sp. A15-62. The pJU87-A15-62-*fciA*$^{-}$ final plasmid was designed by inserting specific guide RNA (gRNA) and 5' and 3' homologous template regions (HTR) into the pJU87 CRISPR backbone containing *cpf1* and *Kan*^{R}. The numbered arrows correspond to primers used to verify the correct insertion of the gRNA and HTR regions into the plasmid. DCO: double crossing over.

IV.2. Results and discussion

In order to better understand how the regulation of the CA4-B process differs from that of CA4-A process, CRISPR constructs were produced to knock out *fciA*, *fciB*, and *unk10* genes, as well as the whole *fciAB* operon, in the model PT 3dB strain *Synechococcus* sp. A15-62. In all cases, sequencing of the constructs proved that pJU87 vectors had well integrated the corresponding gRNA and associated HTR (data not shown), both being essential for double-stranded DNA cleavage and homologous recombination. Furthermore, PCR controls of transformed MC1061 bacteria confirmed the incorporation of the plasmid containing all the elements necessary for genome editing into the competent cells (Fig. 2).

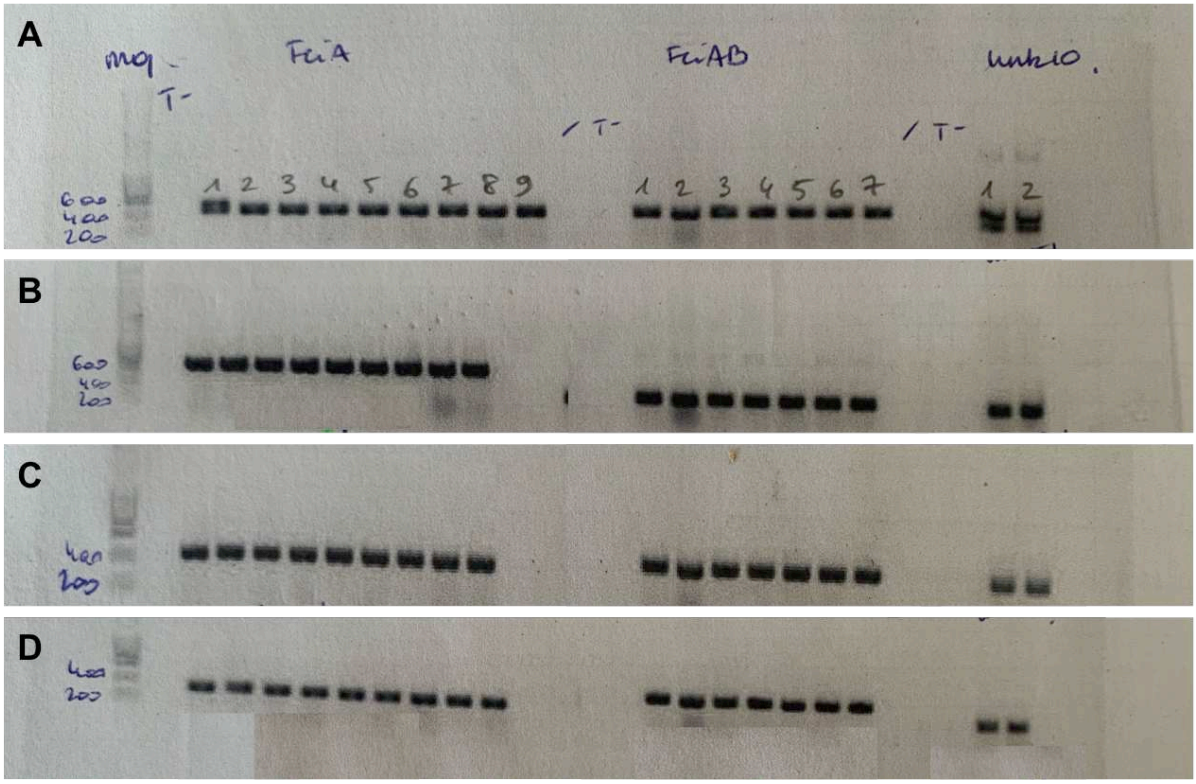

Figure 2: Electrophoresis gel corresponding to the PCR screening of MC1061 bacteria after transformation with pJU87 constructs. Several MC1061 candidates were tested for each targeted gene: nine for *fciA*, seven for *fciAB* and two for *unk10*. The primer couples used were specific of (A) gRNA or of the (B) middle, (C) 5' (D) and 3' zones of the HTR. All observed amplification products had the expected sizes, which indicate that all candidates have been successfully transformed. The same results were observed for *fciB* (data not shown).

Yet, individual colonies isolated following the conjugation step between transformed MC1061 and A15-62 wild-type (WT) cells exhibited the expected bands after PCR screening only for the *fciB* construct (data not shown). After sequencing verification, the *fciB*$^-$ mutant was partially characterized by determining its fluorescence excitation ratio in green (GL) and blue (BL) light. $Exc_{495:545}$ values of 1.43 and 1.52 were measured respectively, in comparison to the classical values of 0.6 – 0.7 and 1.6 – 1.7 found in WT cells. Thus, it seems that the interruption of *fciB* in A15-62 caused a constitutive blue light phenotype characterized by PUB-rich phycobilisomes, and consequently high PUB:PEB ratio. Interestingly, this result is very similar to the one obtained by Sanfilippo and collaborators (2016) for the same gene when muted in the CA4-A model strain RS9916 (Fig. 3). If we assume that the regulatory system encountered in CA4-B is analogous to that of CA4-A, then it is likely that FciB is also a

regulator of the acclimation process. However, its function in PT 3dB strains is probably to directly or indirectly activate *mpeZ*, which binds PEB in GL to Cys-83 of the PE-II α-subunit (Grébert et al., 2021).

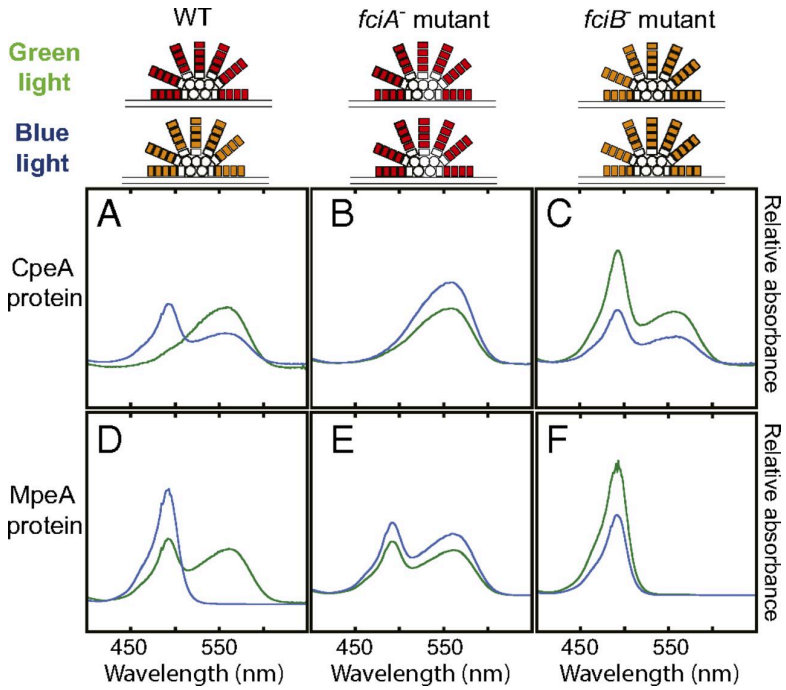

Figure 3: Schematic representation of PBS chromophorylation and associated CpeA (α subunit of PE-I) and MpeA (α subunit of PE-II) absorption spectra in wild-type RS9916 (WT), *fciA*⁻ and *fciB*⁻ mutants grown under blue and green light. Red phycobilisomes indicate high PEB content, while orange indicate high PUB content. (A to C) Absorption spectra of HPLC-purified CpeA and (D to F) MpeA from WT or mutant cells grown under blue light (blue line) and green light (green line; Sanfilippo et al., 2016).

IV.3. Future work

Future attempts to get knockout mutants of the *fciA* and *unk10* genes, as well as *fciAB* operon, should include a PCR step to check whether the plasmids are still detectable in the different cultures. Those that are tested positive should then be transferred to liquid medium without antibiotics so that cultures can get rid of the plasmids, the rationale being that the genomic edition would leave no mark. Subsequently, the cultures should be plated and individual colonies appearing should be picked and tested for *fciA*, *fciAB* and *unk10* disruption by PCR amplification and sequencing. Once mutants are obtained, they will be

characterized by measuring their growth rate by flow cytometry and pigment content (PUB:PEB ratio) by spectrofluorimetry in both BL and GL conditions, to compare their phenotype with that of the wild type strain A15-62. RNA will also be harvested in WT and mutants to look at targeted gene expression by real time RT-PCR, as previously done for *mpeW* and *mpeQ* (Grébert et al., 2021). Finally PBS will also be extracted as described by Six and collaborators (2005) to determine the chromophorylation of PE-I and PE-II subunits, in collaboration with Wendy Schluchter (University of New Orleans) and the mass spectrometry platform of the Indiana University, as previously done (Shukla et al., 2012; Sanfilippo et al., 2016; Grébert et al., 2021).

V. Supplementary material

<u>Supplementary table 1:</u> Sequences of the primers used to generate gRNA and HTR.

	gRNA		HTR -5'		HTR -3'	
	A15-62_ gRNA-F	A15-62_ gRNA-R	A15-62_ HTR5'-F	A15-62_ HTR5'-R	A15-62_ HTR3'-F	A15-62_ HTR3'-R
ficA⁻	AGATGACAATGA AAATAATGAATC	AGACGATTCATT ATTTTCATTGTC	ATGTATTACTCTCCCTTC CATCGTTTTTTCGCAAA CTTC	CATTTTTTTGTCTAGCTT TAATGCGGTAGTTGGTA CCAGCTCCTTCAACTTAA TGCG	GAAGTTTGCGAAAAAA ACGATGGAAGGGAGAG TAATACAT	GCCCGGATTACAGATCC TCTAGAGTCGACGGTAC CTCAAGATGACTTCTAA AATT
fciB⁻	AGATACGGGTGA TCATGGGATTTA	AGACTAAATCCC ATGATCACCCGT	TGCACCTATATTGGC AATCTAATAGATGTT TTCATGTATT	CATTTTTTTGTCTAG CTTTAATGCGGTAGT TGGTACCGTGACTCT CATCGGGAAATC	AATACATGAAAACA TCTATTAGATTGCCA ATATAGGTGCA	GCCCGGATTACAGA TCCTCTAGAGTCGAC GGTACCTAATTTTAT ATGGCAGCGTA
fciAB⁻	AGATCCAACAAA ACATTATTGTAC	AGACGTACAATA ATGTTTTGTTGG	TGCACCTATATTGGCA ATCTTCGTTTTTTCGC AAACTTC	CATTTTTTTGTCTAGCT TTAATGCGGTAGTTGG TACCAGCTCCTTCAACT TAATGCG	GAAGTTTGCGAAAAAA ACGAAGATTGCCAATA TAGGTGCA	GCCCGGATTACAGATC CTCTAGAGTCGAGGT ACCCAATAATTTTATAT GGCAGC
unk10⁻	AGATCCCATTTG CCAATGATGTTG	AGACCAACATCA TTGGCAAATGGG	TTCCTTCATGCAGGT ATAGTTTCAGCACGT GACATGATGA	CATTTTTTTGTCTAG CTTTAATGCGGTAGT TGGTACCGTAGATTT TCAATATCACTA	TCATCATGTCACGTG CTGAAACTATACCTC GATGAAGGAA	GCCCGGATTACAGA TCCTCTAGAGTCGAC GGTACCTCATTTGTA TGGCGCCAATC

Chapter 2:

Culturing approaches to better characterize type IV chromatic acclimation

I. Context of the work

The occurrence of light niche partitioning in the upper lit layer of the ocean between *Synechococcus* populations with different PUB:PEB ratios has been widely documented in the late 20th century using a variety of fluorescence techniques, including fluorescence microscopy, flow cytometry and spectrofluorimetry (Wood, 1985; Olson et al., 1988; Neveux et al., 1999). However, it is only after the discovery that some *Synechococcus* strains could modify the chromophorylation of their phycobilisomes depending on the ambient light color (Palenik, 2001), that one realized that these fluorescence techniques actually could not discriminate chromatic acclimaters from cells with fixed PUB:PEB ratios in the field. This issue was later solved by using molecular markers, and more specifically a combination of three PBS gene markers (*cpcBA*, *mpeBA* and *mpeW*). These allowed Grébert and collaborators (2018) to discriminate all major *Synechococcus* PTs and show unambiguously that green light (GL) specialists, blue light (BL) specialists and chromatic acclimaters co-occurred at different relative abundances in different light niches. In addition, this study revealed the unexpectedly large contribution of the previously overlooked chromatic acclimaters, altogether representing about 42% of all *Synechococcus* cells sampled along the *Tara* Oceans transect. However, the reasons for the prevalence of these chromatic acclimaters in the field, and the light niche in which they could perform better than specialists, remained obscure. Indeed, although Lovindeer and co-workers (2021) proposed that chromatic acclimaters could be favored in conditions of water mixing, their modelling approach did not manage to reproduce the actual distribution pattern of *Synechococcus* PTs observed *in situ*.

The first axis of this chapter aimed at better understanding the differences existing between the two genetically distinct types of chromatic acclimaters, i.e. PT 3dA strains that possess a CA4-A island and PT 3dB cells that have a CA4-B island (Humily et al., 2013). Apart from one study by Sanfilippo and collaborators (2016), who analyzed the variations of the $Exc_{495:545}$ ratio (a PUB:PEB proxy) at various proportions of BL and GL in RS9916 wild-type strain and its *fciA*$^-$ and *fciB*$^-$ mutants, few data were available so far about the behavior of chromatic acclimaters in intermediate blue-green light conditions. In order to fill this gap, and hopefully find a way of distinguishing phenotypically the two different types of

chromatic acclimaters, batch cultures of three PT 3dA and three PT 3dB representatives belonging to different *Synechococcus* clades and subclades were grown in various conditions of temperature, light quality and quantity. During these experiments, growth rate, phycobilin and phycobiliprotein ratios, as well as other cellular parameters (proxies of phycoerythrin and chlorophyll *a* cell content, cell diameter) were measured. Moreover, the time course variations of the $Exc_{495:545}$ ratio after shifting cultures from BL to GL (or conversely) were analyzed in both low and high light at 25°C.

The second objective of this chapter was to assess the respective fitness of the three major PTs of marine *Synechococcus* in the ocean in order to determine whether the CA capability could confer a fitness advantage over fixed pigmentation, and in which condition. To do so, mono- and co-cultures of a GL specialist (PT 3a), a BL specialist (PT 3c) and a chromatic acclimater (PT 3dB) were grown in different conditions of light quality and quantity, an approach similar to the one developed previously by Jef Huisman's group (Stomp et al., 2004, 2008; Luimstra et al., 2020). During our experiments, we followed the growth of the three marine *Synechococcus* strains in light-limited chemostats (Huisman et al., 2002) and acquired several parameters related to the photosynthetic performance, light-harvesting capabilities and pigment content of the strains alone or in mixture, and how they modified their environment (light intensity and quality, pH, nutrient concentrations).

II. Contribution

As concerns continuous mono- and co-cultures, I developed and implemented the experimental set-up with the help of Bastian Gouriou, a Master 2 student who worked under my supervision from January to September 2022. I also supervised Julia Clairet, an undergraduate student, from January to March 2023. Bastian and Julia helped me acquire the extensive dataset presented in the draft article below (see Chapter 2 § IV). I was also responsible for developing and implementing the qPCR approach, with Laurence Garczarek's support. Nutrients samples were analysed by Sarah Bureau. Frédéric Partensky did the comparative genomics. Francesco Mattei, Jolanda Verspagen and Jef Huisman were in charge of the modelling part, which will be included in the manuscript in the forthcoming weeks before submission.

For batch experiments, I acquired the vast majority of the dataset. Analysis and results interpretation were done, for both studies, under the supervision of L. Garczarek and F. Partensky.

I also had the opportunity to be involved in another cultured-based experiment on the comparative thermophysiology of marine *Synechococcus* CRD1 strains in the framework of Mathilde Ferrieux's PhD (Annex 2). More precisely, I participated in growth rate measurements and in acquisition of various associated photophysiological parameters, which helped us define the thermal tolerance range of eight marine *Synechococcus* strains. I also contributed to experiments aimed at determining the PSII repair rate of each strain as a function of temperature. The main outcomes from this study (Ferrieux et al., 2022) were: (i) the confirmation in culture of the occurrence (previously suggested by *in-situ* analyses; Farr ant et al., 2016) of three thermotypes within the CRD1 clade, which predominates in iron-poor areas of the world Ocean; (ii) the precise delineation of the fundamental and realized thermal niches of the three CRD1 thermotypes; and (iii) the discovery of physiological specificities of CRD1 strains with regard to representatives of the four other major *Synechococcus* clades (I to IV) in the Ocean, notably their constitutively low photosystem II quantum yield (F_V/F_M) and high PSII repair rates.

III. Batch experiments

Differential acclimation kinetics of the two forms of Type IV chromatic acclimaters occurring in marine *Synechococcus* cyanobacteria

Louison Dufour[1], Bastian Gouriou[1], Julia Clairet[1], Morgane Ratin[1], Laurence Garczarek[1] and Frédéric Partensky[1]

[1]Sorbonne Université, CNRS, UMR 7144 Adaptation and Diversity in the Marine Environment (AD2M), Station Biologique de Roscoff (SBR), Roscoff, France.

*** Correspondence:**

Corresponding Author: F. Partensky

Keywords: Marine picocyanobacteria, *Synechococcus*, chromatic acclimation

Abstract

Synechococcus is one of two most abundant phytoplanktonic organisms of the Ocean and also displays the widest variety of pigmentation of all marine oxyphototrophs, which makes it ideally suited to colonize the variety of spectral niches occurring in the upper-lit layer of oceans. Seven *Synechococcus* pigment types (PTs) have been described based on the composition and chromophorylation of their light-harvesting complexes, called phycobilisomes (PBS). The most sophisticated and abundant *Synechococcus* PT (3d) gathers cells capable of Type IV chromatic acclimation (CA4), i.e. to reversibly modify the ratio of the blue light-absorbing phycourobilin (PUB) to the green light-absorbing phycoerythrobilin (PEB) in PBS in order to match the ambient light color. Although two genetically distinct types of chromatic acclimaters, so-called PTs 3dA and 3dB, have been evidenced and found to be equally abundant in the Ocean, reasons for their prevalence in natural *Synechococcus* populations remain obscure. Here, acclimation experiments in different blue to green ratios of representatives of these two PTs showed that in mixed blue-green light conditions, PT 3dB strains displayed significantly higher PUB:PEB ratios than their PT 3dA counterparts. Thus, PTs 3dA and 3dB seem to differ in the ratio of blue to green light required to trigger the CA4 process. Furthermore, shift experiments between 100% BL and 100% GL conditions,

and vice-versa, also revealed discrepancies in the acclimation pace between the two types of chromatic acclimaters, which may explain their co-occurrence in some blue green light niches.

Preprint published in bioRxiv: doi.org/10.1101/2023.07.11.548510

Introduction

Phytoplanktonic cells have an obligate requirement for light to perform photosynthesis. In the marine environment this energy source is highly variable quantitatively and qualitatively not only with depth but also along coast-offshore gradients, leaving aside daily oscillations (Kirk, 1994; Holtrop et al., 2021). This variability has triggered an extensive structural and pigment diversification of phytoplankton light-harvesting antennae. These pigment-protein complexes enable cells to considerably enhance the amount and wavelength range of photosynthetically active radiations reaching photosystems. Despite their apparent simplicity compared to algae and higher plants, cyanobacteria possess the most sophisticated form of antennae known in oxyphototrophs, the phycobilisomes (PBS). PBS are huge water-soluble complexes composed of six to eight rods radiating around a central core. Both core and rods are constituted of phycobiliproteins that bind open-chain tetrapyrroles, called phycobilins (Sidler, 1994). While the PBS core is always made of allophycocyanin and is highly conserved, PBS rods display a very large structural flexibility, since they can be made of phycocyanin (PC) only, or of PC and one or two phycoerythrin (PE) types, PE-I and PE-II (Ong and Glazer, 1991; Six et al., 2007b). Additionally, each phycobiliprotein type can bind up to three different kinds of chromophores (or phycobilins). The ultimate degree of sophistication is the capacity for some cyanobacterial cells to modify the composition of their PBS in response to changes in the ambient light color. This process called chromatic acclimation (CA) — the initial term was actually ‘chromatic adaptation’ but was recently replaced in order to best suit this physiological process (Shukla et al., 2012) — was first observed in the early 20th century in freshwater cyanobacteria shifted from red to green light (Engelmann, 1902; Gaidukov, 1903). It was later on attributed to changes in the phycobiliprotein composition of PBS rods: in red light, rods are entirely composed of PC and

cells look green, whereas in green light PC is restricted to the base of the rods and the distal part is made of PE, causing cells to exhibit a bright red color (Boresch, 1922). This type of complementary chromatic acclimation (also called Type 3 chromatic acclimation or CA3) is one among the six different types of CA known so far in Cyanobacteria (Tandeau de Marsac, 1977; Sanfilippo et al., 2019a). While CA2 — a simple type of CA where PE production is induced in GL, generating longer PBS rods, and repressed in red light — and CA3 occur mainly in freshwater and brackish cyanobacteria, CA4 is the main type occurring in the open ocean and is specific to marine *Synechococcus* cyanobacteria (Palenik, 2001; Everroad et al., 2006; Humily et al., 2013). Contrary to CA2 and CA3, CA4 does not involve changes in the phycobiliprotein composition of PBS rods, but in their chromophore composition. Indeed, in response to shifts between green light (GL) and blue light (BL), chromatic acclimaters can modify the relative amount of the two chromophores bound to PE-I and PE-II, in order to match the predominant ambient light color. In BL they exhibit a high ratio of the BL-absorbing phycourobilin (PUB, λ_{max} = 495 nm) to the GL-absorbing phycoerythrobilin (PEB, λ_{max} = 550 nm), and vice-versa in GL (Everroad et al., 2006; Shukla et al., 2012). Variations in PUB:PEB ratio are generally assessed by measuring the relative ratio of whole cell fluorescence excitation at 495 and 545 nm ($Exc_{495:545}$) with emission at 580 nm, which in chromatic acclimaters changes from 0.6 – 0.7 in GL to 1.6 – 1.7 in BL (Palenik, 2001; Everroad et al., 2006). In the nomenclature of *Synechococcus* pigment types (PTs) established by Six and collaborators (2007b), and later modified by Humily and co-workers (2013), chromatic acclimaters are classified as 'PT 3d' cells, meaning that they possess PBS rods made of PC, PE-I and PE-II (a feature shared by all PT 3 strains) and can modify their PUB:PEB ratio. In contrast PTs 3a, 3b and 3c have a constitutively low, medium and high PUB:PEB ratio, respectively. Additionally, two genetically different types of chromatic acclimaters have been described: PTs 3dA and 3dB (Humily et al., 2013). They possess a small genomic island involved in the CA4 process (CA4-A and CA4-B), both forms differing genetically and structurally (Humily et al., 2013). Although long overlooked, CA4 appears to be an ecologically important process for marine *Synechococcus*, since chromatic acclimaters were shown to account for more than 40% of the whole *Synechococcus* population along the *Tara* Oceans expedition transect (Grébert et al., 2018). Moreover, PTs 3dA and 3dB were equally abundant (22.6% and 18.9%, respectively) but distributed in complementary light niches in

the field, the former predominating in temperate and high latitude waters, while the latter was more abundant in warm waters.

The emergence and maintenance of two CA4 types over the course of evolution as well as their differential distribution in the environment suggests that both CA4 types may not be as phenotypically equivalent as previously suggested (Humily et al., 2013). To check this hypothesis, we acclimated three representatives of PTs 3dA and 3dB in batch culture under two conditions of temperature, two irradiances and five light colors to compare their growth rates and PBS characteristics. Furthermore, we performed shifts at different light intensities from BL to GL (and vice-versa) to compare CA4 kinetics between five strains of each PT 3d. Our study indicates that PT 3dA and 3dB strains differ in the BL to GL ratios necessary to trigger the CA4 process. Moreover, we revealed discrepancies in the acclimation pace between the two types of chromatic acclimaters.

Materials and Methods

Biological material and culture conditions

Ten *Synechococcus* strains, of which five PT 3dA and five PT 3dB representatives (Table 1), were retrieved from the Roscoff Culture Collection (https://roscoff-culture-collection.org/). These strains were isolated from very diverse environments and were selected based on genome availability (Doré et al., 2020) and clade affiliation in order to have representatives from all five major clades (I to IV and CRD1) in the global ocean (Farrant et al., 2016), as well as the CA4-A model strain RS9916 (Shukla et al., 2012; Sanfilippo et al., 2016, 2019b).

TABLE 1: Characteristics of the *Synechococcus* strains used in this study.

Strain name	RCC #[1]	Subcluster[2]	Clade[2]	Subclade[3]	Pigment type [4]	Isolation region
BIOS-U3-1	2533	5.1	CRD1	n.a.	3dA	Chilean upwelling
BL107	515	5.1	IV	IVa	3dA	Balearic Sea
MITS9220	2571	5.1	CRD1	n.a.	3dA	Equatorial Pacific
RS9916	555	5.1	IX	n.a.	3dA	Gulf of Aqaba
WH8020	751	5.1	I	Ia	3dA	Sargasso Sea
A15-62	2374	5.1	II	IIa	3dB	Offshore Mauritania
A18-40	n.a.	5.1	III	IIIa	3dB	Atlantic Ocean
MINOS11	2319	5.1	n.a.	n.a.	3dB	Mediterranean Sea
PROS-U-1	2369	5.1	II	IIh	3dB	Moroccan upwelling
RS9915	2553	5.1	III	IIIA	3dB	Gulf of Aqaba

[1]Roscoff Culture Collection, [2]Farrant et al. (2016), [3]Mazard et al. (2012), [4]Humily et al. (2013).

Cells were grown in 50 mL flasks (Sarstedt) in PCR-S11 medium (Rippka et al., 2000) supplemented with 1 mM sodium nitrate, and pre-acclimated for at least three weeks in continuous light provided by blue and/or green LEDs (Alpheus) in temperature-controlled chambers.

Acclimation experiments

A selection of six out of the ten abovementioned strains (BL107, RS9916 and WH8020 for PT 3dA and A15-62, PROS-U-1 and RS9915 for PT 3dB; Table 1) were grown in the following conditions: (i) two temperatures: 18 and 25°C; (ii) two irradiances: low light (LL, 15 µmol photons m^{-2} s^{-1}, hereafter µE) and high light (HL, 75 µE); (iii) five light qualities: blue light (100% BL), green light (100% GL), as well as three mixtures of blue to green light: 25% BL – 75% GL, 50% BL – 50% GL and 75% BL – 25% GL. The LEDs spectra were measured in these different conditions using a PG200N Spectral PAR Meter (UPRtek). Each strain was grown in triplicates and inoculated at an initial cell density of 3×10^6 cells mL^{-1}. Samples were harvested every day to measure cell concentration and fluorescence parameters by flow

cytometry, and once during the exponential phase to measure phycobilin content by spectrofluorimetry (see below).

Shift experiments

Shift experiments between 100% low BL (LBL) and 100% low GL (LGL), and vice-versa, as well as the equivalent experiments between 100% high BL (HBL) and 100% high GL (HGL), were performed on all ten *Synechococcus* strains (Table 1), but only at 25°C. Each strain was diluted with fresh medium before the beginning of the experiments and regularly transferred in order to avoid limitation by nutrients. Aliquots were collected two to three times a day, depending on light intensity, to measure phycobilin content by spectrofluorimetry (see below).

Flow cytometry

Culture aliquots were sampled twice a day, fixed using 0.25% (v/v) glutaraldehyde (grade II, Sigma Aldrich) and stored at −80°C until analysis (Marie et al., 1999a). Cell density was determined using a Guava easyCyte flow cytometer equipped with a 488 nm laser and the Guavasoft software (Luminex Corporation). Average fluorescence at 583 nm and 695 nm were used as proxies of phycoerythrin (PE) and chlorophyll *a* (Chl *a*) contents per cell, respectively. Forward scatter (FSC) was used as a proxy of cell diameter. Both fluorescence and FSC signals were normalized to that of standard fluorescent 0.95 µm silica beads.

Spectrofluorimetry

In vivo fluorescence spectra were recorded at 240 nm min^{-1} with slits fixed at 10 nm once during the exponential phase using a spectrofluorimeter FL6500 (Perkin-Elmer). Excitation spectra were acquired between 450 and 560 nm (with an emission set at 580 nm, which corresponds to the maximum emission of PE). Emission spectra were recorded between 550 and 750 nm (with an excitation set at 530 nm, which corresponds to the maximum

absorption of PUB). Spectra were monitored and analyzed with the Fluorescence software (Perkin-Elmer). The excitation ratio ($Exc_{495:545}$) was considered as a proxy for PUB:PEB ratio, an indicator of the phycoerythrobilin and phycourobilin content of the PBS rods. The fluorescence emission ratios ($Em_{560:650}$) and ($Em_{650:680}$) were respectively used as proxies of phycoerythrin (PE) to phycocyanin (PC) and PC to PBS terminal acceptor (TA) ratios. Those provided information about the electron transfer efficiency within the PBS, the length of PBS rods and the coupling of the PBS to PSII reaction center chlorophylls.

RESULTS

Acclimation experiments

Growth rate

The growth rates of all six tested strains were globally higher at 25°C (Fig. 1C and D) than at 18°C (Fig. 1A and B). Similarly, most strains grew significantly faster at HL than LL at 25°C, while little difference between the two irradiances was observed at 18°C. Consequently, maximum growth rates (μ) were reached at 25°C in HL, with all strains but WH8020 achieving more than one cell division per day ($\mu > 0.69$ day^{-1}; Fig. 1D). While for any given strain, the growth rate varied little between the different light quality conditions, significant differences were observed between PTs 3dA and 3dB at 18°C and LL under four out of five light quality conditions, with PT 3dA strains growing slightly faster than their PT 3dB counterparts (Fig. 1A). This was also the case for the 100% BL condition at HL and 18°C (Fig. 1B), as well as at 50% BL – 50% GL and 100% GL at LL and 25°C (Fig. 1C). No statistically significant differences between the two PTs were observed at 25°C HL.

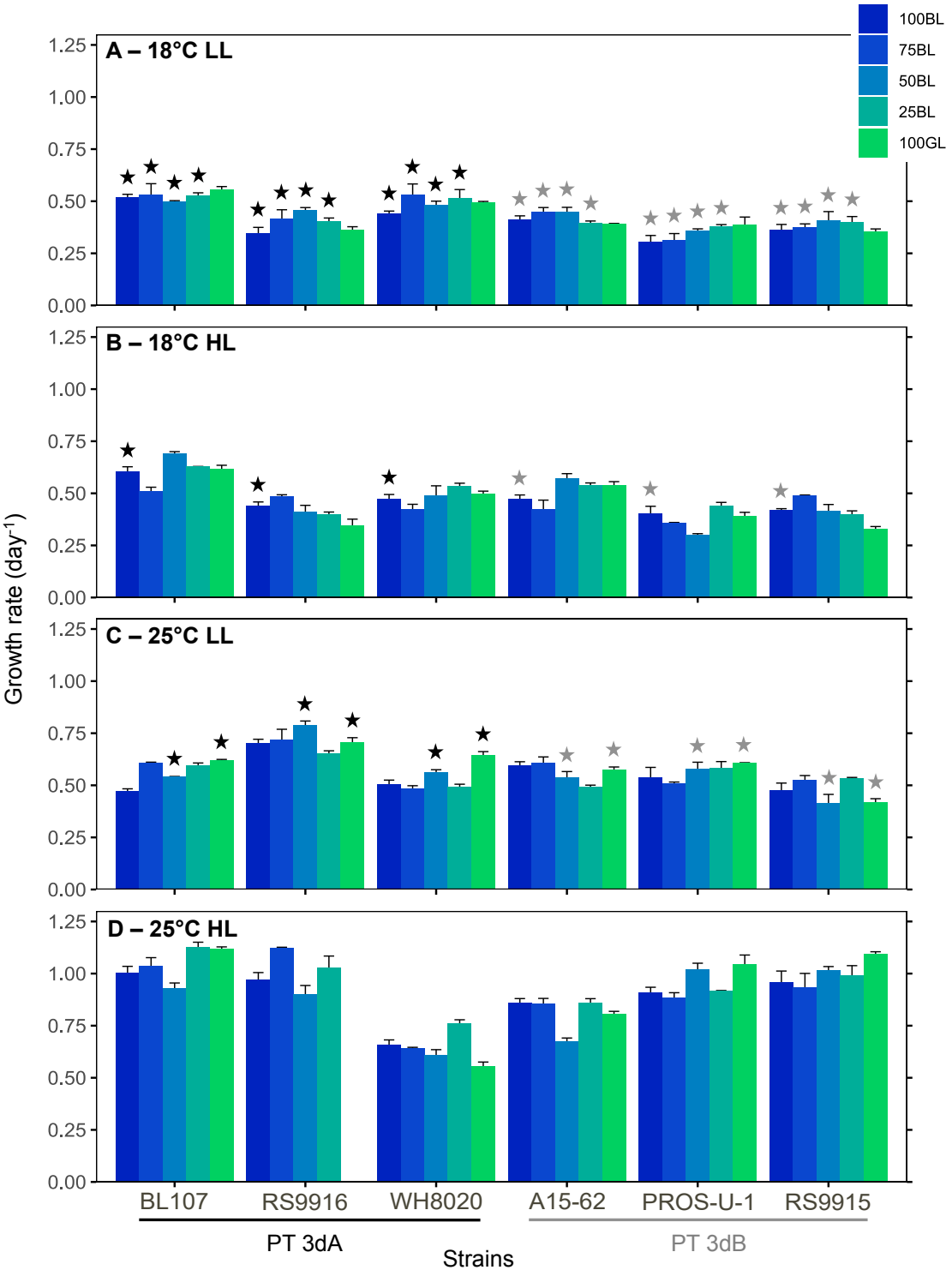

Figure 1: Growth rate of six *Synechococcus* strains grown in different conditions of temperature, light quantity and quality. (A) 18°C low light. **(B)** 18°C high light. **(C)** 25°C low light. (**D**) 25°C high light. Histograms represent average and standard deviations of triplicate measurements. Stars above histograms indicate significantly different values between PT 3dA and 3dB representatives in a given condition of light quality and temperature (Student test or Wilcoxon-Mann-Whitney test, depending on normality and variance homogeneity, p-value < 0.05).

Chlorophyll a and phycoerythrin fluorescence

A downward trend in flow cytometric red (Chl *a*) and orange (PE) fluorescence signals was observed from 100% BL to 100% GL, regardless of irradiance and temperature (Fig. 2 and 3). Both fluorescence signals were higher in LL (Fig. 2A and C, 3A and C) than in HL (Fig. 2B and D, 3B and D), but also at 25°C (Fig. 2C and D, 3C and D) in comparison to 18°C (Fig. 2A and B, 3A and B). Significant differences between PTs 3dA and 3dB were detected only at LL. At 18°C, the Chl *a* fluorescence of PT 3dB strains was higher than for PT 3dA cells at 25% BL – 75% GL and 100% GL (Fig. 2A). The same was true for PE fluorescence in all tested light qualities except 100% BL (Fig. 3A). At 25°C, PT 3dB strains exhibited higher Chl *a* fluorescence in the three light mixtures (Fig. 2C) and PE fluorescence in three out of the five light quality conditions (Fig. 3C).

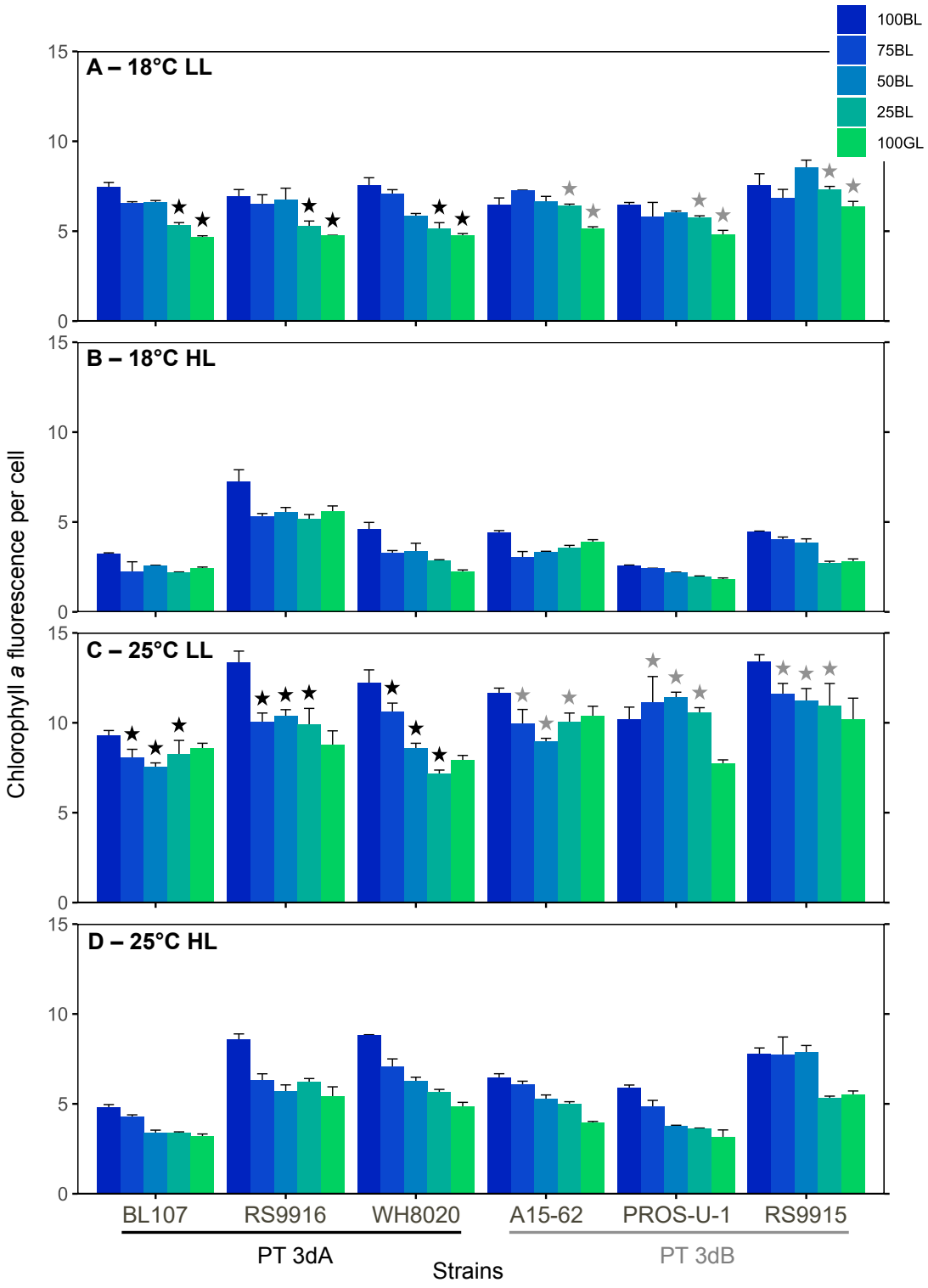

Figure 2: Average flow cytometric chlorophyll *a* fluorescence per cell of six *Synechococcus* strains grown in different conditions of temperature, light quantity and quality. (A) 18°C low light. **(B)** 18°C high light. **(C)** 25°C low light. (**D**) 25°C high light. Histograms represent average and standard deviations of triplicate measurements. Stars above histograms indicate significantly different values between PT 3dA and 3dB representatives in a given condition of light quality and temperature (Student test or Wilcoxon-Mann-Whitney test, depending on normality and variance homogeneity, p-value < 0.05).

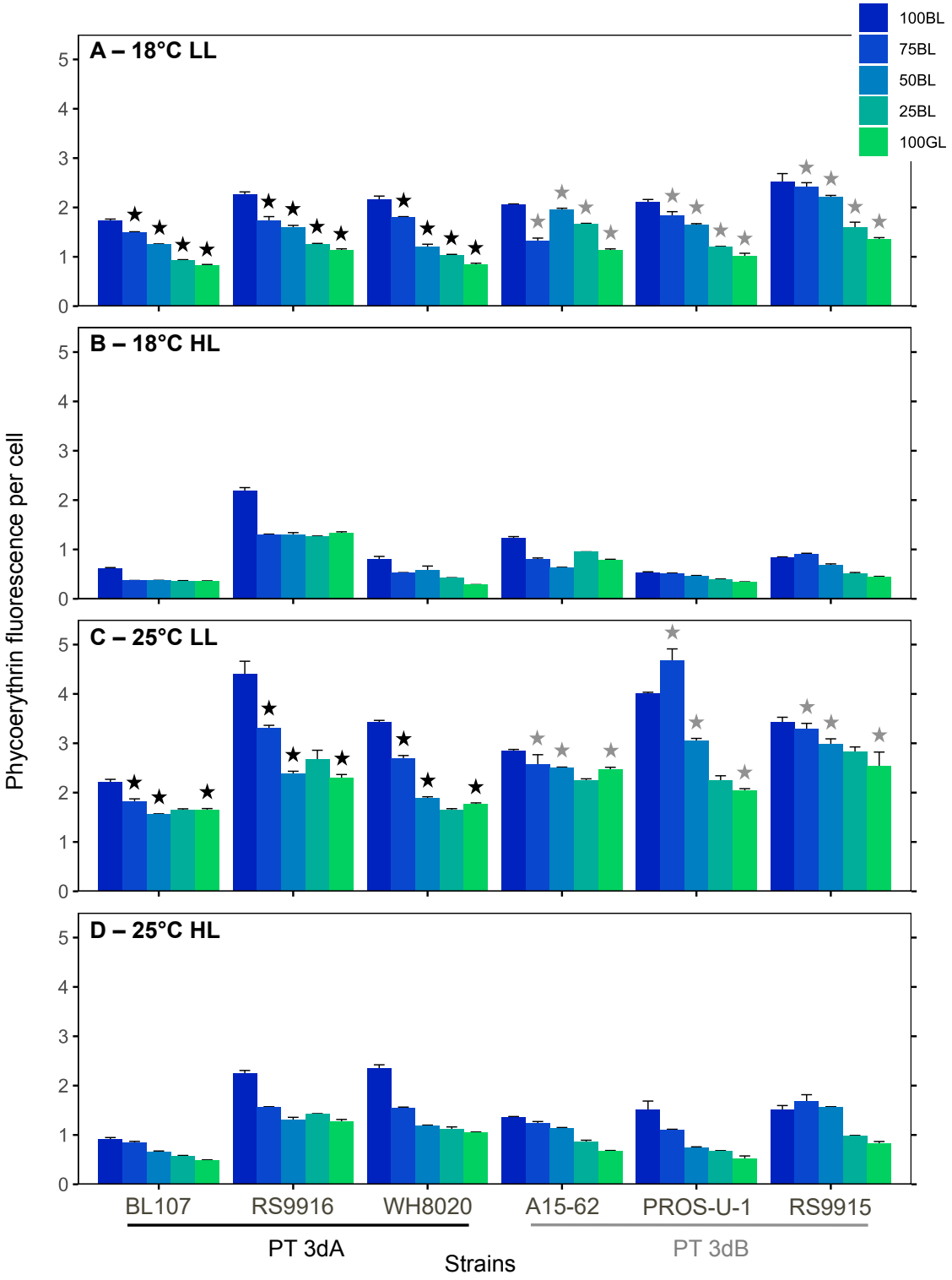

Figure 3: Average flow cytometric phycoerythrin fluorescence per cell of six *Synechococcus* strains grown in different conditions of temperature, light quantity and quality. (A) 18°C low light. **(B)** 18°C high light. **(C)** 25°C low light. (**D**) 25°C high light. Histograms represent average and standard deviations of triplicate measurements. Stars above histograms indicate significantly different values between PT 3dA and 3dB representatives in a given condition of light quality and temperature (Student test or Wilcoxon-Mann-Whitney test, depending on normality and variance homogeneity, p-value < 0.05).

Phycobilin content

As expected, the $Exc_{495:545}$ fluorescence excitation ratio, a proxy of the PUB:PEB ratio of the cells, decreased from 100% BL to 100% GL in all conditions tested (Fig. 4A to D). With a few exceptions, all strains displayed typical $Exc_{495:545}$ ratios for chromatic acclimaters when acclimated to 100% GL (0.6 – 0.7) or 100% BL (1.6 – 1.7; Humily et al., 2013). It is important to note that the LEDs that were used to get the 100% GL condition actually peaked at 515 nm, which is at the blue edge of the green wavelength range (Supplementary Fig. 1). Yet, the fact that all tested chromatic acclimaters exhibited the lowest possible $Exc_{495:545}$ ratio shows that they all 'sensed' this light quality as being GL.

Statistical tests revealed that PT 3dB representatives almost always displayed significantly higher $Exc_{495:545}$ ratios than their PT 3dA counterparts, except in 100 % BL (Fig. 4A to D and Supplementary Fig. 1). Comparison between LL and HL showed that under LL, most cells exhibited progressively decreasing $Exc_{495:545}$ ratios in the three mixed blue-green light conditions (Fig. 4A and C), whereas in HL there was generally a more abrupt shift to a ratio typical of 100% GL acclimation (Fig. 4B and D). As concerns temperature, its effect on PUB:PEB ratios appeared to be much less marked.

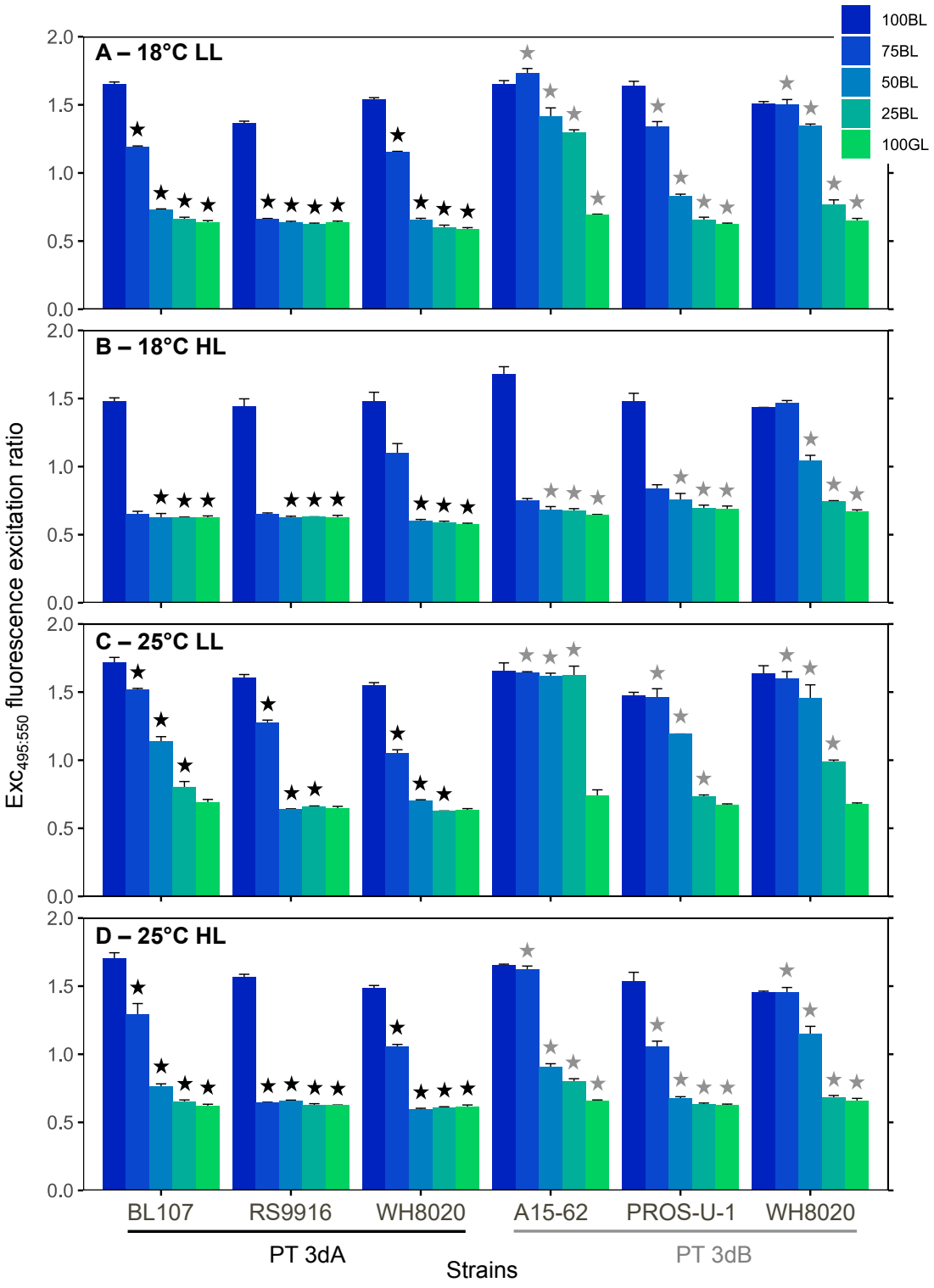

Figure 4: $Exc_{495:545}$ fluorescence excitation ratio (a proxy of PUB:PEB ratio) of six *Synechococcus* strains grown in different conditions of temperature, light quantity and quality. (A) 18°C low light. **(B)** 18°C high light. **(C)** 25°C low light. (**D**) 25°C high light. Histograms represent average and standard deviations of triplicate measurements. The stars above histograms indicate significantly different values between PT 3dA and 3dB representatives in a given condition of light quality and temperature (Student test or Wilcoxon-Mann-Whitney test, depending on normality and variance homogeneity, p-value < 0.05).

Phycobiliprotein content

Two different patterns were identified concerning the variations of $Em_{560:650}$ fluorescence emission ratio, a proxy of PBS PE:PC ratio. Indeed, a decrease in this ratio was most often observed from 100% BL to 100% GL in PT 3dA strains, while it remained fairly stable in PT 3dB representatives, whatever the light color (Fig. 5A to D). The effects of temperature and irradiance were much less clear since the $Em_{560:650}$ ratio did not vary dramatically with these two parameters. Statistically significant differences between PTs 3dA and 3dB were found in a number of conditions, but in contrast to $Exc_{495:545}$ ratio, PT 3dA cells exhibited the highest $Em_{560:650}$ values.

As concerns the $Em_{650:680}$ fluorescence emission ratio, a proxy of the PC:TA ratio, little variations were observed for a given strain, with values always between 1 and 2 whatever the conditions, except for RS9916 that displayed values above 2 (Supplementary Fig. 2A to D). Yet, PT 3dA strains had significantly higher values than their PT 3dB counterparts almost exclusively in HL (Supplementary Fig. 2C and D).

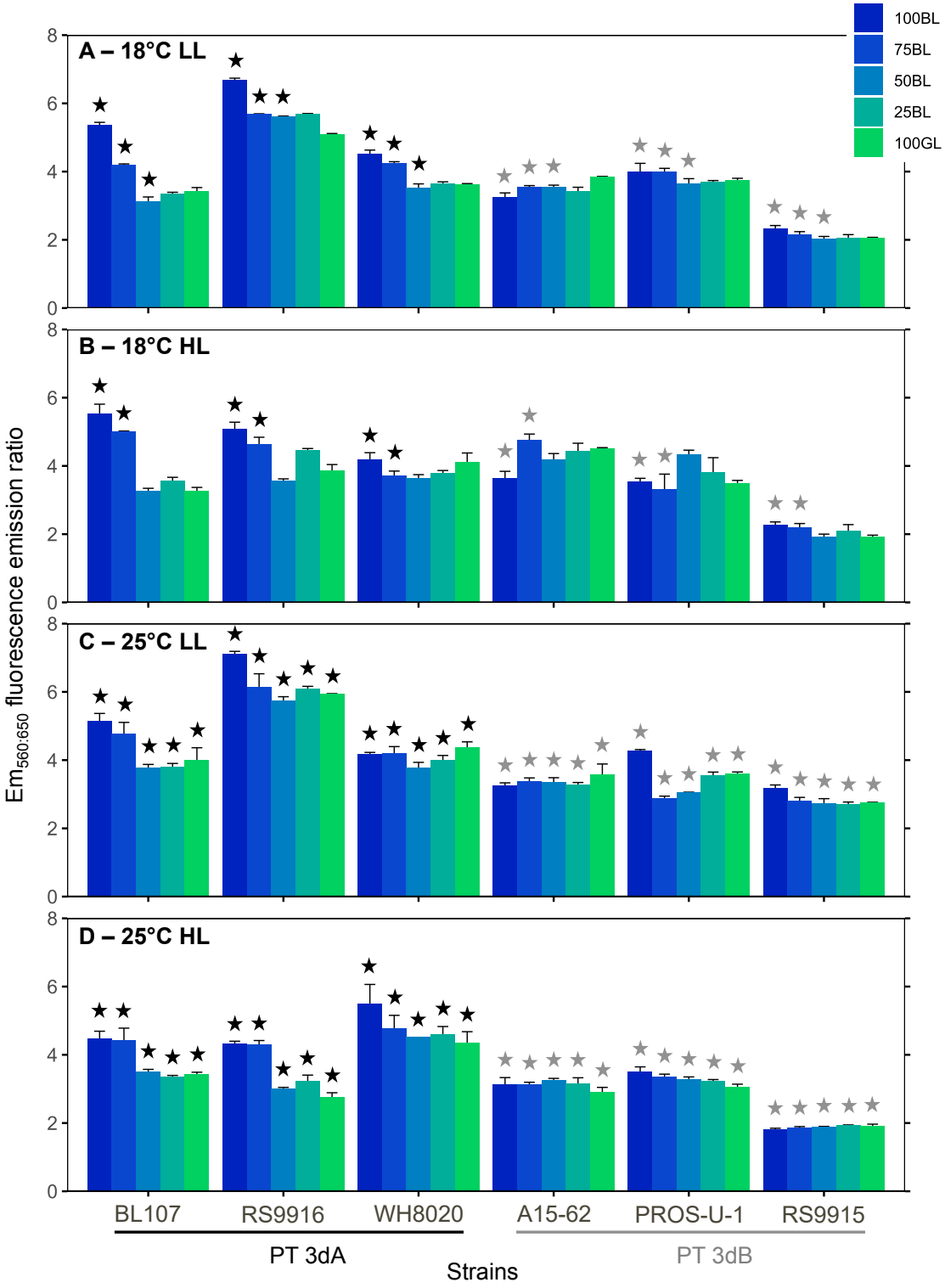

Figure 5: $Em_{560:650}$ fluorescence emission ratios (a proxy of PE:PC ratio) of six *Synechococcus* strains grown in different conditions of temperature, light quantity and quality. (A) 18°C low light. **(B)** 18°C high light. **(C)** 25°C low light. (**D**) 25°C high light. Histograms represent average and standard deviations of triplicate measurements. The stars above histograms indicate significantly different values between PT 3dA and 3dB representatives in a given condition of light quality and temperature (Student test or Wilcoxon-Mann-Whitney test, depending on normality and variance homogeneity, p-value < 0.05).

Cell diameter

In general, the FSC, a proxy of cell diameter, varied little with light quality (Supplementary Fig. 3A to D). As concerns light intensity and temperature, different patterns were observed. For example, the diameter of BL107 seemed to remain constant, regardless of the tested conditions. In others strains, such as PROS-U-1 and RS9915, notable variations in FSC were observed with minimum values achieved for both strains in HL and at 25°C (Supplementary Fig. 3D). Finally, the greatest variations were observed in RS9916 (> 3 times), as well as A15-62 and WH8020 (> 2.5 times), with maximum FSC values in HL but at 18 or 25 °C depending on the strains (Supplementary Fig. 3B and D). Statistical tests showed that PT 3dB cells had significantly larger diameter than PT 3dA strains in some conditions of LL, at 18 and 25°C (Supplementary Fig. 3A and C).

Shift experiments

Shift experiments from GL to BL, and reverse shifts, in either LL or HL conditions were carried out with five PT 3dA and five PT 3dB representatives (Table 1). As expected from a previous study (Humily et al., 2013), the BIOS-U3-1 strain and another representative of the CRD1 clade (MITS9220) did not fully acclimate to HBL and remained stuck at an $Exc_{495:545}$ ratio of about 1.2 (Supplementary Fig. 4B and D). We therefore compared the kinetics and amplitude of $Exc_{495:545}$ variations between PTs 3dA and 3dB with respect to the initial value without including the CRD1 members (Fig. 6A to D). As expected, PT 3dA and 3dB cells exhibited significantly slower kinetics of chromatic acclimation in LL than in HL, CA4 taking about seven days in LL and four days in HL. Furthermore, comparison between the two PTs for a given shift showed that the acclimation kinetics was significantly faster for PT 3dA than PT 3dB from LGL to LBL (Fig. 6A). In contrast, PT 3dB strains exhibited faster acclimation kinetics than their PT 3dA counterparts during the shift from HBL to HGL (Fig. 6D). It is worth noting that, although not significant, similar trends were observed for the two other shift conditions (Fig. 6B and C).

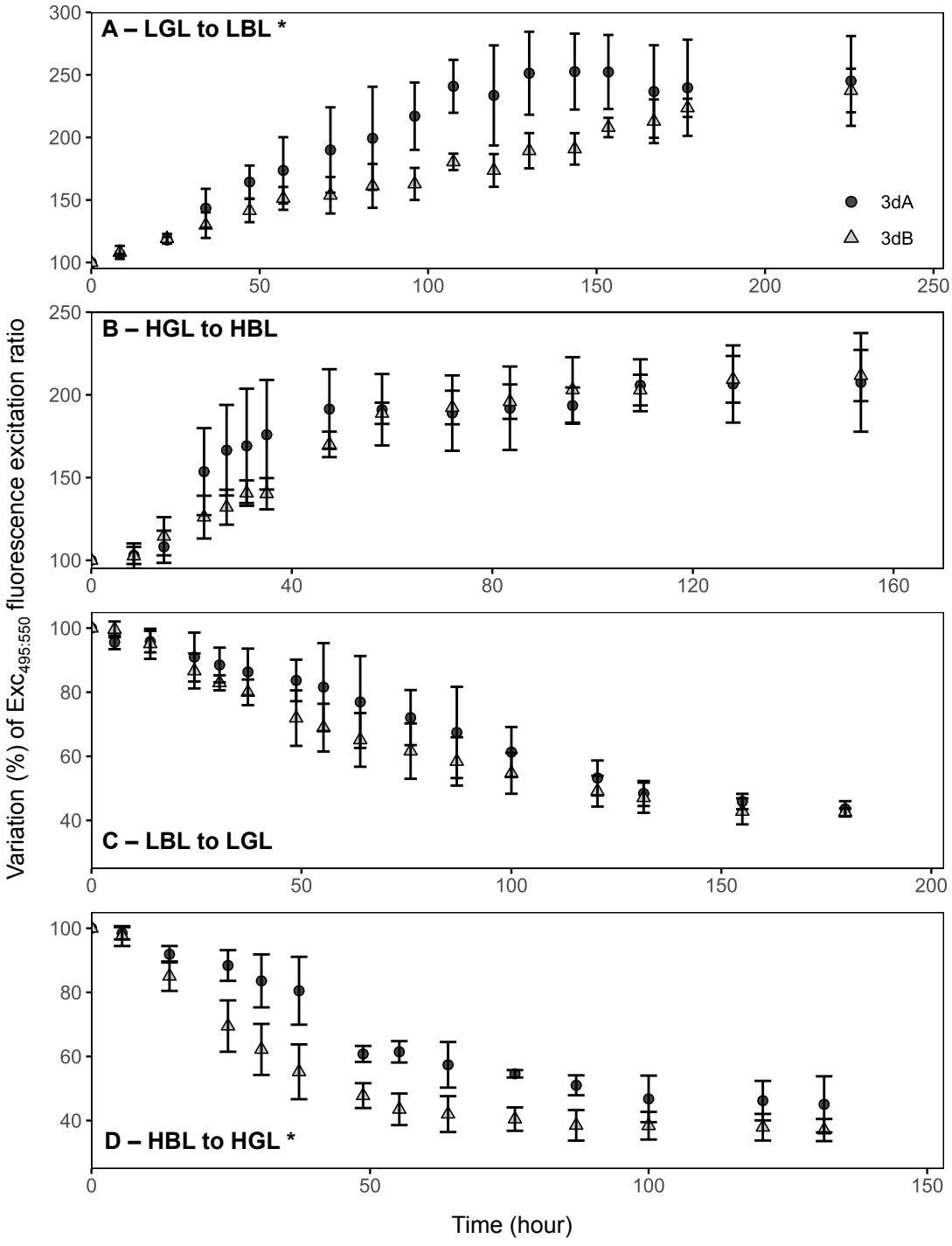

Figure 6: Variation of PUB:PEB compared to initial value of the ten *Synechococcus* strains after an abrupt shift of light quality. (A) LGL to LBL. **(B)** HGL to HBL. **(C)** LBL to LGL. (**D**) HBL to HGL. Each point represents average and standard deviations of three to five measurements. The stars indicate significantly different values between PT 3dA and 3dB representatives (Wilcoxon-Mann-Whitney test, p-value < 0.05).

Discussion

Variations in the underwater light field occur in the upper-lit layer of oceans in response to vertical and horizontal gradients of physico-chemical parameters. These create a number of light niches, to which the different coexisting phytoplankton species are more or less well fitted, depending on their intrinsic pigment content. Recently, Holtrop and collaborators (2021) found that the open ocean shelters five different spectral niches, based on the absorption properties of water molecules as well as the variable concentrations of colored dissolved organic matter and non-algal particles. Thanks to their specific antenna complexes binding divinyl derivatives of Chl *a* and *b* (Ralf and Repeta, 1992), *Prochlorococcus* cells appear to be well adapted to the violet niche (401 – 449 nm), which corresponds to the central oceanic gyres. *Synechococcus* blue light specialists, i.e. cells displaying a high PUB:PEB ratio, are well suited to the blue niche (449 – 514 nm), which encompasses most other marine areas up to polar waters. As concerns green light specialists, i.e. cells displaying a low PUB:PEB ratio, they preferentially thrive in the green niche (514 – 605 nm), which is essentially found in ocean border areas (Holtrop et al., 2021). In this context, *Synechococcus* cells capable of CA4, i.e. to match their PUB:PEB ratio to the ambient light color in order to optimize photon collection, expectedly colonize both the blue and green niches where they can constitute a large part of *Synechococcus* population, especially at high latitude (Xia et al., 2017; Grébert et al., 2018). The occurrence of two genetically distinct types of chromatic acclimaters (Humily et al., 2013; Grébert et al., 2018, 2021, 2022), however made us wonder whether they occupy the very same spectral niche in the marine environment or not. To tackle this question, we looked at the interplay between light quality, light quantity as well as temperature in order to try finding out possible slight differences in pigment phenotypes and/or acclimation kinetics between PTs 3dA and 3dB.

Comparisons of PT 3dA and 3dB cells acclimated to various light qualities ranging from 100% BL to 100% GL at two temperatures and two irradiance levels revealed a number of differences. One of the most striking one was that, in all tested light quality conditions except 100% BL, PT 3dB strains displayed significantly higher $Exc_{495:545}$ ratios than their PT 3dA counterparts, independently of temperature or irradiance levels (Fig. 4). The observed differences are seemingly due to a more progressive decrease of the $Exc_{495:545}$ ratio in intermediate light colors between 100% BL to 100% GL, as well as a slightly higher $Exc_{495:545}$

ratio in the 100% GL condition in PT 3dB than PT 3dA representatives. Indeed, PT 3dA strains were more frequently found in the GL- than the BL-acclimated state with some of them, such as RS9916 in most conditions, even shifting their $Exc_{495:545}$ ratio to the BL-acclimated state only in 100% BL (Fig. 4). In contrast, PT 3dB cells tended to longer remain in the BL-acclimated state, even when the proportion of green light was important, an extreme case being A15-62 at 25°C LL that shifted to the GL-acclimated $Exc_{495:545}$ ratio only in 100% GL (Fig. 4C). Interestingly, it has been hypothesized that the ancestral PT 3dA genotype may have derived from a former GL-specialist having acquired the CA4 capacity by integrating a CA4-A island, while the PT 3dB genotype may have been derived from a former BL specialist having integrated a CA4-B island (Sanfilippo et al., 2019a; Grébert et al., 2021). Our results are consistent with this hypothesis as they suggest that PT 3dA strains need a large proportion of blue photons to induce the CA4-A response, while on the contrary PT 3dB cells require a large proportion of green photons to induce the CA4-B response. In other words, the two PTs seemingly differ in the BL:GL ratio necessary to trigger the CA4 process.

The molecular basis of the difference in PUB:PEB ratio between chromatic acclimaters fully acclimated to either BL or GL has been well documented, and was found to be the same in both the PT 3dA model strain RS9916 (Shukla et al., 2012; Sanfilippo et al., 2016, 2019b) and the PT 3dB model strain A15-62 (Grébert et al., 2021). Both CA4-A and -B processes indeed consist in an exchange of one out of the five phycobilins bound to the α-PE-II subunit (Cys-139) and two out of the six phycobilins bound to the β-PE-II subunit (Cys-83 and Cys-140). More precisely, PUB molecules are bound to these positions in BL, and PEB in GL. However, the observation of intermediate $Exc_{495:545}$ ratios in mixed blue-green light conditions (Fig. 4; see also (Sanfilippo et al., 2019b) remains difficult to interpret, as it may translate different, but not mutually exclusive, sources of variability. Indeed, this observation may be explained by (i) heterogeneous populations of *Synechococcus* cells with PBS either fully acclimated to BL or to GL; (ii) homogeneous populations of *Synechococcus* cells, all having different phycobilins at the three swing sites; (iii) individual cells containing PBS with different chromophorylation states; and/or (iv) heterogeneity in phycobiliprotein chromophorylation within single PBS, i.e. PBS having rods with different chromophorylation states. Unfortunately, there is currently no simple experimental way to demonstrate which of these hypotheses is most likely.

In contrast to light quality, both temperature and irradiance seemingly had little effects on the $Exc_{495:545}$ ratios. In the HL condition, growth rates of all six strains used for acclimation experiments were significantly higher at 25°C (the optimal growth temperature of most marine *Synechococcus* strains tested so far), than at 18°C (Fig. 1), consistent with previous literature (Pittera et al., 2014; Breton et al., 2020; Doré et al., 2020; Ferrieux et al., 2022). Yet, the positive effect of increased temperature on growth rate was much less important at LL than HL, whatever the strain, showing that temperature and irradiance have a synergistic effect on growth of chromatic acclimaters, as previously observed in the model *Synechococcus* PT 3a strain WH7803 (Guyet et al., 2020). Of note, whatever the temperature, all chromatic acclimaters were also able of classical photoacclimation, i.e. to adjust the surface of photosynthetic membranes to reduce the incoming photon flux (Kana and Glibert, 1987; Moore et al., 1995; Six et al., 2004), as shown by the strong decrease of both Chl *a* and PE contents per cell between LL and HL (Fig. 2 and 3). Interestingly, both parameters also slightly decreased in most strains in response to progressive changes in light quality from 100% BL to 100% GL, suggesting that cells used GL more efficiently than BL. They thus needed to slightly adjust the surface of photosynthetic membranes (i.e. both photosystems and PBS) in BL in order to maximize the collection of available photons and maintain their growth rate, which in contrast to pigment ratios did not significantly vary with light quality (Fig. 1). Of note, a direct comparison of the excitation spectra of chromatic acclimaters with LEDs spectra in the different light quality conditions (Supplementary Fig. 1) showed that the light provided by blue LEDs, which peaked at 475 nm, excited both Chl *a* (λ_{max} = 440 nm) and PUB (λ_{max} = 495 nm), but not PEB (λ_{max} = 550 nm). In GL, LEDs emission at 515 nm excited both PUB and PEB (Supplementary Fig. 1). In this context, Lovindeer and co-workers (2021) also recently showed that chromatic acclimaters were characterized by much higher light use efficiency in GL than in BL, often associated with faster growth rate. The latter difference with our results can be explained by the fact that the blue LEDs used in this previous study had a peak at 440 nm, mainly absorbed by Chl *a* (λ_{max} = 440 nm) but very poorly by PUB (λ_{max} = 495 nm), resulting in strong limitation of the production of chemical energy by photosynthesis in their BL condition.

Another parameter that differentiated PTs 3dA and 3dB is the $Em_{560:650}$ fluorescence emission ratio, which is often interpreted as a proxy for the PE:PC ratio. This was significantly

higher in the PT 3dA strains, especially in the bluest light conditions (Fig. 5). Indeed, this ratio tended to decrease from BL to GL in PT 3dA cells, while it was more stable in PT 3dB representatives. Since PE fluorescence per cell decreased in PT 3dA from 100% BL to 100% GL (Fig. 3) and the PC:TA ratio was somewhat constant (Supplementary Fig. 2), this may indicate a lower within-rod energy transfer efficiency than in their PT 3dB counterparts. Another alternative is that PBS rods were progressively shortened from 100% BL to 100% GL in PT 3dA cells but not in PT 3dB. Indeed, the distal PUB-rich PE-II hexamers were previously shown to be eliminated as a result of photoacclimation in *Synechococcus* sp. WH8102 (Six et al., 2004). In PT 3dB representatives, the PE:PC ratio stability, associated with decreasing PE fluorescence, rather suggests that other kinds of structural changes occurred, such as a reduction in the PBS number per cell or in thylakoidal surface area.

Finally, shifts experiment in both LL and HL conditions between 100% BL and 100% GL conditions, and conversely, confirmed previous observations of Humily and collaborators (2013) that PT 3dA cells generally exhibit more variable acclimation kinetics than PT 3dB, especially in HL conditions. Indeed, two PT 3dA strains belonging to the CRD1 clade (BIOS-U3-1 and MITS9220) were stuck at a $Exc_{495:545}$ ratio of around 1.2 in HBL (corresponding to 'phenotypic group 2' in Humily et al., 2013). Moreover, MITS9220 and another PT 3dA representative (BL107) showed a delay in initiation of CA4 from LBL to LGL, but not in the reverse condition, as previously reported for BL107 by these authors and characterized as 'phenotypic group 3'. Furthermore, some PT 3dA strains, common to both studies (RS9916 and WH8020), exhibited different behaviors since these strains reached a significantly lower $Exc_{495:545}$ at HBL than LBL in the previous but not the present study, strengthening the idea that PT 3dA cells have a more variable acclimation phenotype in HBL. In contrast, the majority of PT representatives had typical dynamics, defined by Humily and collaborators (2013) as 'phenotypic group 1'. This difference might be attributed to variability in the genomic localization of the CA4-A island, which can be found virtually anywhere in the genome for PT 3dA strains, including the 5'-end of the PBS region, while the CA4-B island is systematically located in the middle of the PBS rod region on their PT 3dB counterparts (Humily et al., 2013; Grébert et al., 2022). Certainly, the most striking outcome of the shift experiments performed in the present study was the discrepancy in acclimation pace between the two types of chromatic acclimaters, more particularly in two out of four shifts.

Indeed, in the LGL to LBL shift, the PT 3dA representatives reached maximum $Exc_{495:545}$ ratio before PT 3dB strains, while the opposite was observed in the HBL to HGL shift. These results are somehow counterintuitive since during acclimation experiments, PT 3dA cells tended to remain in their basal state (i.e., low $Exc_{495:545}$ ratio) until the BL:GL ratio reached 75 to 100%, and conversely for PT 3dB strains for which the basal state is a high $Exc_{495:545}$ ratio (Fig. 4). Altogether, this could indicate that chromatic acclimaters require a large proportion of photons opposite to their basal state to trigger CA4 process, and that once they are abruptly shifted to the light condition opposite to their basal state (i.e. 100 % BL or GL), the CA4 kinetics is faster than for the other PT (Fig. 6).

In conclusion, our study showed that PTs 3dA and 3dB exhibit subtle differences in their phenotypes, which may explain that in a spectral niche with a mix of blue and green wavelengths, they can coexist not only with blue and green light specialists, but also with their chromatic acclimater counterparts (Huisman et al., 2002; Stomp et al., 2004; Luimstra et al., 2020). Future studies should confirm these hypotheses, either using co-culture experiments of different PTs or by studying the variations of the relative abundance of PTs triggered by changes of the underwater light field.

Data Availability Statement

The authors confirm that the data supporting the findings of this study are available within the article and/or its supplementary materials.

Conflict of interest

The authors declare no conflict of interest.

Author contributions

LD, FP and LG conceived the experiments, analyzed the data and wrote the paper. LD, BG, JC and MR collected the samples and performed the physiological measurements. LD, BG and JC ran the flow cytometry analyses. LD made the figures. All the authors read and approved the final manuscript.

Funding

This work was supported by the French “Agence Nationale de la Recherche” Programs EFFICACY (ANR-19-CE02-0019).

Acknowledgements

We would like to thank Priscillia Gourvil, Martin Gachenot and Michele Grego from the Roscoff Culture Collection (http://roscoff-culture-collection.org/) for maintaining the *Synechococcus* strains used in this study.

Supplementary material

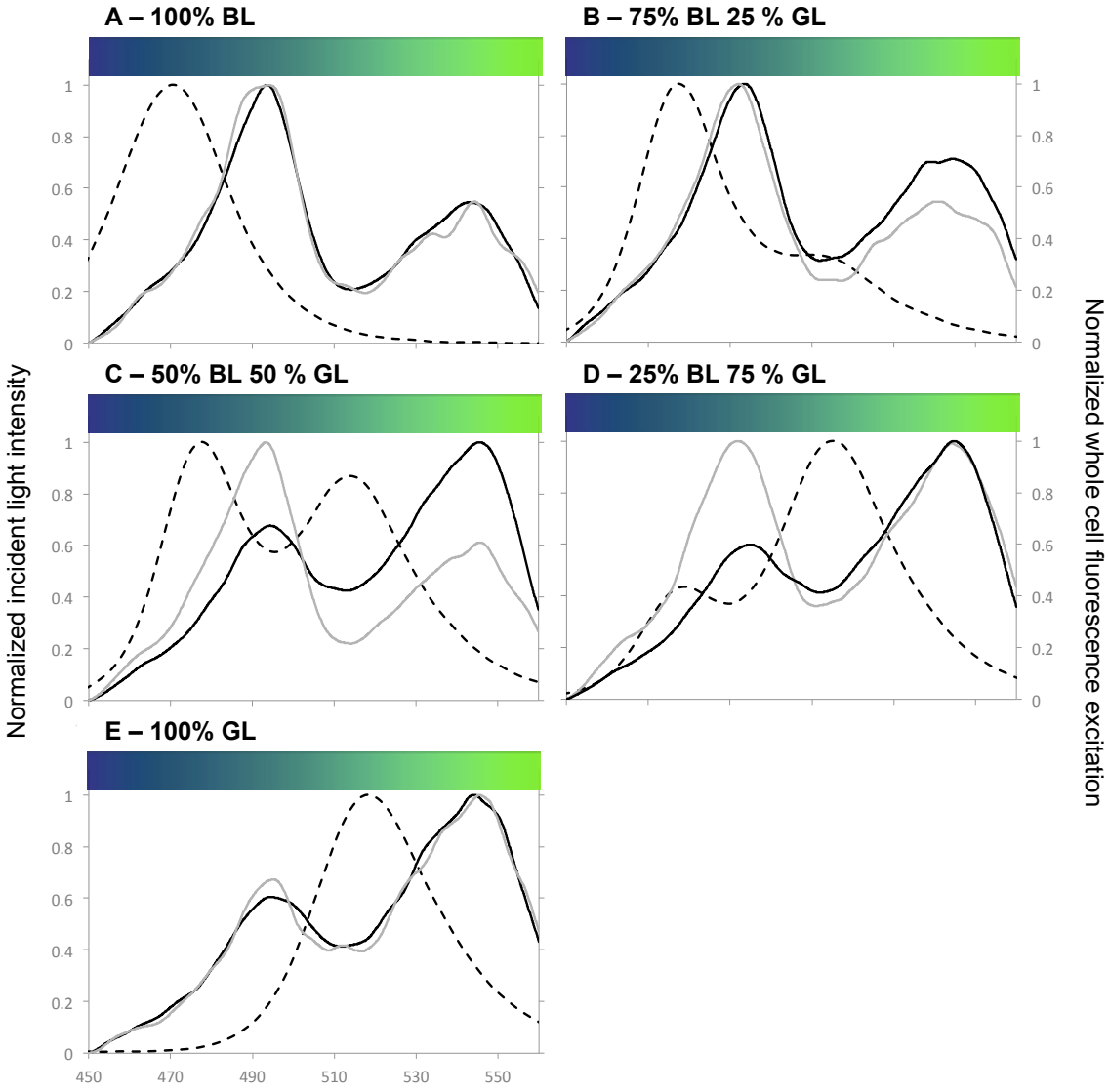

Supplementary figure 1: Representative fluorescence excitation spectra of *Synechococcus* strains RSS9916 (PT 3dA) and RS9915 (PT3 dB) grown in the various mixtures of blue and green light used in this study in low light and at 25°C. (A) 100% BL. **(B)** 75% BL – 25% GL. **(C)** 50% BL – 50% GL. **(D)** 25% BL – 75% GL. **(E)** 100% GL. The LEDs spectra are shown in black dashed line while the excitation spectra of RS9916 and RS9915 are represented by solid dark and light grey lines, respectively.

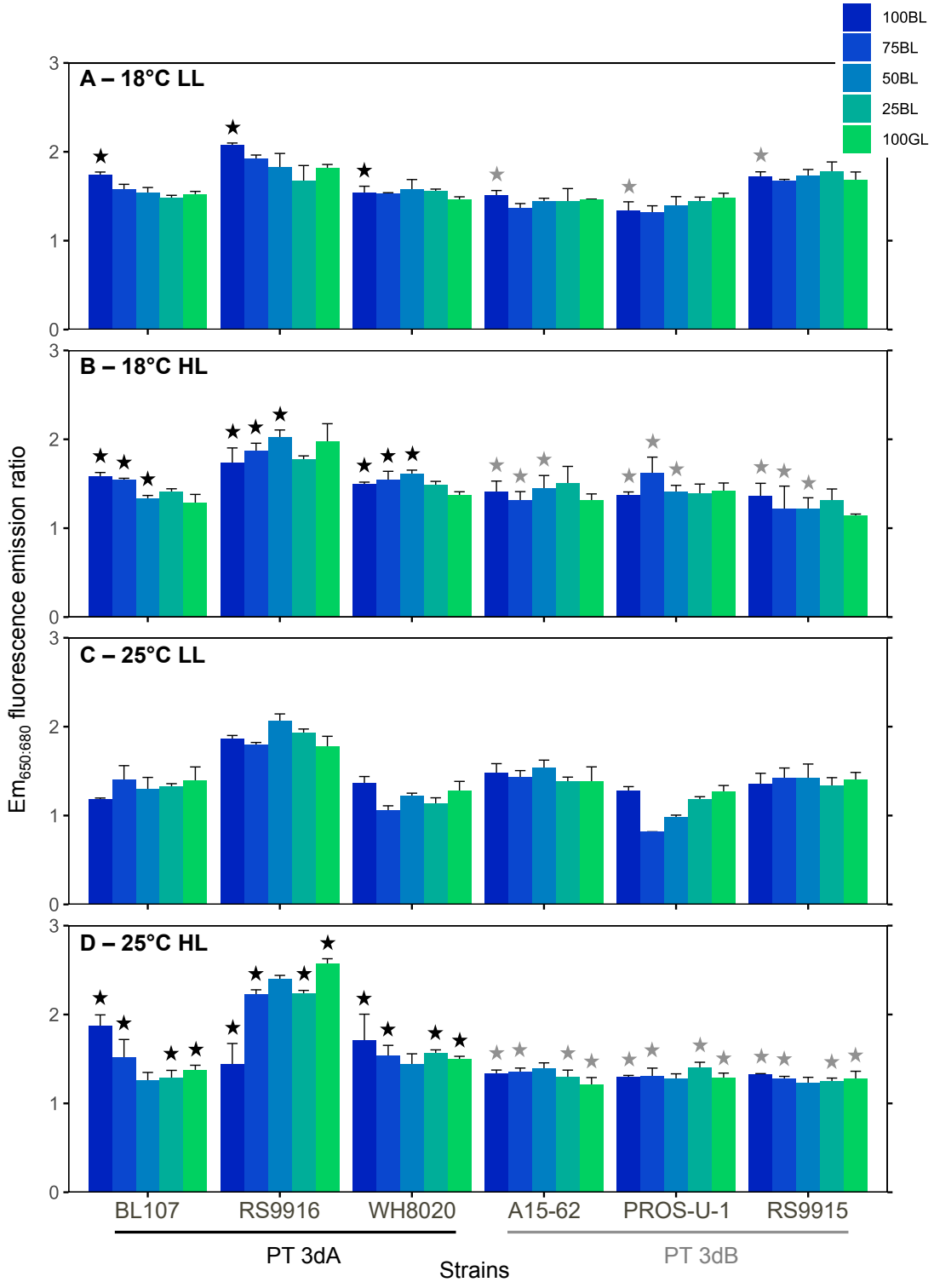

<u>Supplementary figure 2:</u> Average $Em_{650:680}$ fluorescence emission ratio (a proxy of PC:TA ratio) of six *Synechococcus* strains grown in different conditions of temperature, light quantity and quality. (A) 18°C low light. **(B)** 18°C high light. **(C)** 25°C low light. (**D**) 25°C high light. Histograms represent average and standard deviations of triplicate measurements. Stars above histograms indicate significantly different values between PT 3dA and 3dB representatives in a given condition of light quality and temperature (Student test or Wilcoxon-Mann-Whitney test, depending on normality and variance homogeneity, p-value < 0.05).

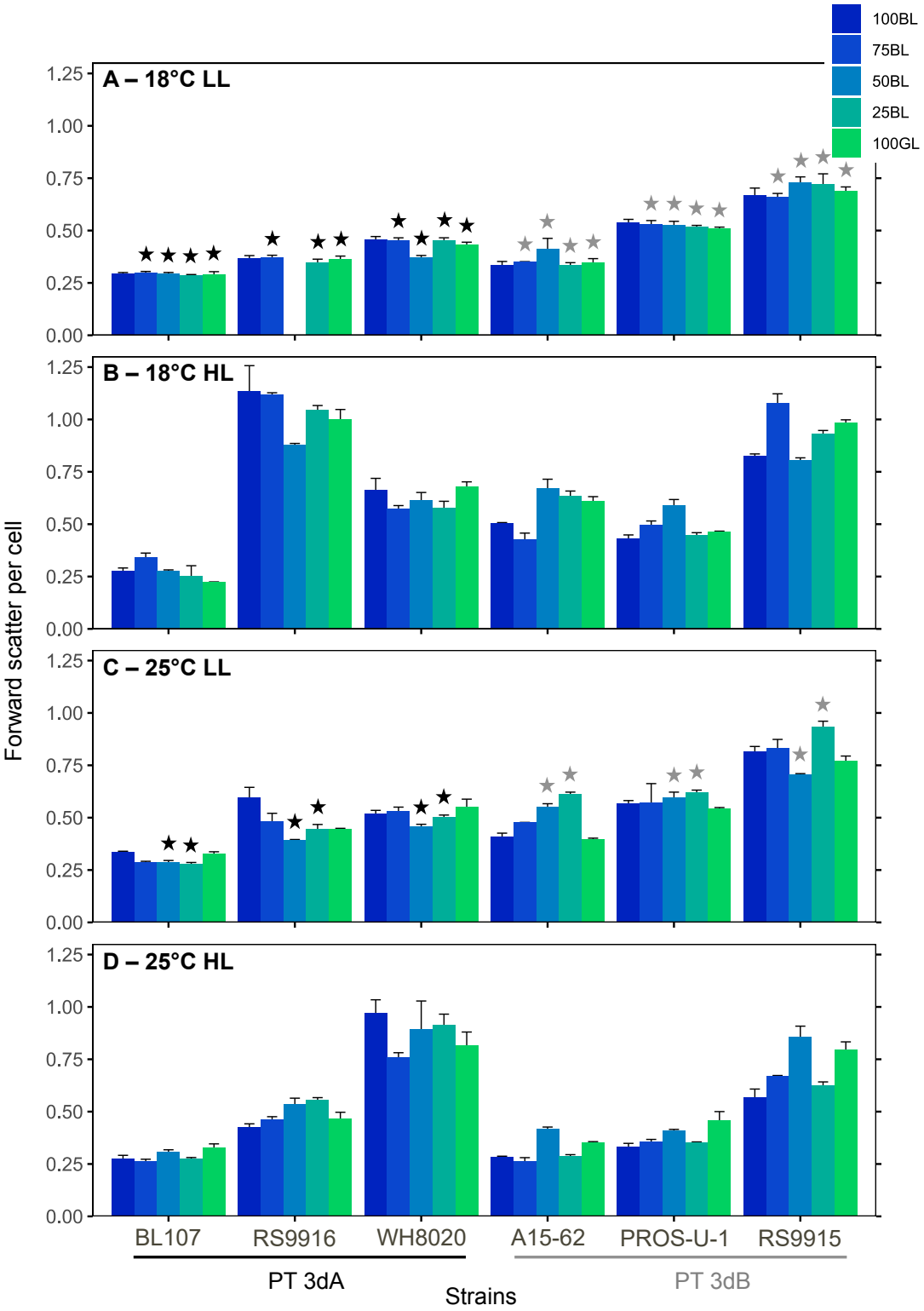

Supplementary figure 3: Average flow cytometric forward scatter (a proxy of cell diameter) of six *Synechococcus* strains grown in different conditions of temperature, light quantity and quality. (A) 18°C low light. **(B)** 18°C high light. **(C)** 25°C low light. (**D**) 25°C high light. Histograms represent average and standard deviations of triplicate measurements. Stars above histograms indicate significantly different values between PT 3dA and 3dB representatives in a given condition of light quality and temperature (Student test or Wilcoxon-Mann-Whitney test, depending on normality and variance homogeneity, p-value < 0.05).

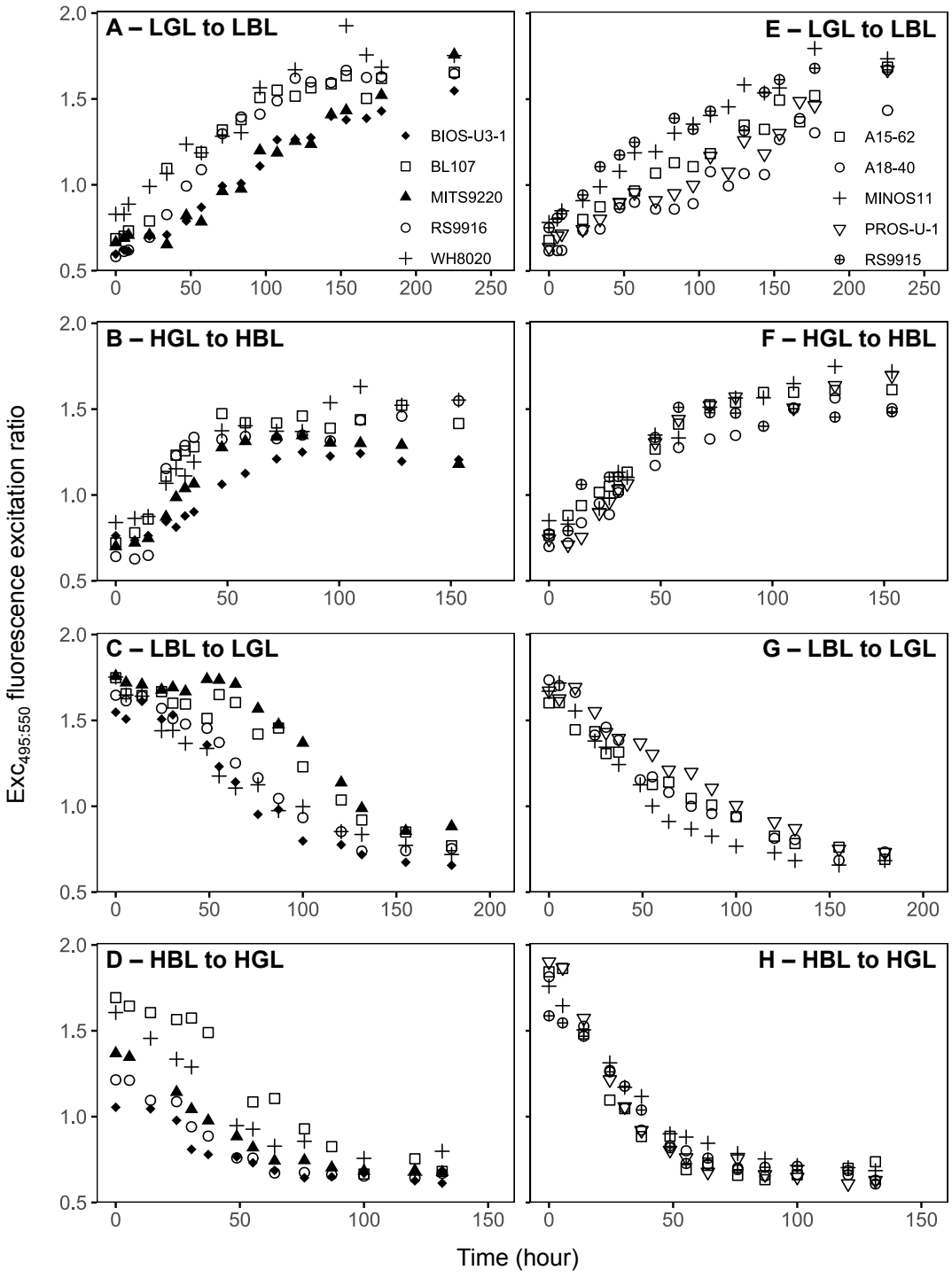

<u>Supplemental Figure 4:</u> $Exc_{495:545}$ fluorescence excitation ratio (a proxy of PUB:PEB ratio) of the ten *Synechococcus* strains after an abrupt shift of light quality. (A, E) LGL to LBL. **(B, F)** HGL to HBL. **(C, H)** LBL to LGL. (**D, H**) HBL to HGL. **(A, B, C, D)** PT 3dA. **(E, F, G, H)** PT 3dB. Each point represents one measurement.

IV. Mono- and co-culture experiments

Competition for light color between marine *Synechococcus* strains with fixed and variable pigmentation

Louison Dufour[1], Laurence Garczarek[1], Francesco Mattei[2], Bastian Gouriou[1], Julia Clairet[1], Morgane Ratin[1], David M. Kehoe[3], Jef Huisman[4], Jolanda Verspagen[4] and Frédéric Partensky[1]

[1]Sorbonne Université, CNRS, UMR 7144 Adaptation and Diversity in the Marine Environment (AD2M), Station Biologique de Roscoff (SBR), Roscoff, France.

[2]Laboratoire d'Océanographie de Villefranche (LOV), Institut de la Mer de Villefranche (IMEV), Villefranche-sur-Mer, France.

[3]Department of Biology, Indiana University, Bloomington, IN 47405.

[4]Department of Freshwater and Marine Ecology (FAME), Institute for Biodiversity and Ecosystem Dynamics, University of Amsterdam, Amsterdam, the Netherlands.

*** Correspondence:**

Corresponding Author: F. Partensky

Keywords: Marine picocyanobacteria, *Synechococcus*, pigment type, chromatic acclimation, competition

Introduction

Marine phytoplankton accounts for about half of global primary production. However, this contribution is highly variable spatially depending upon community composition, which itself strongly fluctuates with environmental conditions (Field et al., 1998; Behrenfeld et al., 2006). Despite its apparent continuity, the world's oceans are composed of many different ecological niches, delineated mostly by temperature gradients and changes in the relative availability of two types of essential resources for which phytoplankton taxa compete: light and nutrients. Light, which provides the energy required for photosynthesis, varies both quantitatively and qualitatively in the water column. The exponential decrease of light

irradiance with depth is indeed accompanied by a progressive narrowing of the visible light spectrum. The latter also strongly varies horizontally from coastal particle-rich to clear open ocean waters (Kirk, 1992; Stomp, 2008). Recently, Holtrop and collaborators (2021) defined five distinct light niches in aquatic ecosystems (violet, blue, green, orange and red niches), the first three being most frequently encountered in the marine environment. In this context, competition for light among phytoplankton species has triggered a wide diversification of both photoprotective pigments needed to cope with strong irradiances in the upper euphotic layer and photosynthetic pigments used to collect Photosynthetically Active Radiations (PAR). This wide pigment diversity allows different phytoplankton taxa to coexist by collecting distinct parts of the visible light spectrum, that is, by spectral niche differentiation (Stomp et al., 2004; Striebel et al., 2009). A striking example of this pigment diversification can be seen in marine *Synechococcus*. With an estimated global abundance of 7×10^{26} cells, this ubiquitous picocyanobacterium is the second organism in the world's ocean (Flombaum et al., 2013) and exhibits the largest pigment diversity known so far within a single phytoplankton lineage (Six et al., 2007b; Humily et al., 2013; Grébert et al., 2022).

Like most other cyanobacteria, *Synechococcus* use large hydrophilic light-harvesting complexes called phycobilisomes (PBS) to collect photons and transfer their energy to photosystems (PS) I and II (Glazer, 1989; Ong and Glazer, 1991). *Synechococcus* PBS are comprised of a core from which extend six to eight peripheral rods. Both core and rods are made of alpha-beta heterodimers of phycobiliproteins held together by linker proteins. While the PBS core is predominantly composed of allophycocyanin (APC, absorption wavelength maximum λ_{max} = 652 nm), rods can be made of either phycocyanin (PC, λ_{max} = 620 nm), or a combination of PC and one to two additional types of phycoerythrin (PE-I and PE-II, λ_{max} = 560 nm; (Ong and Glazer, 1991; Six et al., 2007b). These phycobiliproteins covalently bind one to three types of chromophores: phycocyanobilin (PCB, λ_{max} = 650 nm), phycoerythrobilin (PEB, λ_{max} = 550 nm) and phycourobilin (PUB, λ_{max} = 495 nm; Sidler, 1994). Based on the variation in PBS composition among *Synechococcus* strains, different pigment types (PTs) have been defined, with PT 1 possessing only PC, PT 2 containing both PC and PE-I, and PT 3 having PC, PE-I and PE-II. PT 3 was further divided into subtypes, based on their relative content of PEB and PUB. In subtype 3a, the PUB:PEB ratio, as estimated by the

relative ratio of fluorescence excitation at 495 and 545 nm with emission set at 580 nm, is low ($Exc_{495:545} < 0.5$), while it is high ($Exc_{495:545} \geq 1.6$) in subtype 3c and variable in subtype 3d (Six et al., 2007b; Humily et al., 2013). The pigmentation of PT 3a and 3c strains remain fixed in changing light qualities so they are usually referred as 'blue light (BL) specialists' and 'green light (GL) specialists', respectively (Sanfilippo et al., 2016). PT 3d strains are capable of reversibly modifying their $Exc_{495:545}$ ratio from 0.6 in BL to 1.6 in GL, a process that typically occurs over several days and is called 'Type IV chromatic acclimation' (hereafter CA4; Palenik, 2001; Everroad et al., 2006). Two phenotypically close but genetically distinct types of chromatic acclimaters (PTs 3dA and 3dB) have been described (Humily et al., 2013). Each possesses a ca. 4-5 kilobase pair genomic island called CA4-A or CA4-B, respectively. These islands contain one gene encoding a phycobilin lyase (*mpeZ* or *mpeW*, respectively), one gene encoding a protein of unknown function (*unk10*) and two genes that encode regulatory proteins (*fciA* and *fciB*; Sanfilippo et al., 2016). A gene encoding a third putative regulator (*fciC*) is found in the CA4-A island only (Humily et al., 2013). The mechanistic differences between the two CA4 processes have recently begun to be deciphered. In both cases, part of the mechanism involves competition between two enzymes that attach a different phycobilin at cysteine-83 of the PE-II alpha subunit. In the CA4-A process, the BL-expressed lyase-isomerase MpeZ attaches a PUB at this position in BL, replacing the activity of the constitutively expressed lyase MpeY, which attaches a PEB to the same site in GL (Shukla et al., 2012; Sanfilippo et al., 2019b). Conversely, in the CA4-B process, the GL-expressed lyase MpeW attaches a PEB to Cys-83 of α-PE-II in GL, replacing the activity of the constitutively expressed lyase-isomerase MpeQ, which attaches a PUB to the same site in BL (Grébert et al., 2021). It has been suggested that the acquisition of the CA4-A island conferred the ability to chromatically acclimate to GL specialists, and that the CA4-B island conferred the same ability to BL specialists (Sanfilippo et al., 2019a; Grébert et al., 2021). The ecological significance of the CA4 process long remained elusive due to the lack of an effective method to discriminate CA4-A and CA4-B strains from GL and BL specialists. However, using three different PBS gene markers, Grébert and collaborators (2018) were recently able to quantify the relative abundances of the different *Synechococcus* PTs throughout much of the world's oceans by using metadata from the *Tara* Oceans expedition transect. The authors demonstrated that CA4 cells accounted for 41.5% of total marine *Synechococcus* population,

with CA4-A and CA4-B capable strains being almost equally abundant (22.6 and 18.9%, respectively) but colonizing complementary light niches in the field. Interestingly, CA4-A capable cells dominate in temperate and high latitude waters while CA4-B able cells are more abundant in warm tropical waters. By comparison, the GL and BL specialists were found to represent 20.3% and 33.4%, respectively, of the global *Synechococcus* population. The former was shown to prefer near-coastal particle-rich waters, where green light predominates, while the latter colonize clear open ocean waters, where blue wavelengths are the more abundant (Stomp, 2008; Grébert et al., 2018).

The prevalence of chromatic acclimaters in marine ecosystems suggests that, in particular light conditions, CA4 may confer a fitness advantage that allow them to co-occur with, and even sometimes outgrow, cells with fixed pigmentation. To test this hypothesis, we performed continuous mono- and co-culture experiments of a BL specialist, a GL specialist and a chromatic acclimater in light-limited chemostats (Huisman et al., 2002) under different conditions of light quantity (15 and 75 µmol photons m^{-2} s^{-1}) and quality (blue and green). To better understand the distinct adaptive values of each PT, we also carried out a series of photo-physiological measurements on each strain in all conditions tested. A similar approach was previously used to study competition for light between a red-orange absorbing (PT 1) *Synechococcus*, a green-absorbing (PT 2) *Synechococcus* and a marine filamentous cyanobacterium capable of 'Type III chromatic acclimation' (CA3), which involves changing its PBS absorption maximum from red to green by modifying the composition of its rods from phycocyanin only to mostly phycoerythrin (Stomp et al., 2004, 2008). Here, we demonstrated that the chromatic acclimater outcompetes cells with fixed pigmentation in high blue light (HBL) and grows as well as a GL specialist in a high blue-green light (HBGL) mixture.

Materials and Methods

Biological material and culture conditions

Three *Synechococcus* strains, a GL specialist (RS9907, PT 3a), a BL specialist (RS9902, PT 3c) and a CA4-strain (RS9915, PT 3dB; Table 1) were selected from the Roscoff Culture

Collection (https://roscoff-culture-collection.org/). All were isolated from the upper mixed layer at Station A in the Gulf of Aqaba (Red Sea) in 1999, but at different seasons (Fuller et al., 2003). Cells were grown in PCR-S11 medium (Rippka et al., 2000) supplemented with 175 µM K_2HPO_4,$3H_20$ and 2 mM $NaNO_3$ to avoid any nutrient deprivation.

TABLE 1: Characteristics of the marine *Synechococcus* strains used in this study.

Strain name	**RS9902**	**RS9907**	**RS9915**
RCC #[1]	2676	2382	2553
Subcluster[2]	5.1	5.1	5.1
Clade[2]	II	II	III
Subclade[2]	IIa	IIa	IIIa
Pigment type[3]	3c (BL specialist)	3a (GL specialist)	3dB (CA4 strain)
Isolation date[4]	1999-03-29	1999-08-23	1999-10-18

[1]Roscoff Culture Collection, [2]Farrant et al. (2016), [3]Humily et al. (2013), [4]Fuller et al. (2003).

Before starting the experiments, cultures were pre-acclimated for at least one month in temperature-controlled chambers at 25°C to the five different light conditions tested in this study: low blue light (LBL), low green light (LGL), high blue light (HBL), high green light (HGL) and high blue-green light (HBGL). Low (LL) and high light (HL) conditions corresponded to 15 and 75 µmol photons m^{-2} s^{-1} (hereafter µE), respectively. Spectra of incident light and maximum emission wavelengths (λ_{maxBL} = 475 nm, λ_{maxGL} = 515 nm) are illustrated in Figure 1. Continuous light was provided by blue and/or green LEDs (Alpheus).

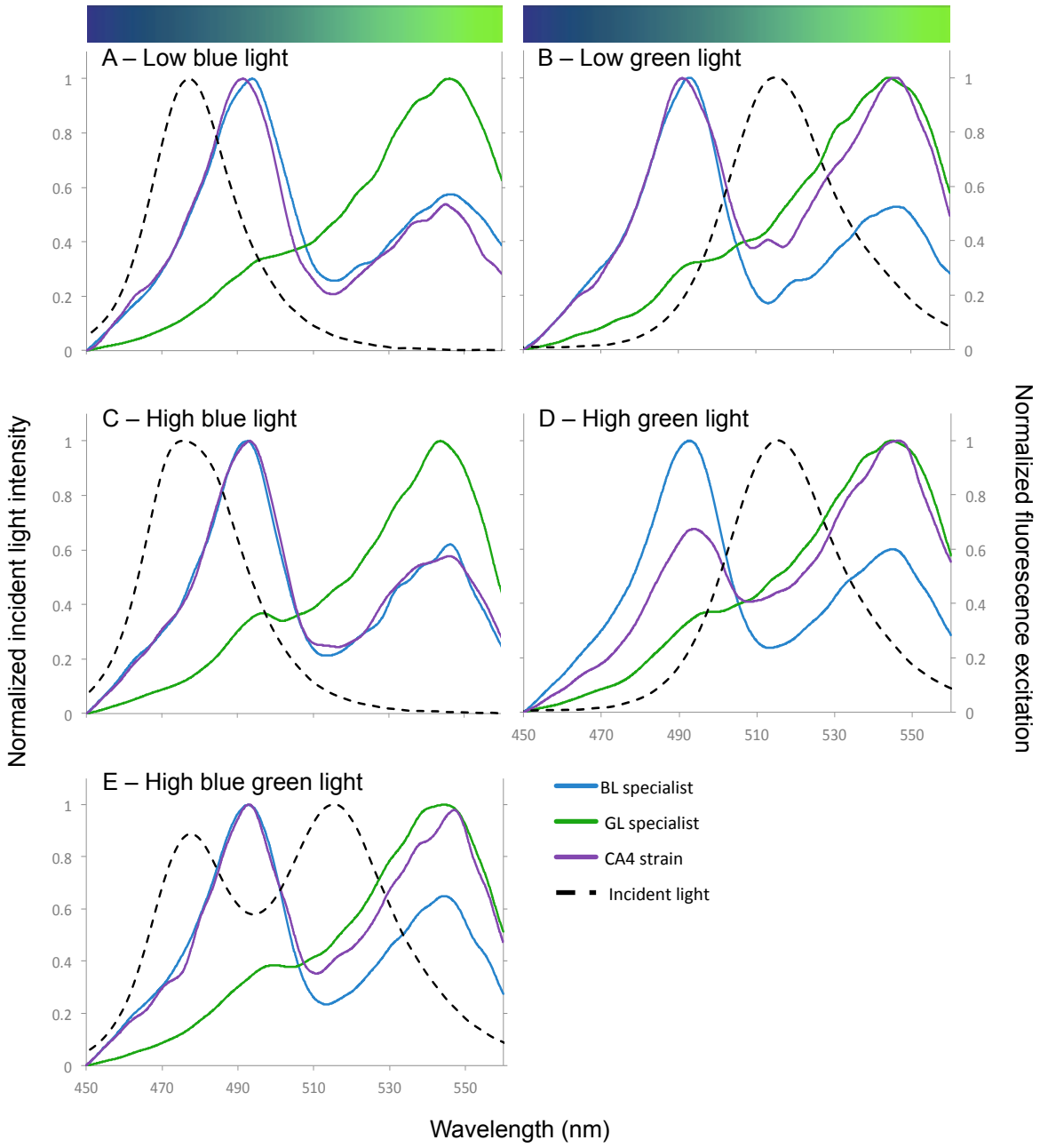

<u>Figure 1:</u> Representative fluorescence excitation spectra of the three *Synechococcus* strains grown in the different light conditions used in this study. (A) Low blue light. **(B)** Low green light. **(C)** High blue light. **(D)** High green light. **(E)** High blue green light. The LEDs spectra are shown in black dashed line while the excitation spectra of the green light specialist, the blue light specialist and the chromatic acclimater are represented in green, blue and purple solid lines, respectively.

For each light condition, mono- and co-cultures of the three *Synechococcus* PTs were grown in light-limited chemostats (Huisman et al., 2002) inoculated at an initial cell density of 3×10^6 cells mL^{-1} of each strain, so that co-cultures started with an initial concentration of

9×10^6 cells mL^{-1}. Cells were continuously diluted in Pyrex® Roux flasks (SCI Labware) for 30 to 60 days until the culture reached steady state, i.e. at least five consecutive days with less than 10% variation in cell density (Burson et al., 2018). Each flask was equipped with a 5-inlet silicone cap for (i) passive ventilation through a 0.2 µm air filter (Midisart 2000, Sartorius), (ii) continuous supply (41.67 µL min^{-1}, corresponding to a dilution rate of 0.1 day^{-1}) of PCR-S11 medium using peristaltic pumps (Ismatec Reglo ICC, Cole-Parmer), (iii) continuous removal of the overflow so that the volume remained constant over time, (iv) bubbling with 3% CO_2-enriched air to control the pH of the cultures and avoid carbon deficiencies, and finally (v) sample collection (Fig. 2). All experiments were done in biological replicates unless specified otherwise.

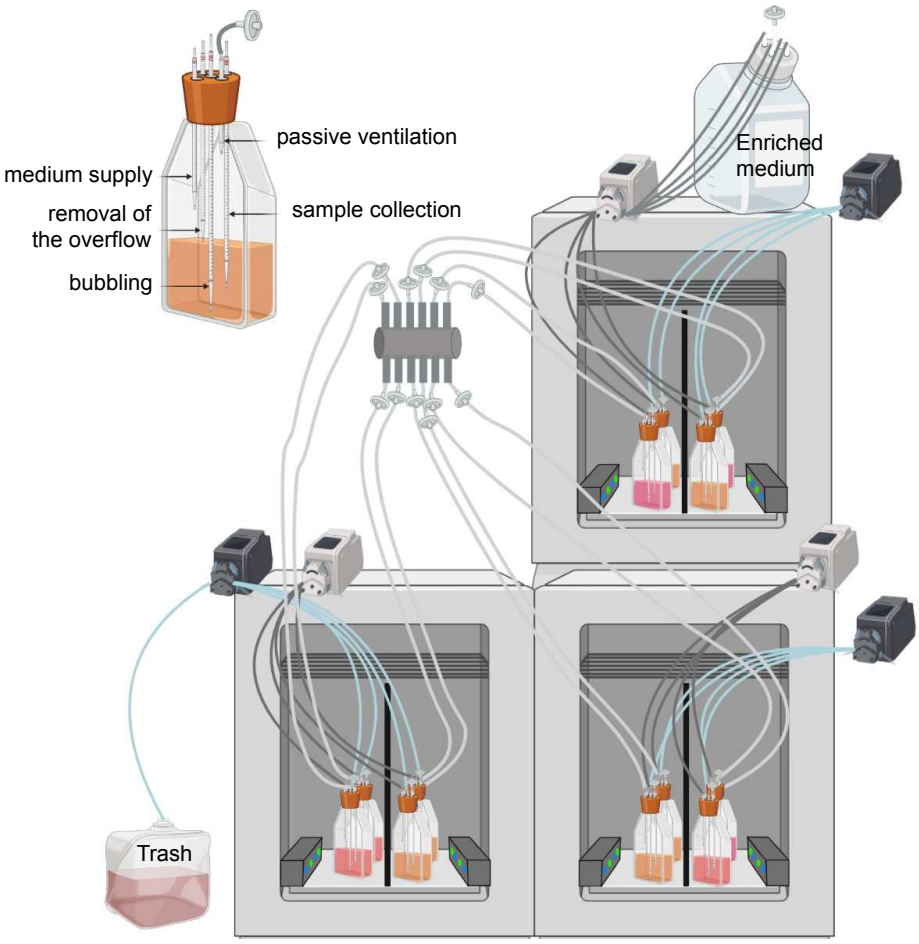

Figure 2: Experimental set-up for mono- and co-cultures in continuous dilution. (Created with BioRender.com).

For each mono and co-culture, samples were harvested every day or two to measure *Synechococcus* cell concentration, PSII quantum yield, pigment ratio and pH. Light intensity transmitted through the flasks was also recorded using a PG200N Spectral PAR Meter (UPRtek). In addition, 5 mL aliquots from each of the co-cultures were collected at the same frequency, filtered through 0.2 µm Supor filters (Pall Life Sciences) and kept at -80 °C until analysis by real-time quantitative PCR. Other measurements were carried out more punctually, as described below.

Synechococcus cell density

Culture aliquots were sampled every day, fixed using 0.25% (v/v) glutaraldehyde (grade II, Sigma Aldrich) and stored at −80°C until analysis (Marie et al., 1999a). *Synechococcus* cell densities were determined using a Guava easyCyte flow cytometer equipped with a 488 nm laser and the Guavasoft software (Luminex Corporation).

Photosynthetically Active Radiation (PAR) measurements

Before starting the experiments, the incident light intensity (I_{in}) integrated over 400 – 700 nm and the light transmission through the flasks filled with fresh PCR-S11 medium were measured with a PG200N Spectral PAR Meter (UPRtek). During the experiments, the light intensity transmitted through the flasks (I_{out}) as well as the light absorption spectra were measured daily with the same device.

Fluorimetry

PSII quantum yield

Measurements of the PSII quantum yield (F_V/F_M), a proxy of the maximum photosynthetic activity of the cells, were carried out three times per week with a multi-wavelength fluorimeter Phyto-PAM II (Walz), as previously described (Pittera et al., 2014) except that five wavelengths (440, 480, 540, 590, or 625 nm) of modulated light were used.

PSII cross-section

The PSII cross-section σ(II), which represents the effective size of photosynthetic antennae, was measured once during the experiments (growth phase) and only in mono-cultures. The O-I1 fluorescence fast kinetics, which refers to the increase of fluorescence yield induced by a strong actinic light, was recorded with a Phyto-PAM II, as described elsewhere (Six et al., 2021). PSII cross-section values at 480 (cyan) and 540 (green) nm ($\sigma(II)_{480nm}$ and $\sigma(II)_{540nm}$, respectively) were calculated using the Phytowin 3 software (Walz; (Schreiber et al., 2012).

PSII electron transport

Like the PSII cross-section, the linear electron transport rate through PSII (ETRII) was measured once during the growth phase of mono-cultures. Measurements were done at 480 and 540 nm, the two wavelengths most used by *Synechococcus*. As described by Six and collaborators (2021), the basal fluorescence F_0 was recorded before samples were exposed to 13 steps of increasing light irradiance (90 sec each). At the end of each step, the instantaneous (F_t) and maximal (F_M') fluorescence levels were recorded, allowing the computing of PSII quantum yield under illuminated conditions (F_V'/F_M'). The ETRII ($e^-PSII^{-1}s^{-1}$) at each step was calculated as follows:

$$ETRII = \frac{\left(\left(\frac{F_{V'}}{F_{M'}}\right) \times \sigma(II)_{\lambda nm} \times I \times 0.6022\right)}{\frac{F_V}{F_M}}$$

With I, instantaneous irradiance at a defined step (Schreiber et al., 2012).

Finally, ETRII values for each step were plotted against their corresponding light irradiance. In fitting the photosynthesis Platt model (Platt and Gallegos, 1980), several parameters such as the initial slope (α), which refers to PSII efficiency under non-saturating light, the saturation irradiance (E_K) and the maximum PSII electron transport rate ($ETRII_{max}$) were computed (Six et al., 2021).

PUB:PEB ratio determination

In vivo fluorescence spectra were recorded once during the exponential phase using a spectrofluorimeter FL6500 (Perkin-Elmer) and analyzed with the Fluorescence software (Perkin-Elmer), as described elsewhere (Dufour et al., 2023). Briefly, excitation spectra were acquired between 450 and 560 nm (with emission set at 580 nm) and emission spectra between 550 and 750 nm (with excitation set at 530 nm). The $Exc_{495:545}$ fluorescence excitation ratio was then used as a proxy for the PUB:PEB ratio and the $Em_{560:650}$ and $Em_{650:680}$ emission ratios to estimate the PE to PC ratio and the PC to PBS terminal acceptor (TA) ratio, respectively. PE:PC ratios provided insights into the electron transfer efficiency within the PBS and the length of PBS rods and PC:TA ratios into the coupling between the PBS and PSII reaction center chlorophylls.

Quantification of different pigment types in co-culture

Faced with the impossibility of differentiating pigment types under some conditions (and more particularly under BL where the chromatic acclimater and the BL specialist had too similar fluorescence signals), a real-time quantitative PCR approach was developed to follow the abundances of the three pigment types within the co-cultures.

Design of the probes and optimization

For each strain, a couple of primers were designed using Geneious® (version 11.0.5). Targeted genes were selected as being: (i) single copy, to readily derive cell numbers from gene copy numbers, and (ii) strain-specific, based on phyletic patterns in the Cyanorak information system (Table 2; Garczarek et al., 2021). Each couple of primers was tested for specificity and optimized (annealing temperature, primers concentration) using DNA extracted from cultures of the three studied strains.

TABLE 2: Real time PCR primers used in this study.

Strain	RS9902	RS9907	RS9915
Gene name	n.a.	*cpeF*	*mpeW*
Product	bacterial Ig-like domain-containing protein	PEB:Cys-50,61 beta-phycoerythrin lyase	PEB:Cys-83 alpha-phycoerythrin II lyase
Cyanorak cluster	CK_00042914	CK_00008055	CK_00020700
Forward primer	qRS9902_CK_00042914_5389F	qRS9907_cpeF_679F	qRS9915_mpeW_841F
Sequence	GGAGCAGGTCTAGAAGCGAT	ATGGGCAAGCTCAACGAAAG	GGCATAGAGACGAAGAACGC
Reverse primer	qRS9902_CK_00042914_5445	qRS9907_cpeF_791R	qRS9915_mpeW_890R
Sequence	GTCGACTCCTAATGCTCCGA	TCCTCCAGTTTCATCAGCGA	TTAGACCAGAAACCGGCCAA
Product size (bp)	57	113	69

Sample collection

Five mL of each co-culture was sampled daily, filtered through 0.2 µm Supor filters of 25 mm diameter (Pall Life Sciences) and stored in 2 mL Eppendorf tubes at -80°C until analysis.

Cell lysis, extraction and purification of DNA from co-culture samples

DNA was extracted from 0.2 µm Supor filters following a protocol adapted from Tai and Palenik (2009) and Gutiérrez-Rodríguez and collaborators (2014). After thawing the filters on ice, 350 µL of lysis buffer (50 mM TRIS, 20 mM EDTA, pH 8.0) and a 5 mm steel bead were added to each Eppendorf. The samples were then grounded for 30 sec at 30 Hz using a TissueLyser (MM300, Retsch) to break the cell wall. To ensure complete cell lysis, filters were incubated under homogenization with 175 µL lysozyme (50 mg mL^{-1}, Sigma-Aldrich) for 45 min at 37°C. 70 µL of SDS (10%, Invitrogen) and 35 µL of proteinase K (20 mg mL^{-1}, Sigma-Aldrich) were added and filters were again incubated under homogenization for 2.5 h at 55°C. RNA was removed by adding 70 µL of RNAse (20 mg mL^{-1}, Sigma-Aldrich) during 10 min

at room temperature. Right after, the filters and the aqueous phases were transferred to 2 mL Phase Lock GelTM tubes (PGL, QuantaBio, VWR). To dissolve the filters, increase DNA extraction efficiency and get rid of protein contaminants, two phenol:chloroform:isoamyl alcohol (25:24:1; Eurobio) and one chloroform:isoamyl alcohol (24:1; Sigma-Aldrich) extractions were performed in a row. For each of them, 700 µL of phenol mix was added to the PGL tubes which were subsequently centrifuged for 5 min at 1500 x *g* and 18°C using an Eppendorf 5417R. Between each extraction, the aqueous phase was gently recovered and transferred to new PGL tubes. Finally, the DNA in the aqueous phase was purified using silica gel columns (DNeasy Blood and Tissue Kit, Qiagen) following the manufacturer's protocol for Gram-negative bacteria. DNA was eluted in 200 µL nuclease-free water (Invitrogen). DNA 260:280 and 260:230 ratios were measured using a ND-1000 spectrophotometer (Nanodrop).

Preparation of real time PCR standards from Synechococcus *cultures*

Template DNA was obtained from exponential phase cultures harvested by centrifugation in presence of 0.01% Pluronic acid (Sigma-Aldrich). Samples were centrifuged at 4°C, 14 000 x *g* for 10 min using an Eppendorf 5804R. A volume of 200 µL of ATL buffer (Qiagen) was added to the pellets before a grinding step using a 5 mm steel bead, as described above. Then, samples were incubated under homogenization with 10 µL lysozyme (50 mg mL^{-1}) for 45 min at 37°C. After addition of 200 µL of AL buffer (Qiagen) and 15 µL of proteinase K (20 mg mL^{-1}), samples were then incubated under homogenization for 2.5 h at 55°C. Right after, a volume of 200 µL ethanol 100% (Sigma-Aldrich) was added to the samples, which were vortexed and then purified using silica gel columns (DNeasy Blood and Tissue Kit, Qiagen) following the manufacturer's instructions. DNA was eluted in 100 µL nuclease free water. As for the co-culture samples, DNA 260:280 and 260:230 ratios, as well as concentrations, were quantified using a ND-1000 spectrophotometer.

Real time PCR

Reactions for real time PCR were prepared by mixing 6 µL of ONEGreen® FAST qPCR Premix (Ozyme), 0.12 µL of forward and reverse primers stock (300 µmol L^{-1}, Eurogentec), 0.76 µL of nuclease free water and 5 µL of template DNA. Template DNA for the standard curves was serially diluted 10-fold over 7 orders of magnitude to obtain standard concentrations ranging from 50 to 5.10^{-6} ng per well. Template DNA from co-cultures samples was not diluted. Each reaction was performed in triplicate. Real-time SYBR Green fluorescence data were acquired using a LightCycler® 480 (Roche) and the program recommended by the manufacturer. The baseline and threshold cycle (C_t) were estimated automatically with the 'Abs Quant/2^{nd} Derivative Max' program of the LightCycler® 480 software (version 1.5.0, Roche). For co-culture samples, each quantification cycle (C_q) was converted to DNA concentration based on the standard curve equation. The number of target gene copy per well was then estimated using the formula of Dhanasekaran and collaborators (2010) and converted to copy per mL based on the volumes of filtered co-culture, DNA elution and template DNA added in each well. Results were expressed as percentage of each strain at any given time of the co-culture experiment.

Determination of pigment content

Volumes of 100 mL of each mono-culture were harvested in presence of 0.01% pluronic acid once during growth phase. Samples were processed as described elsewhere (Ferrieux et al., 2022) with the following changes: (i) 100 mL of cultures were harvested by two cycles of centrifugation at 4°C, 14 000 x *g* for 10 min using an Eppendorf 5804R; (ii) an additional step was added during which pellets were resuspended and transferred to 15 mL tubes and centrifuged one more time under the same conditions; (iii) pellets were then resuspended and transferred to 2 mL Eppendorf tubes and centrifuged at 4°C, 14 000 x *g* for 7 min using an Eppendorf 5417R. Samples were stored at -80°C until analysis. As previously described (Partensky et al., 2018), pellets were resuspended in 100% cold methanol (Sigma-Aldrich) and centrifuged twice at 4°C, 14 000 x *g* for 7 min to get rid of all debris. Extracts were brought to 10% Milli-Q water and injected in a High-Performance Liquid Chromatography

1100 Series System (Hewlett-Packard) equipped with a C8 column (Waters) to analyze liposoluble pigment content.

Biovolume

For each tested light condition, the biovolume of each strain was estimated in steady state using an Eclipse 80i fluorescence microscope equipped with a Cy3 filter (Nikon). Photographs were taken at x100 magnification using a SPOT RT3 camera (Diagnostic Instruments Inc.) under GL excitation (λ = 550 nm) to observe their natural orange fluorescence. Analysis of the photographs was done with SpotAdvanced software (Diagnostic Instruments Inc.) to measure the length (L) and width (W) of 100 cells. Biovolume (V, μm^{-3}) was calculated assuming that *Synechococcus* cells have a 'tic-tac' shape, using the following formula:

$$V = (L - W) \times \pi \times (W/2)^2 + [4/3 \times \pi \times (W/2)^3]$$

Dissolved nutrient analyses

To ensure that mono- and co-cultures were not nutrient limited, phosphate, nitrate and ammonium concentrations were quantified in steady state following standardized protocols (Aminot and Kérouel, 2007; Oriol et al., 2014).

Comparative genomics

The repertoire of genes involved in the biosynthesis or regulation of phycobilisome components was compared between the three marine *Synechococcus* strains using the Cyanorak genome database (Garczarek et al., 2021; www.sb-roscoff.fr/cyanorak/). The phycobilin lyase content was then used to predict the chromophorylation of each phycobiliprotein subunit based on current literature on lyase function.

Results

Strain growth

Mono-cultures

Under low light conditions, comparison of the growth of *Synechococcus* strains in LBL showed that the BL specialist grew faster and thus reached maximum cellular concentrations (~6.7 x 10^7 cells mL^{-1}) around the 20^{th} day of monitoring (Fig. 3A). The chromatic acclimater reached similar cell densities (~6.8 x 10^7 cells mL^{-1}) in steady state, but only after 50 days of continuous culture. Despite several attempts (n=10), the GL specialist was not able to grow in continuous dilution in this specific light condition. In contrast, it grew well in LGL and reached high cell concentrations (~1.2 x 10^8 cells mL^{-1}; Fig. 3D). However, the LGL condition was clearly limiting the growth of the two other strains. In the sole successful trial, the chromatic acclimater density stabilized at a much lower plateau (~1.7 x 10^7 cells mL^{-1}) than the GL specialist. As concerns the BL specialist, it failed to reach a steady state even after 60 days of continuous culture.

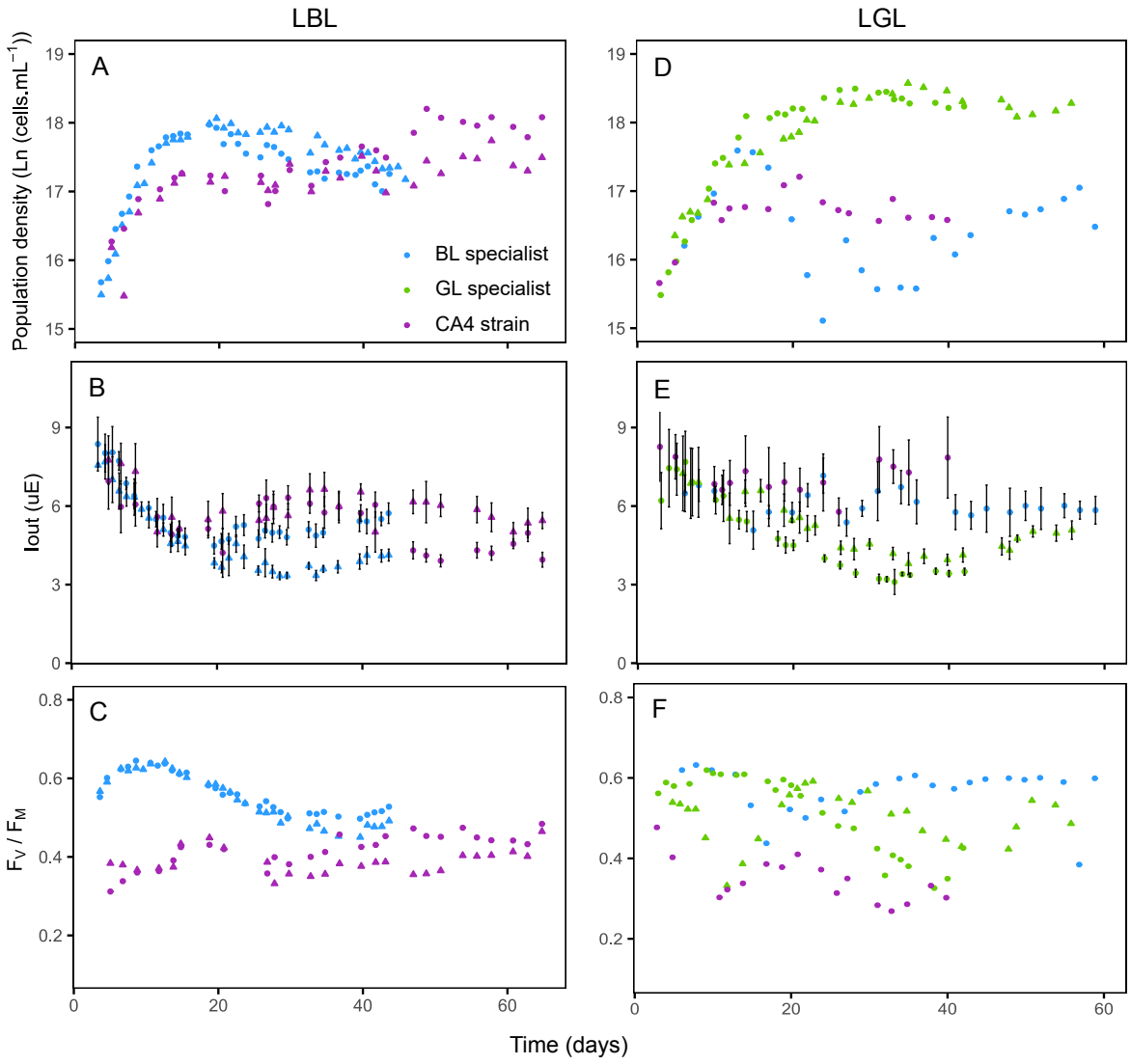

<u>Figure 3:</u> Mono-cultures of marine *Synechococcus* strains representative of different pigment types in low light conditions. (A-C) Low blue light. **(D-F)** Low green light. **(A, D)** Cell concentration. **(B, E)** Light transmission (I_{out} in µmol photons m^{-2} s^{-1}). **(C, F)** Photosystem II quantum yield (F_V/F_M). Error bars in panels B and E correspond to the average and standard deviation of five different light measurements on the side of the flask opposite to the light source. Shapes indicate the different replicates of each strain.

Three high light conditions were tested, namely 100% blue light (HBL), 100% green light (HGL) and an intermediate ratio of both (HBGL; Fig. 1E). In HBL, the BL and GL specialists grew faster than the chromatic acclimater, the BL specialist reaching its highest cell concentrations (~9.6 x 10^8 cells mL^{-1}) two weeks after the beginning of the experiments (Fig.

4A). However, the three PTs stabilized at similar cell densities in steady state (~2.2 x 10^8 cells mL^{-1}). In HBGL, the specialists had comparable growth kinetics and stabilized at similar cell numbers (~5.2 x 10^8 cells mL^{-1}) while the chromatic acclimater grew more slowly and reached a lower plateau (~1.9 x 10^8 cells mL^{-1}; Fig. 4D). Finally, in HGL, while both specialists grew faster than the chromatic acclimater at the beginning of the monitoring and reached high densities around day 6, the maximum cell concentration (~6.3 x 10^8 cells mL^{-1}) was achieved by the GL specialist and the chromatic acclimater in steady state (Fig. 4G).

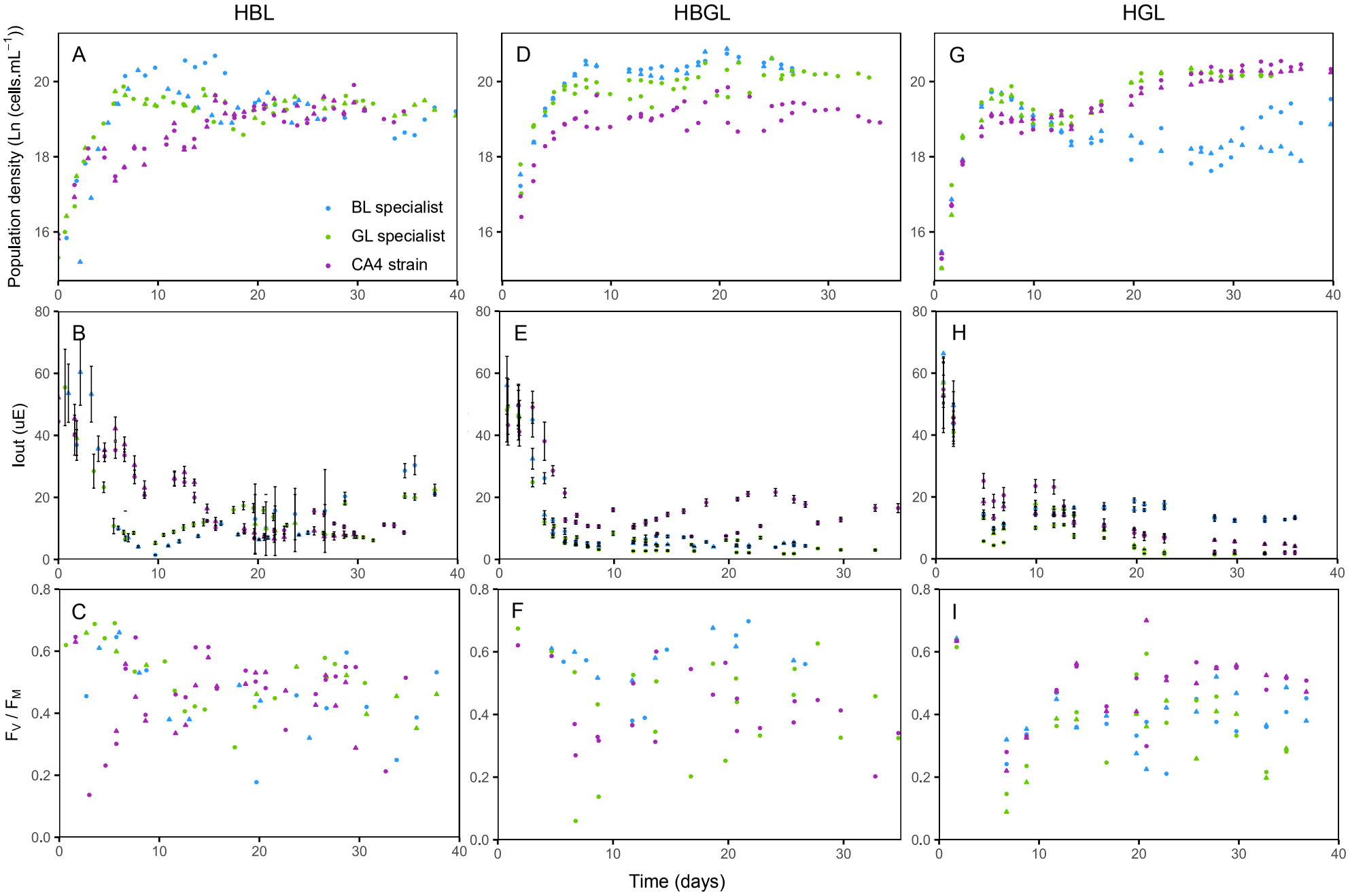
HBL
HBGL
HGL
A
B
C
D
E
F
G
H
I
Population density (Ln (cells.mL^{-1}))
Iout (uE)
F_V / F_M
Time (days)
BL specialist
GL specialist
CA4 strain

Figure 4: Mono-cultures of marine *Synechococcus* strains representative of different pigment types in high light conditions. (A-C) High blue light. **(D-F)** High blue-green light. **(G-I)** High green light. **(A, D, G)** Cell concentration. **(B, E, H)** Light transmission (I_{out} in µmol photons m^{-2} s^{-1}). **(C, F, I)** Photosystem II quantum yield (F_V/F_M). Error bars in panels B, E and H correspond to the average and standard deviation of five different light measurements on the side of the flask opposite to the light source. Shapes indicate the different replicates of each strain.

Co-cultures

When the three strains were grown in co-culture in LL conditions, the specialist of the tested light color always won the competition while the two other strains disappeared more or less quickly. Yet, consistent with data from mono-cultures, the chromatic acclimater seemingly maintained itself in the mixture slightly longer in LBL than LGL, and the BL specialist was less rapidly diluted out in LGL than the GL specialist in LBL (Fig. 5A and D).

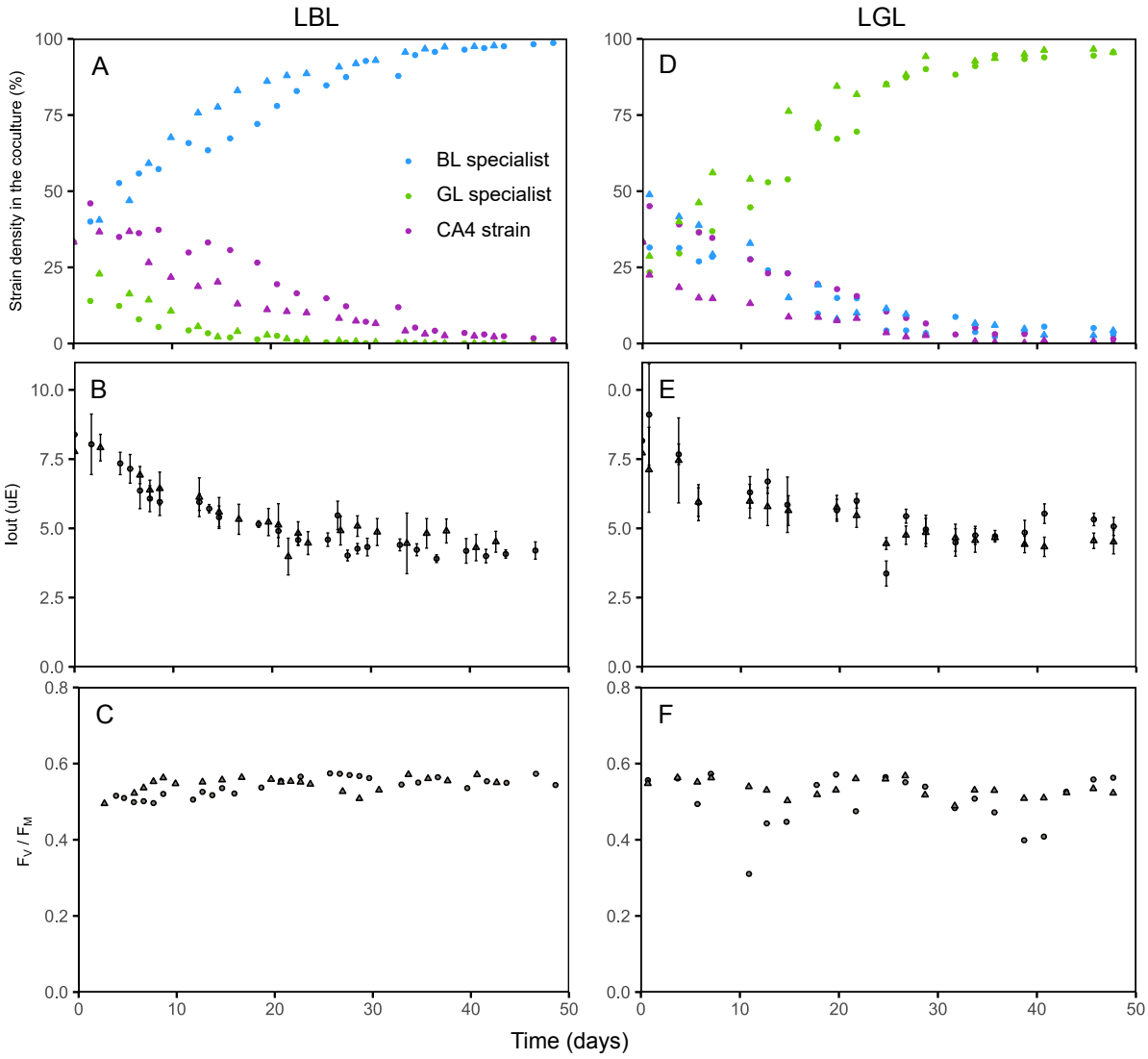

Figure 5: Co-cultures of marine *Synechococcus* strains representative of different pigment types in low light conditions. (A-C) Low blue light. **(D-F)** Low green light. **(A, D)** Cell proportion. **(B, E)** Light transmission (I_{out} in µmol photons m^{-2} s^{-1}). **(C, F)** Photosystem II quantum yield (F_V/F_M). Error bars in panels B and E correspond to the average and standard deviation of five different light measurements on the side of the flask opposite to the light source. Shapes indicate the different replicates of each strain.

The temporal dynamics of the different strains in co-culture were more variable between replicates in HL than LL conditions, but in all cases one strain was generally able to take over the two other strains. In HBL, the BL specialist was the most abundant strain for the 10 first days before being overgrown by the chromatic acclimater, which at the end of the experiment represented 85% to 90% of the total *Synechococcus* population (Fig. 6A). In

HBGL replicate 1, the GL specialist grew fast and quickly supplanted the other two strains (Fig. 6D). In HBGL replicate 2, the BL specialist was the most abundant strain for 10 days, before being gradually replaced by the GL specialist. Interestingly, the latter represented about 70% of the total population at the end of the monitoring in both replicates, while the chromatic acclimater accounted for the last 30%, suggesting that different PTs may co-exist in certain light conditions. In HGL replicate 1, the chromatic acclimater grew fast and was the most abundant strain in the mixture for over two weeks, representing more than 60% of total *Synechococcus* population, while the BL specialist crashed (Fig. 6G). In replicate 2, it was the latter that represented 25% to 40% of the total population during the first two weeks of the experiment, while the chromatic acclimater crashed. Still, in both replicates, the two strains ended up being completely outcompeted by the GL specialist, which was the only remaining strain at the end of the monitoring.

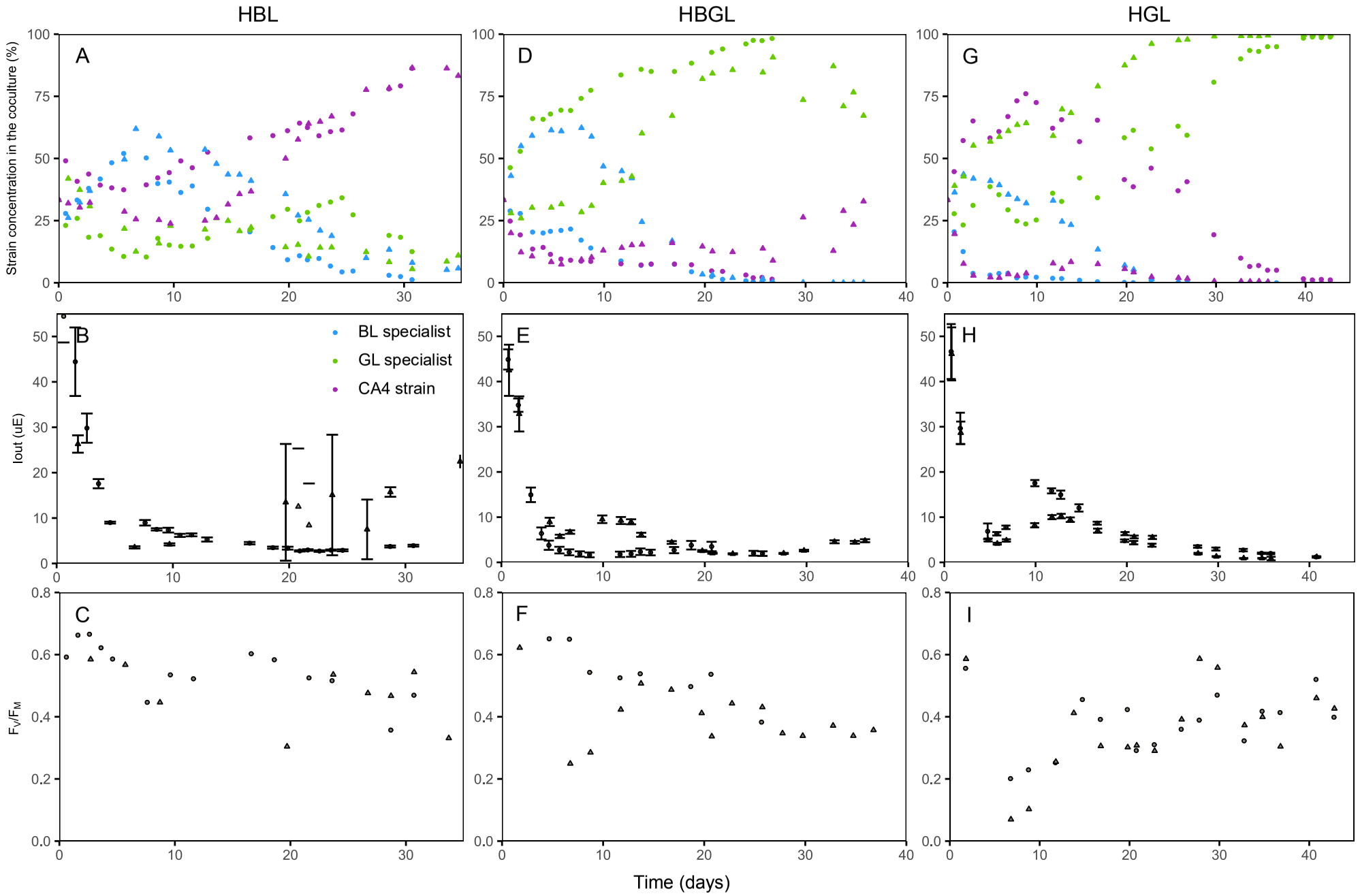
HBL
HBGL
HGL
A
B
C
D
E
F
G
H
I
Strain concentration in the coculture (%)
Iout (uE)
F_V/F_M
Time (days)
BL specialist
GL specialist
CA4 strain

Figure 6: Co-cultures of marine *Synechococcus* strains representative of different pigment types in high light conditions. (A-C) High blue light. **(D-F)** High blue-green light. **(G-I)** High green light. **(A, D, G)** Cell proportion. **(B, E, H)** Light transmission (I_{out} in µmol photons m^{-2} s^{-1}). **(C, F, I)** Photosystem II quantum yield (F_V/F_M). Error bars in panels B, E and H correspond to the average and standard deviation of five different light measurements on the side of the flask opposite to the light source. Shapes indicate the different replicates of each strain.

Light environment

Light transmission and critical light intensities

The lowest critical light intensity (I^*_{out}), i.e. the light penetrating through the culture measured at steady state (Huisman and Weissing, 1994; Huisman et al., 1999), reached very similar values for the BL specialist and the chromatic acclimater in LBL (5.3 ± 0.3 and 4.98 ± 0.8; Fig. 3B). The same pattern was observed in HBL (Fig. 4B), with I^*_{out} reaching 8.91 ± 1.7 for the BL specialist, 8.12 ± 1.0 for the GL specialist and 8.56 ± 1.5 for the chromatic acclimater. In the three other conditions, the lowest critical light intensities were observed for the GL specialist (3.90 ± 0.6 in LGL, 1.64 ± 0.2 in HGL, 2.63 ± 0.5 in HBGL; Fig. 3E and 4E, H).

Light quality

The spectra of light transmitted through each flask indicated that the light quality varied during the experiments in HL but not significantly in LL conditions (Supplementary Fig. 1 and 2), where the maximal biomass at steady state was lower. Indeed, a shift of the absorption peak of a few nanometers (515 – 516 to 520 nm) was observed during the HGL experiments in mono-cultures of the BL specialist (Supplementary Fig. 2I) and the chromatic acclimater (Supplementary Fig. 2K). This pattern also occurred in HBGL for all cultures, more or less intensely, the most important shift (516 to 522 nm) being associated with the BL specialist (Supplementary Fig. 2E to H). In these intermediate conditions, variations in the BL:GL light ratio ($I_{out\ 477:515}$) also occurred. Indeed, the $I_{out\ 477:515}$ decreased from 0.7 to 0.09 and from 0.7 to 0.31 during the course of the GL specialist and CA4-strain monoculture experiments, respectively. The opposite scenario was observed for the GL specialist with an increase in the

$I_{out\ 477:515}$ ratio from 0.7 to 1.09 during the experiments. This indicated that, at least in the conditions used in this study, the BL specialist and chromatic acclimater preferentially absorbed BL while the GL specialist mainly used GL. Concerning the co-cultures, the $I_{out\ 477:515}$ ratio decreased but substantially less than in mono-cultures (from 0.7 to 0.53).

Photophysiology

Photosynthetic activity

The monitoring of F_V/F_M indicated that the photosynthetic activity of all mono-cultures under LL could vary significantly during the course of the experiments without any clear pattern (Fig. 3C and F). Yet, it is worth noting that the chromatic acclimater had systematically lower F_V/F_M values than the specialists under both LBL and LGL conditions, suggesting that it is less efficient to photosynthesize at LL. In contrast, no notable difference was observed between the chromatic acclimater and the two specialists under HL (Fig. 4C, F and I). All three strains indeed exhibited a strong variability of F_V/F_M values over the course of the experiments. Similarly, F_V/F_M was more stable in LL than in HL conditions in co-cultures (Fig. 5C, F and 6C, F, I).

Effective size of photosynthetic antenna

Measurements of the effective size of photosynthetic antenna (σ) demonstrated that for a given strain and light condition, this parameter did not vary over the course of the experiments as shown by the very low standard deviations in Figure 7A and B. As expected, the BL specialist had higher σ values at 480 (cyan) than at 540 (green) nm in all tested light conditions, while the opposite was observed for the GL specialist. The BL specialist exhibited the highest σ_{480nm} in HL, with a maximum in HBGL, but not in LL conditions. The GL specialist reached its maximum σ_{540nm} in HGL, while no significant difference in the effective size of its photosynthetic antenna was observed under all other light conditions. Still, it exhibited the maximum values of all strains at 540 nm. The chromatic acclimater displayed intermediate characteristics between the specialists, with higher σ_{480nm} than σ_{540nm} in LBL, LGL and HBL

but comparable σ values at both wavelengths in HGL and HBGL. To note, the photosynthetic antenna of the chromatic acclimater had a highest effective size in LBL than the BL specialist.

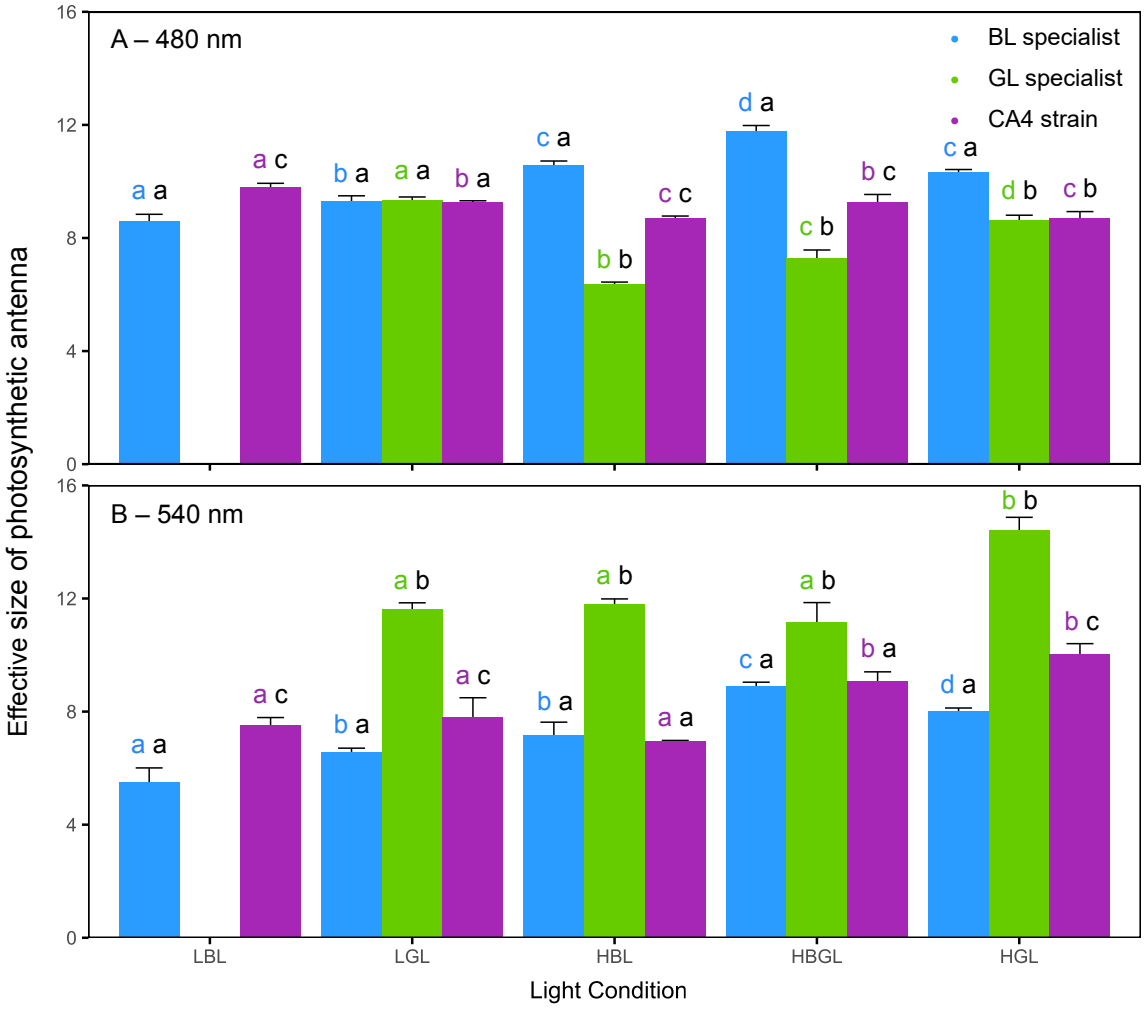

Figure 7: Effective size of photosynthetic antenna (σ) for the three *Synechococcus* strains grown in mono-culture in different light conditions. (A) At 480 nm. **(B)** At 540 nm. Different letters above histograms indicate significantly different values (Kruskall-Wallis followed by Wilcoxon-Mann-Whitney, p-value < 0.05). Histograms represent average and standard deviations of minimum six measurements done during growth phase and steady state. The first colored letter compares the values obtained for a given strain in different light conditions at a given excitation wavelength. The second letter in black compares the different strains in a given light condition and excitation wavelength.

Light-harvesting capabilities

Light response curves were also performed on mono-cultures to compare the photosynthetic performances of the three PTs in the different light conditions. The PSII

efficiency under non-saturating light (α) of the BL specialist was significantly higher at 480 nm in HL, with a maximum in HGL (Fig. 8A and B). In LL, the three PTs exhibited closer α_{480nm}, with the chromatic acclimater and the GL specialist displaying the maximum values in LBL and LGL, respectively. The GL specialist exhibited a significant higher α_{540nm} compared to the other strains in all conditions except HBGL, where it was similar to the BL specialist. The highest PSII efficiency under non-saturating light was measured in HGL at 540 nm for the GL specialist.

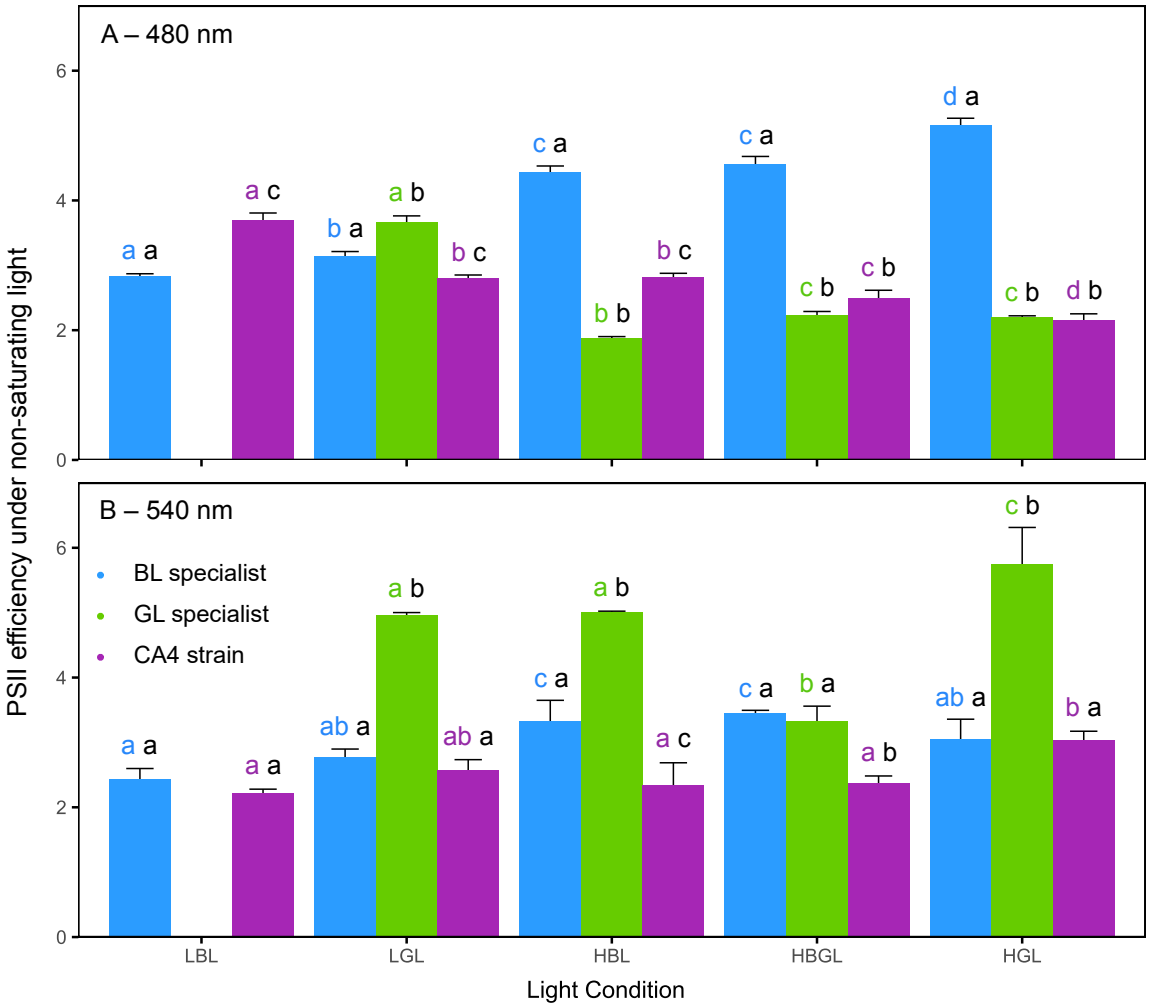

Figure 8: PSII efficiency under non-saturating light (α) for the three *Synechococcus* strains grown in mono-culture in different light conditions. (A) At 480 nm. **(B)** At 540 nm. Different letters above histograms indicate significantly different values (Kruskall-Wallis followed by Wilcoxon-Mann-Whitney, p-value < 0.05). Histograms represent average and standard deviations of minimum six measurements done during growth phase and steady state. The first colored letter compares the values obtained for a given strain in different light conditions at a given excitation wavelength. The second letter in black compares the different strains in a given light condition and excitation wavelength.

The comparison of maximum PSII electron transport rate ($ETRII_{max}$) between strains proved that, at 480 nm, the chromatic acclimater had the highest rate in LBL as well as in the three HL conditions, with a maximum in HBL (Fig. 9A and B). The BL specialist presented the highest $ETRII_{max}$ of all strains at 480 nm in LGL, even if its maximum was actually measured in HGL. At 540 nm, the GL specialist had the highest $ETRII_{max}$ regardless of the condition, with a maximum in HBL.

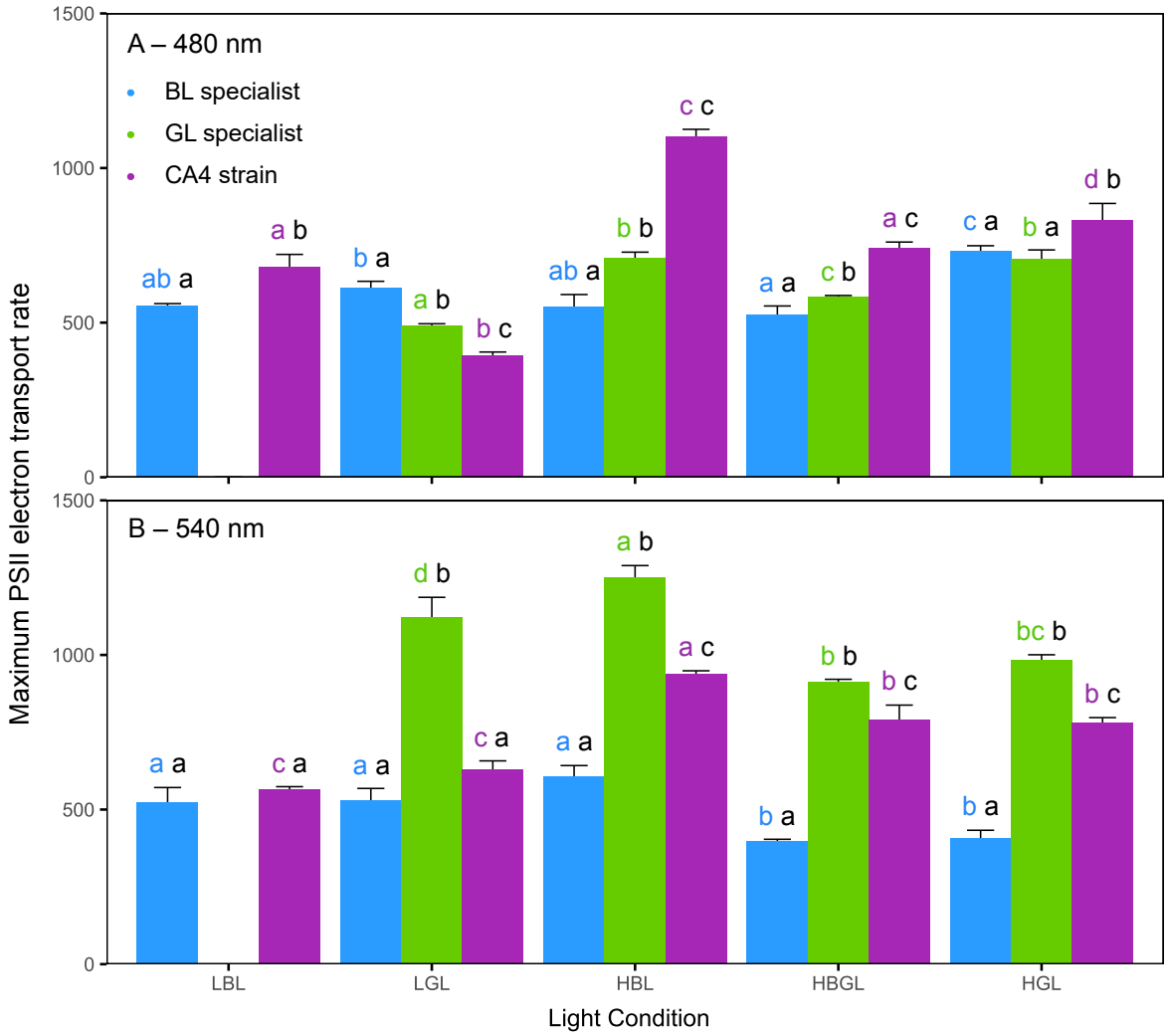

Figure 9: Maximum PSII electron transport rate ($ETRII_{max}$) for the three *Synechococcus* strains grown in mono-culture in different light conditions. (A) At 480 nm. **(B)** At 540 nm. Different letters above histograms indicate significantly different values (Kruskall-Wallis followed by Wilcoxon-Mann-Whitney, p-value < 0.05). Histograms represent average and standard deviations of minimum six measurements done during growth phase and steady state. The first colored letter compares the values obtained for a given strain in different light conditions at a given excitation wavelength. The second letter in black compares the different strains in a given light condition and excitation wavelength.

Finally, the saturation irradiances (E_k) were quite comparable for the three strains in LL conditions at both 480 and 540 nm (Supplementary Fig. 3A and B). The BL specialist has a significantly lower E_k than the two other strains in all HL conditions. In contrast, the chromatic acclimater exhibited the highest E_k values in all light conditions at 540 nm and in HL conditions at 480 nm.

Phycobiliprotein content

The ratio of whole cell fluorescence emission at 560 nm and 650 nm ($Em_{560:650}$), i.e. the phycoerythrin to phycocyanin (PE:PC) emission ratio, sometimes varied during the first ten days of the experiments then stabilized (data not shown). Indeed, increases in the PE:PC ratio were seen in the chromatic acclimater in LBL and LGL before stabilization (from 2.6 to 3.6 and 3.8, respectively). The opposite trend was noticed for the GL specialist in HBL and HBGL, with a decrease of the ratio before stabilization (from 5 to 2.1 and from 3.4 to 2). The $Em_{560:650}$ were systematically higher for the BL specialist in comparison to the GL specialist, even though both exhibited some slight but statistically significant variations of their ratios depending on light conditions (Fig. 10). As for the chromatic acclimater, it exhibited $Em_{560:650}$ values similar to the BL specialist in LL conditions and to the GL specialist in HL conditions. By comparison, the ratio of whole cell fluorescence emission at 650 nm and 680 nm ($Em_{650:680}$), i.e. the PC to terminal acceptor emission ratio, showed no significant variation between strains nor between light treatments (average $Em_{650:680}$ of 1.2; data not shown).

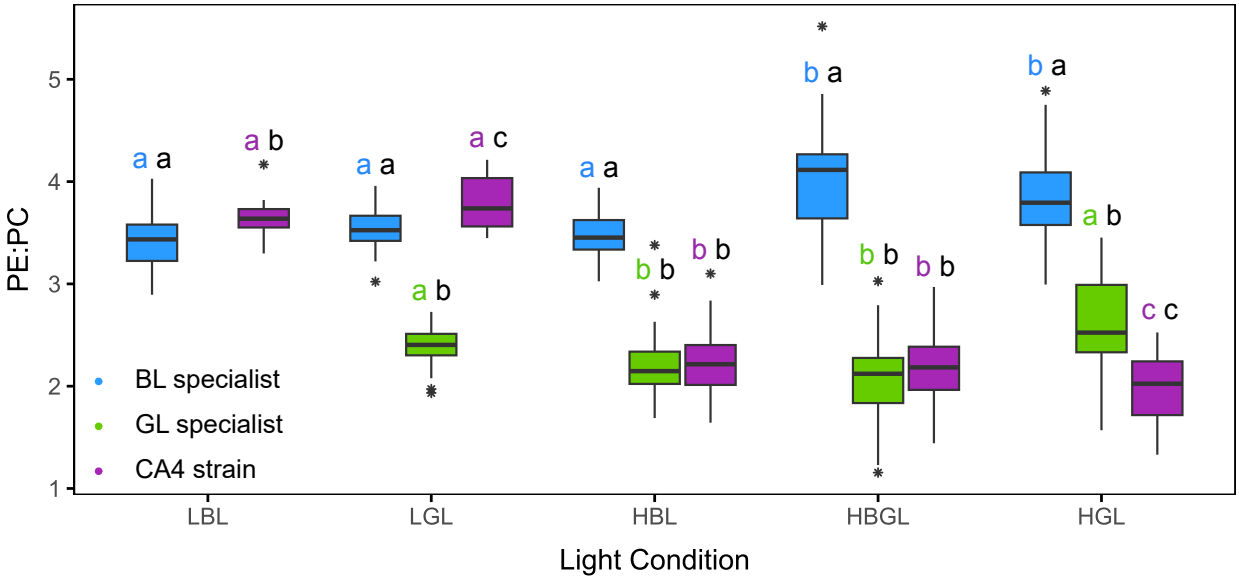

Figure 10: Whole cell $Em_{560:650}$ fluorescence emission ratio (a proxy of PE:PC ratio) for the three *Synechococcus* strains grown in mono-culture in different light conditions. Different letters above boxplots indicate significantly different values (Kruskall-Wallis followed by Wilcoxon-Mann-Whitney, p-value < 0.05). Boxplots represent average and standard deviations of all measurements made during the experiments. The first colored letter compares the values obtained for a given strain in different light conditions. The second letter in black compares the different strains in a given light condition.

Pigment content

Phycobilins

The whole cell excitation ratio at 495 and 545 nm ($Exc_{495:545}$), a proxy of the PUB:PEB ratio of the cells, was invariant during the experiments and between conditions both for the BL specialist (1.58 ± 0.04) and the GL specialist (0.39 ± 0.01), as expected from their fixed PT. On average, the chromatic acclimater displayed typical $Exc_{495:545}$ ratios for a chromatic acclimater in HGL (0.72 ± 0.07) and LBL (1.69 ± 0.06), but slightly lower values in HBL (1.52 ± 0.07; Table S1). More surprisingly, the $Exc_{495:545}$ ratio of the chromatic acclimater changed during the time course of the LGL and HBGL experiments. It indeed increased from a low value of 0.7 at the beginning of the experiments to an intermediate value of 1.03 at steady state in both LGL (1.03 ± 0.11) and HBGL (1.03 ± 0.14; data not shown).

Liposoluble pigment content

The β-carotene to chlorophyll *a* (β-car:Chl *a*) and zeaxanthin to chlorophyll *a* (Zea:Chl *a*) ratios were computed to look at liposoluble pigments variations (Fig. 11). No clear differences were observed for the β-car/Chl *a* between conditions and strains, while the Zea:Chl *a* ratio was only significantly higher in HL compared to LL for the chromatic acclimater. Furthermore, the only difference between strains occurred in LGL condition, where the GL specialist exhibited a significantly higher Zea:Chl *a* ratio than the two other strains.

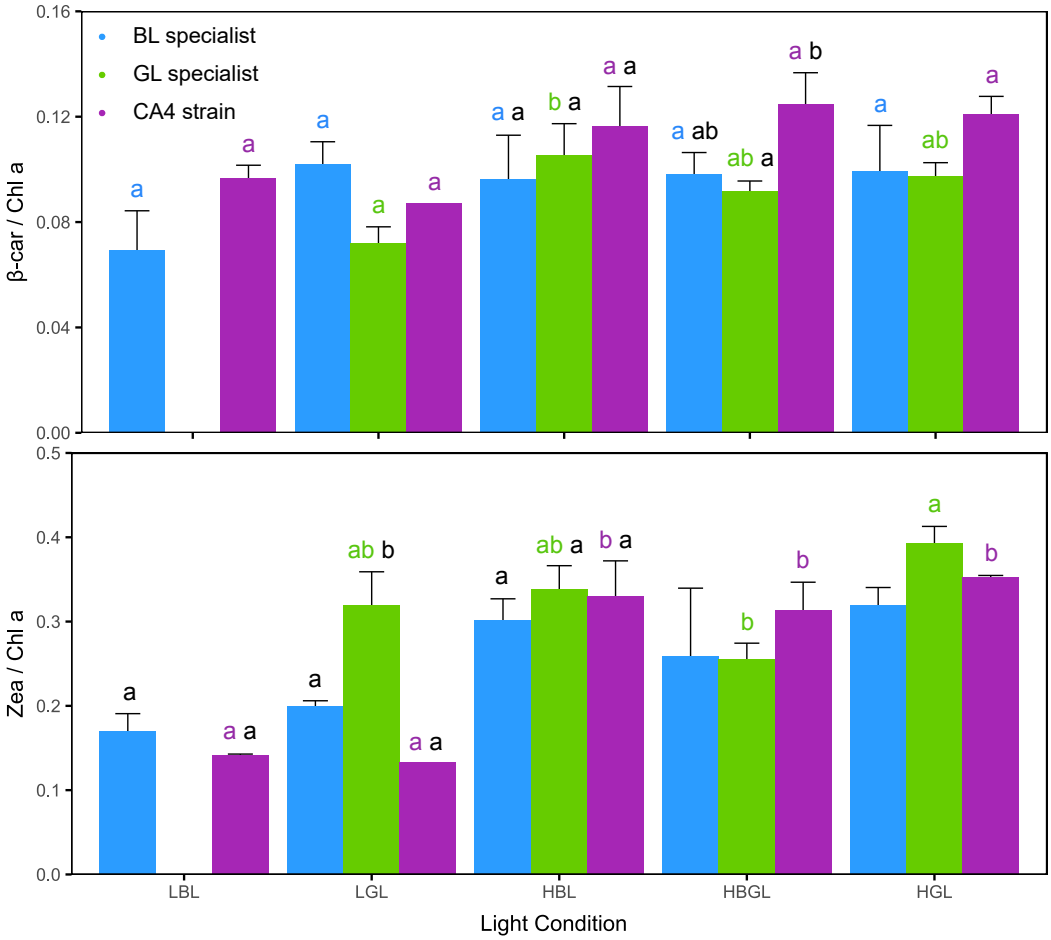

Figure 11: β-carotene to chlorophyll *a* (β-car/Chl *a*) and zeaxanthin to chlorophyll *a* (Zea/Chl *a*) ratios of the three *Synechococcus* strains grown in mono-culture in different light conditions. Different letters above histograms indicate significantly different values (Kruskall-Wallis followed by Wilcoxon-Mann-Whitney, p-value < 0.05). Histograms represent average and standard deviations of minimum three measurements done during growth phase. The first colored letter compares the value obtained for a given strain in different light conditions. The second letter in black compares the different strains in a given light condition. No letters means that no differences in the dataset were identified by the statistical tests.

Comparative genomics

Comparison of the phycobilisome gene content of the three *Synechococcus* strains used in this study showed that all of them exhibit a typical set of genes for their respective pigment type, namely PT 3a (RS9907, GL specialist), 3c (RS9902, BL specialist) and 3dB (RS9915, chromatic acclimater; Table S2). All possess: (i) a *rpcE-F* operon, suggesting that they bind a PEB (and not a PUB) at Cys-84 of the α-phycocyanin subunit (Six et al., 2007b; Blot et al., 2009); and (ii) an ApcE of similar size with only three REP domains, indicating that they have a typical PBS allophycocyanin core made of three cylinders (Sidler, 1994). The examination of the phycobilin lyase content of each strain, combined with data from previous literature, allowed us to predict their chromophorylation at each cysteine binding site (Table S2), thus to derive the total molar PUB:PEB ratio per phycobilisome (Table S3). This showed that the BL specialist and the chromatic acclimater acclimated to BL exhibit the same molar PUB:PEB ratio (1.18). In GL, this ratio is almost twice lower for the GL specialist (0.22) than for the chromatic acclimater (0.39), in agreement with the difference in the $Exc_{495:545}$ ratio between these strains (about 0.4 for the GL specialist vs. 0.6 for the chromatic acclimater).

Discussion

While chromatic acclimaters constitute the most prevalent *Synechococcus* pigment type in open ocean waters (Grébert et al., 2018), the reasons for their ecological success have not been established. One of the main current hypotheses, first evoked to explain the fitness advantage of a cyanobacterium exhibiting CA3 over its counterparts with fixed pigment content (PTs 1 and 2; Stomp et al., 2008), is that chromatic acclimaters would be better adapted than specialists to sustain growth in a fluctuating underwater light field (Lovindeer et al., 2021). Using a mathematical model of the ocean column, the latter authors indeed found that deeper mixed layers selected for chromatic acclimaters in simulated mixtures of *Synechococcus* PTs. However, results from this model seemingly did not match the actual distribution of PTs in the ocean, since no correlation was found between the relative abundance of chromatic acclimaters and mixed layer depths. It is also possible that

chromatic acclimaters could actually perform better than specialists in specific constant light conditions, e.g. in BL/GL mixes and/or at low or high light intensities. To test this hypothesis, we compared the behavior and photo-physiologic characteristics of representatives of BL and GL specialists and a chromatic acclimater in mono and co-cultures. These were carried out in different conditions of light quantity and quality until the strains reached a light-limited steady state.

Mono-cultures grown in LL conditions showed that the BL and GL specialists were respectively characterized by a fast growth in their favorite light color, reaching maximum densities quicker than the two other strains. In contrast, the GL specialist was unable to sustain growth in LBL and the BL specialist failed to reach steady state in LGL (Fig. 3A and D), likely because the ambient photon flux was too low to sufficiently feed photosynthetic light reactions. This seems particularly true for the GL specialist, since there was only a limited overlap between the wavelength range emitted by the blue LEDs and the fluorescence excitation spectrum of this strain (Fig. 1A). As a result, the population losses due to the continuous culture dilution (D = 0.1 day^{-1}) exceeded the growth rate, leading to a rapid disappearance of the cells, a scenario previously evoked by Huisman and collaborators (2002) to describe the competition for light between two microalgae.

Theory predicts that, if species compete for a single color of light, the phytoplankton strain having the lowest critical light intensity (I^*_{out}) should be the best competitor for light and therefore should competitively displace other phytoplankton species (Huisman and Weissing, 1994; Huisman et al., 1999). Here, the GL specialist, which displayed the lowest I^*_{out} in the LGL mono-cultures (Fig. 3E), was indeed the only remaining strain in steady state in the co-cultures (Fig. 5D). In LBL, the chromatic acclimater and the BL specialist had very similar I^*_{out} (Fig. 3B), which could not explain why the latter systematically won the competition in co-culture (Fig. 5A). In this context, photophysiological measurements provided some additional information about the differential behavior of PTs in LL-limited chemostats. In LBL, the effective size of photosynthetic antenna (σ), PSII efficiency under non-saturating light (α) and maximum PSII electron transport rate ($ETRII_{max}$) were mostly higher at 480 nm (cyan) than at 540 nm (green) both for the BL specialist and the chromatic acclimater (Fig. 7 to 9), implying that both strains were better suited for harvesting BL than

GL. Moreover, the chromatic acclimater exhibited slightly higher σ_{480}, α_{480} and $ETRII_{max480}$ than the BL specialist, which should be in favor of the former PT. However, the CA4-strain displayed significantly lower PSII quantum yield (F_V/F_M) all over the course of the experiment (Fig. 3C), indicating that its photophysiological status was suboptimal in LL, in contrast to the BL specialist. This may explain why the chromatic acclimater took longer to reach high concentrations in mono-culture in LBL (Fig. 3A) and was less competitive than the BL specialist in the corresponding co-culture (Fig. 5A).

While the GL specialist performed so poorly in LBL that it did not grow at all despite multiple attempts, it was by far the best suited PT for the LGL condition. Indeed, it exhibited the highest σ_{540}, α_{540} and $ETRII_{max540}$ (Fig. 7 to 9), which is consistent with its rapid growth and high density in steady state in the LGL mono-culture (Fig. 3D) as well as its ability to overgrow the two other strains in the corresponding co-culture (Fig. 5D). Of note, the comparison of the PBS gene sets between the different PTs indicated that PBS rods of the GL specialist are expected to be shorter than those of the other two strains (two vs. three PE-II hexamers respectively). However, even though it possesses less PEB molecules per PBS than the chromatic acclimater (720 vs. 792 PEB respectively; Table S4), the GL specialist exhibited a significantly lower molar PUB:PEB (and $Exc_{495:545}$) ratio than the two other strains (0.22 *vs* 1.18 for the BL specialist and 0.39 for the chromatic acclimater in GL), making it significantly better suited to harvest green photons. Interestingly, during the first two weeks of LGL mono-culture experiments, the chromatic acclimater adjusted its $Exc_{495:545}$ ratio from ca. 0.7 to an intermediate value of ca 1.0. This could imply that it no longer perceived the ambient color as true GL when the mono-culture became denser. It must be stressed that the green LEDs used in our study peaked at 515 nm, i.e. in the valley between the PUB and PEB excitation peaks (Fig. 1). The observed adjustment of the $Exc_{495:545}$ ratio in the chromatic acclimater may thus be a strategy to also catch the blue range of ambient light, in order to optimize light harvesting in conditions of light limitation. The differential overlap between the excitation spectra of strains and emission spectra of the green and blue LEDs may also explain why the BL specialist seemingly performed better in LGL than the GL specialist in LBL.

In contrast to LL, the GL and BL specialists were initially able to grow as fast in both colors in HL conditions, likely because the incident light was not limiting, at least during the first

five days of the experiment. In HBL, the BL specialist reached the highest cell densities, yet all three PTs stabilized at similar cell concentrations in steady state (Fig. 4A). As a result, their critical light intensities (I^*_{out}) were similar (Fig. 4B), making it difficult to identify the best competitor on the basis of this parameter alone. Interestingly, the competition was won by the chromatic acclimater, representing 85 – 90% of the total *Synechococcus* population at the end of the experiment, the remaining being shared by the two specialists (Fig. 6A). This result is seemingly at odds with models predicting that flexible phenotypes would be weaker competitors than specialists in mono-color conditions (Stomp et al., 2008; Lovindeer et al., 2021). As in LBL, the photophysiological measurements made in HBL were mostly higher at 480 nm for the BL specialist and the chromatic acclimater than for the GL specialist, which again exhibited maximum values at 540 nm (Fig. 7 to 9). Consequently, the light-harvesting abilities of the GL specialist were expectedly lower in HBL, consistent with the mismatch between its excitation spectrum and the LEDs emission spectrum, as described above for LBL (Fig. 1C). As concerns the other PTs, the BL specialist displayed the largest effective photosynthetic antennae (σ_{480}) as well as the highest PSII efficiency (α_{480}) in HBL, consistent with its high densities in co-culture during the first two weeks of experiment. In contrast, the chromatic acclimater exhibited much higher maximal electron transport rate ($ETRII_{max480}$) and saturation irradiance (E_{k480}). This indicates that the chromatic acclimater is better adapted to HL conditions than the BL specialist, even though both exhibited similar excitation spectra (Fig. 1C), molar PUB and PEB content per PBS (Table S4) and Zea:Chl *a* and β-car:Chl *a* ratios (Fig. 11). Moreover, the PE:PC emission ratio was almost twice higher in the BL specialist than in the two other strains, suggesting that it displayed a lower within-rod energy transfer efficiency, although the reason for this discrepancy remains to be determined.

In the HGL mono-culture, all three strains grew rapidly at the beginning of the experiments, but the GL specialist and the chromatic acclimater achieved similar and much higher cell densities than the BL specialist in steady state (Fig. 4G). The GL specialist reached the lowest I^*_{out} (Fig. 4H) and exhibited maximum σ_{540}, α_{540} and $ETRII_{max540}$. Accordingly, it accounted for 100% of the total *Synechococcus* population after more than 40 days of growth in the corresponding co-culture (Fig. 6G). In the HBGL mono-culture, the two

specialists grew faster and stabilized at similar and higher cell concentrations than the chromatic acclimater in steady state (Fig. 4D). The GL specialist again displayed the lowest I^*_{out} value (nearly seven times lower than the chromatic acclimater, Fig. 4E) and consequently dominated at the end of the co-culture experiments (Fig. 6D). However, in contrast to the HGL condition where the GL specialist completely displaced its competitors, a final increase in the relative abundance of the chromatic acclimater was observed in both biological replicates in HBGL. Also noteworthy, in one of the two HBGL co-culture replicates, the BL specialist largely dominated the population at the beginning of the experiment, consistent with its fast growth in mono-culture and its I^*_{out} value quite close to that of the GL specialist. The temporal succession of PTs observed in the co-culture in HBGL might be due to the fact that this light condition offered more opportunities for light niche differentiation than the four other tested conditions. One possible explanation for this population dynamics is the progressive diminution of BL availability during the course of the experiments, as shown by the gradual decrease in the 477:514 nm ratio in the HBGL co-culture from 0.75 to 0.53. In the HBGL mono-cultures, variations over time of the spectrum of the transmitted light (Supplementary Fig. 2) indicated that, although both BL and GL were available, the BL specialist absorbed preferentially photons in the blue part of the spectrum while the GL specialist mostly absorbed the green part. The chromatic acclimater, which exhibited an intermediate $Exc_{495:545}$ ratio of 1.0 in HBGL, also had a preference for BL but was able to use more GL than the BL specialist. In this context, we can imagine that the latter was at some point overgrown by the two other strains because of the too low proportion of BL in the co-culture, while the chromatic acclimater could maintain itself using GL. The behavior of the chromatic acclimater, which can finely tune its PUB:PEB ratio to match the ambient light quality, is somehow reminiscent of that of a CA3-capable strain, which modify its PE:PC ratio to harvest the part of the light spectrum not used by its competitor (Stomp et al., 2004).

Conclusion

Previous light competition studies predicted that flexible phenotypes would be weaker competitors than specialists in mono-color conditions. Here, we confirmed that specialists were the winners at LL in their favorite light color and that the GL specialist outcompeted

the other strains in HGL. However, we demonstrated that the chromatic acclimater was the best competitor in HBL and was also capable of co-existing with the GL specialist in HBGL. Additionally, this study revealed previously unknown capacity of chromatic acclimaters to adjust their PE:PC emission ratio depending on the light intensity, which could allow them to adjust the energy transfer efficiency along PBS rods.

If we interpret these data in terms of light niche partitioning in the Ocean (Holtrop et al., 2021), this would imply that each PT dominates in a specific light niche: the GL specialists preferentially thriving in greenish, coastal, nutrient-rich waters; the BL specialists at depth in the open ocean; and the chromatic acclimaters in the upper lit layer of the ocean as well as at intermediate depth, when the underwater light field consist of a mix of blue and green light. Still, given the interplay between competition for the underwater light spectrum, nutrients (Burson et al., 2018; Grébert et al., 2018) and temperature (Six et al., 2021), more studies are needed to better understand the spatio-temporal variability of the distribution of the different *Synechococcus* PTs.

Conflict of interest

The authors declare that the research was conducted in the absence of any commercial or financial relationships that could be construed as a potential conflict of interest.

Funding

This work was supported by the French “Agence Nationale de la Recherche” Program EFFICACY (ANR-19-CE02-0019).

Acknowledgments

We would like to thank the CRBM (Roscoff) for sharing the temperature-controlled room and CO_2 system used in this study, as well as Sarah Bureau for taking care of nutrients analyses. We are also most grateful to Christophe Six and Sarah Garric for technical hints on PAM fluorimetry and HPLC

analyses, as well as Priscillia Gourvil and Martin Gachenot from the Roscoff Culture Collection (http://roscoff-culture-collection.org/).

Supplementary material

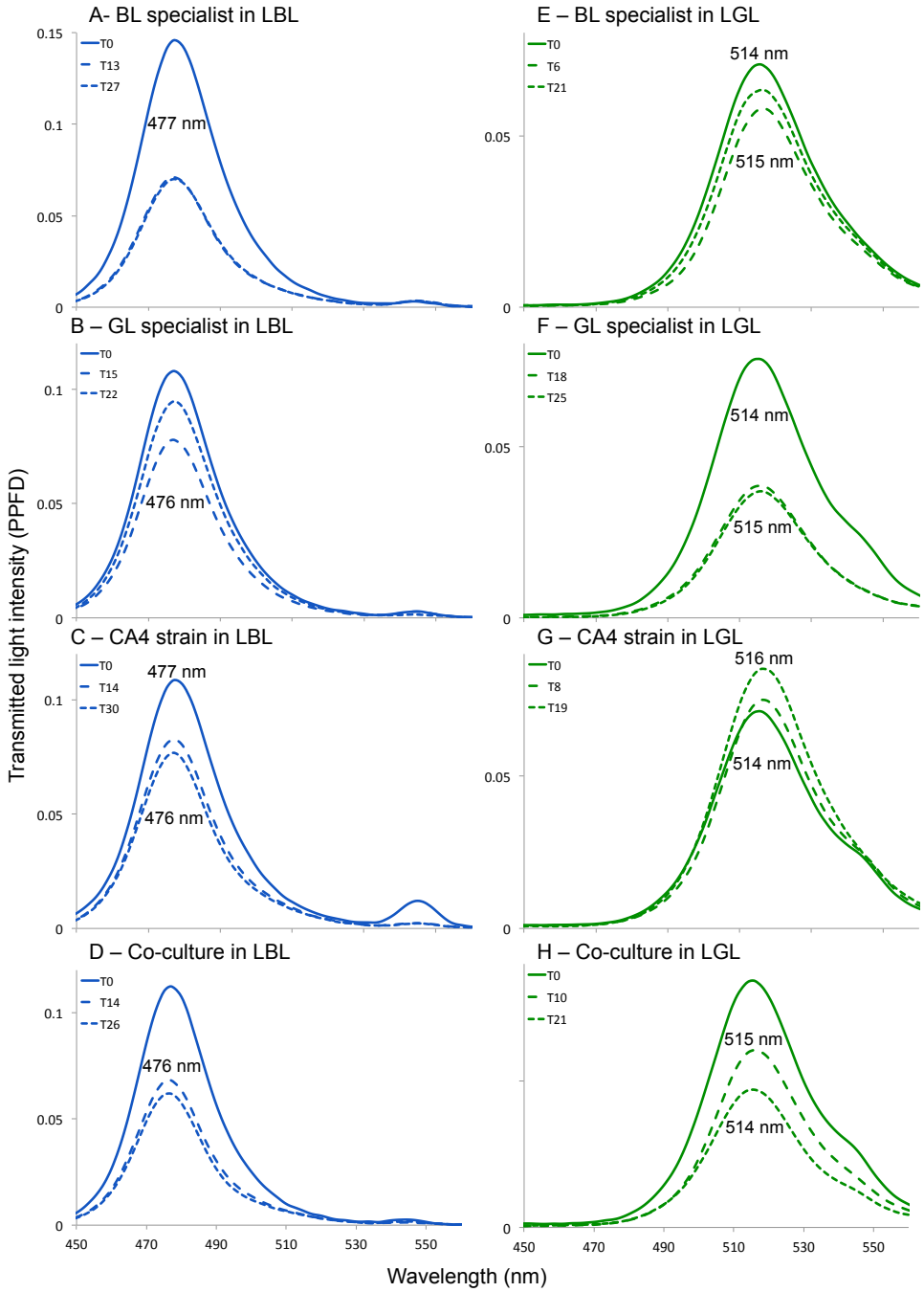

Supplementary figure 1: Spectra of light transmitted through culture flasks in LL conditions. (A-D) Low blue light. **(E-H)** Low green light. **(A, E)** Blue light specialist. **(B, F)** Green light specialist. **(C, G)** chromatic acclimater. **(D, H)** Co-culture.

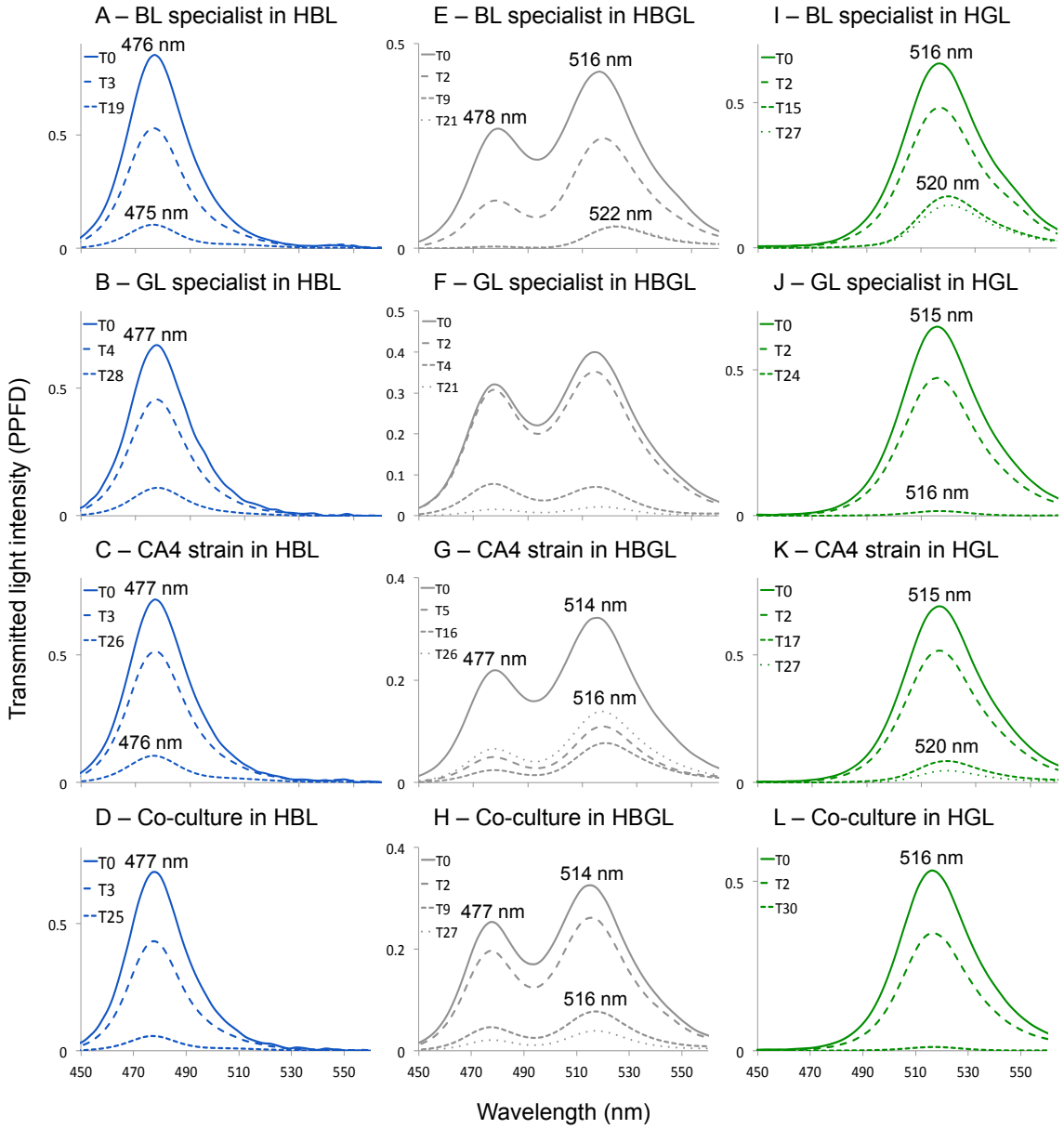

<u>Supplementary figure 2:</u> Spectra of light transmitted through culture flasks in HL conditions. (A-D) High blue light. **(E-H)** High blue-green light**. (I-L)** High green light. **(A, E, I)** BL specialist. **(B, F, J)** GL specialist**. (C, G, K)** chromatic acclimater. **(D, H, L)** Co-culture.

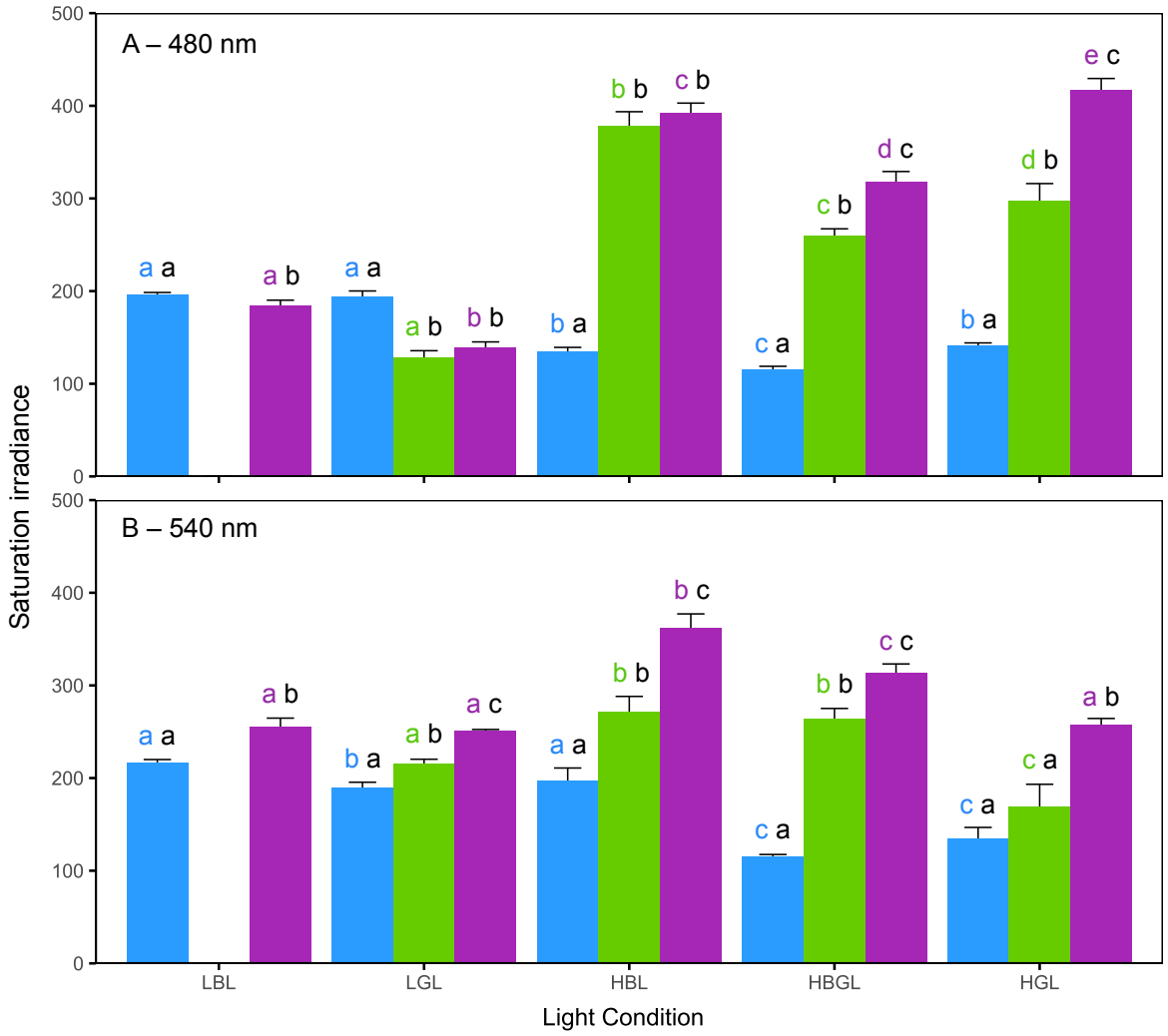

Supplementary figure 3: Saturation irradiance (E_k) for the three *Synechococcus* strains grown in mono-culture in different light conditions. (A) At 480 nm. **(B)** At 540 nm. Different letters above histograms indicate significantly different values (Kruskall-Wallis followed by Wilcoxon-Mann-Whitney, p-value < 0.05). Histograms represent average and standard deviations of minimum six measurements done during growth phase and steady state. The first colored letter compares the values obtained for a given strain in different light conditions at a given excitation wavelength. The second letter in black compares the different strains in a given light condition and excitation wavelength.

Supplementary table 1: Ratios of whole cell fluorescence excitation at 495 nm and 545 nm ($Exc_{495:545}$) with emission set at 560 nm, a proxy of PUB:PEB ratio, for the three *Synechococcus* strains grown in mono-culture in different light conditions. Values are average ± standard deviation of all measurements made during the experiments. *Conditions in which the CA4-strain exhibited an increase of its PUB:PEB ratio during the course of the experiment (10.7% increase in LGL and 13.6% in HBGL).

Strain (PT)	LBL	LGL	HBL	HBGL	HGL
RS9902 (PT 3c, BL specialist)	1.55 ± 0.07	1.59 ± 0.09	1.59 ± 0.1	1.53 ± 0.07	1.64 ± 0.09
RS9907 (PT 3a, GL specialist)	n.a.	0.38 ± 0.03	0.39 ± 0.02	0.39 ± 0.02	0.39 ± 0.01
RS9915 (PT 3dB, CA4 strain)	1.69 ± 0.06	1.03 ± 0.11*	1.52 ± 0.07	1.03 ± 0.14*	0.72 ± 0.07

Supplementary table 2: Phycobilisome gene content of the three *Synechococcus* strains used in this study.

			Strains and pigment types			
			RS9902	**RS9907**	**RS9915**	
Cyanorak cluster	**Gene name**	**Product**	**PT 3c**	**PT 3a**	**PT 3dB**	**Comments**
CK_00008006	*apcA*	allophycocyanin, alpha chain	1	1	1	
CK_00008007	*apcB*	allophycocyanin, beta chain	1	1	1	
CK_00008008	*apcD*	allophycocyanin alpha-B chain	1	1	1	
CK_00000004	*apcF*	allophycocyanin beta-18 chain	1	1	1	
CK_00001646	*apcC*	phycobilisome core linker polypeptide (Lc), allophycocyanin-associated	1	1	1	
CK_00001645	*apcE*	phycobilisome core-membrane linker polypeptide (Lcm)	1	1	1	All 3 strains have an ApcE of similar size. Their structure indicate all 3 strains have a 3-cylinder APC core.
CK_00008001	*cpcA*	phycocyanin, alpha chain	1	1	1	
CK_00007999	*cpcB*	phycocyanin beta chain	1	1	1	
CK_00009072	*cpcG1*	phycobilisome rod-core linker polypeptide CpcG1 (Lrc)	1	1	1	
CK_00000044	*cpcL*	photosystem-I-associated phycobilisome rod-core linker	1	1	1	

		polypeptide-like protein CpcL				
CK_00001528	*cpcS*	PCB:Cys-82 beta-phycocyanin lyase, CpcS subunit	1	1	1	All 3 strains have CpcS (+CpcU), RpcT and RpcE-F lyases but no RpcG lyase. This indicates that their PC binds one PCB and two PEB chromophores (like *Synechococcus* sp. WH7803).
CK_00001592	*cpcU*	PCB:Cys-82 beta-phycocyanin lyase, CpcU subunit	1	1	1	
CK_00001982	*rpcE*	PEB Cys-84 alpha-phycocyanin lyase, RpcE subunit	1	1	1	
CK_00001983	*rpcF*	PEB:Cys-84 alpha-phycocyanin lyase, RpcF subunit	1	1	1	
CK_00001393	*rpcT*	PEB:Cys-153 beta-phycocyanin lyase	1	1	1	
CK_00000069	*cpeA*	C-phycoerythrin class I, alpha subunit	1	1	1	
CK_00008004	*cpeB*	C-phycoerythrin class I, beta subunit	1	1	1	
CK_00001760	*cpeC*	phycobilisome rod linker polypeptide (Lr), C-phycoerythrin class I-associated	1	1	1	
CK_00008020	*cpeE*	phycobilisome rod linker polypeptide (Lr), C-phycoerythrin class I-associated (CpeE)	1	1	1	
CK_00001759	*cpeR*	phycoerythrin operon regulator	1	1	1	
CK_00008055	*cpeF*	PEB:Cys-50,61 beta-phycoerythrin lyase	1	0	0	RS9907 has CpeF so it must bind a PEB at Cys-50-61 of beta-PE-I and likely PE-II as well.
CK_00001397	*cpeS*	PEB:Cys-82 beta-phycoerythrin lyase	1	1	1	
CK_00001572	*cpeT*	PEB:Cys-165 beta-phycoerythrin lyase CpeT	1	1	1	
CK_00001757	*cpeU*	putative PEB:phycoerythrin lyase CpeU	1	1	1	
CK_00001570	*cpeY*	PEB:Cys-82 alpha-phycoerythrin lyase, CpeY subunit	1	1	1	
CK_00001571	*cpeZ*	CpeY lyase activity enhancer	1	1	1	
CK_00007994	*mpeA*	C-phycoerythrin class II, alpha chain	1	1	1	
CK_00008005	*mpeB*	C-phycoerythrin class II, beta chain	1	1	1	

CK_00008012	*mpeC*	phycobilisome rod linker polypeptide (Lr), C-phycoerythrin II-associated (C-phycoerythrin II gamma subunit)	0	1	1	The PT 3a strain RS9907 has no MpeC linker, suggesting its PBS rods are shorter (1 less PE-II disk) than the other two strains (1 PC + 2 PE-I + 3 PE-II disks), according to Six et al. J. Bact. (2005).
CK_00008022	*mpeD*	phycobilisome rod linker polypeptide (Lr), C-phycoerythrin I and II-associated	1	1	1	
CK_00008016	*mpeE*	phycobilisome rod linker polypeptide (Lr), C-phycoerythrin II-associated	1	1	1	
CK_00024045	*mpeH*	possible phycobilisome rod linker polypeptide (Lr), C-phycoerythrin II-associated	1	1	1	
CK_00000136	*mpeU*	putative PEB:phycoerythrin-II lyase-isomerase	0	1	1	RS9902 and RS9915 have MpeU and likely bind a PUB at Cys-50-61 of beta-PC.
CK_00057672	*mpeQ*	PEB:alpha-83-phycoerythrin II lyase-isomerase	0	1	1	
CK_00001396	*mpeY*	PEB:alpha-83-phycoerythrin II lyase	1	0	0	
CK_00002124	*fciA*	AraC-type transcriptional regulator involved in type IV chromatic acclimation	0	0	1	The *fciA-B-mpeW* island is responsible for the RS9915 capacity to perform CA4.
CK_00002123	*fciB*	AraC-type transcriptional regulator involved in type IV chromatic acclimation	0	0	1	
CK_00020700	*mpeW*	PEB:Cys-83 alpha-phycoerythrin II lyase	0	0	1	
CK_00001691	*unk1*	conserved hypothetical protein	1	1	1	
CK_00002915	*unk2A*	conserved hypothetical protein	1	1	1	
CK_00001398	*unk3*	uncharacterized conserved membrane protein	1	1	1	

CK_00001762	*unk4*	conserved hypothetical protein	1	1	1	
CK_00001761	*unk5*	pentapeptide repeat-containing protein	1	1	1	
CK_00005948	*unk6*	conserved hypothetical protein	1	1	1	
CK_00001836	*unk7*	nif11-like leader peptide domain protein	0	1	1	
CK_00002116	*unk8*	nif11-like leader peptide domain protein	0	1	1	
CK_00033153	*unk8-unk7*	nif11-like leader peptide bi-domain fusion protein (Unk8-Unk7)	1	0	0	
CK_00001835	*unk9*	possible nif11-like leader peptide domain protein	1	1	1	
CK_00002279	*unk10*	conserved hypothetical protein	0	1	1	
CK_00002548	*unk11*	conserved hypothetical protein	1	1	1	
CK_00001758	*unk12*	conserved hypothetical protein	1	1	1	
CK_00001834	*unk13*	conserved hypothetical protein	1	1	1	
CK_00000072	*unk14 A*	conserved hypothetical protein	1	1	1	

<u>Supplementary table 3:</u> Chromophorylation of phycobiliprotein subunits and linker polypeptides for the three strains used in this study, as predicted from their phycobilin lyase content and/or characterization of *Synechococcus* spp. strains belonging to the same pigment type.

		Strain and pigment type			
		RS9907	**RS9902**	**RS9915**	
Phycobiliprotein or linker	**Binding sites**	**PT 3a**	**PT 3c**	**PT 3dB**	**References**
Allophycocyanin	α-81	PCB	PCB	PCB	Saunée et al. (2008) J. Biol. Chem. 283: 7513–7522
		CpcS+CpcU	CpcS+CpcU	CpcS+CpcU	
	β-81	PCB	PCB	PCB	
		CpcS+CpcU	CpcS+CpcU	CpcS+CpcU	
	αβ-81	PCB	PCB	PCB	
		CpcS+CpcU	CpcS+CpcU	CpcS+CpcU	
	β18-81	PCB	PCB	PCB	
		CpcS+CpcU	CpcS+CpcU	CpcS+CpcU	
Phycocyanin	α-84	PEB	PEB	PEB	Ong & Glazer

		RpcE-F	RpcE-F	RpcE-F	(1987) J. Biol. Chem. 262: 6323-6327 Six et al. (2007) Genome Biol. 8, R259
	β-82	PCB	PCB	PCB	Saunée et al. (2008) J. Biol. Chem. 283: 7513–7522
		CpcS+CpcU	CpcS+CpcU	CpcS+CpcU	
	β-153	PEB	PEB	PEB	Six et al. (2007) Genome Biol. 8: R259
		RpcT	RpcT	RpcT	
Phycoerythrin-I	α-82	PEB	PEB	PEB	Biswas et al. (2011) J. Biol. Chem. 286: 35509-35521
		CpeY-Z	CpeY-Z	CpeY-Z	
	α-139	PEB	PEB	PEB	Ong & Glazer (1991) J. Biol. Chem. 266: 9515–9527 Grébert et al. (2021) PNAS 118:e2019715118
		?	?	?	
	β-50/61	PEB	PEB	PEB	Kronfel et al. (2019) J. Biol. Chem. 294: 3987-3999 Mahmoud et al. (2017) Front Microbiol 8:243
		CpeF	MpeU?	MpeU?	
	β-82	PEB	PEB	PEB	Kronfel et al. (2019) J. Biol. Chem. 294: 3987-3999 Mahmoud et al. (2017) Front Microbiol 8:243
		CpeS	CpeS	CpeS	
	β-165	PEB	PEB	PEB	Nguyen et al.

		CpeT	CpeT	CpeT	(2020) BBA Bioenrg. 1861: 148284
Phycoerythrin-II	α-75	PUB	PUB	PUB	Ong & Glazer (1991) J. Biol. Chem. 266: 9515–9527 Grébert et al. (2021) PNAS 118:e2019715118
		?	?	?	
	α-83	PEB	PUB	PEB in GL / PUB in BL	
		MpeY	MpeQ	MpeQ in BL / MpeW in GL	
	α-140	PUB	PUB	PEB in GL / PUB in BL	
		?	?	?	
	β-50/61	PEB	PUB	PUB	Kronfel et al. (2019) J. Biol. Chem. 294: 3987-3999 Mahmoud et al. (2017) Front Microbiol 8:243
		CpeF	MpeU?	MpeU?	
	β-82	PEB	PEB	PEB	Kronfel et al. (2019) J. Biol. Chem. 294: 3987-3999 Mahmoud et al. (2017) Front Microbiol 8:243
		CpeS	CpeS	CpeS	
	β-159	PEB	PEB	PEB	Nguyen et al. (2020) BBA Bioenrg. 1861: 148284
		CpeT?	CpeT?	CpeT?	
MpeC	49/64	Absent	PUB	PUB	Wilbanks & Glazer (1983) J. Biol. Chem. 268: 1236-1241 Six et al. (2005) J. Bacteriol. 187: 1685-1694
MpeD	44/59[a]	PUB	PUB	PUB	
MpeE	49/64[b]	PUB	PUB	PUB	

[a]Cysteins positions are 41/56 in RS9907 MpeD; [b]Cysteins positions are 63/78 in RS9915 MpeE.

<u>Supplementary table 4:</u> Total number of chromophores per phycobiliprotein, linker and whole phycobilisome for the three strains used in this study, as derived from Table S3.

	Strain and pigment type			
	RS9907	**RS9902**	**RS9915**	
Total chromophores per phycobiliprotein or linker	**PT 3a**	**PT 3c**	**PT 3dB**	**References**
Allophycocyanin PCB	72	72	72	Sidler, 1994
Phycocyanin PCB	36	36	36	
Phycocyanin PEB	72	72	72	
Phycoerythrin-I PEB in BL	360	216	216	Ong and Glazer, 1991
Phycoerythrin-I PEB in GL	360	216	288	
Phycoerythrin-I PUB in BL	0	144	144	
Phycoerythrin-I PUB in GL	0	144	72	
Phycoerythrin-II PEB in BL	288	216	216	
Phycoerythrin-II PEB in GL	288	216	432	
Phycoerythrin-II PUB in BL	144	432	432	
Phycoerythrin-II PUB in GL	144	432	216	
Phycoerythrin-II Linker PUB	12	18	18	Six et al., 2005
Total chromophores per phycobilisome				
Total PCB	108	108	108	This study
Total PEB in BL	720	504	504	This study
Total PEB in GL	720	504	792	This study
Total PUB in BL	156	594	594	This study
Total PUB in GL	156	594	306	This study
Molar PUB:PEB ratio per phycobilisome				
PUB:PEB in BL	0.22	1.18	1.18	This study
PUB:PEB in GL	0.22	1.18	0.39	This study

Chapter 3:

Environmental approaches to better characterize type IV chromatic acclimation

I. Context of the work

Analyses of the huge sequence datasets collected during global expeditions (Zwirglmaier et al., 2007, 2008; Sohm et al., 2015; Farrant et al., 2016; Grébert et al., 2018) or more localized cruises (Fuller et al., 2006; Mella-Flores et al., 2011; Paulsen et al., 2016; Xia et al., 2017, 2018; Zhang et al., 2022) have provided cyanobacteriologists a wide knowledge on the genetic and pigment diversity of *Synechococcus* communities at large spatial scales, as well as on the vertical distributions of *Synechococcus* ecotypes. The temporal dynamics of natural populations was also studied at some specific sites, such as the Scripps pier Laboratory (Tai and Palenik, 2009), station A in the Gulf of Aqaba (Fuller et al., 2005), stations NM3 and NM7 in the Hongkong area (Xia et al., 2015), or the Martha's Vineyard Coastal Observatory (Hunter-Cevera et al., 2016b). However, the temporal variability of *Synechococcus* PTs has little been explored so far. In this context, the objective of this chapter was to characterize the seasonal variations of the different PTs at two French long-term observatory stations with contrasting oceanic regimes (BOUSSOLE in the northwestern Mediterranean Sea and SOMLIT-Astan in the English Channel), and to relate them to abiotic factors. During two consecutive years, routine seawater analyses performed at these sites were complemented by acquiring depth profiles of water color spectra, as well as collecting seawater samples for analysing the genetic, pigment and functional diversity of picocyanobacteria using a metagenomic approach. It is important to note that the data generated during this study will help improve a biogeochemical model simulating the present distribution and relative abundance of *Synechococcus* PTs at the global scale. Such a model is currently being developed by Francesco Mattei (Laboratoire d'Océanographie de Villefranche-sur-Mer, LOV), a postdoc hired on the ANR EFFICACY project, in close collaboration with two colleagues involved in the DARWIN project, namely Stephanie Dutkiewicz (MIT, USA) and Anna Hickman (University of Southampton, UK). In the future, this model should also enable us to predict the effect of global warming on the distribution of the different *Synechococcus* PTs.

II. Contribution

As concerns the SOMLIT-Astan station, I was in charge every two weeks for two years (June 2020 to October 2022) of the sampling of seawater in subsurface for flow cytometry and HPLC analyses, as well as of the deployment of the CTD and a multi-spectral radiometer (Compact Optical Profiling System, C-OPS, Biospherical Instruments) used in routine at the BOUSSOLE station. Other ECOMAP team members were involved in sampling large volume of seawater (about 20 L) for metagenomics and metatranscriptomics. Members of the 'Service d'Observation en Milieu Littoral' (SOMLIT), who sampled the same site two to three hours before or after us, performed nutrient quantification (as well as CTD and flow cytometry analyses for intercomparison of the two sampling series). At the BOUSSOLE station, sampling was done by members of the OMTAB (Marine Optics, Remote sensing and Biogeochemical Applications) team (LOV, Villefranche-sur-Mer). I only participated in the first sampling in order to train OMTAB team members to filter seawater for metagenomics. Sampling at BOUSSOLE was done once per month from March 2020 to August 2022 at four depths within the upper lit layer.

Many people were involved in sample processing: Morgane Ratin, Bastian Gouriou and myself for cryo-grinding and DNA/RNA extraction from filters; Dominique Marie, Martin Gachenot, Julia Clairet and myself for flow cytometry; Eric Macé and Melek Golbol for CTD; Vicenzo Vellucci for C-OPS; Céline Dimier and Joséphine Ras for HPLC; Sarah Bureau and Emilie Diamond Riquier for nutrients. I gathered all datasets, performed analyses and interpreted the results under the supervision of L. Garczarek and F. Partensky. Unfortunately, metagenomic data were still being sequenced at the time of writing this thesis manuscript, so I could not include data on the relative abundance of *Synechococcus* PTs in my thesis. This part of the work should be done in the forthcoming months.

Concerning the modelling study, I grew several strains representative of GL specialists (PT 3a), BL specialists (PT 3c) and chromatic acclimaters (PTs 3dA and 3dB) in various light quality conditions. The goal was to produced a dataset (PUB:PEB ratio as assessed by spectrofluorimetry, cell numbers by flow cytometry, absorption spectra of whole cell normalized to chlorophyll *a*) that will be further used by Francesco Mattei to calibrate its

adaptation of the DARWIN model. More precisely, measurements were done on twelve strains fully acclimated to BL or GL, and at different times after a shift from BL to GL.

In the context of this chapter, I also took part in Flavien Petit's study on the assessment of phytoplankton community composition using *in-situ* fluorescence, and its potential for application to BGC-Argo profiling floats (Petit et al., in preparation). More precisely, I was in charge of acclimating and growing ten phytoplankton strains, as well as assessing their physiological status and concentration before each experiment. In parallel to the multispectral fluorescence measurements realized by Flavien, I prepared the filters for measurements of chlorophyll *a* concentration by HPLC, which were extracted and analyzed on the SAPIGH platform in Villefranche-sur-Mer.

III. Temporal dynamics of *Synechococcus* pigment types in the English Channel and in the Mediterranean Sea: the biogeochemical context

III.1. Materials and Methods

III.1.a. Sampling location

The SOMLIT-Astan station is located in the Western English Channel, 2.5 km off Roscoff in Britanny (48°46'18''N-3°58'6"W; Guilloux et al., 2013), while the BOUSSOLE station is situated in the Ligurian Sea, which constitutes an arm of the Mediterranean Sea, 59 km off Villefranche-sur-Mer (7°54'E-43°22'N; Antoine et al., 2006). Both are part of long-term time series sampled at regular intervals for hydrological, plankton and/or optical analyses. SOMLIT-Astan monitoring started in 2000 and is carried out twice a month by the SOMLIT (Service d'Observation en Milieu LITtoral; https://www.somlit.fr) team members. As concerns BOUSSOLE project (BOUée pour l'acquiSition d'une Série Optique à Long termE; www.obs-vlfr.fr/Boussole/html/home/home.php), the monitoring started in 2001 and is performed monthly by the Laboratoire d'Océanographie de Villefrance (LOV). The two sites are characterized by contrasting oceanic regimes and depths. Permanent mixed waters and maximum depths of 60 meters are found at SOMLIT-Astan (Sournia and Birrien, 1995; Guilloux et al., 2013), while strong seasonality and depths up to 2400 m can be encountered at BOUSSOLE (D'Ortenzio et al., 2005; Antoine et al., 2006). The data used for this study

correspond to: (i) June 2020 to October 2022 in surface only for the first site; and (ii) March 2020 to August 2022 at several depths for the second one.

III.1.b. Physico-chemical and optical parameters

Seawater temperature was measured *in situ* with CTD profilers (Sea-Bird Scientific) equipped with several sensors including a salinometer, a fluorometer as well as a Photosynthetically Active Radiation (PAR) sensor. Dissolved oxygen concentration was assessed using the Winkler method and pH was measured by spectrophotometry, two methods previously standardized and described by the SOMLIT network (https://www.somlit.fr/parametres-et-protocoles/).

Nutrient data were retrieved from the SOMLIT database (https://www.somlit.fr/demande-de-donnees/) for the SOMLIT-Astan station or provided by the LOV for the BOUSSOLE station. Briefly, nitrates, nitrites and phosphates (NO_3^-, NO_2^- and PO_4^{3-}) were quantified following the protocol described by Aminot and Kérouel (2007). Ammonium (NH_4^+) concentration was determined following the method of Koroleff (1969).

Upward irradiance profiles were acquired by deploying a multi-spectral radiometer (Compact Optical Profiling System, C-OPS, Biospherical Instruments Inc.) equipped with 19 optical-filter microradiometers along the water column as previously described by Organelli and collaborators (2016). For a few specific wavelengths, the Remote Sensing Reflectance ($R_{rs(\lambda)}$), which is defined as the ratio between the water leaving radiance (L_W) and the incident solar irradiance (E_S) as measured by an above-water reference sensor, was calculated based on each profile as follows:

$$R_{rs(\lambda)} = L_{W(\lambda)} / E_{S(\lambda)},$$

where λ refers to the wavelength (Organelli et al., 2016).

III.1.c. Phytoplankton counts and pigment content

For flow cytometry analyses, samples of 1.5 mL seawater were fixed with a mix of glutaraldehyde (25%, Sigma-Aldrich) and pluronic acid (10%, Sigma-Aldrich), as recommended in the SOMLIT protocol (https://www.somlit.fr/parametres-et-protocoles/). After 15 min fixation in the dark, samples were flash-frozen and conserved at -80°C until analysis. Pico- and nano-phytoplankton, bacteria as well as virus abundances were determined by flow cytometry using a NovoCyte Advanteon flow cytometer (Agilent) following the protocol described by Marie and co-workers (1999).

Phytoplankton pigment contents were determined by High Performance Liquid Chromatography (HPLC) based on the protocol established by Ras and collaborators (2008). For this purpose, volumes of 2.2 L were vacuum filtered through 25 mm GF/F glass filters (Whatman), flash-frozen and conserved at -80°C until analysis.

III.1.d. Metagenomic material

About 20 L of seawater were collected in surface only by manual pumping at SOMLIT-Astan and at four different depths with a CTD-rosette device at BOUSSOLE. The bacterial-size fraction (0.22–3 µm) was harvested just after sampling by filtration onto 3 µM and 0.2 µM, 142 mm polycarbonate filters (Millipore) as described by Pesant and co-workers (2015). Filters were immediately flash-frozen on board and transferred at -80°C until DNA extraction. Nucleic acid extractions were performed by simultaneous extraction of DNA and RNA using cryogenic grinding of membrane filters, followed by nucleic acid extraction using NucleoSpin RNA kits (Macherey-Nagel) as described by Alberti and collaborators (2020). Extracted DNA was quantified using a ND-1000 spectrophotometer (Nanodrop) and a Qubit PicoGreen assay (Invitrogen). DNA integrity was checked on a Bioanalyzer DNA High Sensitivity chip (Agilent). Library preparations were performed on the Fasteris, Life Science Genesupport SA platform (Plan-Les-Ouates, Switzerland) using the TruSeq DNA Nano Prep kit (Illumina) after a size selection step by mechanical shearing of the DNA to obtain average insert sizes of 250 bp. Libraries were sequenced on Novaseq S4 (Illumina) in a 2 x 150 bp

paired end mode in order to obtain about 160 million reads per sample and a high proportion (> 90%) of merged overlapping read pairs.

III.2. Results

III.2.a. Surface comparison of the two sites

As previously described in the Western English Channel by Tarran and Bruun (2015), seasonal cycles were observed at SOMLIT-Astan for *Synechococcus* (Fig. 1) and for eukaryotes (Fig S1), a group which can be further subdivided into cryptophytes, pico- and nano-eukaryotes based on their distinct flow cytometric signatures. Peak abundances of the picocyanobacterium occurred in summer, between mid-July and mid-August of each year, but with highly variable magnitudes (a maximum concentration of $1.01E^{+5}$ cells mL^{-1} was reached in August 2021). High concentrations of *Synechococcus* were also recorded during the Autumn 2021, while the usual early spring blooms were not detected. In the Mediterranean Sea (BOUSSOLE), a single *Synechococcus* bloom was observed each year in April (maximum concentrations of $3.87E^{+5}$ cells mL^{-1} in 2021 and $6.07E^{+4}$ cells mL^{-1} in 2022). The concentrations measured during the two-year time series at BOUSSOLE were similar to those recorded by Uysal and Köksalan (2006) in the Northern Levantine Basin shelf waters (annual average of $3.9E^{+4}$ cells mL^{-1} and maximum of $1.53E^{+5}$ cells mL^{-1}). However, this previous study reports the highest *Synechococcus* concentrations during summer and early autumn, and not during spring.

The occurrence of *Prochlorococcus* at the SOMLIT-Astan station at the end of 2022 was unexpected (Fig. 1). This genus is indeed known to be systematically absent from English Channel waters (Humily et al., 2014; Tarran and Bruun, 2015) as was the case over the rest of the sampling period, an observation independently confirmed by the absence of divinyl chlorophyll *a* and *b*, two *Prochlorococcus*-specific pigment markers (Ralf and Repeta, 1992; Ras et al., 2008), in the corresponding HPLC analyses (data not shown). At the BOUSSOLE station, high *Prochlorococcus* concentrations were measured at the end of 2020 – early 2021, as well as at the end of 2021. This seasonality differs slightly from those previously observed for this genus in the central North Pacific Ocean, Sargasso Sea and Red Sea

(Campbell et al., 1994; Lindell and Post, 1995; DuRand et al., 2001), with maximum concentrations measured in summer and autumn. Interestingly, *Prochlorococcus* did not reach as high concentrations as *Synechococcus*, whereas it is generally more abundant than its counterpart in oligotrophic areas (Partensky et al., 1999).

Bacteria and viruses were respectively more abundant than picocyanobacteria, but their abundances showed no clear evidence of seasonality (Supplementary Fig. 1).

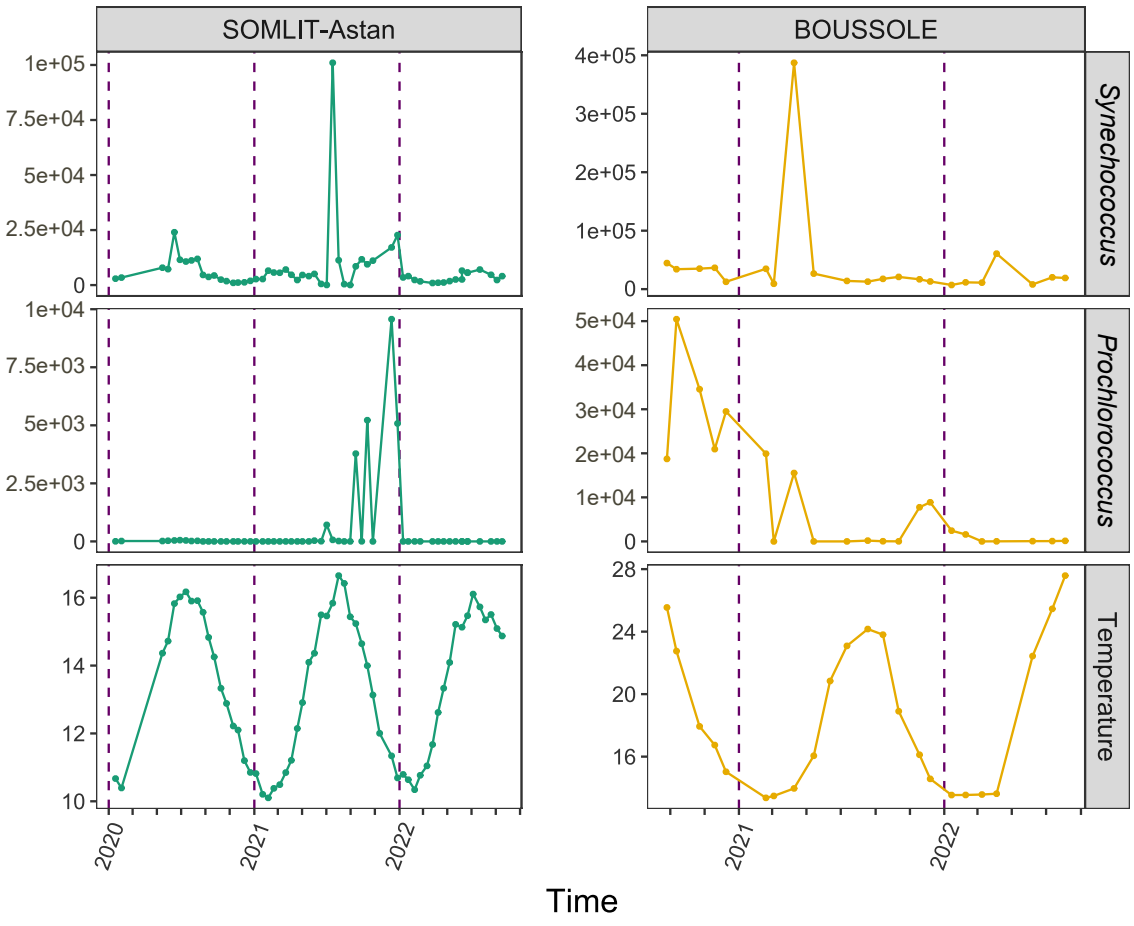

Figure 1: Seasonal dynamics of *Synechococcus*, *Prochlorococcus* and seawater temperature in subsurface in the Western English Channel (SOMLIT-Astan, left panels) and in the Mediterranean Sea (BOUSSOLE, right panels). Sampling was performed twice a month from 2020-02 to 2022-10 at SOMLIT-Astan and every month from 2020-08 to 2022-08 at BOUSSOLE. Picocyanobacterial cell concentrations were measured by flow cytometry and seawater temperature with a CTD profiler.

Variations of chlorophyll *a*, zeaxanthin and carotenes (Fig. 2) were in agreement with *Synechococcus* dynamics. High concentrations of the three pigments were indeed measured during blooms of this picocyanobacterium at both sites. This result is not very surprising as the combination of the three signals is expected to reflect pretty well the abundance of *Synechococcus* (Ras et al., 2008).

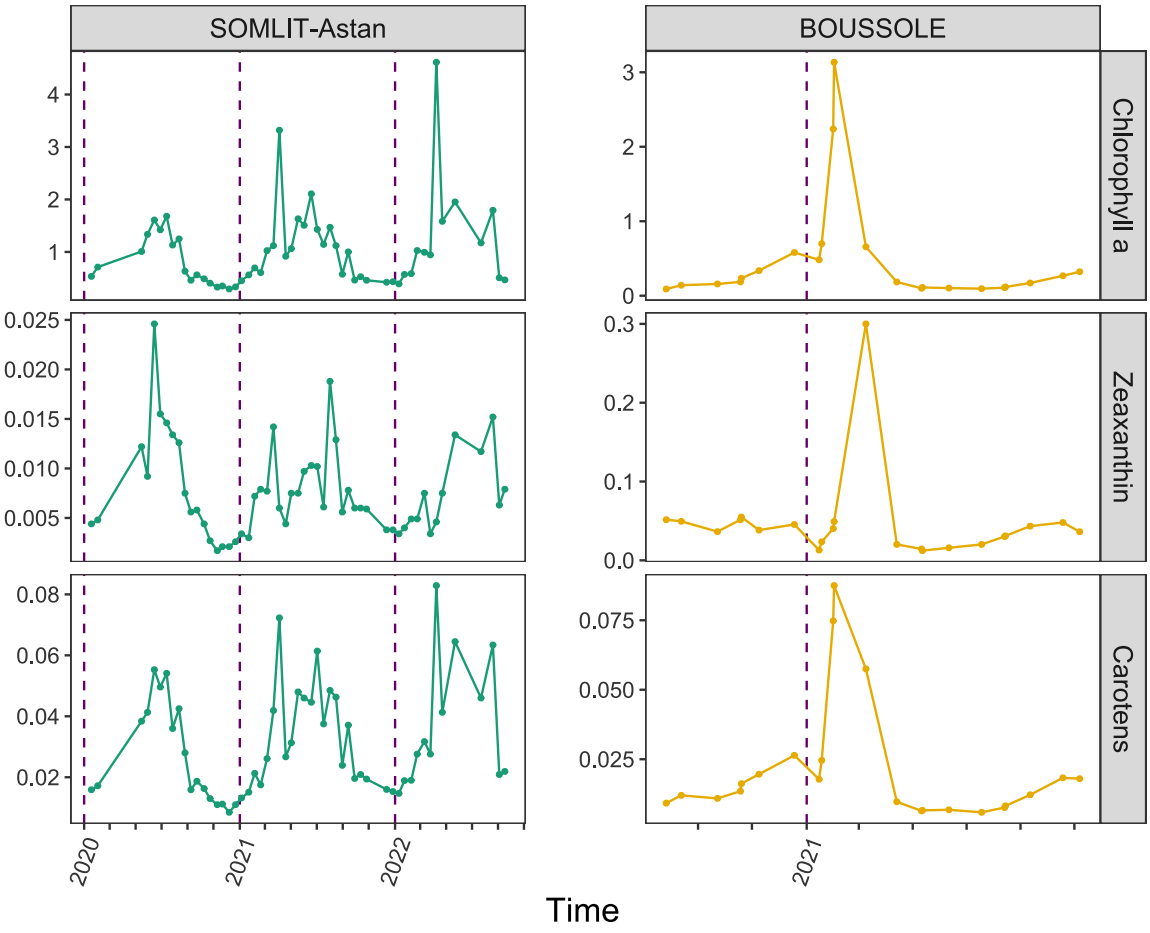

<u>Figure 2:</u> Seasonal dynamics of liposoluble pigments in subsurface in the Western English Channel (SOMLIT-Astan, left panels) and in the Mediterranean Sea (BOUSSOLE, right panels). Sampling was performed twice a month from 2020-02 to 2022-10 at SOMLIT-Astan and every month from 2020-08 to 2022-08 at BOUSSOLE. Chlorophyll *a*, zeaxanthin and carotens concentrations (mg per m^3) were estimated by HPLC. Data for the period 2022-01 to 2022-08 was not yet analysed at BOUSSOLE at the time of writing this PhD thesis report.

As expected from previous literature (Sournia and Birrien, 1995; Antoine et al., 2006), temperature displayed a clear seasonal pattern at both stations, with minimum and maximum values being achieved during winter and late summer respectively (Fig. 1). Interestingly, *Synechococcus* abundance peaks coincided with the warmest waters of the year at the SOMLIT-Astan station, while it occurred shortly after the temperature minimum at BOUSSOLE. Yet, given the sharp difference in the ranges of annual surface seawater temperatures between the two stations, *Synechococcus* abundance actually peaked at similar temperature (around 16°C) at both sites.

As concerns nutrients, although concentrations were highly variable throughout the year and followed marked seasonal cycles at both sites, all were generally less abundant in the northwestern Mediterranean Sea than in the English Channel water at a given time of the year (Fig. 3). This is consistent with the fact that these sites are representative of temperate oligotrophic and mesotrophic areas, respectively (Sournia and Birrien, 1995; L'Helguen et al., 1996; Antoine et al., 2008). At the BOUSSOLE station, nitrate, nitrite and phosphate concentrations all peaked early in the year, after the winter mixing and just before the annual peak of *Synechococcus* abundance. At the SOMLIT-Astan station, nitrate and phosphate concentrations exhibited very similar variations, with maximum measured in winter/spring, while nitrite and ammonium were more abundant in autumn and summer, respectively. As a consequence, *Synechococcus* summer blooms in the English Channel were associated to low nitrate, nitrite and phosphate, but high ammonium concentrations.

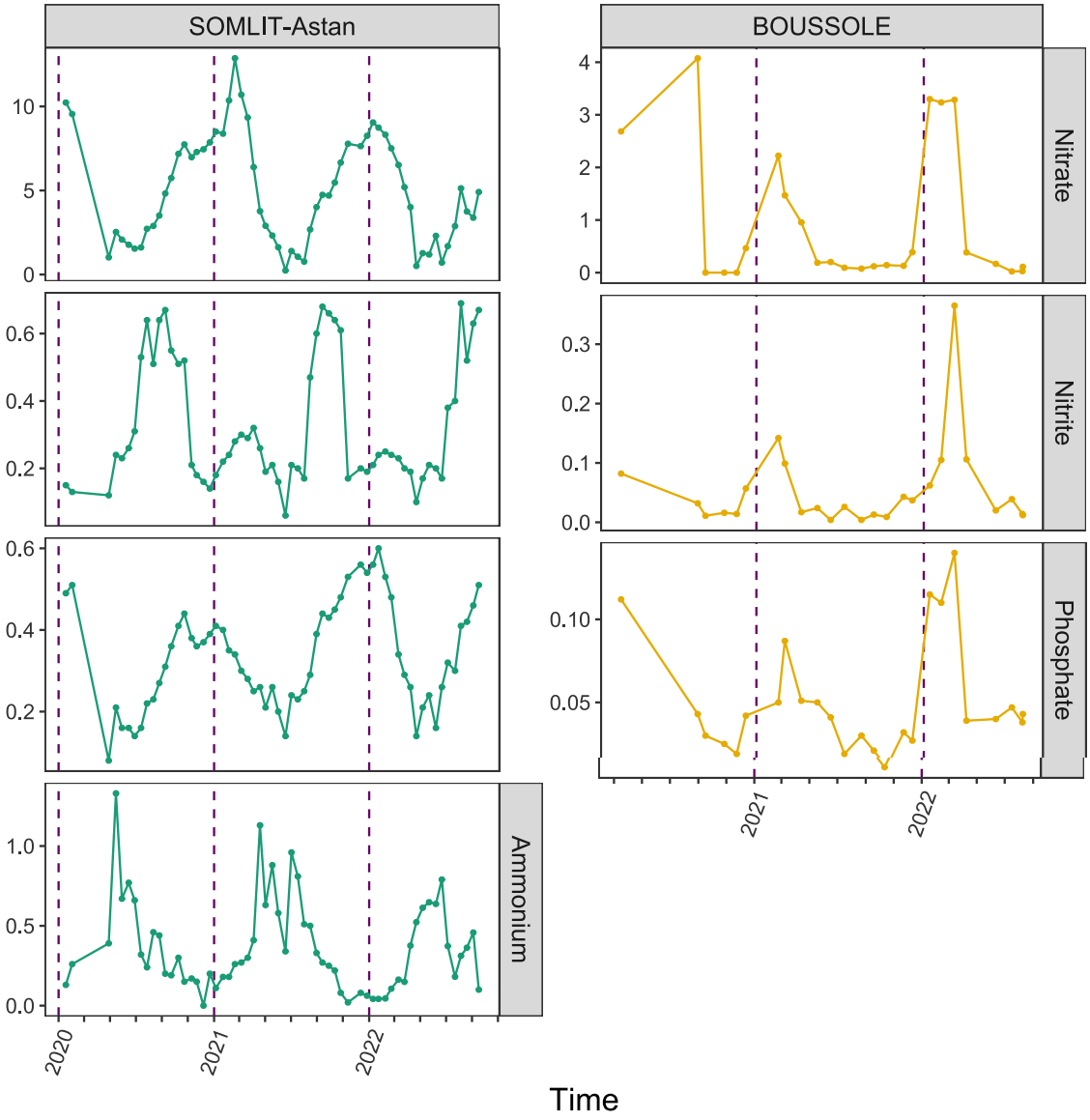

Figure 3: Seasonal dynamics of nutrients (µM) in the Western English Channel (SOMLIT-Astan, left panels) and in the Mediterranean Sea (BOUSSOLE, right panels). Sampling was performed twice a month from 2020-02 to 2022-10 at SOMLIT-Astan and every month from 2020-03 to 2022-08 at BOUSSOLE. Ammonium concentrations were measured only at SOMLIT-Astan.

The remote-sensing reflectance (R_{rs}), a measure of the water-leaving radiance normalized by the downwelling solar irradiance, was estimated for each time point at three selected wavelengths (at 443 and 490 nm for the blue part of the visible light spectrum, at 555 nm for the green part). Two ratios, $R_{rs(443)}$:$R_{rs(555)}$ and $R_{rs(490)}$:$R_{rs(555)}$ were further computed in order to describe the light quality available for *Synechococcus* cells in subsurface at both sites. At

BOUSSOLE, the two ratios were most of the time greater that 1.0 (Fig. 4), indicating that subsurface waters were mostly blue all year round. Yet, a clear seasonal cycle occurred, with the highest ratios being reached in summer and fall. In contrast, the temporal variations of the $R_{rs(443)}$:$R_{rs(555)}$ and $R_{rs(490)}$:$R_{rs(555)}$ were more erratic at the SOMLIT-Astan station, fluctuating between values below and above 1.0. Surface waters seemed to rapidly alternate between blue and green, a dynamic pattern likely related to the extensive water mixing due to strong tides and possibly to the highly variable cloud cover occurring at this station. Although a seasonal cycle of light quality seemingly occurs, with higher ratios in summer/fall and lower ones in winter/spring, it is largely hindered by these local processes.

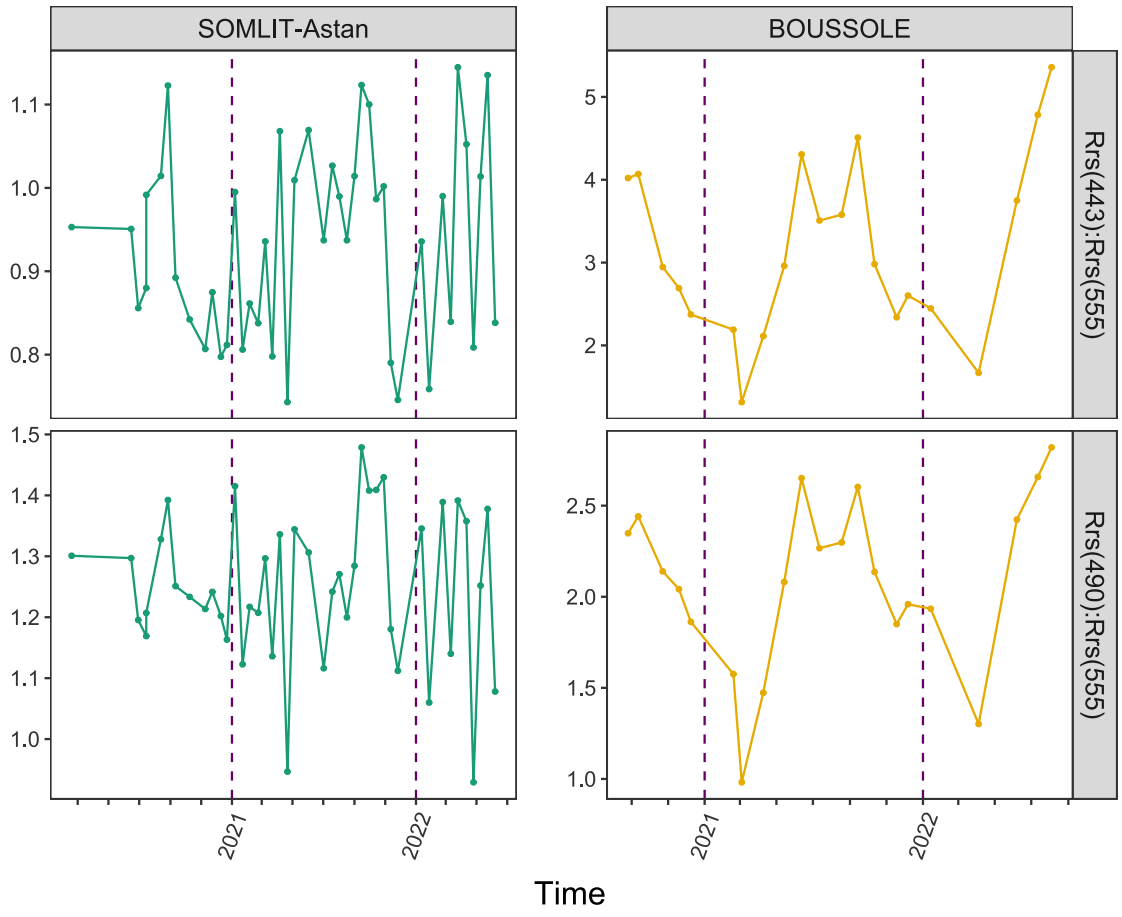

Figure 4: Seasonal dynamics of spectral remote reflectance sensing (R_{rs}) ratios in the Western English Channel (SOMLIT-Astan, left panels) and in the Mediterranean Sea (BOUSSOLE, right panels). Sampling was performed twice a month from 2020-02 to 2022-06 at SOMLIT-Astan and every month from 2020-08 to 2022-08 at BOUSSOLE. R_{rs}, which is defined as the ratio of upwelling radiance emerging from the ocean to downwelling irradiance reaching the water, was assessed at three wavelengths (443, 490 and 555 nm) from C-OPS data. Two R_{rs} ratios, $R_{rs(443)}$:$R_{rs(555)}$ and $R_{rs(490)}$:$R_{rs(555)}$, were further computed for each sampling date.

Vertical profiles performed with the multi-spectral radiometer (C-OPS) also enabled us to look at changes in irradiance occurring with depth at specific wavelengths. Again, two ratios $Irr_{443:555}$ and $Irr_{490:555}$ were computed in order to characterize the underwater light color. Results similar to those described for remote-sensing reflectance were obtained. Both ratios were in fact mostly above 1.0 at the BOUSSOLE station, meaning that blue light predominated (Fig. 5). The effect was even more marked at depth, since the ratios increased from the surface to the bottom of the euphotic layer. This result is consistent with the fact that the northwestern Mediterranean Sea is oligotrophic. In these environments, blue light is indeed scattered by water molecules and thus penetrates deeply into the water column (Stomp, 2008). At SOMLIT-Astan, the $Irr_{443:555nm}$ ratio was again more variable and mostly comprised between 0 and 1.0, the few values higher than 1.0 corresponding to the surface. This result is in line with previous studies on coastal environments which have demonstrated that green light penetrates the deepest, the high concentrations of Chl *a* and organic matter effectively absorbing red and blue regions of the visible light spectrum (Stomp, 2008).

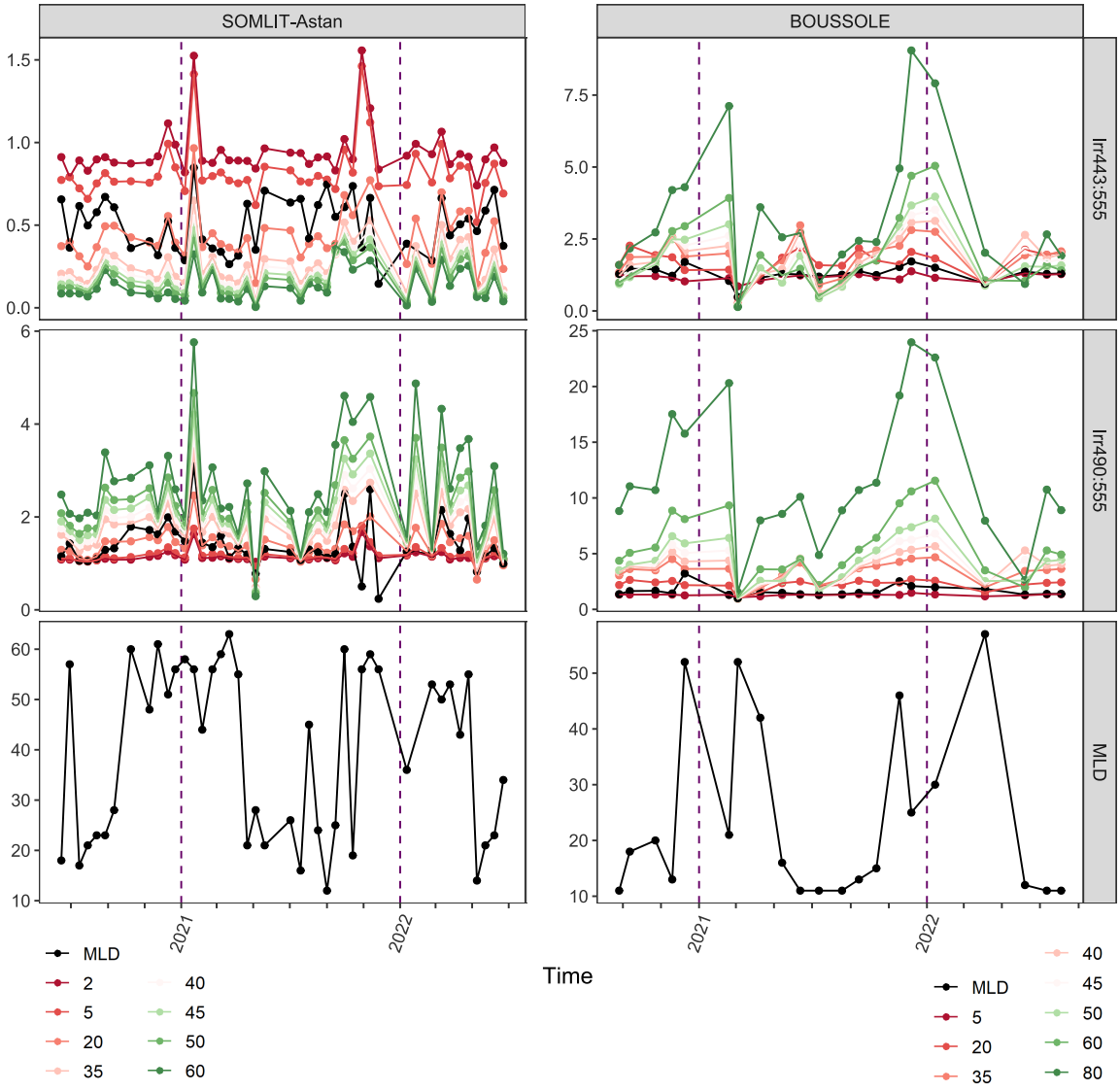

Figure 5: Seasonal dynamics of irradiance (Irr) ratios in the Western English Channel (SOMLIT-Astan, left panels) and in the Mediterranean Sea (BOUSSOLE, right panels), and depth of the mixed layer (MLD). Sampling was performed twice a month from 2020-02 to 2022-06 at SOMLIT-Astan and every month from 2020-08 to 2022-08 at BOUSSOLE. Two irradiance ratios, $Irr_{443:555}$ and $Irr_{490:555}$, were computed from C-OPS data for each sampling date. The mixed layer depth (m) was also assessed from C-OPS data.

Another striking result is the fact that the mixed layer depth varied according to the season in SOMLIT-Astan (Fig. 5), while the site has always been described as permanently mixed.

III.2.b. Vertical profiles at the BOUSSOLE station

An Ocean Data View map of *Synechococcus* abundance (Fig. 6A) at the BOUSSOLE station confirmed what was described above in subsurface, with blooms mainly occurring in spring. This marine picocyanobacterium was poorly detected below 60 m, as previously observed (Partensky et al., 1999; Mella-Flores et al., 2011), but was able to achieve high cellular concentrations from the surface down to 50 m. In contrast, *Prochlorococcus* was most abundant between 25 and 50 m, and detected at greater depths than its counterpart (Fig. 6B).

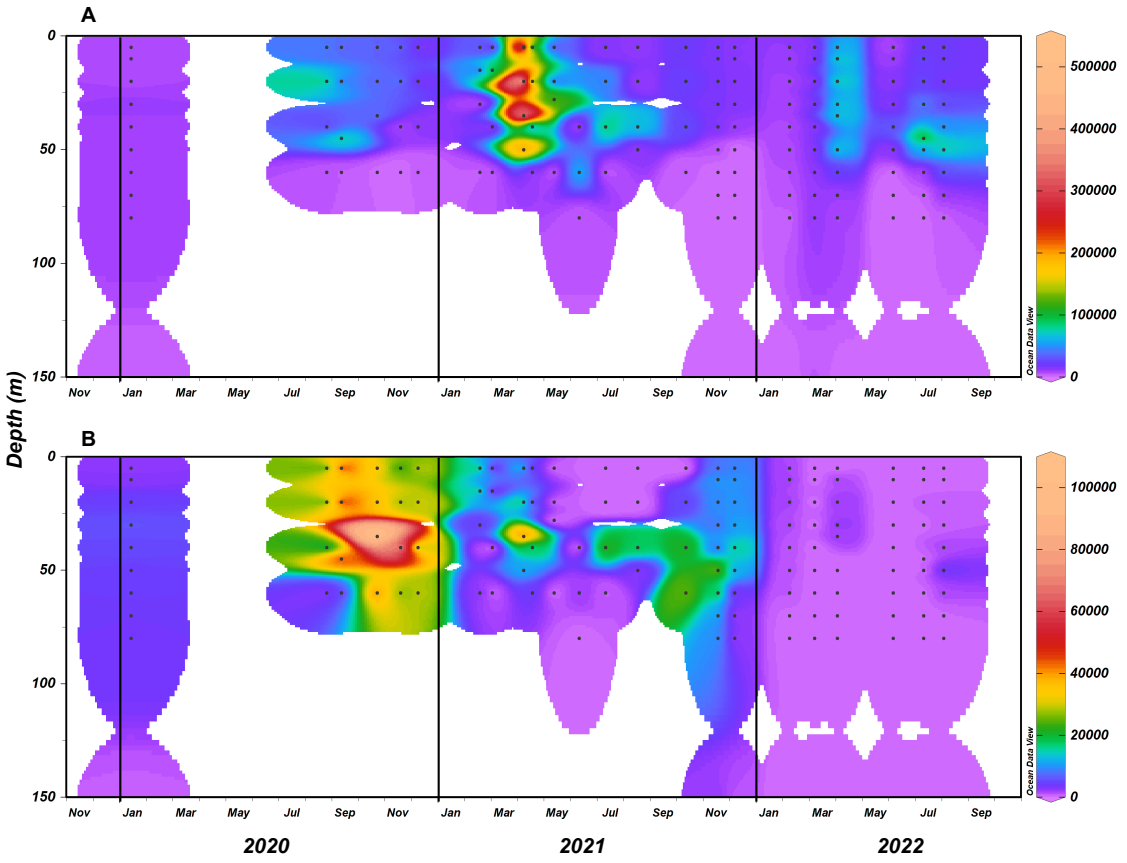

Figure 6: Contour plot of (A) *Synechococcus* and (B) *Prochlorococcus* abundances (cells per mL) for the BOUSSOLE time series. Small blacks dots correspond to collected samples (Ocean Data View (ODV) software, version 5.6.5, Schlitzer, R., https://odv.awi.de, 2018).

Chlorophyll *a*, zeaxanthin and carotenes were only detectable in the upper part of the water column, and more precisely from the surface down to 50 m, or more rarely 75 m (Fig. 7). The highest concentrations of zeaxanthin (Fig. 7B), a pigment marker quasi-specific to

Cyanobacteria (Ras et al., 2008), matched well with *Synechococcus* depth distribution. As concerns chlorophyll *a* (Fig. 7A), which is considered as a universal proxy for phytoplankton, and carotenes (Fig. 7C) that are found in a variety of taxa, both exhibited larger temporal distributions. Divinyl chlorophyll *a* and *b* were detected only at 25 m and below (Supplementary Fig. 3), which fitted well with the high *Prochlorococcus* abundances found at these depths in fall.

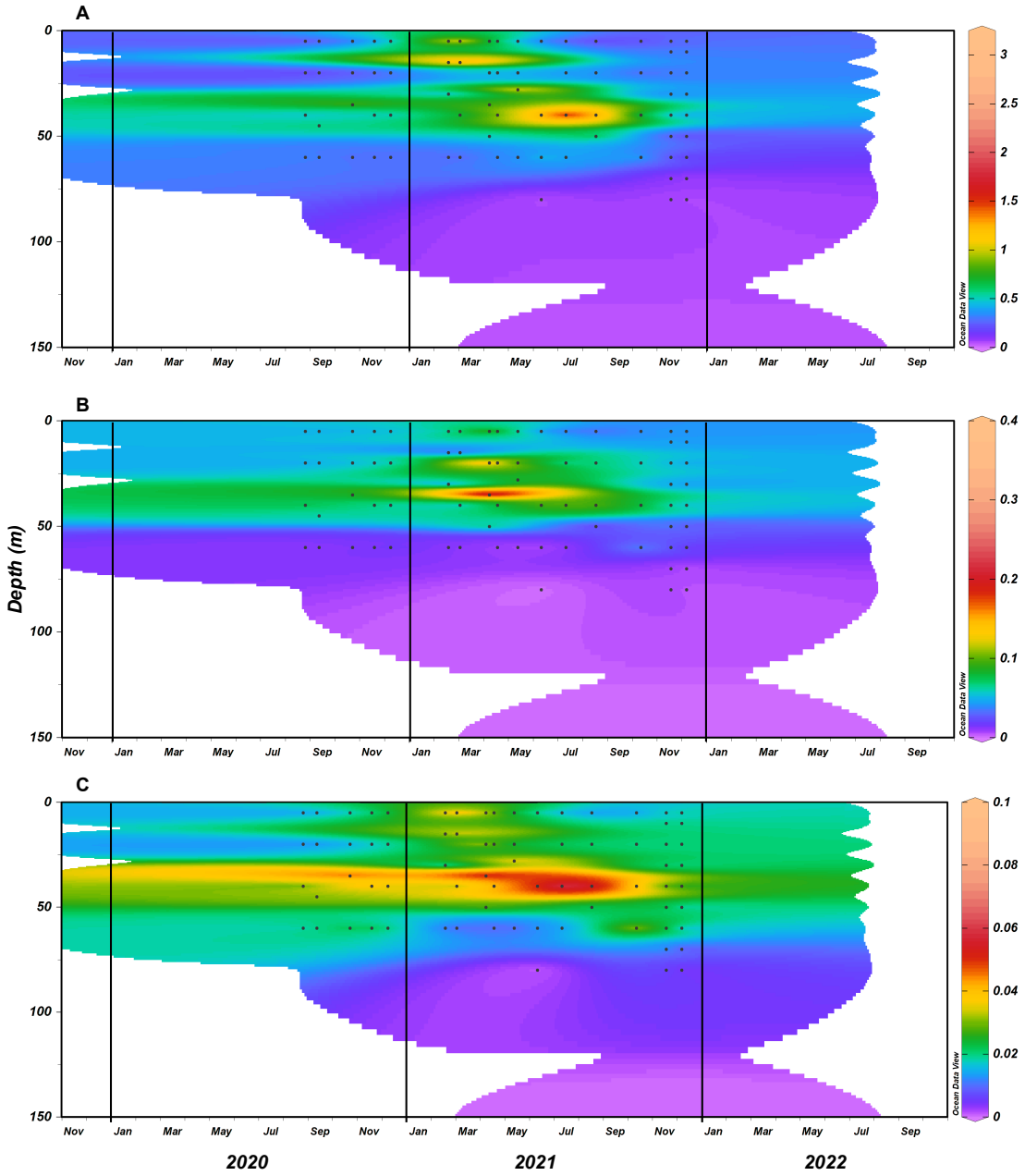

Figure 7: Contour plot of (A) chlorophyll *a*, (B) zeaxanthin and (C) carotenes (mg per m^{-3}) for the BOUSSOLE time series. Small blacks dots correspond to collected samples (Ocean Data View (ODV) software, version 5.6.5, Schlitzer, R., https://odv.awi.de, 2018).

Temperature and nutrient maps clearly highlighted: (i) stratification periods, as the one that lasted from March to the end of November 2021; and (ii) winter mixing events, as those that took place from December 2021 to April 2022 (Fig. 8). These alternations are typical of this marine region and have been extensively studied and described (Bustillos-Guzman et al., 1995). Each year, stratification sets when surface waters warm up, isolating the upper mixed layer from the deeper depths. During spring and summer, phytoplankton blooms consume all available nutrients in the surface layer. It is only in winter that the upwelling of deep cold nutrient-rich waters disrupt the stratification, and thus provide a new stock of nutrients that will be used by the phytoplankton during the following spring.

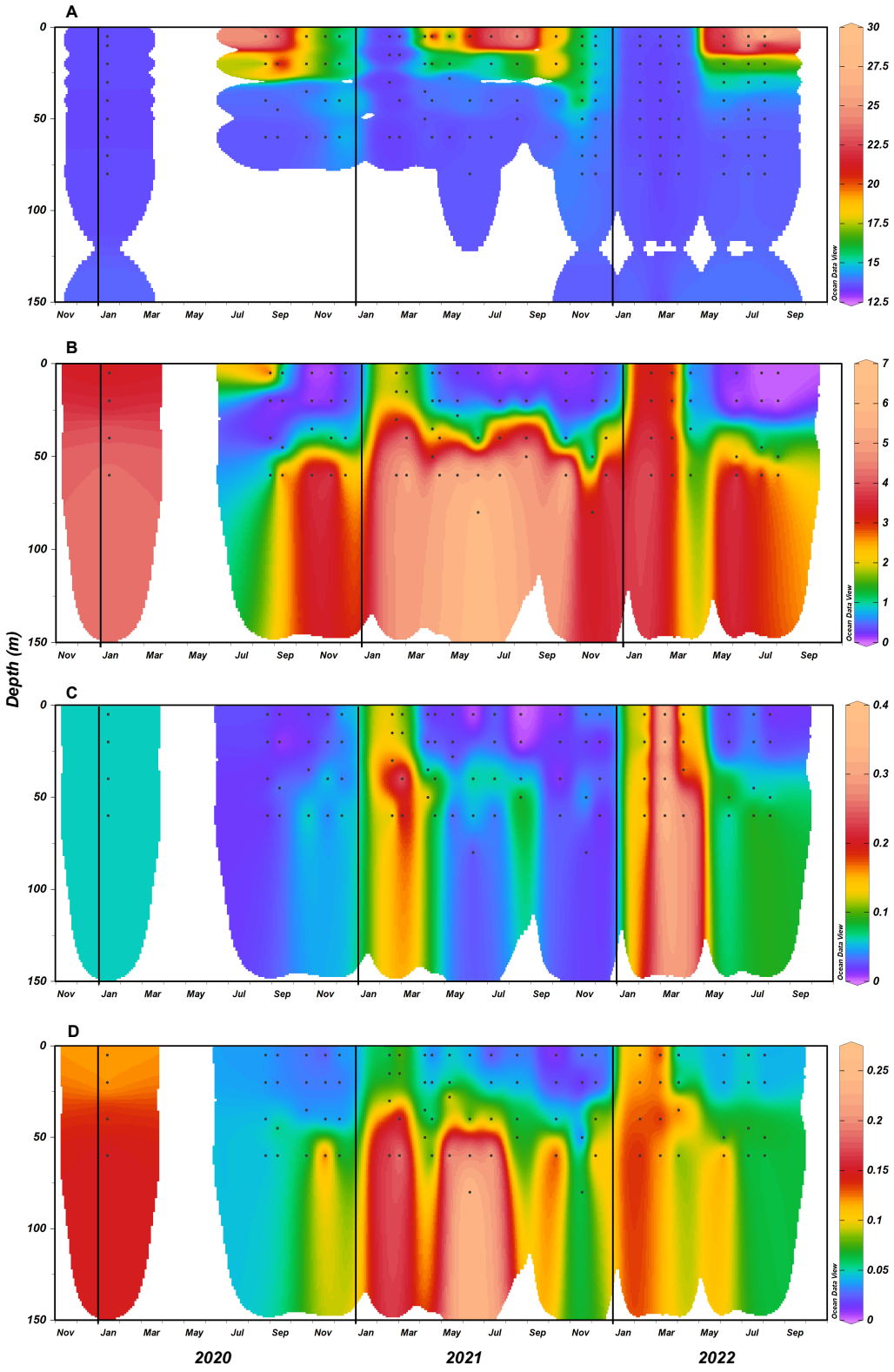

Figure 8: Contour plot of (A) temperature and (B) nitrate, (C) nitrite and (D) phosphate concentrations (in µM) for the BOUSSOLE time series. Small blacks dots correspond to collected samples (Ocean Data View (ODV) software, version 5.6.5, Schlitzer, R., https://odv.awi.de, 2018).

Even if metagenomics analyses could unfortunately not be performed before the submission of this thesis manuscript, it is possible to draw some hypotheses about *Synechococcus* PTs spatial and temporal distribution. Our expectations are that there will be virtually no PT 1 and 2 representatives at both stations, as previously reported in May 2012 at SOMLIT-Astan (Humily et al., 2014) and in summer in the Mediterranean Sea (Grébert et al., 2018). These two PTs are indeed usually restricted to marine estuaries and near coastal waters (Xia et al., 2017). However, a seasonal succession of PT 3 subtypes should occur at both sites, with distinct timing and relative proportions of PT 3a, 3c and 3dA and/or 3dB cells.

III.3. Future work

Analyses of the metagenomes collected at both stations will be performed in near future since sequencing results should be available in a couple of weeks. For this purpose, existing custom-designed pipelines will be adapted and used to recruit reads from both taxonomic (*petB*; Farrant et al., 2016) and phycobilisome gene markers (*cpcBA*, *mpeBA*, *mpeW*; Grébert et al., 2018) from the metagenomes. The relative abundance of the different *Synechococcus* clades and pigment types will then be correlated to ancillary parameters (temperature, nutrients availability, light quality, etc.), which I have already gathered into a single database to simplify further multivariate statistical analyses. These analyses will finally allow us to describe the temporal dynamics of *Synechococcus* PTs at two oceanographically contrasted sites, and nicely complement the previous findings from the *Tara* Oceans circumnavigation (Grébert et al., 2018). This study could also provide invaluable inputs for the global Ocean Darwin model, since seasonal variations of biotic and abiotic parameters are important factors to consider when modelling the spatial and temporal distribution of phytoplankton.

IV. Supplementary figures

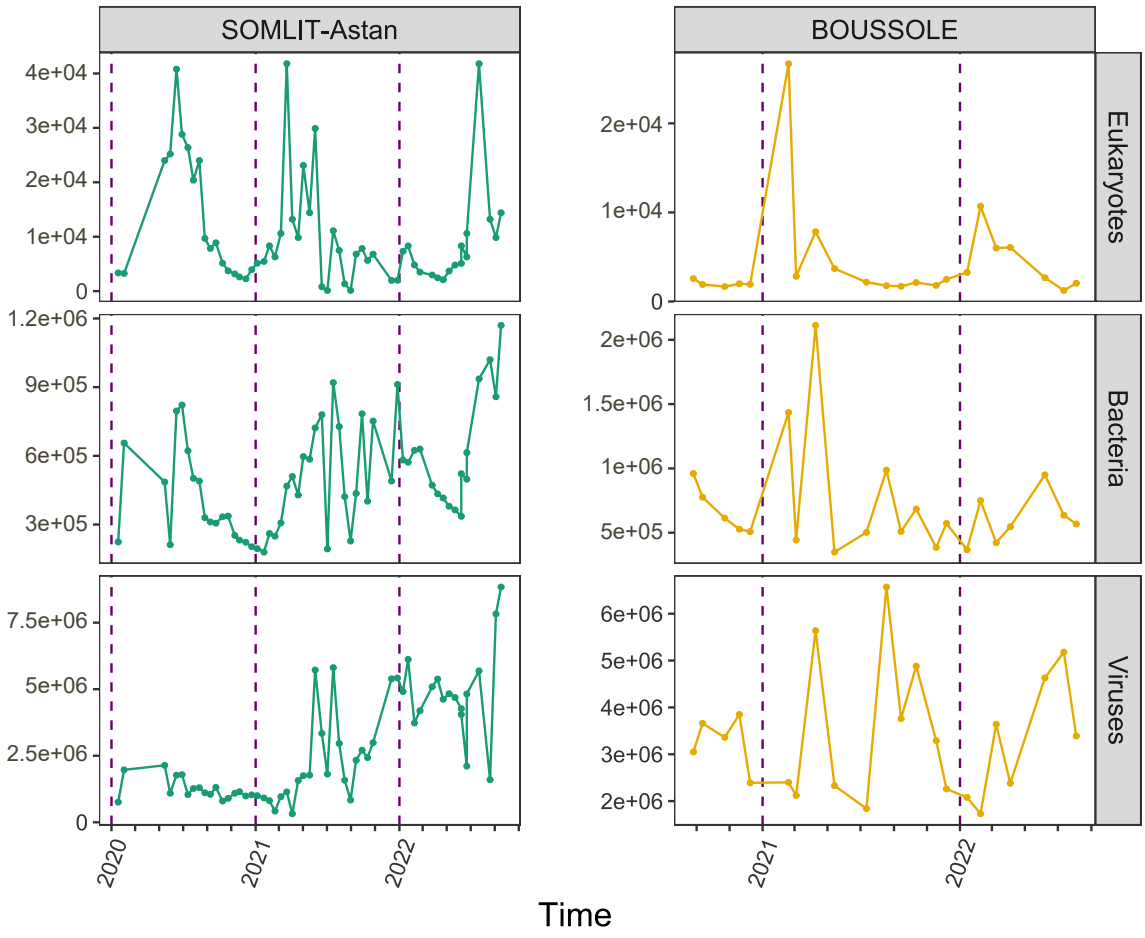

<u>Supplementary figure 1:</u> Seasonal dynamics of total eukaryotes, bacteria and viruses in the Western English Channel (SOMLIT-Astan, left panels) and in the Mediterranean Sea (BOUSSOLE, righ panels). The number of cells per mL of seawater was estimated by flow cytometry for each sampling date from 2020-02 to 2022-10 for SOMLIT-Astan and 2020-08 to 2022-08 for BOUSSOLE.

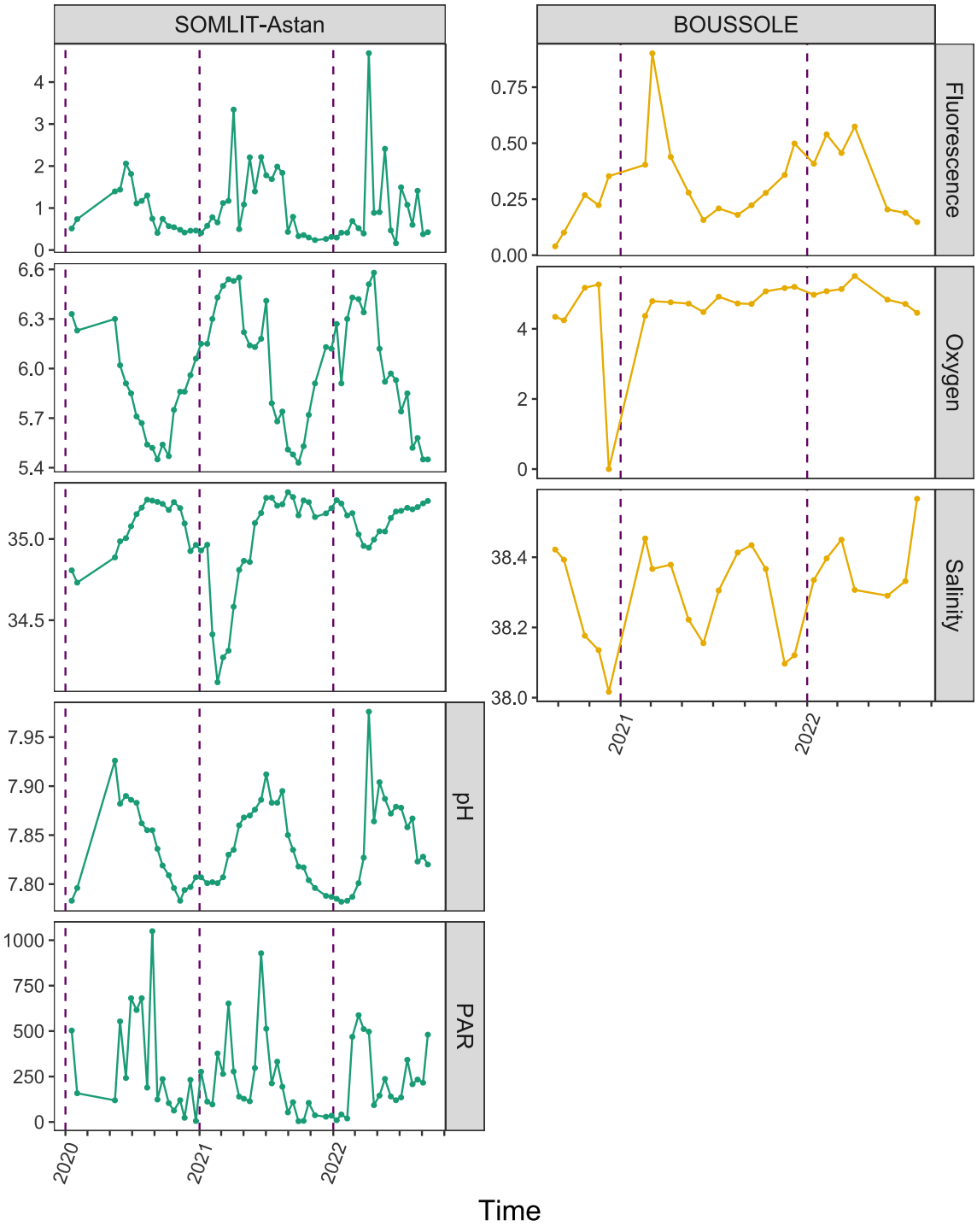

<u>Supplementary figure 2:</u> Seasonal dynamics of additional abiotic parameters in the Western English Channel (SOMLIT-Astan, left panels) and in the Mediterranean Sea (BOUSSOLE, right panels). Fluorescence (RFU), oxygen (mL L^{-1}), salinity (PSU), pH and photosynthetically active radiations (µE m^{-2} s^{-1}) were measured by sensors deployed on a CTD profiler for each sampling date from 2020-02 to 2022-10 for SOMLIT-Astan and 2020-08 to 2022-08 for BOUSSOLE.

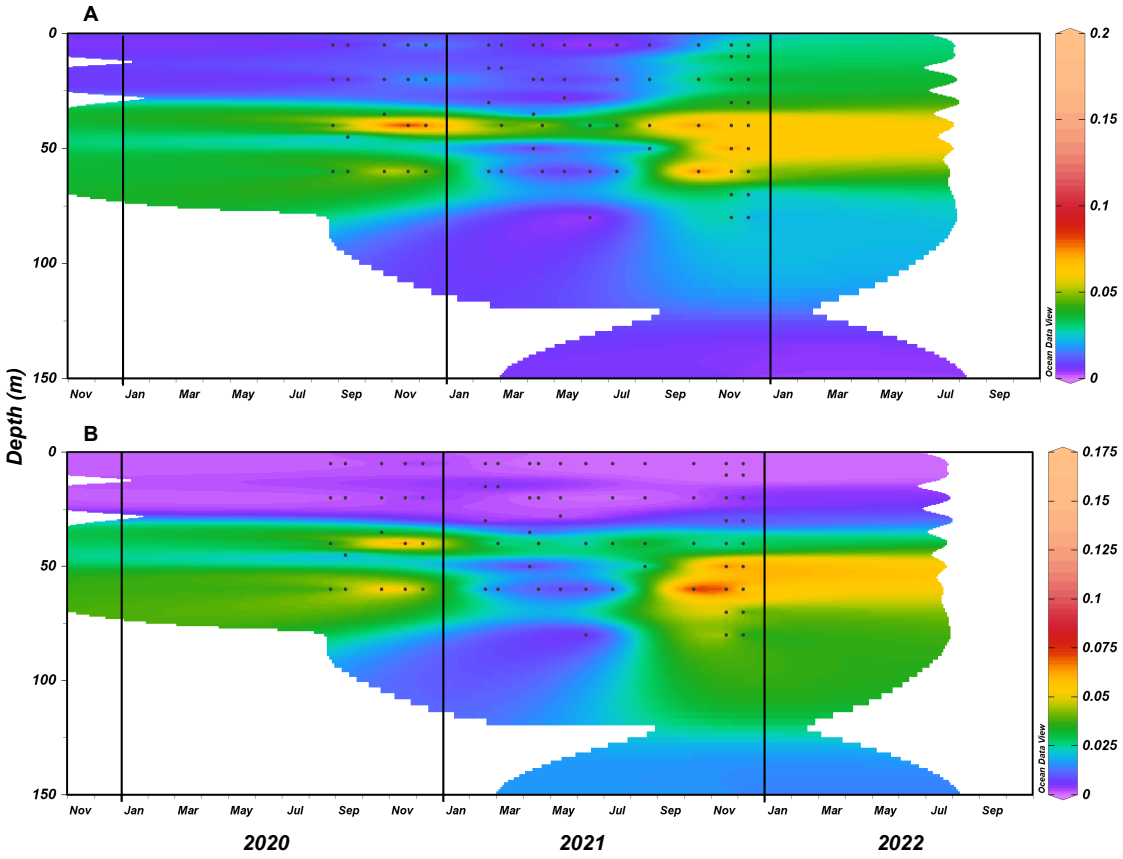

Supplementary figure 3: Contour plot of (A) divinyl-chlorophyll *a* and (B) divinyl-chlorophyll *b* (mg per m^{-3}) for the BOUSSOLE time series. Small blacks dots correspond to collected samples (Ocean Data View (ODV) software, version 5.6.5, Schlitzer, R., https://odv.awi.de, 2018).

V. Adaptation of Darwin model

The DARWIN model is a global ocean circulation and biogeochemistry model. It was developed in the framework of the DARWIN project (http://darwinproject.mit.edu/research/), and proved very powerful to study the diversity and biogeography of plankton communities. For example, by including multispectral optical properties and light absorption characteristics of various phytoplankton taxa, Hickman and collaborators (2010) were able to explore the role of nutrients, temperature and spectral light preferences in the competition among the different microorganisms in the South Atlantic Gyre. Moreover, the authors managed to reproduce a realistic vertical niche partitioning with (i) co-dominance of high-light adapted *Prochlorococcus* and *Synechococcus* in the upper layer; (ii) and low-light adapted *Prochlorococcus* and picoeukaryotes deeper in

the water column. Using another version of the DARWIN model, Dutkiewicz and co-workers (2015) demonstrated that all phytoplankton taxa will not react in the same way to the on-going global change, and particularly to ocean acidification. More recently, Dutkiewicz and collaborators (2019) showed that alterations of ocean color will greatly impact phytoplankton biomass and community structure, with an increase of the relative contribution of picophytoplankton at the expense of larger cells.

Among the many advantages of the DARWIN model is the possibility: (i) first, to parameterize the underwater light field and include the effects of optically active seawater constituents such as phytoplankton functional types, detrital particles and colored dissolved organic matter; (ii) second, to predict how climate change will affect these parameters. Therefore, this model seems ideally suited to predict the short and long-term variations of the relative abundances of *Synechococcus* PTs at the global scale.

At the time this manuscript was submitted, the dataset I produced on twelve strains representative of PTs 3a, 3c, 3dA and 3dB (PUB:PEB ratios, cell numbers, absorption spectra of whole cell normalized to chlorophyll *a*) was analysed and used by Francesco Mattei to calibrate the model. These data generated in BL, GL, as well as during a shift from BL to GL, proved very helpful to (i) implement realistic absorption spectra for PTs 3c and 3d, which were under-represented in the literature; (ii) assess the variability between and within pigment types; and finally (iii) provide new insights into the intermediate acclimation states that CA4 cells can display during a shift. All these data enabled Francesco to better encode the CA4 process into the model. Several simulations were carried out to examine the annual distribution of the three most abundant *Synechococcus* PTs (3a, 3c, 3d) on the global scale over the 200 first meters of the water column (Fig. 9). Although Francesco is still fine-tuning the model to get more refined and realistic results, the present simulations provided very promising and interesting results. As expected, PTs 3a and 3c exhibited complementary distributions in the field, the first being highly represented at high latitudes and the second in oligotrophic zones. As concerns chromatic acclimaters, they appeared widely distributed with particularly high contribution to the total *Synechococcus* population in transition zones between areas dominated by green or blue light specialists, respectively. The DARWIN model should therefore soon make it possible to describe, with a fine temporal scale, the

horizontal and vertical distribution of the different *Synechococcus* PTs according to the season. It should also provide further insights on the adaptive advantage of CA4, notably by describing the importance of each acclimation state of chromatic acclimaters (6 states in total: 2 fully acclimated to BL or GL and 4 in between) at the global scale.

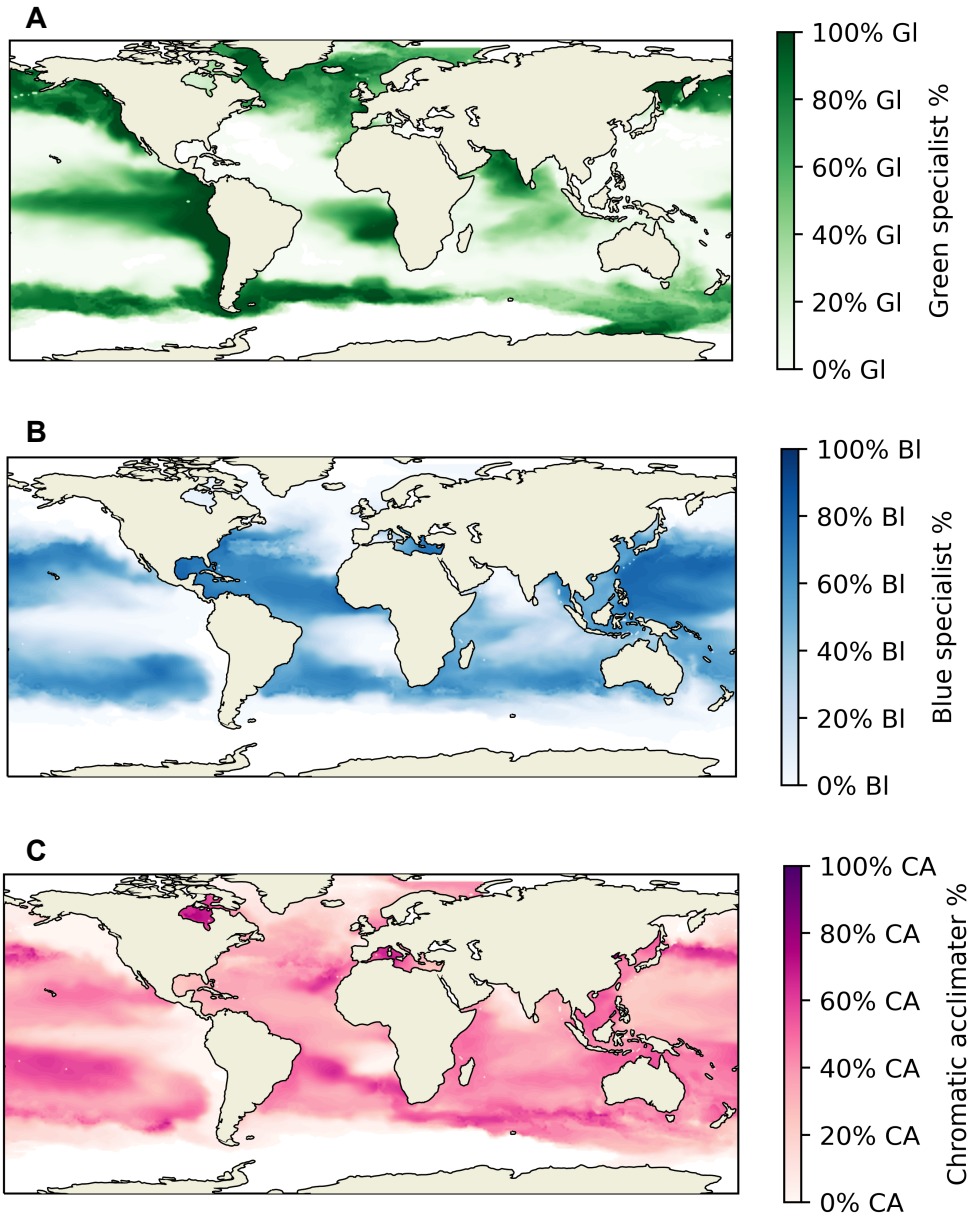

Figure 9: Map of annual distribution of the three most abundant *Synechococcus* pigment types at the global scale. (A) Green light specialist, or PT 3a. **(B)** Blue light specialists, or PT 3c. **(C)** Chromatic acclimaters, or PT 3d. Abundances were integrated over the 200 first meters of the water column (from Francesco Mattei).

Conclusions and Perspectives

In the framework of this PhD, I have studied the CA4 process in marine *Synechococcus* at three different organization scales: genes (Chapter 1), cells (Chapter 2) and populations (Chapter 3). I also contributed to a study dealing with the global ocean modelling of this process (Mattei et al., in prep.), which constitutes the fourth and largest organization scale. All confirmed that *Synechococcus* is a highly pertinent model in microbial ecology, as was stated before for *Prochlorococcus* (Coleman and Chisholm, 2007). *Synechococcus* is however better suited for experimental work, since it is easier to grow and several hundreds of clonal strains are available in culture collections (including about 500 in the RCC), compared to a few dozen *Prochlorococcus* strains (including less than ten in the RCC). Moreover, it is genetically tractable, an approach which remains so far inaccessible to *Prochlorococcus*. Furthermore, numerous *Synechococcus* genomes have been sequenced and annotated (97 in Cyanorak v2.1, of which 81 are non-redundant and cover fairly well the broad genetic and pigment diversity of the genus; Doré et al., 2020; Garczarek et al., 2021). These constitute an extensive reference genome data set available for researchers. In addition to being well suited for comparative physiology experiments and functional studies, *Synechococcus* also has the advantage of being an ecologically relevant model. Compared to *Prochlorococcus*, *Synechococcus* is more ubiquitous and its estimated contribution to the oceanic net primary production is twice higher (16 vs. 8%; Flombaum et al., 2013).

I. Molecular characterization of the genes and proteins involved in CA4

The molecular tool used in this thesis, the CRISPR-Cas system, was discovered in 1987 in *Escherichia coli* (Ishino et al., 1987) but its function remained unknown for a long time. Notable advances were made in the early 2000s, leading to the hypothesis that CRISPR-Cas are involved in adaptive immunity, an assumption further tested and confirmed in several bacterial models (Barrangou, 2013; Marraffini, 2015). Since then, these systems have been used to develop tools for genome editing (modulation of gene expression, epigenetic modifications, immunization; Croteau et al., 2018; Donohoue et al., 2018) in a wide variety of organisms such as insects, mammals or plants. Still, this technology has not been used to the same extent in cyanobacteria. This is notably due to the fact that: (i) a high expression of Cas9, one of the best described endonucleases so far, can be toxic to these microorganisms

(Wendt et al., 2016); (ii) many cyanobacteria have a high level of ploidy (Griese et al., 2011); (iii) the effectiveness of the method is highly variable depending on the strain (Till et al., 2020). To overcome these issues, Ungerer and Pakrasi (2016) recently used the Cpf1 endonuclease (also called Cas12) from *Francisella novicida*. This alternate enzyme appeared to be globally efficient, precise, specific and easy to use in three cyanobacterial model strains (*Anabaena* PCC 7129, *Synechococcus elongatus* UTEX 2973 and *Synechocystis* PCC 6803). However, the application of CRISPR-Cas-mediated mutagenesis is still not routine in marine *Synechococcus*.

The first part of my thesis consisted in producing mutants of *Synechococcus* PT 3dB strain A15-62. Several genes were targeted: (i) the individual *fciA* and *fciB* genes, both having similar C-terminal regions to AraC family transcription factors (Sanfilippo et al., 2016) which form a large class of proteins that activate or repress transcription in many cellular responses (Gallegos et al., 1997); (ii) the whole *fciAB* operon; and finally (iii) *unk10*, which presents no clear sequence homology to any known protein except for the presence of a Nif11-like N-terminal domain (Grébert et al., 2022) potentially involved in the biosynthesis of ribosomally produced peptides (Haft et al., 2010). Unfortunately, inactivation of these genes in our model strain A15-62 using a CRISPR-Cpf1-mediated genome editing approach is still in progress, except for *fciB* (see Chapter 1). As a consequence, the role of these genes in the CA4-B process could not be demonstrated before submitting this thesis manuscript. Still, it is possible to draw a provisional model of CA4-B regulation, based on the one proposed by Sanfilippo and collaborators (2016) for CA4-A (Fig. 1A) and complemented by the partial phenotype of the A15-62 *fciB*$^-$ mutant. Indeed, CA4-A and B genetic islands being quite similar, we can postulate that their respective regulatory systems are analogous. In this context, it is most likely that FciB, whose interruption causes a constitutive BL phenotype, is also a regulator of the CA4 process. However, while FciB was suggested in PT 3dA cells to repress the expression of *mpeZ*, which encodes a lyase isomerase binding PEB to Cys-83 of the PE-II α-subunit and isomerising it into PUB in BL (Shukla et al., 2012), the function of FciB in PT 3dB strains is probably to directly or indirectly activate *mpeW*, which encodes a lyase that binds PEB to the same site in GL (Grébert et al., 2021). Moreover, if FciA also has an opposite function to FciB in CA4-B, as it is the case in the CA4-A system, then it should act as

a direct or indirect repressor of MpeW activity in BL (Fig. 1B). Of note, the expression of the *unk10* gene was found to be strongly upregulated in BL in both CA4-A and B representative strains (Doré 2013; Sanfilippo et al., 2016), which suggests that, like in PT 3dA cells, Unk10 is directly or indirectly activated by FciA in BL and repressed by FciB in GL in PT 3dB strains. This different regulation pathway between PTs 3dA and 3dB is possibly related to the specific presence of the phage-like regulator FciC in PT 3dA only. Still, these assumptions remain highly speculative and their confirmation still awaits the complete characterization of the *fciA*, *fciB* and *unk10* genes (PUB:PEB ratio, genes expression, PBS chromophorylation) in *Synechococcus* sp. A15-62.

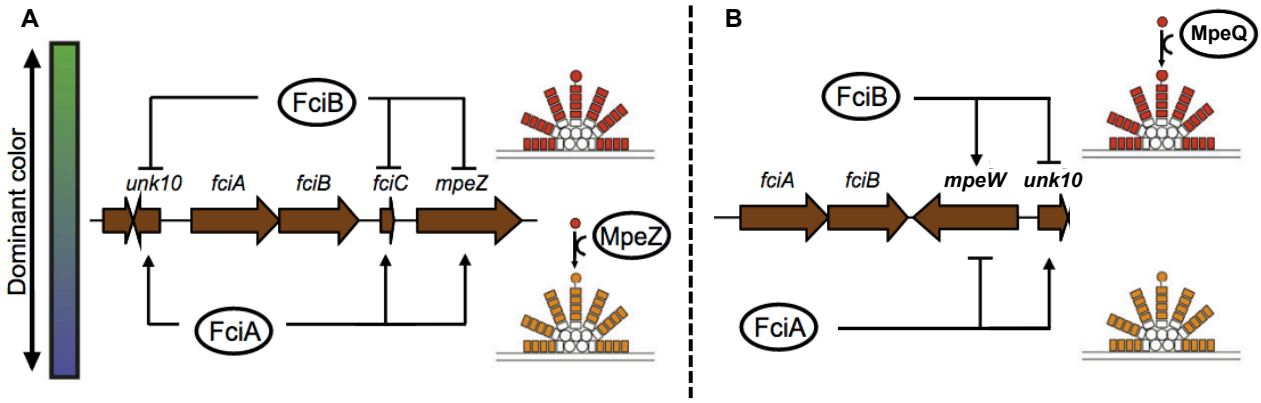

Figure 1: Hypothetical model of CA4-B regulation, as compared to the model previously proposed for CA4-A regulation. (A) in CA4-A, FciA activates the expression of *mpeZ*, *fciC* and *unk10*, leading to PBS containing more PUB when BL predominates. When GL is prevalent, FciB represses the expression of the same three genes, leading to PEB-rich PBS (Sanfilippo et al., 2016). MpeZ, which converts PEB into PUB and attaches it to MpeA-C83, is more highly expressed in BL (Shukla et al., 2012). It competes with a lyase encoded outside the CA4-A genomic island, MpeY, which attaches PEB to the same site and is not light regulated (Sanfilippo et al., 2019b). The function of FciC and Unk10 is unknown yet, but the expression of both genes is up-regulated in BL, suggesting that they also have a role in the CA4 process. (B) The CA4-B genomic island is composed of fewer genes. By homology with the CA4-A process and the partial phenotype of *fciB*$^{-}$ mutant, one may assume that FciA and FciB could be direct or indirect regulators of the CA4-B process, FciB activating and FciA repressing *mpeW* expression. MpeW, which attaches PEB to MpeA-C83, is more expressed in GL. It competes with a lyase-isomerase encoded outside the CA4-B genomic island, which converts PEB into PUB at the same site and is not light regulated (Grébert et al., 2021). Since *unk10* expression is up-regulated in BL and down regulated in GL in the CA4-B process, one may assume that, like in the CA4-A process, it is activated by FciA and repressed by FciB (modified from Sanfilippo et al., 2016).

However, if these predictions hold true, this would reinforce the hypothesis that PT 3dB strains are former BL specialists who have gained the ability to also use green light by acquisition of the CA4-B island, and conversely that PT 3dA strains are former GL specialists who have acquired CA4 capacity thanks to the acquisition of a CA4-A island (Sanfilippo et al., 2019a; Grébert et al., 2021). To further confirm this hypothesis, it would be interesting to transform several BL and GL specialists with either CA4-A or CA4-B genomic islands, and to test that they have acquired CA4 capacity. Of note, Théophile Grébert has already successfully cloned the CA4-B genomic island from *Synechococcus* sp. A15-62 into an autonomously replicating plasmid, and further introduced it into two *Synechococcus* PT 3c strains (CC9605 and WH8102). As expected, both transformed strains were capable of decreasing their PUB:PEB ratio after transfer to BL, suggesting that the CA4-B genomic island is necessary and sufficient to confer PT 3c strains the ability to perform chromatic acclimation. However, more work is needed to confirm this hypothesis, notably to check if the complementary experiment can also work, given that GL specialists are phenotypically not totally equivalent to chromatic acclimaters acclimated to GL (PUB:PEB ratio of about 0.4 and 0.6, respectively; Humily et al., 2013).

Another unanswered question concerns the sensor(s) that drive(s) the CA4 process. Indeed, unlike CA2 or CA3-capable cyanobacteria, marine *Synechococcus* are unlikely to use cyanobacteriochromes for light color sensing, since no genes encoding such proteins have been identified in their genomes (Sanfilippo et al., 2019a). In this context, the fact that CA4 islands seem to be necessary and sufficient to confer CA ability (Shukla et al., 2012; Humily et al., 2013; Sanfilippo et al., 2016; Grébert, 2017) suggests that genes present in both islands (*fciA*, *fciB* or *unk10*) could be involved in this function. It would thus be interesting to further investigate this hypothesis.

II. Fitness advantage of the different pigment types of marine *Synechococcus*

The ECOMAP team, which has been working on picocyanobacterial models for over 30 years, has accumulated a lot of experience with *Prochlorococcus* and *Synechococcus* culturing techniques. Indeed, numerous comparative physiology experiments have been conducted by the team in batch or cyclostat, under different conditions of temperature

(Pittera et al., 2014; Breton et al., 2020; Six et al., 2021; Ferrieux et al., 2022), nutrient availability (Ferrieux et al., in prep), or irradiance levels (Six et al., 2004, 2007a; Blot et al., 2011; Guyet et al., 2020). During the second part of my this thesis, a new culturing method previously developed by Huisman and collaborators (2002), the chemostat, was successfully implemented in Roscoff and adapted to marine picocyanobacteria. This approach, which made it possible to maintain the same culture for several months, has proved very useful to look at the adaptive value of the different PTs of *Synechococcus* under different conditions of light quality and quantity. Indeed, we demonstrated that the PT 3dB representative was at disadvantage in low light compared to the specialists, but that it was capable of co-existing with them in a mix of high blue and green light. More unexpectedly, the PT 3dB strain won the competition in high blue light. At the scale of the global ocean, where five distinct spectral niches are available for photosynthesis (violet, blue, green, orange and red; Holtrop et al., 2021), a generalization of these results would imply that chromatic acclimaters would be predominant in surface waters characterized by a high abundance of blue light, as well as at intermediate depth where the underwater light field consists in a mix of blue and green wavelengths. As concerns BL specialists, our results indicate that they should preferentially thrive at depth in the open ocean where low blue light predominates, whereas GL specialists should be encountered at all depths in greenish waters. These predictions correspond fairly well to what has been observed *in situ* by Grébert and collaborators (2018). Indeed, PT 3a cells were more abundant in intertropical oceanic borders and regional seas (Red Sea, Arabian Sea, Panama/Gulf of Mexico) associated with green particle-rich waters. PT 3c cells were dominant in transparent, oligotrophic areas (Mediterranean Sea, South Atlantic, Indian Ocean gyres), where blue light penetrates the deepest. As concerns chromatic acclimaters (PTs 3dA and 3dB), they co-occurred with BL specialists in the open ocean and with GL specialists in more coastal and/or mixed temperate waters. However, the observation made by Grébert and co-workers (2018) that chromatic acclimaters were proportionally more abundant at depth and that their relative abundance was correlated with low photosynthetically available radiation, whereas BL specialists were proportionally more abundant in surface, seems somewhat at odds with our result that chromatic acclimaters could outcompete a BL specialist in HBL. Still, it must be noted that the *Tara Oceans* dataset was not ideal for drawing conclusions about the effect

of depth as it comprises only two depths for half of the stations sampled (Grébert et al., 2018). In this context, analyses of the metagenomic dataset from BOUSSOLE, where four depths were sampled over two years, should be very useful to confirm or not their observations.

As mentioned above, mono- and co-cultures have enabled the study of competition between three *Synechococcus* PTs for light quality and quantity. However, Holtrop and collaborators (2021) recently demonstrated that the underwater light spectrum could not completely explain the relative abundance of the major PTs at the global scale. In their study, the blue niche accounted for 21% of the variation in the relative abundance of PUB-rich cells across the globe. As concerns chromatic acclimaters, the co-occurrence of blue and green light explained only 19% of the variations. The percentage was however much higher for the PEB-rich cells, since it rose to 77%. These results are not very surprising since previous studies showed that the distribution of *Synechococcus* was mainly influenced by other abiotic parameters such as nutrient availability (nitrogen, phosphorus, iron), temperature and salinity (Farrant et al., 2016). Moreover, these selective factors are likely to interact, further complicating the distribution of marine picocyanobacteria in the environment. For example, Burson and co-workers (2018) proved that there is an interplay between competition for the underwater light spectrum and nutrient availability in different phytoplankton species. Indeed, photosynthesis and nutrient acquisition are highly connected by a network of physiological interactions, nutrients being needed to produce photosynthetic pigments, and nutrient uptake requiring energy generated through the electron chain transport. In this context, chemostats constitute excellent tools for studying the impact of a specific abiotic factor on representative strains, and combination of different factors could also be considered. However, as Burson and collaborators (2018) pointed out, chemostats are costly, labor intensive and time consuming, limiting the number of experimental conditions and replicates that can be performed at the same time. Still, insights obtained from chemostat experiments could be complemented by modelling in order to better assess the impact of environmental parameters on the actual and future distribution of marine *Synechococcus* at a global scale.

III. Phenotypic differences between the two types of chromatic acclimaters

As the first part of my thesis (Chapter 1) was focused on studying the CA4-B process, we also chose to use a PT 3dB during the chemostat experiments (Chapter 2 § IV). Still, the emergence and maintenance of two genetically different but related forms of CA4 over the course of evolution is quite intriguing. The fact that PTs 3dA and 3dB occupy complementary niches in the environment (Grébert et al., 2018) suggests that they may have distinct adaptive values. Thus, the second part of my thesis also involved searching for possible phenotypic differences between several representatives of both subtypes 3d in various conditions of temperature, light quantity and quality. We found that these differed in the BL to GL ratios necessary to trigger the CA4 process, the PT 3dB strains needing a larger proportion of green light to shift their pigmentation to the GL-acclimated state in comparison to the PT 3dA cells (and conversely for the latter with blue light). These findings lend further support to the above-mentioned hypothesis that PT 3dA and 3dB strains are former BL and GL specialists, respectively, who have gained the ability to also use GL or BL by acquisition of the CA4-B or CA4-A genomic islands, respectively. Furthermore, these results are consistent with mono-culture outcomes where the chromatic acclimater was shown to use BL preferentially to GL, even if both were available for photosynthesis. In this context, it could be worth examining the behaviour of PT 3dA strains in the same condition of culture that should, if consistent, preferably harvest GL.

As concerns the intermediate PUB:PEB ratios measured in mixed blue-green light conditions, several non-exclusive assumptions concerning *Synechococcus* cells pigmentation were proposed, but could not be demonstrated (see Chapter II § III). In order to refine them a little more, it could be interesting to look deeper into PBS chromophorylation of the same PTs 3dA and 3dB representatives acclimated to similar blue and green light mixtures (Shukla et al., 2012; Sanfilippo et al., 2016; Grébert et al., 2021), as well as lyase and lyase-isomerase expression by real-time RT-PCR (Grébert et al., 2021). At the same time, it would be interesting to get PBS images by classical electron microscopy (EM), as previously done by Arteni and collaborators (2009) with *Synechocystis* sp. strain PCC6803, or by cryo-EM, as achieved more recently by Sauer and co-workers (2021) with the same strain. These images

could help decipher if the decrease in the PE:PC ratio in PT 3dA strains from BL to GL is due to rod shortening and/or lower within-rod energy transfer efficiency.

The fact that PTs 3dA and 3dB exhibited differences in acclimation pace, with the former subtype displaying the most variability in terms of kinetics, was certainly one of the major results of this comparative study. The particular case of the two CRD1 representatives, which were stuck into an intermediate PUB:PEB ratio in HBL, is also quite interesting. Members of the CRD1 clade usually dominate *Synechococcus* communities in ultra-oligotrophic, iron poor areas such as the South Pacific gyre, which are likely to further expand as a result of climate change (Polovina et al., 2008; Sohm et al., 2015; Farrant et al., 2016). Interestingly, most CRD1 strains genomes (or metagenome-assembled genomes, MAGs) available to date are natural CA4-A-less mutant populations that are stuck in the BL-acclimated state due to the natural loss of *fciA/B* regulator genes and a degenerated (or missing) *mpeY* gene (Humily et al., 2013; Grébert et al., 2018, 2022). This adaptation is consistent with the fact that ultra-oligotrophic areas belong to the violet niche *sensu* Holtrop et al. (2021), where the ability to capture GL has no adaptive interest. However, CRD1 cells are also found in high-nutrient low chlorophyll (HNLC) areas, such as the Chilean upwelling (Farrant et al., 2016) or the equatorial Pacific Ocean, where the BIOS-U3-1 and MITS9220 strains were isolated, respectively. In such environments, GL is likely more important, possibly explaining why the two strains have kept their ability to perform CA4. However, the fact that they have a lower than expected $Exc_{495:545}$ ratio in HBL imply that they are unable to reach a fully acclimated BL phenotype. Thus, their absorption properties differ from that of specialists in all light quality conditions.

IV. Temporal and spatial dynamics of the different pigment types of marine *Synechococcus*

Following the discovery of the omnipresence and abundance of marine picocyanobacteria in the open ocean Johnson and Sieburth (1979), the distribution of *Synechococcus* in the environment has been extensively studied. In this context, the development and improved accessibility of metagenomics, as well as the advent of global expeditions, constituted two

important revolutions, providing a more detailed picture of *Synechococcus* ubiquity. These also led to new insights into the genetic diversity of the genus, notably by highlighting the ecological importance of five major clades *in situ*, each predominant in contrasting environments (Sohm et al., 2015; Farrant et al., 2016). As concerns *Synechococcus* pigment diversity, it was long assessed using fluorescent-based techniques (epifluorescence microscopy, spectrofluorimetry, flow cytometry; Campbell and Iturriaga, 1988; Olson et al., 1988; Lantoine and Neveux, 1997; Campbell et al., 1998; Wood et al., 1998; Michelle Wood et al., 1999; Neveux et al., 1999; Sherry and Michelle Wood, 2001; Haverkamp et al., 2008), which did not have the resolving power to fully differentiate all PTs and subtypes. Thus, the identification of three molecular markers necessary and sufficient to discriminate all of them (*cpcBA*, *mpeBA* and *mpeW*; Grébert et al., 2018) proved very useful. Indeed, in analysing the metagenomic data from the *Tara* Oceans expedition with those markers, the authors provided a crucial knowledge on the relative abundance and spatial distribution of all PTs at the global scale. However, data concerning their temporal variability were lacking. The last part of my thesis therefore consisted in studying the seasonal variations of the different PTs of *Synechococcus* over two successive years at two stations with contrasting oceanic regimes (SOMLIT-Astan and BOUSSOLE).

Although the metagenomics analysis was still in progress at the time of writing this thesis manuscript, it is possible to draw some working hypotheses about the relative abundance and seasonal successions of PTs 3a, 3c and 3d in the field. As the water tends to be bluer at BOUSSOLE, we can expect to observe high proportion of PT 3c representatives all year round, and especially at depth where blue light predominates over other wavelengths (Stomp, 2008) and light intensity decreases (see Chapter 2 § IV). However, remote sensing reflectance and irradiance data revealed that the proportion of GL could be significant at certain times of the year, and more particularly in surface waters, thus offering an additional spectral niche. Then, we expect to also find chromatic acclimaters, and perhaps more PT 3dB cells. These hypotheses are mainly based on the PTs assemblage observed by Grébert and collaborators (2018) in the Mediterranean Sea, with a majority of 3c strains, a significant proportion of chromatic acclimaters (3dB being slightly more abundant than 3dA), and a minority of 3a representatives (see Introduction, Fig. 36). At SOMLIT-Astan, remote sensing

reflectance and irradiance data indicated that the underwater light field varied greatly throughout the year, although it tended to be greenish. Consequently, one can expect to see a high contribution of PT 3a representatives to the *Synechococcus* population at this site, and even more at depth where green light is the most abundant (Stomp, 2008) and the light intensity is weaker (see Chapter 2 § IV). Also, we expect to observe CA4-A-capable strains in surface waters, where the underwater light field consists of a mix of blue and green wavelengths. These hypotheses, which are mainly based on the observation of PTs 3a and 3d co-dominance in a SOMLIT-Astan seawater sample (Humily et al., 2014), still await confirmation from upcoming metagenomic analyses.

In addition to providing information on seasonal variations of *Synechococcus* PTs, the data generated during my thesis will serve to improve the adaptation of the DARWIN model developed by Francesco Mattei. As highlighted by Dutkiewicz and collaborators (2019), these time series are highly desirable, and should be implemented as much as possible, as they enable improvement in the ability to detect phytoplankton diversity from space. With the on-going global change due to continued anthropogenic forcing, it is essential to be able to identify and predict variations in the diversity and abundance of phytoplankton communities, which are 'centrally important to the biology of the planet' (Hoegh-Guldberg and Bruno, 2010). These changes could indeed have dramatic effects, as phytoplankton are located at the base of trophic chains and consequently impact higher trophic levels and therefore whole marine ecosystems. In fact, the latter have a critical feedback role on Earth's climate regulation, notably via the sequestration of atmospheric CO_2, and provide socio-economic services critical to human wellbeing (Henson et al., 2021).

References

Adir, N. (2005). Elucidation of the molecular structures of components of the phycobilisome: reconstructing a giant. *Photosynthesis Research*, *85*, 15-32.

Adir, N., Bar-Zvi, S., & Harris, D. (2020). The amazing phycobilisome. *Biochimica et Biophysica Acta (BBA)-Bioenergetics*, *1861*(4), 148047.

Adir, N., Dines, M., Klartag, M., McGregor, A., & Melamed-Frank, M. (2006). Assembly and disassembly of phycobilisomes. *Complex intracellular structures in prokaryotes*, 47-77.

Ahlgren, N. A., & Rocap, G. (2012). Diversity and distribution of marine *Synechococcus*: multiple gene phylogenies for consensus classification and development of qPCR assays for sensitive measurement of clades in the ocean. *Frontiers in Microbiology*, *3*, 213.

Alberti, A., Poulain, J., Engelen, S., Labadie, K., Romac, S., Ferrera, I., ... & Wincker, P. (2020). Handling of genomics samples.

Aminot, A., & Kérouel, R. (2007). *Dosage automatique des nutriments dans les eaux marines: méthodes en flux continu.* Editions Quae.

Anderson, L. K., & Toole, C. M. (1998). A model for early events in the assembly pathway of cyanobacterial phycobilisomes. *Molecular Microbiology*, *30*(3), 467-474.

Antoine, D., Chami, M., Claustre, H., d'Ortenzio, F., Morel, A., Bécu, G., ... & Adams, D. (2006). *BOUSSOLE: A joint CNRS-INSU, ESA, CNES, and NASA ocean color calibration and validation activity* (No. Rept-2007-00282-0).

Antoine, D., d'Ortenzio, F., Hooker, S. B., Bécu, G., Gentili, B., Tailliez, D., & Scott, A. J. (2008). Assessment of uncertainty in the ocean reflectance determined by three satellite ocean color sensors (MERIS, SeaWiFS and MODIS-A) at an offshore site in the Mediterranean Sea (BOUSSOLE project). *Journal of Geophysical Research: Oceans*, *113*(C7).

Apt, K. E., Collier, J. L., & Grossman, A. R. (1995). Evolution of the phycobiliproteins. *Journal of Molecular Biology*, *248*(1), 79-96.

Aro, E. M., Virgin, I., & Andersson, B. (1993). Photoinhibition of photosystem II. Inactivation, protein damage and turnover. *Biochimica et Biophysica Acta (BBA)-Bioenergetics*, *1143*(2), 113-134.

Arteni, A. A., Ajlani, G., & Boekema, E. J. (2009). Structural organisation of phycobilisomes from *Synechocystis* sp. strain PCC6803 and their interaction with the membrane. *Biochimica et Biophysica Acta (BBA)-Bioenergetics*, *1787*(4), 272-279.

Azam, F., Fenchel, T., Field, J. G., Gray, J. S., Meyer-Reil, L. A., & Thingstad, F. J. M. E. P. S. (1983). The ecological role of water-column microbes in the sea. *Marine Ecology Progress Series. Oldendorf*, *10*(3), 257-263.

Badger, M. R., & Price, G. D. (2003). CO2 concentrating mechanisms in cyanobacteria: molecular components, their diversity and evolution. *Journal of Experimental Botany*, *54*(383), 609-622.

Barrangou, R. (2013). CRISPR-Cas systems and RNA-guided interference. *Wiley Interdisciplinary Reviews: RNA*, *4*(3), 267-278.

Becker, J. W., Berube, P. M., Follett, C. L., Waterbury, J. B., Chisholm, S. W., DeLong, E. F., & Repeta, D. J. (2014). Closely related phytoplankton species produce similar suites of dissolved organic matter. *Frontiers in Microbiology*, *5*, 111.

Behrenfeld, M. J., & Milligan, A. J. (2013). Photophysiological expressions of iron stress in phytoplankton. *Annual Review of Marine Science*, *5*, 217-246.

Behrenfeld, M. J., O'Malley, R. T., Siegel, D. A., McClain, C. R., Sarmiento, J. L., Feldman, G. C., ... & Boss, E. S. (2006). Climate-driven trends in contemporary ocean productivity. *Nature*, *444*(7120), 752-755.

Benett, A. J. J. C. B. (1973). Complementary chromatic adaptation in a filamentous blue-green alga. *J. Cell. Biol.*, *58*, 419-435.

Biard, T. (2015). *Diversité, biogéographie et écologie des Collodaires (Radiolaires) dans l'océan mondial* (Doctoral dissertation, Paris 6).

Biller, S. J., Berube, P. M., Lindell, D., & Chisholm, S. W. (2015). *Prochlorococcus*: the structure and function of collective diversity. *Nature Reviews Microbiology*, *13*(1), 13-27.

Biller, S. J., Schubotz, F., Roggensack, S. E., Thompson, A. W., Summons, R. E., & Chisholm, S. W. (2014). Bacterial vesicles in marine ecosystems. *Science*, *343*(6167), 183-186.

Biswas, A., Boutaghou, M. N., Alvey, R. M., Kronfel, C. M., Cole, R. B., Bryant, D. A., & Schluchter, W. M. (2011). Characterization of the activities of the CpeY, CpeZ, and CpeS bilin lyases in phycoerythrin biosynthesis in *Fremyella diplosiphon* strain UTEX 481. *Journal of Biological Chemistry*, *286*(41), 35509-35521.

Biswas, A., Vasquez, Y. M., Dragomani, T. M., Kronfel, M. L., Williams, S. R., Alvey, R. M., ... & Schluchter, W. M. (2010). Biosynthesis of cyanobacterial phycobiliproteins in *Escherichia coli*: chromophorylation efficiency and specificity of all bilin lyases from *Synechococcus* sp. strain PCC 7002. *Applied and Environmental Microbiology*, *76*(9), 2729-2739.

Blankenship, R. E. (2021). *Molecular mechanisms of photosynthesis*. John Wiley & Sons.

Blankenship, R. E., & Hartman, H. (1998). The origin and evolution of oxygenic photosynthesis. *Trends in Biochemical Sciences*, *23*(3), 94-97.

Blot, N., Mella-Flores, D., Six, C., Le Corguillé, G., Boutte, C., Peyrat, A., ... & Garczarek, L. (2011). Light history influences the response of the marine cyanobacterium *Synechococcus* sp. WH7803 to oxidative stress. *Plant Physiology*, *156*(4), 1934-1954.

Blot, N., Wu, X. J., Thomas, J. C., Zhang, J., Garczarek, L., Böhm, S., ... & Zhao, K. H. (2009). Phycourobilin in trichromatic phycocyanin from oceanic cyanobacteria is formed post-translationally by a phycoerythrobilin lyase-isomerase. *Journal of Biological Chemistry*, *284*(14), 9290-9298.

Boresch, K. (1922). Photokatalysen in Pflanzen. *Naturwissenschaften*, *10*(22), 505-512.

Brahamsha, B. (1996). A genetic manipulation system for oceanic cyanobacteria of the genus *Synechococcus*. *Applied and Environmental Microbiology*, *62*(5), 1747-1751.

Bretaudeau, A., Coste, F., Humily, F., Garczarek, L., Le Corguille, G., Six, C., ... & Partensky, F. (2012). CyanoLyase: a database of phycobilin lyase sequences, motifs and functions. *Nucleic acids research*, *41*(D1), D396-D401.

Breton, S., Jouhet, J., Guyet, U., Gros, V., Pittera, J., Demory, D., ... & Six, C. (2020). Unveiling membrane thermoregulation strategies in marine picocyanobacteria. *New Phytologist*, *225*(6), 2396-2410.

Brierley, A. S. (2017). Plankton. *Current Biology*, *27*(11), R478-R483.

Bryant, D. A., Guglielmi, G., de Marsac, N. T., Castets, A. M., & Cohen-Bazire, G. (1979). The structure of cyanobacterial phycobilisomes: a model. *Archives of Microbiology*, *123*, 113-127.

Buchan, A., LeCleir, G. R., Gulvik, C. A., & González, J. M. (2014). Master recyclers: features and functions of bacteria associated with phytoplankton blooms. *Nature Reviews Microbiology*, *12*(10), 686-698.

Burson, A., Stomp, M., Greenwell, E., Grosse, J., & Huisman, J. (2018). Competition for nutrients and light: testing advances in resource competition with a natural phytoplankton community. *Ecology*, *99*(5), 1108-1118.

Bustillos-Guzman, J., Claustre, H., & Marty, J. C. (1995). Specific phytoplankton signatures and their relationship to hydrographic conditions in the coastal northwestern Mediterranean Sea. *Marine Ecology Progress Series*, *124*, 247-258.

Cabello-Yeves, P. J., Callieri, C., Picazo, A., Schallenberg, L., Huber, P., Roda-Garcia, J. J., ... & Scanlan, D. J. (2022a). Elucidating the picocyanobacteria salinity divide through ecogenomics of new freshwater isolates. *BMC Biology*, *20*(1), 1-24.

Cabello-Yeves, P. J., Haro-Moreno, J. M., Martin-Cuadrado, A. B., Ghai, R., Picazo, A., Camacho, A., & Rodriguez-Valera, F. (2017). Novel *Synechococcus* genomes reconstructed from freshwater reservoirs. *Frontiers in Microbiology*, *8*, 1151.

Cabello-Yeves, P. J., Scanlan, D. J., Callieri, C., Picazo, A., Schallenberg, L., Huber, P., ... & Puxty, R. J. (2022). α-cyanobacteria possessing form IA RuBisCO globally dominate aquatic habitats. *The ISME Journal*, *16*(10), 2421-2432.

Cai, H., Wang, K., Huang, S., Jiao, N., & Chen, F. (2010). Distinct patterns of picocyanobacterial communities in winter and summer in the Chesapeake Bay. *Applied and Environmental Microbiology*, *76*(9), 2955-2960.

Campbell, L., & Iturriaga, R. (1988). Identification of *Synechococcus* spp. in the Sargasso Sea by immunofluorescence and fluorescence excitation spectroscopy performed on individual cells. *Limnology and Oceanography*, *33*(5), 1196-1201.

Campbell, L., Landry, M. R., Constantinou, J., Nolla, H. A., Brown, S. L., Liu, H., & Caron, D. A. (1998). Response of microbial community structure to environmental forcing in the Arabian Sea. *Deep Sea Research Part II: Topical Studies in Oceanography*, *45*(10-11), 2301-2325.

Campbell, L., Nolla, H. A., & Vaulot, D. (1994). The importance of *Prochlorococcus* to community structure in the central North Pacific Ocean. *Limnology and oceanography*, *39*(4), 954-961.

Capuano, V., Braux, A. S., de Marsac, N. T., & Houmard, J. (1991). The "anchor polypeptide" of cyanobacterial phycobilisomes. Molecular characterization of the *Synechococcus* sp. PCC 6301 apce gene. *Journal of Biological Chemistry*, *266*(11), 7239-7247.

Caron, David A., et al. "Marine protistan diversity." *Annual Review of Marine Science* 4 (2012): 467-493.

Carrigee, L. A., Frick, J. P., Karty, J. A., Garczarek, L., Partensky, F., & Schluchter, W. M. (2021). MpeV is a lyase isomerase that ligates a doubly linked phycourobilin on the β-subunit of phycoerythrin I and II in marine *Synechococcus*. *Journal of Biological Chemistry*, *296*.

Carrigee, L. A., Frick, J. P., Liu, X., Karty, J. A., Trinidad, J. C., Tom, I. P., ... & Schluchter, W. M. (2022). The phycoerythrobilin isomerization activity of MpeV in *Synechococcus* sp. WH8020 is prevented by the presence of a histidine at position 141 within its phycoerythrin-I β-subunit substrate. *Frontiers in Microbiology*, *13*, 1011189.

Casadaban, M. J., & Cohen, S. N. (1980). Analysis of gene control signals by DNA fusion and cloning in *Escherichia coli*. *Journal of Molecular Biology*, *138*(2), 179-207.

Chang, L., Liu, X., Li, Y., Liu, C. C., Yang, F., Zhao, J., & Sui, S. F. (2015). Structural organization of an intact phycobilisome and its association with photosystem II. *Cell Research*, *25*(6), 726-737.

Chen, F., Wang, K., Kan, J., Suzuki, M. T., & Wommack, K. E. (2006). Diverse and unique picocyanobacteria in Chesapeake Bay, revealed by 16S-23S rRNA internal transcribed spacer sequences. *Applied and Environmental Microbiology*, *72*(3), 2239-2243.

Chisholm, S. W., Frankel, S. L., Goericke, R., Olson, R. J., Palenik, B., Waterbury, J. B., ... & Zettler, E. R. (1992). *Prochlorococcus marinus* nov. gen. nov. sp.: an oxyphototrophic marine prokaryote containing divinyl chlorophyll *a* and *b*. *Archives of Microbiology*, *157*, 297-300.

Chisholm, S. W. RJ Olson, ER Zettler, R. Goericke, J. Waterbury, and N. Welschmeyer. 1988. A novel free-living prochlorophyte abundant in the oceanic euphotic zone. *Nature*, *334*, 340-343.

Coleman, M. L., & Chisholm, S. W. (2007). Code and context: *Prochlorococcus* as a model for cross-scale biology. *Trends in Microbiology*, *15*(9), 398-407.

Collier, J. L., & Grossman, A. (1994). A small polypeptide triggers complete degradation of light-harvesting phycobiliproteins in nutrient-deprived cyanobacteria. *The EMBO Journal*, *13*(5), 1039-1047.

Croteau, F. R., Rousseau, G. M., & Moineau, S. (2018). Le système CRISPR-Cas-Au-delà de l'édition génomique. *Médecine/sciences*, *34*(10), 813-819.

Dhanasekaran, S., Doherty, T. M., Kenneth, J., & TB Trials Study Group. (2010). Comparison of different standards for real-time PCR-based absolute quantification. *Journal of Immunological Methods*, *354*(1-2), 34-39.

Domínguez-Martín, M. A., Sauer, P. V., Kirst, H., Sutter, M., Bína, D., Greber, B. J., ... & Kerfeld, C. A. (2022). Structures of a phycobilisome in light-harvesting and photoprotected states. *Nature*, *609*(7928), 835-845.

Donohoue, P. D., Barrangou, R., & May, A. P. (2018). Advances in industrial biotechnology using CRISPR-Cas systems. *Trends in Biotechnology*, *36*(2), 134-146.

Doré, H. (2017). *Adaptation à la niche écologique chez deux représentants majeurs du phytoplancton marin,* Synechococcus *et* Prochlorococcus*: des gènes à l'écosystème* (Doctoral dissertation, Université Pierre et Marie Curie-Paris VI).

Doré, H., Farrant, G. K., Guyet, U., Haguait, J., Humily, F., Ratin, M., ... & Garczarek, L. (2020). Evolutionary mechanisms of long-term genome diversification associated with niche partitioning in marine picocyanobacteria. *Frontiers in Microbiology*, *11*, 567431.

Doré, H., Guyet, U., Leconte, J., Farrant, G. K., Alric, B., Ratin, M., ... & Garczarek, L. (2023). Differential global distribution of marine picocyanobacteria gene clusters reveals distinct niche-related adaptive strategies. *The ISME Journal*, *17*(5), 720-732.

D'Ortenzio, F., Iudicone, D., de Boyer Montegut, C., Testor, P., Antoine, D., Marullo, S., ... & Madec, G. (2005). Seasonal variability of the mixed layer depth in the Mediterranean Sea as derived from in situ profiles. *Geophysical Research Letters*, *32*(12).

Dufour, L., Gouriou, B., Clairet, J., Ratin, M., Garczarek, L., & Partensky, F. (2023). Differential acclimation kinetics of the two forms of Type IV chromatic acclimaters occurring in marine *Synechococcus* cyanobacteria. *bioRxiv*, 2023-07.

Dufresne, A., Ostrowski, M., Scanlan, D. J., Garczarek, L., Mazard, S., Palenik, B. P., ... & Partensky, F. (2008). Unraveling the genomic mosaic of a ubiquitous genus of marine cyanobacteria. *Genome Biology*, *9*(5), 1-16.

DuRand, M. D., Olson, R. J., & Chisholm, S. W. (2001). Phytoplankton population dynamics at the Bermuda Atlantic Time-series station in the Sargasso Sea. *Deep Sea Research Part II: Topical Studies in Oceanography*, *48*(8-9), 1983-2003.

Dutkiewicz, S., Hickman, A. E., Jahn, O., Henson, S., Beaulieu, C., & Monier, E. (2019). Ocean colour signature of climate change. *Nature Communications*, *10*(1), 578.

Dutkiewicz, S., Morris, J. J., Follows, M. J., Scott, J., Levitan, O., Dyhrman, S. T., & Berman-Frank, I. (2015). Impact of ocean acidification on the structure of future phytoplankton communities. *Nature Climate Change*, *5*(11), 1002-1006.

Dvořák, P., Casamatta, D. A., Poulíčková, A., Hašler, P., Ondřej, V., & Sanges, R. (2014). *Synechococcus*: 3 billion years of global dominance. *Molecular Ecology*, *23*(22), 5538-5551.

Elhai, J., & Wolk, C. P. (1988). [83] Conjugal transfer of DNA to cyanobacteria. In *Methods in Enzymology* (Vol. 167, pp. 747-754). Academic Press.

Engelmann, T. W. (1902). Ueber experimentelle Erzeugung zweckmassiger Aenderrungen der Farbung pflanzlicher Chromophylle durch farbiges Licht. *Arch. Anat. Physiol. Lpz.; Physiol. Abt*, 333-335.

Everroad, C., Six, C., Partensky, F., Thomas, J. C., Holtzendorff, J., & Wood, A. M. (2006). Biochemical bases of type IV chromatic adaptation in marine *Synechococcus* spp. *Journal of Bacteriology*, *188*(9), 3345-3356.

Everroad, R. C., & Wood, A. M. (2012). Phycoerythrin evolution and diversification of spectral phenotype in marine *Synechococcus* and related picocyanobacteria. *Molecular Phylogenetics and Evolution*, *64*(3), 381-392.

Fairchild, C. D., & Glazer, A. N. (1994). Oligomeric structure, enzyme kinetics, and substrate specificity of the phycocyanin alpha subunit phycocyanobilin lyase. *Journal of Biological Chemistry*, *269*(12), 8686-8694.

Fairchild, C. D., Zhao, J., Zhou, J., Colson, S. E., Bryant, D. A., & Glazer, A. N. (1992). Phycocyanin alpha-subunit phycocyanobilin lyase. *Proceedings of the National Academy of Sciences*, *89*(15), 7017-7021.

Farrant, G. K., Doré, H., Cornejo-Castillo, F. M., Partensky, F., Ratin, M., Ostrowski, M., ... & Garczarek, L. (2016). Delineating ecologically significant taxonomic units from global patterns of marine picocyanobacteria. *Proceedings of the National Academy of Sciences*, *113*(24), E3365-E3374.

Ferrieux, M., Dufour, L., Doré, H., Ratin, M., Guéneuguès, A., Chasselin, L., ... & Garczarek, L. (2022). Comparative thermophysiology of marine *Synechococcus* CRD1 strains isolated from different thermal niches in iron-depleted areas. *Frontiers in Microbiology*, *13*, 893413.

Field, C. B., Behrenfeld, M. J., Randerson, J. T., & Falkowski, P. (1998). Primary production of the biosphere: integrating terrestrial and oceanic components. *Science*, *281*(5374), 237-240.

Fischer, W. W., Hemp, J., & Johnson, J. E. (2016). Evolution of oxygenic photosynthesis. *Annual Review of Earth and Planetary Sciences*, *44*, 647-683.

Flombaum, P., Gallegos, J. L., Gordillo, R. A., Rincón, J., Zabala, L. L., Jiao, N., ... & Martiny, A. C. (2013). Present and future global distributions of the marine Cyanobacteria *Prochlorococcus* and *Synechococcus*. *Proceedings of the National Academy of Sciences*, *110*(24), 9824-9829.

Fournier, G. P., Moore, K. R., Rangel, L. T., Payette, J. G., Momper, L., & Bosak, T. (2021). The Archean origin of oxygenic photosynthesis and extant cyanobacterial lineages. *Proceedings of the Royal Society B*, *288*(1959), 20210675.

Frankenberg, N., Mukougawa, K., Kohchi, T., & Lagarias, J. C. (2001). Functional genomic analysis of the HY2 family of ferredoxin-dependent bilin reductases from oxygenic photosynthetic organisms. *The Plant Cell*, *13*(4), 965-978.

Fuller, N. J., Marie, D., Partensky, F., Vaulot, D., Post, A. F., & Scanlan, D. J. (2003). Clade-specific 16S ribosomal DNA oligonucleotides reveal the predominance of a single marine *Synechococcus* clade throughout a stratified water column in the Red Sea. *Applied and Environmental Microbiology*, *69*(5), 2430-2443.

Fuller, N. J., Tarran, G. A., Yallop, M., Orcutt, K. M., & Scanlan, D. J. (2006). Molecular analysis of picocyanobacterial community structure along an Arabian Sea transect reveals distinct spatial separation of lineages. *Limnology and Oceanography*, *51*(6), 2515-2526.

Fuller, N. J., West, N. J., Marie, D., Yallop, M., Rivlin, T., Post, A. F., & Scanlan, D. J. (2005). Dynamics of community structure and phosphate status of picocyanobacterial populations in the Gulf of Aqaba, Red Sea. *Limnology and Oceanography*, *50*(1), 363-375.

Gaidukov, N. (1903). Weitere Untersuchungen uber den Einfluss farbigen Lichtes auf die Farbung der Oscillarien. *Ber. Disch. Bot. Ges.*, *21*, 484-492.

Gallegos, M. T., Schleif, R., Bairoch, A., Hofmann, K., & Ramos, J. L. (1997). Arac/XylS family of transcriptional regulators. *Microbiology and Molecular Biology Reviews*, *61*(4), 393-410.

Gantt, E. (1981). Phycobilisomes. *Annual Review of Plant Physiology*, *32*(1), 327-347.

Gantt, E., & Conti, S. F. (1965). The ultrastructure of *Porphyridium cruentum*. *The Journal of Cell Biology*, *26*(2), 365-381.

Gantt, E., & Conti, S. F. (1966). Granules associated with the chloroplast lamellae of *Porphyridium cruentum*. *The Journal of Cell Biology*, *29*(3), 423-434.

Garczarek, L., Dufresne, A., Blot, N., Cockshutt, A. M., Peyrat, A., Campbell, D. A., ... & Six, C. (2008). Function and evolution of the psbA gene family in marine *Synechococcus*: *Synechococcus* sp. WH7803 as a case study. *The ISME Journal*, *2*(9), 937-953.

Garczarek, L., Guyet, U., Doré, H., Farrant, G. K., Hoebeke, M., Brillet-Guéguen, L., ... & Partensky, F. (2021). Cyanorak v2. 1: a scalable information system dedicated to the visualization and expert curation of marine and brackish picocyanobacteria genomes. *Nucleic Acids Research*, *49*(D1), D667-D676.

Gasper, R., Schwach, J., Hartmann, J., Holtkamp, A., Wiethaus, J., Riedel, N., ... & Frankenberg-Dinkel, N. (2017). Distinct features of cyanophage-encoded T-type phycobiliprotein lyase ΦCpeT: The role of auxiliary metabolic genes. *Journal of Biological Chemistry*, *292*(8), 3089-3098.

Glazer, A. N. (1988). [32] Phycobilisomes. In *Methods in Enzymology* (Vol. 167, pp. 304-312). Academic Press.

Glazer, A. N. (1989). Light guides: directional energy transfer in a photosynthetic antenna. *Journal of Biological Chemistry*, *264*(1), 1-4.

Glazer, A. N., Apell, G. S., Hixson, C. S., Bryant, D. A., Rimon, S., & Brown, D. M. (1976). Biliproteins of cyanobacteria and Rhodophyta: Homologous family of photosynthetic accessory pigments. *Proceedings of the National Academy of Sciences*, *73*(2), 428-431.

Grébert, T. (2017). *Pigment diversity in marine* Synechococcus *sp.: Molecular basis, evolution and ecological role* (Doctoral dissertation, Université Pierre et Marie Curie-Paris VI).

Grébert, T., Doré, H., Partensky, F., Farrant, G. K., Boss, E. S., Picheral, M., ... & Garczarek, L. (2018). Light color acclimation is a key process in the global ocean distribution of *Synechococcus* cyanobacteria. *Proceedings of the National Academy of Sciences*, *115*(9), E2010-E2019.

Grébert, T., Garczarek, L., Daubin, V., Humily, F., Marie, D., Ratin, M., ... & Partensky, F. (2022). Diversity and evolution of pigment types in marine *Synechococcus* cyanobacteria. *Genome Biology and Evolution*, *14*(4), evac035.

Grébert, T., Nguyen, A. A., Pokhrel, S., Joseph, K. L., Ratin, M., Dufour, L., ... & Partensky, F. (2021). Molecular bases of an alternative dual-enzyme system for light color acclimation of marine *Synechococcus* cyanobacteria. *Proceedings of the National Academy of Sciences*, *118*(9), e2019715118.

Greenwood, D. R., & Wing, S. L. (1995). Eocene climates and latitudinal gradients for North America and Australia. *Geology*, *23*(11), 1040-1048.

Griese, M., Lange, C., & Soppa, J. (2011). Ploidy in cyanobacteria. *FEMS Microbiology Letters*, *323*(2), 124-131.

Grossman, A. R., Schaefer, M. R., Chiang, G. G., & Collier, J. (1993). The phycobilisome, a light-harvesting complex responsive to environmental conditions. *Microbiological Reviews*, *57*(3), 725-749.

Guidi, L., Chaffron, S., Bittner, L., Eveillard, D., Larhlimi, A., Roux, S., ... & Gorsky, G. (2016). Plankton networks driving carbon export in the oligotrophic ocean. *Nature*, *532*(7600), 465-470.

Guilloux, L., Rigaut-Jalabert, F., Jouenne, F., Ristori, S., Viprey, M., Not, F., ... & Simon, N. (2013). An annotated checklist of Marine Phytoplankton taxa at the SOMLIT-Astan time series off Roscoff (Western English Channel, France): data collected from 2000 to 2010. *Cah. Biol. Mar*, *54*, 247-256.

Gutiérrez-Rodríguez, A., Slack, G., Daniels, E. F., Selph, K. E., Palenik, B., & Landry, M. R. (2014). Fine spatial structure of genetically distinct picocyanobacterial populations across environmental gradients in the Costa Rica Dome. *Limnology and Oceanography*, *59*(3), 705-723.

Guyet, U., Nguyen, N. A., Doré, H., Haguait, J., Pittera, J., Conan, M., ... & Garczarek, L. (2020). Synergic effects of temperature and irradiance on the physiology of the marine *Synechococcus* strain WH7803. *Frontiers in Microbiology*, *11*, 1707.

Hackl, T., Laurenceau, R., Ankenbrand, M. J., Bliem, C., Cariani, Z., Thomas, E., ... & Chisholm, S. W. (2023). Novel integrative elements and genomic plasticity in ocean ecosystems. *Cell*, *186*(1), 47-62.

Haft, D. H., Basu, M. K., & Mitchell, D. A. (2010). Expansion of ribosomally produced natural products: a nitrile hydratase-and Nif11-related precursor family. *BMC Biology*, *8*, 1-15.

Havaux, M., Guedeney, G., He, Q., & Grossman, A. R. (2003). Elimination of high-light-inducible polypeptides related to eukaryotic chlorophyll *a/b*-binding proteins results in aberrant photoacclimation in *Synechocystis* PCC6803. *Biochimica et Biophysica Acta (BBA)-Bioenergetics*, *1557*, 21-33.

Haverkamp, T., Acinas, S. G., Doeleman, M., Stomp, M., Huisman, J., & Stal, L. J. (2008). Diversity and phylogeny of Baltic Sea picocyanobacteria inferred from their ITS and phycobiliprotein operons. *Environmental Microbiology*, *10*(1), 174-188.

Haverkamp, T. H., Schouten, D., Doeleman, M., Wollenzien, U., Huisman, J., & Stal, L. J. (2009). Colorful microdiversity of *Synechococcus* strains (picocyanobacteria) isolated from the Baltic Sea. *The ISME journal*, *3*(4), 397-408.

He, Q., Dolganov, N., Björkman, O., & Grossman, A. R. (2001). The high light-inducible polypeptides in *Synechocystis* PCC6803: expression and function in high light. *Journal of Biological Chemistry*, *276*(1), 306-314.

Henson, S. A., Cael, B. B., Allen, S. R., & Dutkiewicz, S. (2021). Future phytoplankton diversity in a changing climate. *Nature Communications*, *12*(1), 5372.

Herdman, M. (2001). Subsection I.(Formerly Chroococcales Wettstein 1924, emends. Rippka, Deruelles, Waterbury, Herdman and Stanier 1979). *Bergey's Manual of Systematic Bacteriology*, *1*, 493-514.

Hess, W. R., Partensky, F., Van der Staay, G. W., Garcia-Fernandez, J. M., Börner, T., & Vaulot, D. (1996). Coexistence of phycoerythrin and a chlorophyll *a/b* antenna in a marine prokaryote. *Proceedings of the National Academy of Sciences*, *93*(20), 11126-11130.

Hess, W. R., Steglich, C., Lichtlé, C., & Partensky, F. (1999). Phycoerythrins of the oxyphotobacterium *Prochlorococcus marinus* are associated to the thylakoid membrane and are encoded by a single large gene cluster. *Plant Molecular Biology*, *40*, 507-521.

Hickman, A. E., Dutkiewicz, S., Williams, R. G., & Follows, M. J. (2010). Modelling the effects of chromatic adaptation on phytoplankton community structure in the oligotrophic ocean. *Marine Ecology Progress Series*, *406*, 1-17.

Hoegh-Guldberg, O., & Bruno, J. F. (2010). The impact of climate change on the world's marine ecosystems. *Science*, *328*(5985), 1523-1528.

Holtrop, T., Huisman, J., Stomp, M., Biersteker, L., Aerts, J., Grébert, T., ... & Woerd, H. J. V. D. (2021). Vibrational modes of water predict spectral niches for photosynthesis in lakes and oceans. *Nature Ecology & Evolution*, *5*(1), 55-66.

Horton, P., Ruban, A. V., & Walters, R. G. (1996). Regulation of light harvesting in green plants. *Annual Review of Plant Biology*, *47*(1), 655-684.

Huang, S., Wilhelm, S. W., Harvey, H. R., Taylor, K., Jiao, N., & Chen, F. (2012). Novel lineages of *Prochlorococcus* and *Synechococcus* in the global oceans. *The ISME Journal*, *6*(2), 285-297.

Huisman, J., Jonker, R. R., Zonneveld, C., & Weissing, F. J. (1999). Competition for light between phytoplankton species: experimental tests of mechanistic theory. *Ecology*, *80*(1), 211-222.

Huisman, J., Matthijs, H. C., Visser, P. M., Balke, H., Sigon, C. A., Passarge, J., ... & Mur, L. R. (2002). Principles of the light-limited chemostat: theory and ecological applications. *Antonie van Leeuwenhoek*, *81*, 117-133.

Huisman, J., & Weissing, F. J. (1994). Light-limited growth and competition for light in well-mixed aquatic environments: an elementary model. *Ecology*, *75*(2), 507-520.

Humily, F., Farrant, G. K., Marie, D., Partensky, F., Mazard, S., Perennou, M., ... & Garczarek, L. (2014). Development of a targeted metagenomic approach to study a genomic region involved in light harvesting in marine *Synechococcus*. *FEMS Microbiology Ecology*, *88*(2), 231-249.

Humily, F., Partensky, F., Six, C., Farrant, G. K., Ratin, M., Marie, D., & Garczarek, L. (2013). A gene island with two possible configurations is involved in chromatic acclimation in marine *Synechococcus*. *PloS One*, *8*(12), e84459.

Hunter-Cevera, K. R., Neubert, M. G., Olson, R. J., Solow, A. R., Shalapyonok, A., & Sosik, H. M. (2016a). Physiological and ecological drivers of early spring blooms of a coastal phytoplankter. *Science*, *354*(6310), 326-329.

Hunter-Cevera, K. R., Post, A. F., Peacock, E. E., & Sosik, H. M. (2016). Diversity of *Synechococcus* at the Martha's Vineyard coastal observatory: Insights from culture isolations, clone libraries, and flow cytometry. *Microbial Ecology*, *71*, 276-289.

Ishino, Y., Shinagawa, H., Makino, K., Amemura, M., & Nakata, A. (1987). Nucleotide sequence of the *iap* gene, responsible for alkaline phosphatase isozyme conversion in *Escherichia coli*, and identification of the gene product. *Journal of Bacteriology*, *169*(12), 5429-5433.

Johnson, P. W., & Sieburth, J. M. (1979). Chroococcoid cyanobacteria in the sea: a ubiquitous and diverse phototrophic biomass 1. *Limnology and Oceanography*, *24*(5), 928-935.

Johnson, Z. I., Zinser, E. R., Coe, A., McNulty, N. P., Woodward, E. M. S., & Chisholm, S. W. (2006). Niche partitioning among *Prochlorococcus* ecotypes along ocean-scale environmental gradients. *Science*, *311*(5768), 1737-1740.

Kana, T. M., & Glibert, P. M. (1987). Effect of irradiances up to 2000 µE m− 2 s− 1 on marine *Synechococcus* WH7803—I. Growth, pigmentation, and cell composition. *Deep Sea Research Part A. Oceanographic Research Papers*, *34*(4), 479-495.

Katano, T., & Nakano, S. I. (2006). Growth rates of *Synechococcus* types with different phycoerythrin composition estimated by dual-laser flow cytometry in relationship to the light environment in the Uwa Sea. *Journal of Sea Research*, *55*(3), 182-190.

Ke, B. (2001). *Photosynthesis photobiochemistry and photobiophysics* (Vol. 10). Springer Science & Business Media.

Kehoe, D. M., & Gutu, A. (2006). Responding to color: the regulation of complementary chromatic adaptation. *Annu. Rev. Plant Biol.*, *57*, 127-150.

Kirk, J. T. (1992). The nature and measurement of the light environment in the ocean. In *Primary productivity and biogeochemical cycles in the sea* (pp. 9-29). Boston, MA: Springer US.

Kirk, John TO. *Light and photosynthesis in aquatic ecosystems*. Cambridge University press, 1994.

Koroleff, F. (1969). Determination of total nitrogen in natural waters by means of persulfate oxidation.

Kronfel, C. M., Hernandez, C. V., Frick, J. P., Hernandez, L. S., Gutu, A., Karty, J. A., ... & Schluchter, W. M. (2019). CpeF is the bilin lyase that ligates the doubly linked phycoerythrobilin on β-phycoerythrin in the cyanobacterium *Fremyella diplosiphon*. *Journal of Biological Chemistry*, *294*(11), 3987-3999.

Kumarapperuma, I., Joseph, K. L., Wang, C., Biju, L. M., Tom, I. P., Weaver, K. D., ... & Yang, X. (2022). Crystal structure and molecular mechanism of an E/F type bilin lyase-isomerase. *Structure*, *30*(4), 564-574.

Kützing, F. T. (1843). *Phycologia generalis oder Anatomie, Physiologie und Systemkunde der Tange: Textbd* (Vol. 1). Brockhaus.

Kylin, H. (1910). Über Phykoerythrin und Phykocyan bei Ceramium rubrum (Huds.) Ag.

Kylin, H. (1912). Über die roten und blauen Farbstoffe der Algen.

Lantoine, F., & Neveux, J. (1997). Spatial and seasonal variations in abundance and spectral characteristics of phycoerythrins in the tropical northeastern Atlantic Ocean. *Deep Sea Research Part I: Oceanographic Research Papers*, *44*(2), 223-246.

Larsson, J., Celepli, N., Ininbergs, K., Dupont, C. L., Yooseph, S., Bergman, B., & Ekman, M. (2014). Picocyanobacteria containing a novel pigment gene cluster dominate the brackish water Baltic Sea. *The ISME Journal*, *8*(9), 1892-1903.

Latifi, A., Ruiz, M., & Zhang, C. C. (2009). Oxidative stress in cyanobacteria. *FEMS Microbiology Reviews*, *33*(2), 258-278.

Ledermann, B., Béjà, O., & Frankenberg-Dinkel, N. (2016). New biosynthetic pathway for pink pigments from uncultured oceanic viruses. *Environmental Microbiology*, *18*(12), 4337-4347.

L'Helguen, S., Madec, C., & Le Corre, P. (1996). Nitrogen uptake in permanently well-mixed temperate coastal waters. *Estuarine, Coastal and Shelf Science*, *42*(6), 803-818.

Li, Y., Zhang, J., Xie, J., Zhao, J., & Jiang, L. (2001). Temperature-induced decoupling of phycobilisomes from reaction centers. *Biochimica et Biophysica Acta (BBA)-Bioenergetics*, *1504*(2-3), 229-234.

Lindell, D., & Post, A. F. (1995). Ultraphytoplankton succession is triggered by deep winter mixing in the Gulf of Aqaba (Eilat), Red Sea. *Limnology and Oceanography*, *40*(6), 1130-1141.

Liu, H., Jing, H., Wong, T. H., & Chen, B. (2014). Co-occurrence of phycocyanin-and phycoerythrin-rich *Synechococcus* in subtropical estuarine and coastal waters of Hong Kong. *Environmental Microbiology Reports*, *6*(1), 90-99.

Liu, L. N., Chen, X. L., Zhang, Y. Z., & Zhou, B. C. (2005). Characterization, structure and function of linker polypeptides in phycobilisomes of cyanobacteria and red algae: an overview. *Biochimica et Biophysica Acta (BBA)-Bioenergetics*, *1708*(2), 133-142.

Lokstein, H., Steglich, C., & Hess, W. R. (1999). Light-harvesting antenna function of phycoerythrin in *Prochlorococcus marinus*. *Biochimica et Biophysica Acta (BBA)-Bioenergetics*, *1410*(1), 97-98.

Lovindeer, R., Abbott, L., Medina, H., & Mackey, K. R. (2021). Costs and limitations of marine *Synechococcus* blue-green chromatic acclimation. *Frontiers in Marine Science*, *8*, 689998.

Luimstra, V. M., Verspagen, J. M., Xu, T., Schuurmans, J. M., & Huisman, J. (2020). Changes in water color shift competition between phytoplankton species with contrasting light-harvesting strategies. *Ecology*, *101*(3), e02951.

Lundell, D. J., Yamanaka, G., & Glazer, A. N. (1981). A terminal energy acceptor of the phycobilisome: the 75,000-dalton polypeptide of *Synechococcus* 6301 phycobilisomes--a new biliprotein. *The Journal of Cell Biology*, *91*(1), 315-319.

MacColl, R. (1998). Cyanobacterial phycobilisomes. *Journal of structural biology*, *124*(2-3), 311-334.

Mahmoud, R. M., Sanfilippo, J. E., Nguyen, A. A., Strnat, J. A., Partensky, F., Garczarek, L., ... & Schluchter, W. M. (2017). Adaptation to blue light in marine *Synechococcus* requires MpeU, an enzyme with similarity to phycoerythrobilin lyase isomerases. *Frontiers in Microbiology*, *8*, 243.

Marie, Dominique, et al. "Enumeration of phytoplankton, bacteria, and viruses in marine samples." *Current Protocols in Cytometry* 10.1 (1999): 11-11.

Marraffini, L. A. (2015). CRISPR-Cas immunity in prokaryotes. *Nature*, *526*(7571), 55-61.

Mazard, S., Ostrowski, M., Partensky, F., & Scanlan, D. J. (2012). Multi-locus sequence analysis, taxonomic resolution and biogeography of marine *Synechococcus*. *Environmental Microbiology*, *14*(2), 372-386.

Mella-Flores, D., Mazard, S., Humily, F., Partensky, F., Mahé, F., Bariat, L., ... & Garczarek, L. (2011). Is the distribution of *Prochlorococcus* and *Synechococcus* ecotypes in the Mediterranean Sea affected by global warming?. *Biogeosciences*, *8*(9), 2785-2804.

Meyer, R., Figurski, D., & Helinski, D. R. (1977). Physical and genetic studies with restriction endonucleases on the broad host-range plasmid RK2. *Molecular and General Genetics MGG*, *152*(2), 129-135.

Meyers, L. A., & Bull, J. J. (2002). Fighting change with change: adaptive variation in an uncertain world. *Trends in Ecology & Evolution*, *17*(12), 551-557.

Wood, A. M., Lipsen, M., & Coble, P. (1999). Fluorescence-based characterization of phycoerythrin-containing cyanobacterial communities in the Arabian Sea during the Northeast and early Southwest Monsoon (1994–1995). *Deep Sea Research Part II: Topical Studies in Oceanography*, *46*(8-9), 1769-1790.

Moon-van der Staay, S. Y., De Wachter, R., & Vaulot, D. (2001). Oceanic 18S rDNA sequences from picoplankton reveal unsuspected eukaryotic diversity. *Nature*, *409*(6820), 607-610.

Moore, C. M., Mills, M. M., Arrigo, K. R., Berman-Frank, I., Bopp, L., Boyd, P. W., ... & Ulloa, O. (2013). Processes and patterns of oceanic nutrient limitation. *Nature Geoscience*, *6*(9), 701-710.

Moore, L. R., Goericke, R., & Chisholm, S. W. (1995). Comparative physiology of *Synechococcus* and *Prochlorococcus*: influence of light and temperature on growth, pigments, fluorescence and absorptive properties. *Marine Ecology Progress Series*, 259-275.

Moore, L. R., Rocap, G., & Chisholm, S. W. (1998). Physiology and molecular phylogeny of coexisting *Prochlorococcus* ecotypes. *Nature*, *393*(6684), 464-467.

Morrissey, J., & Bowler, C. (2012). Iron utilization in marine cyanobacteria and eukaryotic algae. *Frontiers in Microbiology*, *3*, 43.

Muller, P., Li, X. P., & Niyogi, K. K. (2001). Non-photochemical quenching. A response to excess light energy. *Plant Physiology*, *125*(4), 1558-1566.

Mullineaux, C. W. (2014). Electron transport and light-harvesting switches in cyanobacteria. *Frontiers in plant science*, *5*, 7.

Neveux, J., Lantoine, F., Vaulot, D., Marie, D., & Blanchot, J. (1999). Phycoerythrins in the southern tropical and equatorial Pacific Ocean: Evidence for new cyanobacterial types. *Journal of Geophysical Research: Oceans*, *104*(C2), 3311-3321.

Nishiyama, Y., Allakhverdiev, S. I., & Murata, N. (2006). A new paradigm for the action of reactive oxygen species in the photoinhibition of photosystem II. *Biochimica et Biophysica Acta (BBA)-Bioenergetics*, *1757*(7), 742-749.

Olson, R. J., Chisholm, S. W., Zettler, E. R., & Armbrust, E. V. (1988). Analysis of *Synechococcus* pigment types in the sea using single and dual beam flow cytometry. *Deep Sea Research Part A. Oceanographic Research Papers*, *35*(3), 425-440.

Olson, R. J., Chisholm, S. W., Zettler, E. R., & Armbrust, E. V. (1990). Pigments, size, and distributions of *Synechococcus* in the North Atlantic and Pacific Oceans. *Limnology and Oceanography*, *35*(1), 45-58.

Ong, L. J., & Glazer, A. N. (1991). Phycoerythrins of marine unicellular cyanobacteria. I. Bilin types and locations and energy transfer pathways in *Synechococcus* spp. phycoerythrins. *Journal of Biological Chemistry*, *266*(15), 9515-9527.

Organelli, E., Bricaud, A., Gentili, B., Antoine, D., & Vellucci, V. (2016). Retrieval of Colored Detrital Matter (CDM) light absorption coefficients in the Mediterranean Sea using field and satellite ocean color radiometry: Evaluation of bio-optical inversion models. *Remote Sensing of Environment*, *186*, 297-310.

Oriol, L., Garcia, N., Cariou, T., FERREIRA, S., & JOLLY, O. (2014). Dosage de l'azote ammoniacal en milieu marin par fluorimétrie. *Procédure: Protocole National. SOMLIT*, 1-14.

Palenik, B. (2001). Chromatic adaptation in marine *Synechococcus* strains. *Applied and Environmental Microbiology*, *67*(2), 991-994.

Partensky, F., & Garczarek, L. (2010). *Prochlorococcus*: advantages and limits of minimalism. *Annual Review of Marine Science*, *2*, 305-331.

Partensky, F., Hess, W. R., & Vaulot, D. (1999). *Prochlorococcus*, a marine photosynthetic prokaryote of global significance. *Microbiology and Molecular Biology Reviews*, *63*(1), 106-127.

Partensky, F., Mella-Flores, D., Six, C., Garczarek, L., Czjzek, M., Marie, D., ... & Prášil, O. (2018). Comparison of photosynthetic performances of marine picocyanobacteria with different configurations of the oxygen-evolving complex. *Photosynthesis Research*, *138*, 57-71.

Paulsen, M. L., Dore, H., Garczarek, L., Seuthe, L., Mueller, O., Sandaa, R. A., ... & Larsen, A. (2016). *Synechococcus* in the Atlantic gateway to the Arctic Ocean. *Frontiers in Marine Science*, *3*, 191.

Pesant, S., Not, F., Picheral, M., Kandels-Lewis, S., Le Bescot, N., Gorsky, G., ... & Searson, S. (2015). Open science resources for the discovery and analysis of *Tara* Oceans data. *Scientific data*, *2*(1), 1-16.

Pick, F. R. (1991). The abundance and composition of freshwater picocyanobacteria in relation to light penetration. *Limnology and Oceanography*, *36*(7), 1457-1462.

Pittera, J., Humily, F., Thorel, M., Grulois, D., Garczarek, L., & Six, C. (2014). Connecting thermal physiology and latitudinal niche partitioning in marine *Synechococcus*. *The ISME Journal*, *8*(6), 1221-1236.

Pittera, J., Jouhet, J., Breton, S., Garczarek, L., Partensky, F., Maréchal, E., ... & Six, C. (2018). Thermoacclimation and genome adaptation of the membrane lipidome in marine *Synechococcus*. *Environmental Microbiology*, *20*(2), 612-631.

Pittera, J., Partensky, F., & Six, C. (2017). Adaptive thermostability of light-harvesting complexes in marine picocyanobacteria. *The ISME Journal*, *11*(1), 112-124.

Platt, T., & Gallegos, C. L. (1980). Modelling primary production. In *Primary productivity in the sea* (pp. 339-362). Boston, MA: Springer US.

Polovina, J. J., Howell, E. A., & Abecassis, M. (2008). Ocean's least productive waters are expanding. *Geophysical Research Letters*, *35*(3).

Ralf, G., & Repeta, D. J. (1992). The pigments of *Prochlorococcus* marinus: The presence of divinylchlorophyll *a* and *b* in a marine procaryote. *Limnology and Oceanography*, *37*(2), 425-433.

Ras, J., Claustre, H., & Uitz, J. (2008). Spatial variability of phytoplankton pigment distributions in the Subtropical South Pacific Ocean: comparison between in situ and predicted data. *Biogeosciences*, *5*(2), 353-369.

Richardson, T. L., & Jackson, G. A. (2007). Small phytoplankton and carbon export from the surface ocean. *Science*, *315*(5813), 838-840.

Rippka, R., Coursin, T., Hess, W., Lichtlé, C., Scanlan, D. J., Palinska, K. A., ... & Herdman, M. (2000). *Prochlorococcus marinus* Chisholm et al. 1992 subsp. pastoris subsp. nov. strain PCC 9511, the first axenic chlorophyll *a2/b2*-containing cyanobacterium (Oxyphotobacteria). *International Journal of Systematic and Evolutionary Microbiology*, *50*(5), 1833-1847.

Roche, J. L., Van der Staay, G. W. M., Partensky, F., Ducret, A., Aebersold, R., Li, R., ... & Green, B. R. (1996). Independent evolution of the prochlorophyte and green plant chlorophyll *a/b* light-harvesting proteins. *Proceedings of the National Academy of Sciences*, *93*(26), 15244-15248.

Sagan, L. (1967). On the origin of mitosing cells. *Journal of Theoretical Biology*, *14*(3), 225-IN6.

Saito, M. A., Rocap, G., & Moffett, J. W. (2005). Production of cobalt binding ligands in a *Synechococcus* feature at the Costa Rica upwelling dome. *Limnology and Oceanography*, *50*(1), 279-290.

Sánchez-Baracaldo, P. (2015). Origin of marine planktonic cyanobacteria. *Scientific reports*, *5*(1), 17418.

Sánchez-Baracaldo, P., Bianchini, G., Di Cesare, A., Callieri, C., & Chrismas, N. A. (2019). Insights into the evolution of picocyanobacteria and phycoerythrin genes (*mpeBA* and *cpeBA*). *Frontiers in Microbiology*, *10*, 45.

Sánchez-Baracaldo, P., & Cardona, T. (2020). On the origin of oxygenic photosynthesis and Cyanobacteria. *New Phytologist*, *225*(4), 1440-1446.

Sandström, S., Ivanov, A. G., Park, Y. I., Öquist, G., & Gustafsson, P. (2002). Iron stress responses in the cyanobacterium *Synechococcus* sp. PCC7942. *Physiologia Plantarum*, *116*(2), 255-263.

Sanfilippo, J. E., Garczarek, L., Partensky, F., & Kehoe, D. M. (2019a). Chromatic acclimation in cyanobacteria: a diverse and widespread process for optimizing photosynthesis. *Annual Review of Microbiology*, *73*, 407-433.

Sanfilippo, J. E., Nguyen, A. A., Garczarek, L., Karty, J. A., Pokhrel, S., Strnat, J. A., ... & Kehoe, D. M. (2019). Interplay between differentially expressed enzymes contributes to light color acclimation in marine *Synechococcus*. *Proceedings of the National Academy of Sciences*, *116*(13), 6457-6462.

Sanfilippo, J. E., Nguyen, A. A., Karty, J. A., Shukla, A., Schluchter, W. M., Garczarek, L., ... & Kehoe, D. M. (2016). Self-regulating genomic island encoding tandem regulators confers chromatic acclimation to marine *Synechococcus*. *Proceedings of the National Academy of Sciences*, *113*(21), 6077-6082.

Sauer, P. V., Dominguez-Martin, M. A., Kirst, H., Sutter, M., Bina, D., Greber, B. J., ... & Kerfeld, C. A. (2021). Structures of the cyanobacterial phycobilisome. *bioRxiv*, 2021-11.

Saunée, N. A., Williams, S. R., Bryant, D. A., & Schluchter, W. M. (2008). Biogenesis of phycobiliproteins: II. CpcS-I and CpcU comprise the heterodimeric bilin lyase that attaches phycocyanobilin to CYS-82 OF β-phycocyanin and CYS-81 of allophycocyanin subunits in *Synechococcus* sp. PCC 7002. *Journal of Biological Chemistry*, *283*(12), 7513-7522.

Scanlan, D. J. (2012). Marine picocyanobacteria. In *Ecology of Cyanobacteria II: Their Diversity in Space and Time* (pp. 503-533). Dordrecht: Springer Netherlands.

Scheer, H. (1981). Biliproteins. *Angewandte Chemie International Edition in English*, *20*(3), 241-261.

Scheer, H., & Zhao, K. H. (2008). Biliprotein maturation: the chromophore attachment. *Molecular microbiology*, *68*(2), 263-276.

Schirrmeister, B. E., Sanchez-Baracaldo, P., & Wacey, D. (2016). Cyanobacterial evolution during the Precambrian. *International Journal of Astrobiology*, *15*(3), 187-204.

Schluchter, W. M., & Glazer, A. N. (1999). Biosynthesis of phycobiliproteins in cyanobacteria. In *The phototrophic prokaryotes* (pp. 83-95). Boston, MA: Springer US.

Schluchter, W. M., Shen, G., Alvey, R. M., Biswas, A., Saunée, N. A., Williams, S. R., ... & Bryant, D. A. (2010). Phycobiliprotein biosynthesis in cyanobacteria: structure and function of enzymes involved in post-translational modification. In *Recent advances in phototrophic prokaryotes* (pp. 211-228). Springer New York.

Schreiber, U., Klughammer, C., & Kolbowski, J. (2012). Assessment of wavelength-dependent parameters of photosynthetic electron transport with a new type of multi-color PAM chlorophyll fluorometer. *Photosynthesis Research*, *113*, 127-144.

Shen, G., Saunee, N. A., Williams, S. R., Gallo, E. F., Schluchter, W. M., & Bryant, D. A. (2006). Identification and characterization of a new class of bilin lyase: the *cpcT* gene encodes a bilin lyase responsible for attachment of phycocyanobilin to Cys-153 on the β-subunit of phycocyanin in *Synechococcus* sp. PCC 7002. *Journal of Biological Chemistry*, *281*(26), 17768-17778.

Shen, G., Schluchter, W. M., & Bryant, D. A. (2008). Biogenesis of phycobiliproteins: I. cpcS-I and cpcU mutants of the cyanobacterium *Synechococcus* sp. PCC 7002 define a heterodimeric phyococyanobilin lyase specific for β-phycocyanin and allophycocyanin subunits. *Journal of Biological Chemistry*, *283*(12), 7503-7512.

Sherry, N. D., & Wood, A. M. (2001). Phycoerythrin-containing picocyanobacteria in the Arabian Sea in February 1995: diel patterns, spatial variability, and growth rates. *Deep Sea Research Part II: Topical Studies in Oceanography*, *48*(6-7), 1263-1283.

Shukla, A., Biswas, A., Blot, N., Partensky, F., Karty, J. A., Hammad, L. A., ... & Kehoe, D. M. (2012). Phycoerythrin-specific bilin lyase–isomerase controls blue-green chromatic acclimation in marine *Synechococcus*. *Proceedings of the National Academy of Sciences*, *109*(49), 20136-20141.

Sidler, W. A. (1994). Phycobilisome and phycobiliprotein structures. In *The molecular biology of cyanobacteria* (pp. 139-216). Dordrecht: Springer Netherlands.

Singh, N. K., Sonani, R. R., Rastogi, R. P., & Madamwar, D. (2015). The phycobilisomes: an early requisite for efficient photosynthesis in cyanobacteria. *EXCLI Journal*, *14*, 268.

Six, C., Joubin, L., Partensky, F., Holtzendorff, J., and Garczarek, L. (2007a). UV-induced phycobilisome dismantling in the marine picocyanobacterium *Synechococcus* sp. WH8102. *Photosynth Res* 92, 75–86. doi: 10.1007/s11120-007-9170-4.

Six, C., Ratin, M., Marie, D., & Corre, E. (2021). Marine *Synechococcus* picocyanobacteria: light utilization across latitudes. *Proceedings of the National Academy of Sciences*, *118*(38), e2111300118.

Six, C., Thomas, J. C., Brahamsha, B., Lemoine, Y., & Partensky, F. (2004). Photophysiology of the marine cyanobacterium *Synechococcus* sp. WH8102, a new model organism. *Aquatic Microbial Ecology*, *35*(1), 17-29.

Six, C., Thomas, J. C., Garczarek, L., Ostrowski, M., Dufresne, A., Blot, N., ... & Partensky, F. (2007b). Diversity and evolution of phycobilisomes in marine *Synechococcusspp*.: a comparative genomics study. *Genome Biology*, *8*(12), 1-22.

Six, C., Thomas, J. C., Thion, L., Lemoine, Y., Zal, F., & Partensky, F. (2005). Two novel phycoerythrin-associated linker proteins in the marine cyanobacterium *Synechococcus* sp. strain WH8102. *Journal of bacteriology*, *187*(5), 1685-1694.

Śliwińska-Wilczewska, S., Konarzewska, Z., Wiśniewska, K., & Konik, M. (2020). Photosynthetic pigments changes of three phenotypes of picocyanobacteria *Synechococcus* sp. under different light and temperature conditions. *Cells*, *9*(9), 2030.

Sohm, J. A., Ahlgren, N. A., Thomson, Z. J., Williams, C., Moffett, J. W., Saito, M. A., ... & Rocap, G. (2016). Co-occurring *Synechococcus* ecotypes occupy four major oceanic regimes defined by temperature, macronutrients and iron. *The ISME Journal*, *10*(2), 333-345.

Sohrin, R., Isaji, M., Obara, Y., Agostini, S., Suzuki, Y., Hiroe, Y., ... & Hidaka, K. (2011). Distribution of *Synechococcus* in the dark ocean. *Aquatic Microbial Ecology*, *64*(1), 1-14.

Soo, R. M., Hemp, J., Parks, D. H., Fischer, W. W., & Hugenholtz, P. (2017). On the origins of oxygenic photosynthesis and aerobic respiration in Cyanobacteria. *Science*, *355*(6332), 1436-1440.

Sournia, A., & Birrien, J. L. (1995). La série océanographique côtière de Roscoff (Manche occidentale) de 1985 à 1992. *Cahiers de Biologie Marine*, *36*(1), 1-8.

Stanier, R. Y., & Cohen-Bazire, G. (1977). Phototrophic prokaryotes: the cyanobacteria. *Annual Review of Microbiology*, *31*(1), 225-274.

Stanier, R. Y., Kunisawa, R., Mandel, M. C. B. G., & Cohen-Bazire, G. (1971). Purification and properties of unicellular blue-green algae (order Chroococcales). *Bacteriological Reviews*, *35*(2), 171-205.

Stomp, M. (2008). *Colourful coexistence: a new solution to the plankton paradox*. Amsterdam: Universiteit van Amsterdam.

Stomp, M., Huisman, J., De Jongh, F., Veraart, A. J., Gerla, D., Rijkeboer, M., ... & Stal, L. J. (2004). Adaptive divergence in pigment composition promotes phytoplankton biodiversity. *Nature*, *432*(7013), 104-107.

Stomp, M., van Dijk, M. A., van Overzee, H. M., Wortel, M. T., Sigon, C. A., Egas, M., ... & Huisman, J. (2008). The timescale of phenotypic plasticity and its impact on competition in fluctuating environments. *The American Naturalist*, *172*(5), E169-E185.

Storf, M., Parbel, A., Meyer, M., Strohmann, B., Scheer, H., Deng, M. G., ... & Zhao, K. H. (2001). Chromophore attachment to biliproteins: Specificity of PecE/PecF, a lyase-isomerase for the photoactive 31-Cys-α84-phycoviolobilin chromophore of phycoerythrocyanin. *Biochemistry*, *40*(41), 12444-12456.

Striebel, M., Behl, S., Diehl, S., & Stibor, H. (2009). Spectral niche complementarity and carbon dynamics in pelagic ecosystems. *The American Naturalist*, *174*(1), 141-147.

Suttle, C. A. (2007). Marine viruses—major players in the global ecosystem. *Nature Reviews Microbiology*, *5*(10), 801-812.

Tai, V., & Palenik, B. (2009). Temporal variation of *Synechococcus* clades at a coastal Pacific Ocean monitoring site. *The ISME Journal*, *3*(8), 903-915.

Takahashi, S., & Murata, N. (2008). How do environmental stresses accelerate photoinhibition?. *Trends in Plant Science*, *13*(4), 178-182.

Tandeau de Marsac, N. (1977). Occurrence and nature of chromatic adaptation in cyanobacteria. *Journal of Bacteriology*, *130*(1), 82-91.

De Marsac, N. T. (2003). Phycobiliproteins and phycobilisomes: the early observations. *Photosynthesis Research*, *76*(1-3), 197-205.

Tarran, G. A., & Bruun, J. T. (2015). Nanoplankton and picoplankton in the Western English Channel: abundance and seasonality from 2007–2013. *Progress in Oceanography*, *137*, 446-455.

Teale, F. W. J., & Dale, R. E. (1970). Isolation and spectral characterization of phycobiliproteins. *Biochemical Journal*, *116*(2), 161.

Till, P., Toepel, J., Bühler, B., Mach, R. L., & Mach-Aigner, A. R. (2020). Regulatory systems for gene expression control in cyanobacteria. *Applied Microbiology and Biotechnology*, *104*(5), 1977-1991.

Ting, C. S., Rocap, G., King, J., & Chisholm, S. W. (2002). Cyanobacterial photosynthesis in the oceans: the origins and significance of divergent light-harvesting strategies. *Trends in Microbiology*, *10*(3), 134-142.

Toledo, G., Palenik, B., & Brahamsha, B. (1999). Swimming marine *Synechococcus* strains with widely different photosynthetic pigment ratios form a monophyletic group. *Applied and Environmental Microbiology*, *65*(12), 5247-5251.

Ulloa, O., Henríquez-Castillo, C., Ramírez-Flandes, S., Plominsky, A. M., Murillo, A. A., Morgan-Lang, C., ... & Stepanauskas, R. (2021). The cyanobacterium *Prochlorococcus* has divergent light-harvesting antennae and may have evolved in a low-oxygen ocean. *Proceedings of the National Academy of Sciences*, *118*(11), e2025638118.

Ungerer, J., & Pakrasi, H. B. (2016). Cpf1 is a versatile tool for CRISPR genome editing across diverse species of cyanobacteria. *Scientific Reports*, *6*(1), 39681.

Urbach, E., Scanlan, D. J., Distel, D. L., Waterbury, J. B., & Chisholm, S. W. (1998). Rapid diversification of marine picophytoplankton with dissimilar light-harvesting structures inferred from sequences of *Prochlorococcus* and *Synechococcus* (Cyanobacteria). *Journal of Molecular Evolution*, *46*, 188-201.

Uysal, Z., & Köksalan, İ. (2006). The annual cycle of *Synechococcus* (cyanobacteria) in the northern Levantine Basin shelf waters (Eastern Mediterranean). *Marine Ecology*, *27*(3), 187-197.

V. Esenbeck, N. (1836). Ueber einen blau-rothen Farbstoff, der sich bei der Zersetzung von Oscillatorien bildet. *Annalen der Pharmacie*, *17*(1), 75-82.

Vaulot, D., Eikrem, W., Viprey, M., & Moreau, H. (2008). The diversity of eukaryotic marine picophytoplankton. *FEMS Microbiol. Rev*, *32*, 795-820.

Walker, P. L. (2022). Mechanisms for High Light Tolerance in a Fast-Growing Cyanobacterium.

Waterbury, J. B. (1989). Subsection I. Order Chroococcales Wettstein 1924, emend. Rippka et al., 1979. *Bergey's Manual of Systematic Bacteriology*, *3*, 1728-1746.

Waterbury, J. B., Watson, S. W., Guillard, R. R., & Brand, L. E. (1979). Widespread occurrence of a unicellular, marine, planktonic, cyanobacterium. *Nature*, *277*(5694).

Wendt, K. E., Ungerer, J., Cobb, R. E., Zhao, H., & Pakrasi, H. B. (2016). CRISPR/Cas9 mediated targeted mutagenesis of the fast growing cyanobacterium *Synechococcus elongatus* UTEX 2973. *Microbial Cell Factories*, *15*, 1-8.

Wiethaus, J., Busch, A. W., Kock, K., Leichert, L. I., Herrmann, C., & Frankenberg-Dinkel, N. (2010). CpeS is a lyase specific for attachment of 3Z-PEB to Cys82 of β-phycoerythrin from *Prochlorococcus marinus* MED4. *Journal of Biological Chemistry*, *285*(48), 37561-37569.

Wilbanks, S. M., & Glazer, A. N. (1993). Rod structure of a phycoerythrin II-containing phycobilisome. I. Organization and sequence of the gene cluster encoding the major phycobiliprotein rod components in the genome of marine *Synechococcus* sp. WH8020. *Journal of Biological Chemistry*, *268*(2), 1226-1235.

Wood, A. M. (1985). Adaptation of photosynthetic apparatus of marine ultraphytoplankton to natural light fields. *Nature*, *316*(6025), 253-255.

Wood, A. M., Phinney, D. A., & Yentsch, C. S. (1998). Water column transparency and the distribution of spectrally distinct forms of phycoerythrin-containing organisms. *Marine Ecology Progress Series*, *162*, 25-31.

Worden, A. Z., Follows, M. J., Giovannoni, S. J., Wilken, S., Zimmerman, A. E., & Keeling, P. J. (2015). Rethinking the marine carbon cycle: factoring in the multifarious lifestyles of microbes. *Science*, *347*(6223), 1257594.

Xia, X., Guo, W., Tan, S., & Liu, H. (2017). *Synechococcus* assemblages across the salinity gradient in a salt wedge estuary. *Frontiers in Microbiology*, *8*, 1254.

Xia, X., Liu, H., Choi, D., & Noh, J. H. (2018). Variation of *Synechococcus* pigment genetic diversity along two turbidity gradients in the China Seas. *Microbial Ecology*, *75*, 10-21.

Xia, X., Vidyarathna, N. K., Palenik, B., Lee, P., & Liu, H. (2015). Comparison of the seasonal variations of *Synechococcus* assemblage structures in estuarine waters and coastal waters of Hong Kong. *Applied and Environmental Microbiology*, *81*(21), 7644-7655.

Xu, H., Vavilin, D., Funk, C., & Vermaas, W. (2004). Multiple deletions of small Cab-like proteins in the cyanobacterium *Synechocystis* sp. PCC 6803: consequences for pigment biosynthesis and accumulation. *Journal of Biological Chemistry*, *279*(27), 27971-27979.

Yona, D., Park, M. O., Oh, S. J., & Shin, W. C. (2014). Distribution of *Synechococcus* and its phycoerythrin pigment in relation to environmental factors in the East Sea, Korea. *Ocean Science Journal*, *49*, 367-382.

Zhang, P., Eisenhut, M., Brandt, A. M., Carmel, D., Silén, H. M., Vass, I., ... & Aro, E. M. (2012). Operon *flv4-flv2* provides cyanobacterial photosystem II with flexibility of electron transfer. *The Plant Cell*, *24*(5), 1952-1971.

Zhang, X., Cheung, S., Wang, J., Zhang, G., Wei, Y., Liu, H., ... & Liu, H. (2022). Highly Diverse *Synechococcus* Pigment Types in the Eastern Indian Ocean. *Frontiers in Microbiology*, *13*, 806390.

Zhao, K. H., Deng, M. G., Zheng, M., Zhou, M., Parbel, A., Storf, M., ... & Scheer, H. (2000). Novel activity of a phycobiliprotein lyase: both the attachment of phycocyanobilin and the isomerization to phycoviolobilin are catalyzed by the proteins PecE and PecF encoded by the phycoerythrocyanin operon. *FEBS Letters*, *469*(1), 9-13.

Zhao, K. H., Wu, D., Wang, L., Zhou, M., Storf, M., Bubenzer, C., ... & Scheer, H. (2002). Characterization of phycoviolobilin phycoerythrocyanin-α84-cystein-lyase-(isomerizing) from *Mastigocladus laminosus*. *European Journal of Biochemistry*, *269*(18), 4542-4550.

Zhao, K. H., Zhang, J., Tu, J. M., Böhm, S., Plöscher, M., Eichacker, L., ... & Zhou, M. (2007). Lyase activities of CpcS-and CpcT-like proteins from *Nostoc* PCC7120 and sequential reconstitution of binding sites of phycoerythrocyanin and phycocyanin β-subunits. *Journal of Biological Chemistry*, *282*(47), 34093-34103.

Zhou, J., Gasparich, G. E., Stirewalt, V. L., De Lorimier, R., & Bryant, D. A. (1992). The *cpcE* and *cpcF* genes of *Synechococcus* sp. PCC 7002. Construction and phenotypic characterization of interposon mutants. *Journal of Biological Chemistry*, *267*(23), 16138-16145.

Zwirglmaier, K., Heywood, J. L., Chamberlain, K., Woodward, E. M. S., Zubkov, M. V., & Scanlan, D. J. (2007). Basin-scale distribution patterns of picocyanobacterial lineages in the Atlantic Ocean. *Environmental Microbiology*, *9*(5), 1278-1290.

Zwirglmaier, K., Jardillier, L., Ostrowski, M., Mazard, S., Garczarek, L., Vaulot, D., ... & Scanlan, D. J. (2008). Global phylogeography of marine *Synechococcus* and *Prochlorococcus* reveals a distinct partitioning of lineages among oceanic biomes. *Environmental Microbiology*, *10*(1), 147-161.

Annex

<u>Annexe 1:</u> The phycoerythrobilin isomerization activity of MpeV in *Synechococcus* sp. WH8020 is prevented by the presence of a histidine at position 141 within its phycoerythrin-I β-subunit substrate.

<u>Annexe 2:</u> Comparative Thermophysiology of Marine *Synechococcus* CRD1 Strains Isolated From Different Thermal Niches in Iron-Depleted Areas.

frontiers | Frontiers in Microbiology

TYPE Original Research
PUBLISHED 15 November 2022
DOI 10.3389/fmicb.2022.1011189

OPEN ACCESS

EDITED BY
Graciela L. Lorca,
University of Florida, United States

REVIEWED BY
Ines Abatedaga,
CONICET Institute of Bionanotechnology of NOA (INBIONATEC), Argentina
Vinod K. Kannaujiya,
Banaras Hindu University, India

*CORRESPONDENCE
Wendy M. Schluchter
wschluch@uno.edu

SPECIALTY SECTION
This article was submitted to Microbial Physiology and Metabolism, a section of the journal Frontiers in Microbiology

RECEIVED 03 August 2022
ACCEPTED 12 October 2022
PUBLISHED 15 November 2022

CITATION
Carrigee LA, Frick JP, Liu X, Karty JA, Trinidad JC, Tom IP, Yang X, Dufour L, Partensky F and Schluchter WM (2022) The phycoerythrobilin isomerization activity of MpeV in *Synechococcus* sp. WH8020 is prevented by the presence of a histidine at position 141 within its phycoerythrin-I β-subunit substrate.
Front. Microbiol. 13:1011189.
doi: 10.3389/fmicb.2022.1011189

The phycoerythrobilin isomerization activity of MpeV in *Synechococcus* sp. WH8020 is prevented by the presence of a histidine at position 141 within its phycoerythrin-I β-subunit substrate

Lyndsay A. Carrigee[1,2], Jacob P. Frick[1], Xindi Liu[1], Jonathan A. Karty[3], Jonathan C. Trinidad[3], Irin P. Tom[4], Xiaojing Yang[4], Louison Dufour[5], Frédéric Partensky[5] and Wendy M. Schluchter[1]*

[1]Department of Biological Sciences, University of New Orleans, New Orleans, LA, United States, [2]Environmental Laboratory, Engineering and Research Development Center, US Army Corps of Engineers, Vicksburg, MS, United States, [3]Department of Chemistry, Indiana University, Bloomington, IN, United States, [4]Department of Chemistry, University of Illinois Chicago, Chicago, IL, United States, [5]Ecology of Marine Plankton Team, UMR 7144 Adaptation and Diversity in the Marine Environment, Station Biologique, Sorbonne Université, CNRS, Roscoff, France

Marine *Synechococcus* efficiently harvest available light for photosynthesis using complex antenna systems, called phycobilisomes, composed of an allophycocyanin core surrounded by rods, which in the open ocean are always constituted of phycocyanin and two phycoerythrin (PE) types: PEI and PEII. These cyanobacteria display a wide pigment diversity primarily resulting from differences in the ratio of the two chromophores bound to PEs, the green-light absorbing phycoerythrobilin and the blue-light absorbing phycourobilin. Prior to phycobiliprotein assembly, bilin lyases post-translationally catalyze the ligation of phycoerythrobilin to conserved cysteine residues on α- or β-subunits, whereas the closely related lyase-isomerases isomerize phycoerythrobilin to phycourobilin during the attachment reaction. MpeV was recently shown in *Synechococcus* sp. RS9916 to be a lyase-isomerase which doubly links phycourobilin to two cysteine residues (C50 and C61; hereafter C50, 61) on the β-subunit of both PEI and PEII. Here we show that *Synechococcus* sp. WH8020, which belongs to the same pigment type as RS9916, contains MpeV that demonstrates lyase-isomerase activity on the PEII β-subunit but only lyase activity on the PEI β-subunit. We also demonstrate that occurrence of a histidine at position 141 of the PEI β-subunit from WH8020, instead of a leucine in its counterpart from RS9916, prevents the isomerization activity by WH8020 MpeV, showing for the first time that both the substrate and the enzyme play a role in the isomerization reaction. We propose a structural-based mechanism for the role of H141 in blocking isomerization. More generally, the knowledge of the amino acid present at position 141 of the β-subunits may be used to

predict which phycobilin is bound at C50, 61 of both PEI and PEII from marine *Synechococcus* strains.

KEYWORDS

bilin lyase, cyanobacteria, chromatic acclimation, phycobilisome, phycoerythrin, phycoerythrobilin, phycourobilin, post-translational modification

Introduction

Marine cyanobacteria are responsible for as much as half of the world's oxygen production and photosynthesis and play a key role in carbon and nutrient cycling (Bengston, 1994; Kasting and Siefert, 2003; Kehoe, 2010). Marine isolates of *Synechococcus* cyanobacteria possess huge light-harvesting complexes (or phycobilisome; hereafter PBS), comprised of up to four types of highly pigmented phycobiliproteins (PBPs). Allophycocyanin constitutes the core of the PBS, surrounded by 6–8 rods made of phycocyanin and up to two types of phycoerythrin (PEI and PEII; Figure 1; Ong and Glazer, 1991; Glazer, 1994; Everroad et al., 2006; Flombaum et al., 2013; Sanfilippo et al., 2019a). This variable PBP content extends the spectral range of the PBS light harvesting capabilities. PEI and PEII are homologous PBP, each composed of an α- and a β-subunit arranged in a torus-like hetero-hexamer $(\alpha\beta)_6$ and stacked together with the help of linker polypeptides to form the distal portion of the PBS rods (Figure 1; Glazer, 1988; Betz, 1997; Schluchter et al., 2010).

The large pigment diversity in marine strains of *Synechococcus* PBS is not only due to its variable PBP content but also to the variable composition of covalently bound linear tetrapyrrole bilins. The latter are post-translationally added to highly conserved cysteine (C) residues of PBP precursors by a variety of bilin lyases. Three major groups or clans of bilin lyases have been characterized to date: the S/U type, the T type, and the E/F type (Fairchild et al., 1992; Fairchild and Glazer, 1994; Shen et al., 2006; Zhao et al., 2007; Saunée et al., 2008). Bilin chromophore and attachment site specificity as well as primary amino acid sequence similarities are trademarks differentiating members of each clan. The crystal structures of the S/U [Protein Data Bank, (PDB): 3BDR; Zhao et al., 2006; Shen et al., 2008;Schluchter et al., 2010; Kronfel et al., 2013; Overkamp et al., 2014] and T (PDB: 4O4O; Zhou et al., 2014; Gasper et al., 2017) lyases show that they adopt a similar antiparallel beta-barrel structure akin to the lipocalin protein family (Schluchter et al., 2010; Kronfel et al., 2013; Overkamp et al., 2014). The E/F lyases adopt all helical structures. While the crystal structure of the heterodimeric CpcE/F lyase was reported to adopt an α-helical structure of a solenoid shape (Zhao et al., 2017), the recent crystal structure of a novel lyase-isomerase, MpeQ (Kumarapperuma et al., 2022), suggested that a question mark-like architecture represents a common protein framework for both single chain and heterodimeric E/F lyases (Andrade et al., 2001; Marcotrigiano et al., 2001; Kozo et al., 2002; Takano and Gusella, 2002; Scheer and Zhao, 2008; Schluchter et al., 2010; Zhao et al., 2017; Kumarapperuma et al., 2022). The S/U lyases exhibit a broad variation in chromophore and PBP substrate specificity but are highly specific with regard to C binding sites (Shen et al., 2006; Saunée et al., 2008; Scheer and Zhao, 2008; Biswas et al., 2010; Schluchter et al., 2010; Kronfel et al., 2013; Zhou et al., 2014; Gasper et al., 2017). In contrast, the E/F lyases display high specificities for the bilin chromophore and bilin binding site on a particular PBP (PDB 5N3U; Fairchild et al., 1992; Swanson et al., 1992; Zhou et al., 1992; Fairchild and Glazer, 1994).

Marine strains of *Synechococcus* containing both PEI and PEII possess a diverse set of E/F lyases (Wilbanks and Glazer, 1993; Six et al., 2007; Shukla et al., 2012), particularly in those strains that undergo Type IV chromatic acclimation (CA4). In the CA4 phenomenon, *Synechococcus* are able to alter the ratio between the blue light-absorbing chromophore phycourobilin (PUB; $\lambda_{max} \sim 495$ nm) and the green light-absorbing chromophore phycoerythrobilin (PEB; $\lambda_{max} \sim 545$ nm) in both PEI and PEII, thereby extending the light harvesting capabilities of PBS (Figures 1, 2; Palenik, 2001; Everroad et al., 2006; Kehoe, 2010; Humily et al., 2013; Sanfilippo et al., 2016, 2019a,b). This unique CA4 phenomenon is conferred by a small genomic island that occurs in two possible configurations, CA4-A or CA4-B, (Supplementary Figure 1; Humily et al., 2013). Each island encodes a transcriptional activator, a repressor, a protein of unknown function, and an E/F-type bilin lyase (PEB lyase MpeW in the CA4-B island) or lyase-isomerase (MpeZ in the CA4-A island; Supplementary Figure 1). A bilin lyase-isomerase is an enzyme that has an additional activity to isomerize PEB to PUB during the ligation reaction (Everroad et al., 2006; Shukla et al., 2012; Humily et al., 2013; Sanfilippo et al., 2016).

Intriguingly, all marine *Synechococcus* containing a CA4-A island also possess a specific member of the E/F clan, MpeV, which

Abbreviations: BL, Blue light; C, Cysteine residue; CA4, Type IV chromatic acclimation; CpeA/CpeB, α–/β-subunit of phycoerythrin type; I; EICs, Extracted ion chromatograms; GL, Green light; HT, Hexahistidine-tagged; H, Histidine; L, Leucine; MpeA/MpeB, α-/β-subunit of phycoerythrin type II; MS, Mass spectrometry; MW, Molecular weight; PAGE, Polyacrylamide gel electrophoresis; PBP, Phycobiliprotein(s); PBS, Phycobilisome(s); PDB, Protein Data Bank; PEI, Phycoerythrin I; PEII, Phycoerythrin II; PEB, Phycoerythrobilin; PUB, Phycourobilin; RS, *Synechococcus* sp. RS9916; SDS, Sodium dodecyl sulfate; WH, *Synechococcus* sp. WH8020..

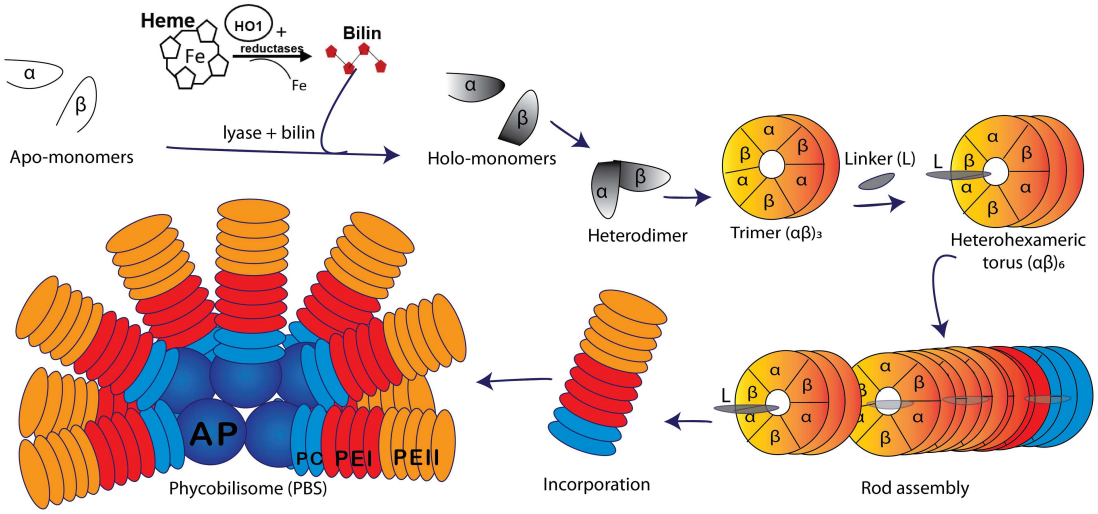

FIGURE 1
Model of a marine *Synechococcus* WH8020 phycobilisome (PBS) containing phycoerythrin I (PEI, red), phycoerythrin II (PEII, orange), phycocyanin (PC, light blue), and an allophycocyanin (AP, deep blue) core. A depiction of PBS rod assembly shows the addition of bilin *via* lyase catalyzed post-translational modification of apo-α and apo-β monomers (white) forming holo-monomers (gray) which come together to form a heterodimer. Heterodimers are subsequently arranged in trimers $(\alpha\beta)_3$ followed by heterohexamers $(\alpha\beta)_6$ and with the help of linker (L) polypeptides, the PBS rod is formed and bound onto the core (Glazer, 1982; Glazer, 1984; Six et al., 2007; Schluchter et al., 2010).

is not involved in the CA4 process (Carrigee et al., 2020b). The *mpeV* gene is located in a large genomic region containing a cluster of genes involved on the biosynthesis of PBS rods, so-called the "PBS genomic region" (Supplementary Figure 1; Wilbanks and Glazer, 1993; Grébert et al., 2021). We recently characterized MpeV from the model *Synechococcus* CA4-A strain RS9916 (hereafter RS9916). In RS9916, we showed that MpeV is integral in the ligation reaction of a doubly-linked PUB at the equivalent position (C50, 61) on the recombinant β-subunits of both PEI (CpeB) and PEII (MpeB), demonstrating that MpeV is a lyase-isomerase capable of attaching the doubly-linked PUB on both subunits (see Figure 2; Carrigee et al., 2020b). This study also showed that RS9916 MpeV activity requires ligation of PEB at C82 position on both CpeB and MpeB by CpeS (a S/U type lyase) and is enhanced by activity of the chaperone-like enzyme CpeZ (a member of the E/F clan; Kronfel et al., 2019a,b; Carrigee et al., 2020b). When all three enzymes (CpeS, CpeZ, and MpeV) from RS9916 were expressed, both CpeB and MpeB possessed a doubly-linked PUB at C50, 61 (Carrigee et al., 2020b).

It has been reported that in *Synechococcus* sp. WH8020 (hereafter WH8020) PEI and PEII, CpeB incorporates PEB while MpeB has PUB at the C50, 61 positions (Ong and Glazer, 1991). Like RS9916, WH8020 is also a CA4-A strain that possesses *mpeV* (Wilbanks and Glazer, 1993; Carrigee et al., 2020b; Grébert et al., 2022). To determine whether MpeV is responsible for ligating PEB on CpeB and PUB on MpeB in WH8020, we employed recombinant protein expression, absorbance and fluorescence spectroscopy, and tandem mass spectrometry. We found that a single amino acid substitution on CpeB, specifically a change from leucine (L) to histidine (H) at position 141, was sufficient to block the isomerase activity of WH8020 MpeV. We further predict that a few other CA4-A strains containing a CpeB with the same substitution might have a similar bilin pattern, and, more generally, that the knowledge of the amino acid present at position 141 of CpeB or MpeB can be used to predict which phycobilin is bound at C50, 61 of both β-subunits from marine *Synechococcus* strains at large. We also propose a structural-based mechanism for the role of H141 in blocking isomerization.

Materials and methods

Plasmids for the characterization of WH8020 MpeV and CpeB

The putative lyase genes *cpeS*, *cpeZ*, and *mpeV* from the RS9916 genome (Supplementary Figure 1) were amplified *via* polymerase chain reaction (PCR) using a standard *Pfu* DNA polymerase system (ThermoFisher Scientific, Waltham, MA) and synthetic forward and reverse oligonucleotide primers with engineered restriction endonuclease sites (Eurofins MWG Operon, Huntsville, AL). Primers used to amplify genes by PCR for the construction of these expression vectors are previously published (Carrigee, 2020; Carrigee et al., 2020a,b). Amplified fragments were separately cloned into compatible Novagen Duet vectors using corresponding restriction enzymes as listed in Supplementary Tables 1, 2 or were previously published (Carrigee, 2020; Carrigee et al., 2020a,b). Expression vectors used in this study (Supplementary Table 2) include two previously described (Shukla et al., 2012; Kronfel et al., 2019b).

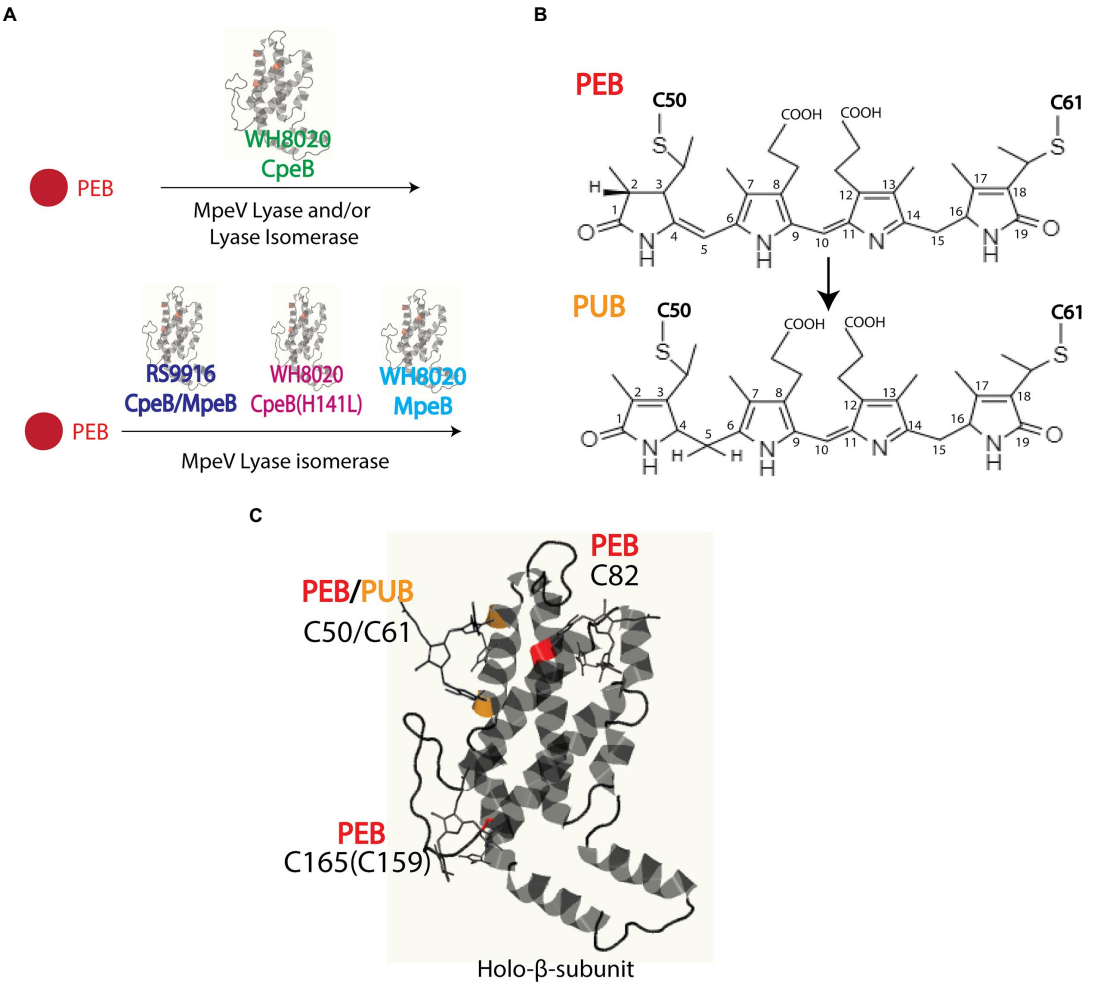

FIGURE 2
(A) Model of *Synechococcus* sp. WH8020 MpeV activity as both a lyase and lyase-isomerase. **(B)** Chemical structures of phycoerythrobilin (PEB) and doubly-linked phycourobilin (PUB). Post-translational pigment attachment is catalyzed by bilin lyases or lyase isomerases with a thioether linkage at the 3^1 carbon of the bilin A ring during single attachment or additionally through the 18^1 carbon of the bilin D ring when doubly attached. **(C)** Bilin structure and ligation sites, representative of RS9916 and WH8020 CpeB. Ribbon diagram generated using Phyre^2 (Kelley et al., 2015). depicting β-subunit of PEI (β-PEI) chromophorylation pattern and lyases involved (bilins in ball and stick). PEB ligated residues are highlighted in red, and PUB ligated residues are highlighted in orange.

The *mpeV* gene from WH8020 was amplified *via* PCR using Platinum SuperFi II DNA Polymerase as a master mix in lieu of the *Pfu* system as previously described (Carrigee et al., 2020b). PCR reactions were performed using the standard High Fidelity PCR protocol from ThermoFisher Scientific (Waltham, MA). WH8020 substrate genes were cloned as an operon for PEI (*cpeBA*) with the beta subunit in frame with a hexahistidine tag (HT) and inserted into pET-DUET independently. WH8020 *mpeV* was cloned in-frame with the coding region of the HT and inserted into pCDF-DUET1. For co-expression of multiple genes required to characterize MpeV, some genes were subcloned into both multiple cloning sites (MCSs) for compatibility as follows. RS9916 *cpeZ* was cloned using Platinum SuperFi PCR protocol and inserted in frame after the sequence encoding a HT into MCSI of pCOLA-Duet containing non-tagged (NT) *cpeS* in MCSII (Carrigee, 2020; Carrigee et al., 2020b). The RS9916 *cpeA* gene sequence was inserted into multiple cloning site I (MCSI) pET-Duet (Novagen, Madison, WI) in frame with the sequence encoding a hexahistidine tag (HT). *cpeB* was subsequently subcloned into MCSII to achieve (MCSI/MCSII/vector) RS9916 HT*cpeA*/HT*cpeB*/pET-DUET and RS9916 HT*mpeA*/HT*mpeB*/pET-DUET as previously described (Carrigee, 2020; Carrigee et al., 2020b).

A single-site variant of WH8020 CpeB was created by mutating the H141 residue to L (H141L) using combined overlap extension PCR method adapted from (Hussain and Chong, 2016) using the Platinum SuperFi protocol (Supplementary Table 1). A PCR fragment containing the entire mutant WH8020 *cpeBA* operon was cloned into MCSI of pET-DUET vector containing resulting plasmids listed in Supplementary Table 2. All plasmids were sequenced for verification of clones and mutations (Eurofins Genomics LLC, Louisville, KY).

Escherichia coli growth conditions and recombinant expression

Initial experiments for heterologous protein expression were performed using *E. coli* grown in Luria Bertani (LB) medium. However, we used modified, auto-induced medium for maximal protein yield (Studier, 2005). This involved a 100-ml LB starter culture of *E. coli* cells grown at 37°C overnight; then this was added to a liter of auto-induced medium composed of LB containing 1 mM $MgSO_4$, 25 mM $(NH_4)_2SO_4$, 50 mM KH_2PO_4, 50 mM Na_2HPO_4, 0.5% glycerol, and 0.05% glucose at 18°C with appropriate combinations of antibiotics ampicillin (Ap: 100 μg·ml^{-1}), chloramphenicol (Cm: 34 μg·ml^{-1}), kanamycin (Km: 50 μg·ml^{-1}), and spectinomycin (Sp: 100 μg·ml^{-1}). With either medium, once the OD_{600nm} reached 0.6, cultures were induced with 1 mM isopropyl 1-β-D-thiogalactopyranoside, after which the cells were allowed to grow at 18°C for an additional 24 h before being harvested by centrifugation at 11,000 ×*g* for 8 min in a Sorvall RC 5C Plus centrifuge (Kendro Laboratory Products, Newtown, CT). Cell pellets were stored at −20°C until ready for purification and analysis. The wet weight of all cell pellets was measured and recorded prior to storage at −20°C.

Protein purification

The histidine-tagged (HT) proteins were purified as previously described (Carrigee et al., 2020b). Briefly, cell pellets were resuspended at 3.0 ml·g^{-1} complete with mini protease cocktail (Thermo Scientific, Waltham, MA), 0.01 mg·ml^{-1} lysozyme (Fisher Scientific, Hampton, NH), and passed through a French Pressure Cell Press at 18,000 psi three times. All samples purified by cobalt affinity chromatography, dialyzed to remove imidazole, and then concentrated by ultrafiltration through an Amicon Ultra centrifugal filter unit (10 kDa cutoff; Novagen/EMD Millipore Corp., Darmstadt, Germany) and stored at −20°C.

Analysis of recombinant protein and bound bilin

Purified protein was quantified using Bradford colorimetric assay (BioRad, Hercules, CA) and diluted to obtain equal concentrations across co-expressions for direct comparison when possible. Absorbance spectroscopy was performed using Perkin Elmer Lambda 35 UV/VIS or Shimadzu UV-2600 UV–Vis spectrophotometers followed by fluorescence spectroscopy using a Perkin Elmer LS55 (Waltham, MA) with excitation at 490 nm (PEB) or 440 nm (PUB; slit widths were set at 10 nm). Proteins were subsequently resolved by 15% (w/v) polyacrylamide gel electrophoresis (PAGE) in the presence of sodium dodecyl sulfate (SDS) and ultimately visualized by Coomassie blue staining (Saunée et al., 2008). To visualize proteins with bound bilin, gels were subjected to zinc-enhanced fluorescence using ChemiDoc MP imaging system (Bio-Rad, Hercules, CA) with excitation at 460–490 nm (PUB) and 520–545 nm (PEB).

Growth of cyanobacterial strains

WH8020 cells were obtained from the Roscoff Culture collection.[1] Cultures of WH8020 were grown at 22°C in PCR-S11 media and acclimated for at least 7 days in either blue light (BL) or green light (GL) and PBS were collected as previously described (Sanfilippo et al., 2016; Mahmoud et al., 2017; Sanfilippo et al., 2019b). Fluorescence excitation spectra were recorded at an emission of 575 nm, using a Perkin Elmer LS-50B spectrofluorometer. The fluorescence excitation 495–545 nm ratio was calculated and used as a proxy for the molar PUB to PEB ratio, as described (Humily et al., 2013).

HPLC separation of PBS, trypsin digestion, and liquid chromatography tandem mass spectrometry

PBS were purified using methods previously described (Shukla et al., 2012; Sanfilippo et al., 2016, 2019a). Samples were dialyzed overnight against 5 mM Na phosphate buffer (pH 7.0) and subsequently purified *via* high performance liquid chromatography (HPLC) using methods outlined in (Shukla et al., 2012; Sanfilippo et al., 2016). Phycobiliproteins were monitored from 210 to 700 nm with specific channels monitoring for total protein (280 nm), PUB (490 nm), and PEB (550 nm). Relevant fractions were vacuum-dried and kept at −20°C prior to digestion for mass spectrometric (MS) analysis as previously described (Biswas et al., 2011; Shukla et al., 2012; Sanfilippo et al., 2016). Purified proteins were dialyzed against 2 mM sodium phosphate buffer (pH 7.0) and 1 mM β-mercaptoethanol. One aliquot of trypsin (dimethylated trypsin from porcine pancreas; Sigma, St. Louis, MO) was added to 2% (w/w) from a 20 μg ml^{-1} stock to the denatured protein mixtures and incubated at 30°C for 3 h in the dark (Shukla et al., 2012). The reaction was quenched by adding 30% (v/v) glacial acetic acid. Digested peptides were passed

1 https://www.roscoff-culture-collection.org/

through a pre-equilibrated C8 Sep-Pak cartridge (Waters Corporation, Milford, MA), and thereafter the eluted sample was vacuum dried and stored at −80°C before LC–MS² on a Thermo Orbitrap Fusion Lumos instrument. MS1 scans were obtained with a resolution of 120,000 and mass range of 300–2,000 m/z. Data dependent HCD were acquired with a 3 s cycle time, quadrupole precursor isolation window of two 2 m/z and resolution of 30,000 with 30% relative collision energy. Samples were separated by an Easy NanoLC1200 HPLC (ThermoFisher) equipped with a 75 μm × 15 cm Acclaim PepMap100 separating column (Thermo Scientific) downstream of a 2 cm guard column (Thermo Scientific). Buffer A was 0.1% formic acid in water. Buffer B was 0.1% formic acid in 80% acetonitrile. Peptides were separated on a 30 min gradient from 4% B to 33% B. All data processing was performed with Thermo XCalibur 4.0, Proteome Discover 2.1 (Thermo Scientific), and a local copy of ProteinPropector 5.22.1 (prospector.ucsf.edu).

Bioinformatics and structural modeling of proteins

Gene sequences from *Synechococcus* strains RS9916 and WH8020 were retrieved from Cyanorak (Garczarek et al., 2021). Amino acid sequences were analyzed using the ClustalW alignment tool from MacVector software V. 12.7.5 (MacVector Inc., Apex, NC) and Phyre² prediction system (Kelley et al., 2015). The model of the MpeV-CpeB complex was obtained using the AlphaFold2 multimer implemented in the ColabFold server based on the protein sequences of MpeV and CpeB from RS9916 (Jumper et al., 2021; Mirdita et al., 2022). The PEB chromophore was then manually docked into the MpeV/MpeB complex structure using Coot (Emsley and Cowtan, 2004).

Results

HPLC analyses of WH8020 PBS

Initially, we wanted to confirm that the bilin composition of PEI and PEII from wild type (WT) WH8020 PBS was as previously described (Ong and Glazer, 1991). Cells used in this previous study were isolated from cultures grown in white light, a light condition known to elicit a pigment phenotype equivalent to GL in CA4 strains (Ong and Glazer, 1991; Everroad and Wood, 2006; Humily et al., 2013). Here we isolated PBS from native WH8020 cells grown in two separate light conditions: GL for maximum PEB production and BL for maximum PUB production (Supplementary Figure 2). PBPs were then separated by HPLC with relative absorbance and chromatograms obtained using 550 nm (PEB) and 495 nm (PUB) for bilin content and 280 nm for total protein (Figures 3A–C; Shukla et al., 2012; Carrigee et al., 2020b). The numbered peaks in Figures 3D–G were collected, digested with trypsin, and analyzed by LC/MS/MS to identify the proteins present in each peak. As shown in Table 1, peaks labeled as MpeA, CpeA, CpeB, and MpeB were verified by MS coverage (Table 1; Figure 3). As expected for this CA4-A strain, variable bilin content was detected among the α-subunits depending on light quality (GL or BL), and the changes in PUB:PEB ratio observed in the spectra for CpeA and MpeA matched those documented for RS9916 during the CA4 process (Figures 3H,I; Kehoe, 2010; Shukla et al., 2012; Nguyen, 2018; Carrigee et al., 2020b). Unfortunately, we were not able to identify all bilins attached at each light condition for each protein by LC tandem MS, but we can infer the likely bilin content from our spectra and using the previous characterizations of WH8020 in white light (equivalent to GL; Ong and Glazer, 1991) and RS9916 in BL and GL (Shukla et al., 2012) as shown in Figure 3I.

As expected from previous work showing that the CA4 process affects only MpeA and CpeA (Shukla et al., 2012), no changes were observed in the MpeB and CpeB proteins in GL vs. BL (Figures 3E,G). As previously reported by Ong and Glazer for WH8020 grown in white light (Ong and Glazer, 1991) and for RS9916 in both GL and BL (Shukla et al., 2012), WH8020 MpeB binds a doubly-linked PUB at C50, 61 and two PEB (C159 and C82) in a 1:2 ratio, or a PUB:PEB of ~0.58 independent of light condition (Figures 3E,G; Ong and Glazer, 1991). However, while RS9916 CpeB maintains bilin composition of one PUB (doubly-linked to C50, 61) and 2 PEB (C82 and C165) for CpeB regardless of growth conditions, HPLC analysis showed that WH8020 CpeB has PEB bound to all sites, including the doubly-linked C50, 61 position, consistent with what Ong and Glazer reported in 1991 (Ong and Glazer, 1991). The fraction collected for CpeB (Figure 3E, peak 2) only contains PEB (no PUB is detected) and no bilin content changes were detected in GL or BL.

Comparative genomics analysis

MpeV was first suggested as a putative lyase by Wilbanks and Glazer, after sequencing of a large fraction of the PBS rod genomic region from WH8020 (Supplementary Figure 1; Wilbanks and Glazer, 1993). ClustalW analysis of protein sequences from RS9916 and WH8020 revealed 97.3% similarity between the CpeB substrates, 97.8% similarity between MpeB substrates, and 72.2% similarity between the MpeV homologs (Supplementary Figure 3). This led us to hypothesize that MpeV could be a lyase acting at C50, 61 on CpeB and perhaps also the lyase-isomerase acting on C50, 61 on MpeB in WH8020.

A comparison of *Synechococcus* CpeB sequences sorted by pigment type (PT) is shown in Supplementary Figure 4A [for review on PTs, see (Six et al., 2007; Humily et al., 2013; Grébert et al., 2022)]. All strains of *Synechococcus* belonging to PT2 (green light specialists with PEI and PEB only), PT3a (green light specialists with PEI, PEII, and a constitutively low PUB:PEB), about half of PT3dA (CA4-A) including WH8020, and the only representative of PT3eA (RCC307 that is genetically undistinguishable from typical PT3dA but exhibits

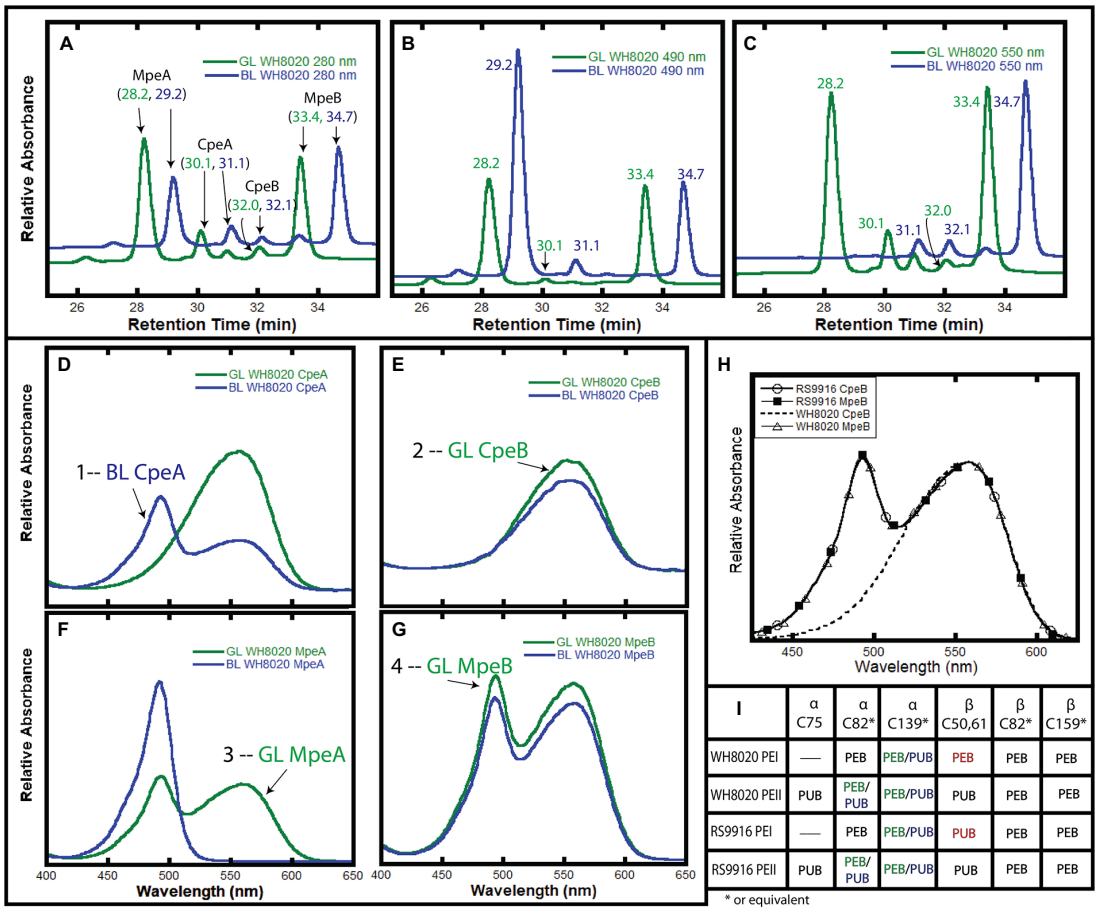

I	α C75	α C82*	α C139*	β C50,61	β C82*	β C159*
WH8020 PEI	—	PEB	PEB/PUB	PEB	PEB	PEB
WH8020 PEII	PUB	PEB/PUB	PEB/PUB	PUB	PEB	PEB
RS9916 PEI	—	PEB	PEB/PUB	PUB	PEB	PEB
RS9916 PEII	PUB	PEB/PUB	PEB/PUB	PUB	PEB	PEB

* or equivalent

FIGURE 3
HPLC analysis of WH8020 PBS. **(A–C).** Chromatograms depicting relative absorbance of total protein (280nm), presence of PUB (490nm), and presence of PEB (560nm). **(D–G)** Relative absorbance spectra of phycoerythrin I (PEI) and II (PEII) phycobiliprotein subunits separated by HPLC and denoted as follows: α-subunit of PEI (CpeA), β-subunit of PEI (CpeB), α-subunit of PEII (MpeA), β-subunit of PEII (MpeB). PBS extracted from WH8020 cells grown in an abundance of green light (GL, green lines) or blue light (BL, blue lines). **(H)** Comparison of the absorbance spectra of RS9916 and WH8020 β-subunits CpeB and MpeB. Note that WH8020 CpeB contains only PEB. **(I)** Table depicting the bilin content of these proteins at specific Cys residues (as inferred from Shukla et al., 2012 and Ong and Glazer, 1991). Sites that change for CA4 are shown as PEB (in green light) and PUB (in blue light) separated by a "/" The CpeB subunit differs at C50,61 between WH8020 and RS9916. Spectra numbered in **(D–G)** correspond with data in **Table** 1. These results are representative of two independent replicates.

only faint variations in the PUB:PEB ratio), all possess a H at position 141 in CpeB. In contrast, all strains that are either PT3c (typical BL specialists), PT3f (a rarer type of BL specialists), PT3dB (CA4-B), the other half of PT3dA including RS9916, and a natural mutant strain (BIOS-E4-1 that also display a BL specialist phenotype; Humily et al., 2013; Grébert et al., 2018) possess a L at position 141 in CpeB (Supplementary Figure 4A, blue highlights). By comparison for MpeB, all PT3a (or 3eA) strains exhibited a H whereas most other strains have a L, consistent with the fact that the former have a PEB and all others a PUB at C50, 61 (Supplementary Figure 4B). The only exception to this rule is PT3f strains which have a M at this position.

Recombinant protein analysis

For simplicity, all recombinant proteins from RS9916 are hereafter prefixed with an "RS" and all WH8020 proteins are hereafter prefixed with a "WH" while generic referral to protein(s) from both strains will remain unprefixed (e.g., CpeA vs. RSCpeA or WHCpeA). We sought to determine the activity of WHMpeV compared to that of RSMpeV using our heterologous *E. coli* expression system with various substrates. All protein co-expressions analyzing β-subunits as substrates were designed to also express α-subunits in an effort to increase solubility of β-subunits as previously shown (Anderson and Toole, 1998; Kronfel et al., 2019b; Carrigee et al., 2020b). Our earlier work with

TABLE 1 Mass spectrometry coverage of phycobilisome peptide fragments from WH8020. Trypsin digested samples of PEI α- (CpeA) and β-(CpeB) subunits and PEII α-(MpeA) and β-(MpeB) subunits showing their MS percent coverage, relative abundance (Rel Abund) and number (Num) of unique peptides found for each protein within each sample. Bold numbers for each sample correspond to numbered absorbance spectra in **Figure** 3.

1—CpeA sample			2—CpeB sample			3—MpeA sample			4—MpeB sample			Protein name
Num unique	% Cov	Rel Abund	Num Unique	% Cov	Rel Abund	Num Unique	% Cov	Rel Abund	Num Unique	% Cov	Rel Abund	
24	80.5	85.9%	17	66.5	4.4%	15	72	0.2%	8	55.5	0.1%	WH8020_CpeA
8	38.6	6.7%	9	46.7	54.9%	7	42.4	0.3%	10	36.4	2.7%	WH8020_CpeB
8	36.4	7.1%	6	36.4	3.7%	38	98.8	98.7%	11	78.2	0.5%	WH8020_MpeA
14	66.9	0.3%	11	51.7	37.0%	10	51.7	0.8%	28	96.6	96.7%	WH8020_MpeB

RS9916 showed that the enzymes RSCpeS and RSCpeZ were required to obtain enough chromophorylated (attaching PEB at C82 of CpeB and MpeB), soluble RSCpeB and RSMpeB substrate to allow RSMpeV to function (Carrigee et al., 2020b). Therefore, these genes from RS9916 were expressed concomitantly in trials testing RSMpeV and WHMpeV activity (Figure 4). Even though detectable amounts of α-subunits (CpeA) co-purified with their respective β-subunits (CpeB; Figures 4E–G), CpeA was expectedly not chromophorylated by the available lyases (see section LC–MS–MS analyses of recombinant co-expressions below). CpeB was present in all co-expressions as determined by total protein staining using Coomassie blue (Figure 4G). Control co-expressions to assess bilin addition and site specificity included CpeB/CpeA expressed without a lyase, or expressed in the presence of RSCpeZ, RSCpeS, and/or MpeV as outlined in Supplementary Table 3. Absorbance spectra from recombinant co-expressions of RSMpeV or WHMpeV enzymes with RSCpeB, WHCpeB, or WHMpeB demonstrate that WHMpeV acts as a PEB lyase-isomerase, doubly ligating PUB on RSCpeB (Figure 4A, co-expression 1, red line; absorbance peak 491.5 nm) and WHMpeB (Supplementary Figure 5; absorbance peak at 493 nm), but it does not isomerize PEB when attaching it to WHCpeB (Figures 4B,C, co-expression 4, black dashed line). The addition of a doubly-ligated PEB on WHCpeB subunit is detected as a prominent shoulder at 534.0 nm in addition to a peak at 556.5 nm from the C82 PEB ligated by RSCpeS (Figures 4B,C, co-expression 4, black dashed line). This is consistent with observations by Kronfel et al. for a paralogous E/F type lyase called CpeF which doubly ligates a PEB on CpeB at an equivalent position in the freshwater cyanobacterium *Fremyella diplosiphon* (Kronfel et al., 2019b). We conclude that WHMpeV is capable of isomerizing activity on both WHMpeB and RSCpeB but that the WHCpeB substrate prevents the isomerization activity of WHMpeV.

Analysis of WHMpeV enzymatic activity using structural modeling and site-directed mutagenesis

As mentioned above, WHCpeB contains H at position 141 whereas RSCpeB contains L at this position (Supplementary Figures 3, 4). Molecular modeling of the structure of WHCpeB suggested that H141 should be positioned close to the C50, 61 bilin position and at ~7.4 Å from C50 (Figure 5). When PEB is docked with its ring A close to C50 and ring D close to C61, aspartic acid (D)54 of WHCpeB is poised toward the bilin, potentially interacting with the pyrrole nitrogen atoms of rings B and C (Figure 5). The arginine (R)57 residue on WHMpeV points toward the propionate chain of the C ring of PEB whereas MpeV-D116/R89 line the binding pocket near D ring (Figure 5B). Linkage at the A ring of PEB to C50 is a critical step in chromophore attachment, isomerization and stability for RSCpeB (Carrigee et al., 2020b). A site-directed mutation was introduced into WHCpeB converting H141 to leucine (H141L; Figure 5; Supplementary Table 1) to test whether this residue affected isomerization activity by WHMpeV. Absorbance data from the co-expressions including RSCpeZ, RSCpeS, and WHMpeV as outlined in Supplementary Table 3 revealed that this single substitution provided sufficient change(s) within the binding pocket to allow isomerization to occur (Figures 4, 5). Indeed, when native WHCpeB is expressed in the presence of RSCpeZ, RSCpeS, and WHMpeV, we see evidence of a doubly-ligated PEB at the C50, 61 position (Figures 4B–D, co-expression 4, black dashed line, and Table 2). However, when we perform this same co-expression using pHTCpeB(H141L)A (Supplementary Table 2), we see a doubly-linked PUB at the C50, 61 position (Figures 4C,D, co-expression 6 purple line, co-expression 5 green line, and Table 2). These findings indicate that the microenvironment of the WHCpeB binding pocket surrounding C50 plays a major role in WHMpeV isomerization activity at C50, 61.

LC–MS–MS analyses of recombinant co-expressions

Table 2 shows peak areas obtained for extracted ion chromatograms $(M+4H)^{4+}$ ions of the tryptic peptide for CpeB containing residues 38–78. The peptide sequence is the same in both the RSCpeB and WHCpeB and is shown in Supplementary Tables 4–7. The negative control sample (WHCpeBA, no MpeV) shows no bilin attachment and interestingly, MS–MS data suggest C61 and C73 are linked by a disulfide bridge. Complete ligation of bilin to C50 and C61 was observed for the positive control sample (WHCpeB + WHMpeV). RSMpeV appears to modify WHCpeB and

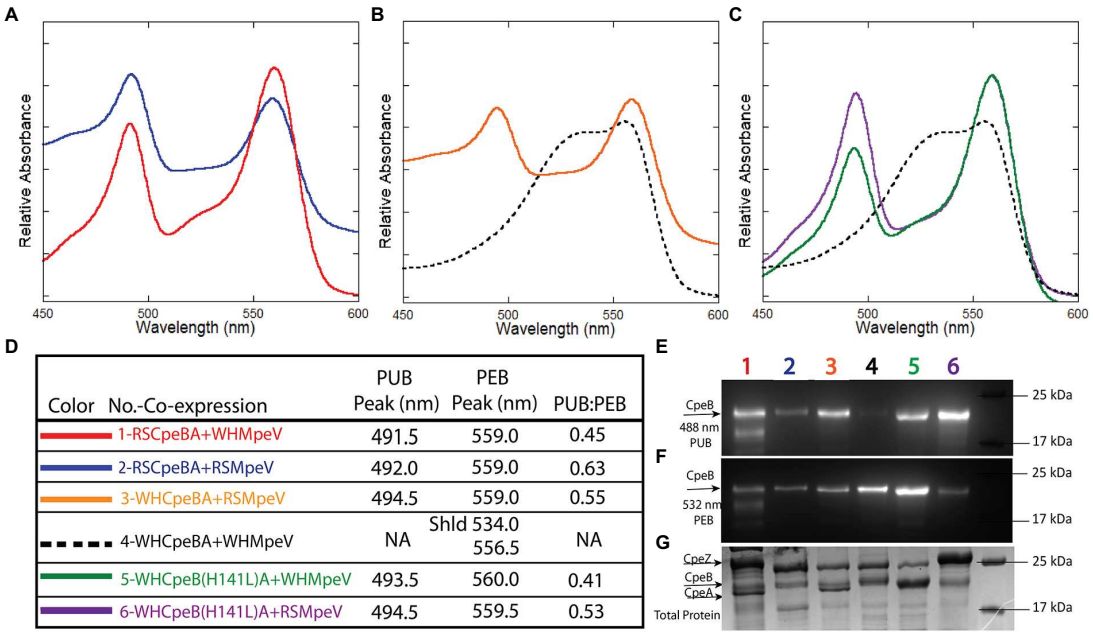

FIGURE 4
Absorbance spectra and SDS-PAGE for *Synechococcus* RS9916 and WH8020 CpeB co-expressions with MpeV. **(A–C)** Relative absorbance spectra depicting bilin addition to RSCpeB and WHCpeB when expressed in the presence of either WHMpeV or RSMpeV (as indicated in the legend in panel **D**). Purified protein substrates were resolved *via* SDS-PAGE and imaged with zinc-enhanced fluorescence at 460–490nm **(E)** which excites PUB and at 520–545nm **(F)** which excites PEB. Lanes are labeled with co-expression numbers and colors as listed in panel **D**. The same gel was then stained with Coomassie blue **(G)** to visualize proteins. All expressions contained RS9916 *cpeS*, *cpeZ*, and *ho1/pebS*. This study is representative of two independent replicates. NA means not applicable.

WHCpeB(H141L) at a slower rate than WHMpeV modifies WHCpeB as we observed unmodified, disulfide linked 38–78 peptide in the mixture. Intriguingly, the co-expressions where WHMpeV acted on RSCpeB or WHCpeB(H141L) showed evidence of bilins singly attached to the 38–78 peptide as well as normal double attachment and some unmodified substrate with no bilins attached at all. It is likely that the disulfide bond formed during purification and processing, as the cytoplasm of *E. coli* is generally a reducing environment (Gąciarz et al., 2017). However, its formation may indicate a lack of sufficient activity by MpeV or insufficient folding by CpeB to achieve the doubly ligated chromophore in some of these combinations (Table 2). Representative mass spectra supporting these observations comprise Supplementary Figures 5–7; Supplementary Tables 4–7, contain lists of tandem mass spectral fragment matches. In all samples containing RSCpeS, a bilin attached at C82 was observed, as previously described (Carrigee et al., 2020b). We did not observe any bilin modifications on CpeA in these co-expressions.

Modeling of MpeV with substrates suggests the role of His141

To explore the possible role of CpeB H141 in conferring the lyase activity of MpeV, we built a structure model of MpeV in complex with two substrates: CpeB and PEB, using manual docking aided by AlphaFold2 implemented in the ColabFold server (Jumper et al., 2021; Mirdita et al., 2022; Figure 5). In this model, the bilin pigment adopts an *anti, syn, anti*-configuration in which the ring A and ring D are in close proximity of their respective C anchors (i.e., C50 and C61 of CpeB) and the pyrrole nitrogen atoms of PEB rings B/C are in hydrogen-bonding distances with CpeB-D54 (Figure 5). Interestingly, we note that the side chain at the 141 position of CpeB would directly interact with the ring B propionate (Figure 5). For example, in WH8020 CpeB, H141 potentially forms a hydrogen bond with the ring B propionate while L141 of RS9916 CpeB cannot. This difference may explain the absence of the isomerase activity of MpeV on the CpeB substrate of WH8020 because the hydrogen bond between H141 and ring B propionate group may confer steric hinderance for the bilin transformation required by the PEB to PUB isomerization during a ligation reaction (Yang et al., 2007).

Discussion

Among the three clans of lyases, only some members of the E/F clan have been reported to have the capability to isomerize bilins during attachment (Everroad et al., 2006; Shukla et al.,

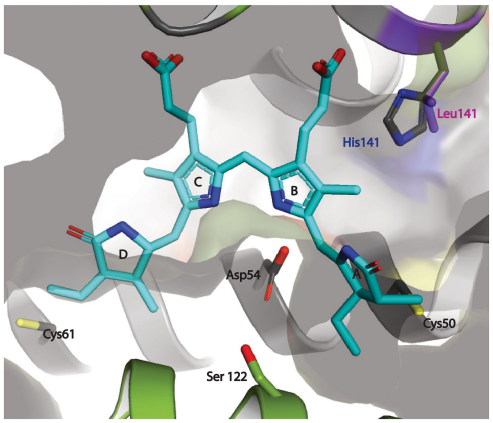

FIGURE 5
Docking of PEB at the putative binding cleft between the MpeV enzyme and WH8020 CpeB substrate. The PEB chromophore (cyan) is modeled in its final *anti, syn, anti*-conformation with ring A and ring D positioned next to their respective covalent anchors, (Cys50 and Cys61 of CpeB in yellow) bound between CpeB (gray ribbon), and MpeV (green ribbon). The pyrrole nitrogen atoms of rings B and C of PEB are stabilized *via* the side chain of the highly conserved Asp54 of CpeB. This model also places the side chain of His141 from WH8020 CpeB ~3.5Å away from the ring B propionate group of PEB. We propose that this hydrogen bond between His141 and PEB potentially plays an important role in preventing the isomerization of PEB to PUB during the ligation reaction. The positioning of the conserved Ser122 of MpeV suggests it may be part of a putative active site for lyase activity.

TABLE 2 LC–MS–MS results for MpeV co-expressions. Extracted ion chromatograms were made using m/z 1200.8254 for 38–78 peptides with a bilin attached; 1053.7513 was extracted for the 38–78 peptide lacking a bilin. Sample abbreviations are defined in **Supplementary Table 1**.

Sample	38–78 peptide cysteine state[a]	Retention time[d]	EIC area[b]
WHCpeBA + RSCpeZ/	2B	N/D	N/D
CpeS, no MpeV	1B	N/D	N/D
	0B	22.34	3.34E+08
WHCpeBA + RSCpeZ/	2B	20.94	2.35E+07
CpeS + WHMpeV	1B	N/D	N/D
	0B	N/D	N/D
WHCpeBA + RSCpeZ/	2B	21.19	7.73E+08
CpeS+ RSMpeV	1B	N/D	N/D
	0B	22.6	1.08E+08
RSCpeBA + RSCpeZ/	2B	25.71,26.44	4.57E+07
CpeS + WHMpeV[c]	1B	27.25	3.59E+07
	0B	27.23	2.32E+07
WHCpeB(H141L)A +	2B	21.14	4.42E+09
RSCpeZ/CpeS +	1B	23.2	6.79E+07
RSMpeV[c]	0B	22.54	8.07E+07
WHCpeB(H141L)A +	2B	25.83,26.48	2.32E+08
RSCpeZ/CpeS +	1B	27.27	2.41E+07
WHMpeV[c]	0B	21.97	7.82E+07

Representative tandem mass spectra for each form of the peptide can be found in Supplementary Figures 5–7.
[a]The 38–78 peptide has C50, C61 and C73. Peptides with doubly-linked bilin bridging C50 and C61 are labeled 2B. Peptides with a singly-linked bilin at C50 are labeled 1B; peptides with no bilin but a disulfide between C60 and C73 are labeled 0B.
[b]All EICs were made using an 8 ppm mass window and a 3 point boxcar smoothing routine. Areas were integrated with the ICIS algorithm of Thermo QualBrowser 4.3.73.11. Results are representative of two independent replicates.
[c]Sample was run separately from the others using a slightly modified gradient.
[d]N/D means not detected.

2012; Humily et al., 2013; Sanfilippo et al., 2016); moreover very few studies regarding the mechanism among substrate-bilin-enzyme interactions during the isomerization reaction have been explored (Zhao et al., 2017; Kumarapperuma et al., 2022). The ability of a member of the E/F-type lyase family (in the present case MpeV) to behave as both a lyase and an isomerase to two very similar substrates has never been reported before and suggests the CpeB (and likely MpeB) substrate environment plays a role in the isomerization process. *Synechococcus* sp. WH8020 is a CA4-A capable strain whose β-subunits share a high sequence similarity with RS9916 β-subunits (Supplementary Figures 1, 3A); however, the doubly ligated bilin at C50, 61 of WHCpeB is a PEB (Ong and Glazer, 1991) rather than a PUB, as on RSCpeB (Shukla et al., 2012), matching the chromophore pattern that is seen *in vivo* in WH8020 PBS (Figure 4). We observed that PEB isomerization to PUB is possible on recombinant WHCpeB at the doubly ligated C50, 61 position as demonstrated when it was co-expressed with RSMpeV in *E. coli* (Figure 5B, co-expression 4, orange line; Table 2), leading us to conclude that the interaction(s) among the lyase, bilin, and β-PE substrate are all important for the isomerization process. These data suggest the WHCpeB substrate may play a role in blocking the isomerization by the WHMpeV bilin lyase during ligation. In examining the alignment between the RSCpeB and WHCpeB sequences and our molecular model of the WHCpeB C50, 61 binding pocket, we identified H141 as potentially important for affecting isomerization by preventing WHMpeV (but not RSMpeV) from isomerizing PEB to PUB under native conditions (Figures 3, 5). By altering WHCpeB with the H141L point mutation, we showed that WHMpeV was able to isomerize PEB to PUB at C50, 61 on this WHCpeB (H141L) mutant during the attachment reaction. One explanation for this phenomenon is steric hinderance of H141 within the binding pocket of WHCpeB due to its bulky side chain and its proximity to C50 on WHCpeB, the site of PEB A-ring attachment and subsequent location of the bond isomerization (Figure 5). Alternatively, H141 may be involved in protonation/deprotonation or hydrogen-bonding dependent activity affecting the bilin conformation within the binding pocket (Kumarapperuma et al., 2022). Our modeling suggested that H141 in CpeB is close to the ring B propionate of PEB. This type of interaction has been seen in bacteriophytochromes previously (Yang et al., 2007). H141 may hydrogen bond to this group, blocking the

movement that has to occur during the isomerization reaction. L (or M) at this position would not be so constrained, allowing the isomerization to occur.

Historically, E/F-type lyases including MpeV exhibit broad variation in chromophore and PBP substrate specificity, while demonstrating high binding-site specificity (e.g., which C residue). Kumarapperuma and collaborators recently determined the crystal structure of the lyase-isomerase MpeQ, proposed a mechanism for the reaction, and compared it to the mechanism for the related PEB lyase MpeW (Kumarapperuma et al., 2022). For MpeQ, Tyrosine 318 was proposed to activate PEB, polarizing the C3 = C3^1 double bond. The side chain of V319 creates a steric conflict with the A-ring of PEB. This conflict is resolved by the PEB/PUB isomerization reaction and then ligation can happen, resulting in the MpeA-PUB product. In the PEB lyase MpeW, ligation happens directly after Tyrosine 318 activates that bond because there is no steric hindrance by the smaller residue of G319 on MpeW. In the case of WHMpeV, we hypothesize that the H141 residue in WHCpeB hydrogen bonds to the ring B propionate, constraining the movement that may occur during the isomerization reaction, favoring ligation before isomerization can take place (Figures 2, 5). RSMpeV is capable of isomerizing WHCpeB (Figure 4B, orange line), so there must be subtle differences within the MpeV enzymes that also control this isomerization reaction. In order to better understand this, we would need a structure of the substrate CpeB with the enzyme MpeV and the substrate PEB, a goal we are currently working toward.

This H at 141 is conserved in all green light specialists, i.e., *Synechococcus* strains that have either no PUB (PT2) or a constitutively low PUB/PEB ratio (PT3a; Supplementary Figure 3; Six et al., 2007; Grébert et al., 2022). Instead of MpeV, these strains possess the PEB lyase CpeF, the most ancient member of the CpeF-MpeV-MpeU E/F lyase family, which ligates doubly-linked PEB at C50/61 (Kronfel et al., 2019b; Carrigee et al., 2020b). In contrast, the blue light specialists, i.e., PT3c and PT3f which constitutively have a high PUB/PEB ratio, and the PT3 dB strains, i.e., chromatic acclimators possessing a CA4-B island (Humily et al., 2013; Grébert et al., 2021), all have a L at CpeB-141, and we posit that these strains must have a PUB at C50, 61 of CpeB. All of them lack CpeF and MpeV, so we hypothesize that the lyase-isomerase necessary to bind a PUB at both CpeB and MpeB C50, 61 in these strains is MpeU, a partially characterized member of this E/F lyase family (Mahmoud et al., 2017; Carrigee et al., 2020b; Grébert et al., 2022). Interestingly, while all PT3dA strains, i.e., chromatic acclimators possessing a CA4-A island, possess MpeV, only half of them, including RS9916, MITS9220, BL107, PROS-9-1 and the natural mutant strain BIOS-E4-1 which has become a BL specialist by selective loss of *fciA*, *fciB*, and *mpeY* genes (Humily et al., 2013; Grébert et al., 2018), have L at CpeB-141, so we hypothesize that they all have PUB at C50, 61 of CpeB, as previously demonstrated for RS9916 (Shukla et al., 2012). The other half of the PT3dA strains, including WH8020, CC9311, BIOS-U3-1 and RCC307, which shows only faint variations of its PUB/PEB ratio (Humily et al., 2013) all have H at this 141 position and consequently must have PEB at CpeB 50–61, like was first shown in WH8020 by Ong and Glazer (1991) and checked by us in the present study. The identity of the amino-acid at position 141 is seemingly also important for MpeB, with all GL specialists that have a PEB at C50, 61 having a H, and all BL specialists and chromatic acclimators that have a PUB at C50, 61 having a L. The only exception to this rule is PT3f strains which have a M at the MpeB 141 position. Even though the phycobiliprotein chromophorylation of strains representative of this pigment type has never been formally determined, it is most likely that they bind a PUB at C50, 61 on both CpeB and MpeB. So, altogether it appears that the chromophore bound at C50, 61 of CpeB and/or MpeB in any PE-containing marine *Synechococcus* can be reliably predicted from the amino acid present at position 141 of these PE β-subunits.

Combined with the structural and mechanistic analyses previously performed on MpeQ (Kumarapperuma et al., 2022), the present study demonstrated that there are residues within the substrate that influence the isomerization reaction of lyase/isomerases, a novel finding. A complete understanding of the mechanisms of these isomerase-capable lyases within the E/F clan is a main challenge for future studies.

Data availability statement

The original contributions presented in the study are publicly available. This data can be found at: MassIVE (https://massive.ucsd.edu/ProteoSAFe/static/massive.jsp), dataset ID number MSV000090019.

Author contributions

LC and WS conceived of the study through discussions with the coauthors. WS supervised the work and together with LC wrote the draft manuscript. LC, JF, and XL conducted the recombinant protein analyses. LD and FP performed the growth and analyses of *Synechococcus* sp. WH8020 cells for PBS purification and performed the bioinformatic analyses of CpeB and MpeB. JK and JT performed the tandem mass spectrometry and analyzed the data. IT and XY modeled the structure of MpeV with CpeB and PEB. All authors contributed to the article and approved the submitted version.

Funding

The Orbitrap Fusion Lumos was purchased with funds from the Precision Health Initiative of the Indiana University Bicentennial Grand Challenges Program. This research project has been supported by awards from the National Science Foundation to WS (MCB 2017171) and XY (MCB 2017274)

and from the Agence Nationale de la Recherche (ANR) program EFFICACY (ANR-19-CE02-0019) to FP.

Acknowledgments

We are grateful to Kes Lynn Joseph for helpful discussions and for assistance with culture prep and maintenance. We are also very grateful to David Kehoe for helpful discussions.

Conflict of interest

The authors declare that the research was conducted in the absence of any commercial or financial relationships that could be construed as a potential conflict of interest.

Publisher's note

Supplementary material

The Supplementary material for this article can be found online at: https://www.frontiersin.org/articles/10.3389/fmicb.2022.1011189/full#supplementary-material

References

Anderson, L. K., and Toole, C. M. (1998). A model for early events in the assembly pathway of cyanobacterial phycobilisomes. *Mol. Microbiol.* 30, 467–474. doi: 10.1046/j.1365-2958.1998.01081.x

Andrade, M. A., Petosa, C., O'Donoghue, S. I., Müller, C. W., and Bork, P. (2001). Comparison of ARM and HEAT protein repeats. *J. Mol. Biol.* 309, 1–18. doi: 10.1006/jmbi.2001.4624

Bengston, S. (1994). *Early Life On Earth. Nobel Symposium No. 84.* Columbia Univ. press: New York.

Betz, M. (1997). One century of protein crystallography: the phycobiliproteins. *Biol. Chem.* 378, 167–176.

Biswas, A., Boutaghou, M. N., Alvey, R. M., Kronfel, C. M., Cole, R. B., Bryant, D. A., et al. (2011). Characterization of the activities of the CpeY, CpeZ, and CpeS Bilin lyases in phycoerythrin biosynthesis in *Fremyella diplosiphon* strain UTEX 481. *J. Biol. Chem.* 286, 35509–35521. doi: 10.1074/jbc.M111.284281

Biswas, A., Vasquez, Y. M., Dragomani, T. M., Kronfel, M. L., Williams, S. R., Alvey, R. M., et al. (2010). Biosynthesis of cyanobacterial phycobiliproteins in *Escherichia coli:* chromophorylation efficiency and specificity of all Bilin lyases from *Synechococcus* sp. strain PCC 7002. *Appl. Environ. Microbiol.* 76, 2729–2739. doi: 10.1128/AEM.03100-09

Carrigee, L. (2020). Characterizing the function of lyases involved in the biosynthesis of phycoerythrin I and II from marine *Synechococcus* cyanobacteria: A PhD dissertation. Univeristy of New Orleans, New Orleans, LA.

Carrigee, L. A., Frick, J. P., Karty, J. A., Garczarek, L., Partensky, F., and Schluchter, W. M. (2020b). MpeV is a lyase isomerase that ligates a doubly linked phycourobilin to the β-subunit of phycoerythrin I and II in marine *Synechococcus*. *J. Biol. Chem.* 296, 1–13. doi: 10.1074/jbc.RA120.015289

Carrigee, L., Mahmoud, R. M., Sanfilippo, J. E., Frick, J. P., Strnat, J. A., Karty, J. A., et al. (2020a). CpeY is a phycoerythrobilin lyase for cysteine 82 of the phycoerythrin I α-subunit in marine *Synechococcus*. *BBA-Bioenergetics* 1861:148215. doi: 10.1016/j.bbabio.2020.148215

Emsley, P., and Cowtan, K. (2004). Coot: model-building tools for molecular graphics. *Acta Crystallogr. Sect. D* 60, 2126–2132. doi: 10.1107/S0907444904019158

Everroad, C., Six, C., Partensky, F., Thomas, J.-C., Holtzendorff, J., and Wood, A. M. (2006). Biochemical bases of type IV chromatic adaptation in marine *Synechococcus* spp. *J. Bacteriol.* 188, 3345–3356. doi: 10.1128/jb.188.9.3345-3356.2006

Everroad, R. C., and Wood, A. M. (2006). Comparative molecular evolution of newly discovered picocyanobacterial strains reveals a phylogenetically informative variable region of beta-phycoerythrin. *J. Phycol.* 42, 1300–1311. doi: 10.1111/j.1529-8817.2006.00282.x

Fairchild, C. D., and Glazer, A. N. (1994). Oligomeric structure, enzyme kinetics, and substrate specificity of the phycocyanin alpha subunit phycocyanobilin lyase. *J. Biol. Chem.* 269, 8686–8694. doi: 10.1016/S0021-9258(17)37022-9

Fairchild, C. D., Zhao, J., Zhou, J., Colson, S. E., Bryant, D. A., and Glazer, A. N. (1992). Phycocyanin α subunit phycocyanobilin lyase. Proc. Natl. Acad. Sci., USA, 89, 7017–7021. doi: 10.1073/pnas.89.15.7017.

Flombaum, P., Gallegos, J. L., Gordillo, R. A., Rincon, J., Zabala, L. L., Jiao, N., et al. (2013). Present and future global distributions of the marine cyanobacteria *Prochlorococcus* and *Synechococcus*. Proc. Natl. Acad. Sci. USA, 110, 9824–9829. doi: 10.1073/pnas.1307701110.

Gąciarz, A., Khatri, N. K., Velez-Suberbie, M. L., Saaranen, M. J., Uchida, Y., Keshavarz-Moore, E., et al. (2017). Efficient soluble expression of disulfde bonded proteins in the cytoplasm of E*scherichia coli* in fed-batch fermentations on chemically defined minimal media. *Microb. Cell Fact.* 16:108. doi: 10.1186/s12934-017-0721-x

Garczarek, L., Guyet, U., Doré, H., Farrant, G. K., Hoebeke, M., Brillet-Guéguen, L., et al. (2021). Cyanorak v2.1: a scalable information system dedicated to the visualization and expert curation of marine and brackish picocyanobacteria genomes. *Nucleic Acids Res.* 49, D667–D676. doi: 10.1093/nar/gkaa958

Gasper, R., Schwach, J., Hartmann, J., Holtkamp, A., Wiethaus, J., Reidel, N., et al. (2017). Distinct features of Cyanophage-encoded T-type Phycobiliprotein Lyase ΦCpeT: the role of auxillary metabolic genes. *J. Biol. Chem.* 292, 3089–3098. doi: 10.1074/jbc.M116.769703

Glazer, A. N. (1982). Phycobilisomes: structure and dynamics. *Annu. Rev. Microbiol.* 36, 173–198. doi: 10.1146/annurev.mi.36.100182.001133

Glazer, A. N. (1984). Phycobilisome: a macromolecular complex optimized for light energy transfer. *Biochim. Biophys. Acta.* 768, 29–51.

Glazer, A. N. (1988). Phycobilisomes. *Methods Enzymol.* 167, 304–312. doi: 10.1016/0076-6879(88)67035-2

Glazer, A. N. (1994). Phycobiliproteins - a family of valuable, widely used fluorophores. *J. Appl. Phycol.* 6, 105–112. doi: 10.1007/BF02186064

Grébert, T., Doré, H., Partensky, F., Farrant, G. K., Boss, E. S., Picheral, M., et al. (2018). Light color acclimation is a key process in the global ocean distribution of *Synechococus* cyanobacteria. *Proc. Natl. Acad. Sci. U. S. A.*, 115, E2010–E2019. doi: 10.1073/pnas.1717069115

Grébert, T., Garczarek, L., Daubin, V., Humily, F., Marie, D., Ratin, M., et al. (2022). Diversity and evolution of pigment types in marine *Synechococcus* cyanobacteria. *Genome Biol. Evol.* 14:evac035. doi: 10.1093/gbe/evac035

Grébert, T., Nguyen, A. A., Pokhrel, S., Joseph, K. L., Ratin, M., Dufour, L., et al. (2021). Molecular bases of an alternative dual-enzyme system for light color acclimation of marine *Synechococcus* cyanobacteria. *Proc. Natl. Acad. Sci. U. S. A.* 118. doi: 10.1073/pnas.2019715118

Humily, F., Partensky, F., Six, C., Farrant, G. K., Ratin, M., Marie, D., et al. (2013). A gene island with two possible confirurations is involved in chromatic acclimation in marine *Synechococcus*. *PLoS One* 8:e84459. doi: 10.1371/journal.pone.0084459

Hussain, H., and Chong, N. F.-M. (2016). Combined overlap extension PCR method for improved site directed mutagenesis. *Hindawi Publish. Corporat. BioMed. Res. Int.* 2016, 1–7. doi: 10.1155/2016/8041532

Jumper, J., Evans, R., Pritzel, A., Green, T., Figurnov, M., Ronneberger, O., et al. (2021). Highly accurate protein structure prediction with AlphaFold. *Nature* 596, 583–589. doi: 10.1038/s41586-021-03819-2

Kasting, J. F., and Siefert, J. L. (2003). Life and the evolution of Earth's atmosphere. *Science* 299:1015. doi: 10.1126/sceince.1071184

Kehoe, D. M. (2010). Chromatic adaptation and the evolution of light color sensing in cyanobacteria. *Proc. Natl. Acad. Sci. U. S. A.* 107, 9029–9030. doi: 10.1073/pnas.1004510107

Kelley, L. A., Mezulis, S., Yates, C. M., Wass, M. N., and Sternberg, M. J. (2015). The Phyre2 web portal for protein modeling prediction and analysis. *Nat. Protoc.* 10, 845–858. doi: 10.1038/nprot.2015.053

Kozo, M., Kazuaki, N., and Masato, N. (2002). Identification of a novel prokaryotic HEAT-repeats-containing protein which interacts with a cyanobacterial IscA homolog. *FEBS Lett.* 519, 123–127. doi: 10.1016/s0014-5793(02)02736-9

Kronfel, C. M., Biswas, A., Frick, J. P., Gutu, A., Blensdorf, T., Karty, J. A., et al. (2019a). The roles of the chaperone-like protein CpeZ and the phycoerythrobilin lyase CpeY in phycoerythrin biogenesis. *Biochim. Biophys. Acta-Bioenerg.* 1860, 249–561. doi: 10.1016/j.bbabio.2019.06.001

Kronfel, C. M., Hernandez, C. V., Frick, J. P., Hernandez, L. S., Gutu, A., Karty, J. A., et al. (2019b). CpeF is the Bilin lyase that ligates the doubly linked phycoerythrobilin on β-phycoerythrin in the cyanobacterium *Fremyella diplosiphon*. *J. Biol. Chem.* 294, 3987–3999. doi: 10.1074/jbc.RA118.007221

Kronfel, C. M., Kuzin, A. P., Forouhar, F., Biswas, A., Su, M., Lew, S., et al. (2013). Structural and biochemical characterization of the Bilin lyase CpcS from *Thermosynechococcus elongatus*. *Biochemistry* 52, 8663–8676. doi: 10.1021/bi401192z

Kumarapperuma, I., Joseph, K. L., Wang, C., Biju, L. M., Tom, I. P., Weaver, K. D., et al. (2022). Crystal structure and molecular mechanism of an E/F type Bilin lyase-isomerase. *Structure* 30, 564–574.e3. doi: 10.1016/j.str.2022.01.007

Mahmoud, R. M., Sanfilippo, J. E., Nguyen, A. A., Strnat, J. A., Partensky, F., Garczarek, L., et al. (2017). Adaptation to blue light in marine *Synechococcus* requires MpeU, an enzyme with similarity to phycoerythrobilin lyase isomerases. *Front. Microbiol.* 8. doi: 10.3389/fmicb.2017.00243

Marcotrigiano, J., Lomakin, I. B., Sonenberg, N., Pestova, T. V., Hellen, C. U., and Burley, S. K. (2001). A conserved HEAT domain within eIF4G directs assembly of the translation initiation machinery. *Mol. Cell* 7, 193–203. doi: 10.1016/S1097-2765(01)00167-8

Mirdita, M., Schütze, K., Moriwaki, Y., Heo, L., Ovchinnikov, S., and Steinegger, M. (2022). ColabFold: making protein folding accessible to all. *Nat. Methods* 19, 679–682. doi: 10.1038/s41592-022-01488-1

Nguyen, A. (2018). *Characterization of genes involved in the biosynthesis of Phycoerythrin I and II in cyanobacteria: A PhD dissertation*. New Orleans, LA: University of New Orleans.

Ong, L. J., and Glazer, A. N. (1991). Phycoerythrins of marine unicellular cyanobacteria. I. Bilin types and locations and energy transfer pathways in *Synechococcus* spp. phycoerythrins. *J. Biol. Chem.* 266, 9515–9527. doi: 10.1016/S0021-9258(18)92851-6

Overkamp, K. E., Gasper, R., Kock, K., Herrmann, C., Hofmann, E., and Frankenburg-Dinkel, N. (2014). Insights into the biosynthesis and assembly of Cryptophycean Phycobiliproteins. *J. Biol. Chem.* 289, 26691–26707. doi: 10.1074/jbc.M114.591131

Palenik, B. (2001). Chromatic adaptation in marine *Synechococcus* strains. *Appl. Environ. Microbiol.* 67, 991–994. doi: 10.1128/AEM.67.2.991-994.2001

Sanfilippo, J. E., Garczarek, L., Partensky, F., and Kehoe, D. M. (2019a). Chromatic acclimation in cyanobacteria: a diverse and widespread process for optimizing photosynthesis. *Annu. Rev. Microbiol.* 73, 407–433. doi: 10.1146/annurev-micro-020518-115738

Sanfilippo, J. E., Nguyen, A. A., Garczarek, L., Karty, J. A., Pokhrel, S., Strnat, J. A., et al. (2019b). Interplay between differentially expressed enzymes contributes to light color acclimation in marine *Synechococcus*. *Proc. Natl. Acad. Sci. U. S. A.*, 1–6. doi: 10.1073/pnas.1810491116

Sanfilippo, J. E., Nguyen, A. A., Karty, J. A., Shukla, A., Schluchter, W. M., Garczarek, L., et al. (2016). Self-regulating genomic island encoding tandem regulators confers chromatic acclimation to marine *Synechococcus*. *Proc. Natl. Acad. Sci. U. S. A.* 113, 6077–6082. doi: 10.1073/pnas.201600625

Saunée, N. A., Williams, S. R., Bryant, D. A., and Schluchter, W. M. (2008). Biogenesis of phycobiliproteins. II. CpcS-I and CpcU comprise the heterodimeric Bilin lyase that attaches phycocyanobilin to Cys-82 of beta -phycocyanin and Cys-81 of allophycocyanin subunits in *Synechococcus* sp. PCC 7002. *J. Biol. Chem.* 283, 7513–7522. doi: 10.1074/jbc.M708165200

Scheer, H., and Zhao, K. (2008). Biliprotein maturation: the chromophore attachment. *Mol. Microbiol.* 68, 263–276. doi: 10.1111/j.1365-2958.2008.06160.x

Schluchter, W. M., Shen, G., Alvey, R. M., Biswas, A., Saunee, N. A., Williams, S. R., et al. (2010). Phycobiliprotein biosynthesis in cyanobacteria: structure and function of enzymes involved in post-translational modification. *Adv. Exp. Med. Biol.* 675, 211–228. doi: 10.1007/978-1-4419-1528-3_12

Shen, G., Saunee, N. A., Williams, S. R., Gallo, E. F., Schluchter, W. M., and Bryant, D. A. (2006). Identification and characterization of a new class of Bilin lyase: the *cpcT* gene encodes a Bilin lyase responsible for attachment of phycocyanobilin to Cys-153 on the beta subunit of phycocyanin in *Synechococcus* sp. PCC 7002. *J. Biol. Chem.* 281, 17768–17778. doi: 10.1074/jbc.M602563200

Shen, G., Schluchter, W. M., and Bryant, D. A. (2008). Biogenesis of phycobiliproteins. I. *cpcS*-I and *cpcU* mutants of the cyanobacterium *Synechococcus* sp. PCC 7002 define a heterodimeric phycocaynobilin lyase specific for beta -phycocyanin and allophycocyanin subunits. *J. Biol. Chem.* 283, 7503–7512. doi: 10.1074/jbc.M708164200

Shukla, A., Biswas, A., Blot, N., Partensky, F., Karty, J. A., Hammad, L. A., et al. (2012). Phycoerythrin-specific biln lyase-isomerase controls blue-green chromatic acclimation in marine *Synechococcus*. *Proc. Natl. Acad. Sci. U. S. A.* 109, 20136–20141. doi: 10.1073/pnas.1211777109

Six, C., Thomas, J.-C., Garczarek, L., Ostrowski, M., Dufresne, A., Blot, N., et al. (2007). Diversity and evolution of phycobilisomes in marine *Synechococcus* spp.: a comparative genomics study. *Genome Biol.* 8:R259. doi: 10.1186/gb-2007-8-12-r259

Studier, F. W. (2005). Protein production by auto-induction in high density shaking cultures. *Protein Expr. Purif.* 41, 207–234. doi: 10.1016/j.pep.2005.01.016

Swanson, R. V., Zhou, J., Leary, J. A., Williams, T., de Lorimier, R., Bryant, D. A., et al. (1992). Characterization of phycocyanin produced by *cpcE* and *cpcF* mutants and identification of an intergenic suppressor of the defect in Bilin attachment. *J. Biol. Chem.* 267, 16146–16154. doi: 10.1016/S0021-9258(18)41979-5

Takano, H., and Gusella, J. (2002). The predominantly HEAT-like motif structure of huntingtin and its association and coincident nuclear entry with dorsal, an NF-kB/Rel/dorsal family transcription factor. *BMC Neurosci.* 3:15. doi: 10.1186/1471-2202-3-15

Wilbanks, S. M., and Glazer, A. N. (1993). Rod structure of a phycoerythrin II-containing phycobilisome I: organization and sequence of the gene cluster encoding the major phycobiliprotein rod components in the genome of marine *Synechococcus* sp. WH8020. *J. Biol. Chem.* 268, 1226–1235. doi: 10.1016/S0021-9258(18)54064-3

Yang, X., Stojković, E. A., Kuk, J., and Moffat, K. (2007). Crystal structure of the chromophore binding domain of an unusual bacteriophytochrome, RpBphP3, reveals residues that modulate photoconversion. *Proc. Natl. Acad. Sci. U. S. A.* 104, 12571–12576. doi: 10.1073/pnas.0701737104

Zhao, C., Hoppner, A., Xu, Q.-Z., Gartner, W., Scheer, H., Zhou, M., et al. (2017). Structures and enzymatic mechanisms of phycobiliprotein lyases CpcE/F and PecE/F. *Proc. Natl. Acad. Sci. U. S. A.* 114, 13170–13175. doi: 10.1073/pnas.1715495114

Zhao, K. H., Su, P., Li, J., Tu, J. M., Zhou, M., Bubenzer, C., et al. (2006). Chromophore attachment to phycobiliprotein beta-subunits: phycocyanobilin:cystein-beta84 phycobiliprotein lyase activity of CpeS-like protein from *anabaena* sp. PCC7120. *J. Biol. Chem.* 281, 8573–8581. doi: 10.1074/jbc.M513796200

Zhao, K.-H., Su, P., Tu, J.-M., Wang, X., Liu, H., Ploscher, M., et al. (2007). Phycobilin:cysteine-84 biliprotein lyase, a near-universal lyase for cysteine-84-binding sites in cyanobacterial phycobiliproteins. *Proc. Natl. Acad. Sci. U. S. A.* 104, 14300–14305. doi: 10.1073/pnas.0706209104

Zhou, W., Ding, W.-L., Zheng, X.-L., Dong, L.-L., Zhao, B., Zhou, M., et al. (2014). Structure and mechanism of the phycobiliprotein Lyase CpcT. *J. Biol. Chem.* 289, 26677–26689. doi: 10.1074/jbc.M114.586743

Zhou, J., Gasparich, G. E., Stirewalt, V. L., de Lorimier, R., and Bryant, D. A. (1992). The *cpcE* and *cpcF* genes of *Synechococcus* sp. PCC 7002: construction and phenotypic characterization of interposon mutants. *J. Biol. Chem.* 267, 16138–16145. doi: 10.1016/S0021-9258(18)41978-3

frontiers | Frontiers in Microbiology

ORIGINAL RESEARCH
published: 09 May 2022
doi: 10.3389/fmicb.2022.893413

Comparative Thermophysiology of Marine *Synechococcus* CRD1 Strains Isolated From Different Thermal Niches in Iron-Depleted Areas

*Mathilde Ferrieux[1], Louison Dufour[1], Hugo Doré[1†], Morgane Ratin[1], Audrey Guéneuguès[2], Léo Chasselin[2], Dominique Marie[1], Fabienne Rigaut-Jalabert[3], Florence Le Gall[1], Théo Sciandra[1], Garance Monier[1], Mark Hoebeke[4], Erwan Corre[4], Xiaomin Xia[5], Hongbin Liu[6], David J. Scanlan[7], Frédéric Partensky[1] and Laurence Garczarek[1,8]**

[1] Sorbonne Université, CNRS, UMR 7144 Adaptation and Diversity in the Marine Environment (AD2M), Station Biologique de Roscoff (SBR), Roscoff, France, [2] Sorbonne Université, CNRS, UMR 7621 Laboratoire d'Océanographie Microbienne (LOMIC), Observatoire Océanologique de Banyuls/mer, Banyuls, France, [3] Sorbonne Université, CNRS, Fédération de Recherche FR2424, Station Biologique de Roscoff, Roscoff, France, [4] CNRS, FR 2424, ABiMS Platform, Station Biologique de Roscoff (SBR), Roscoff, France, [5] Key Laboratory of Tropical Marine Bio-Resources and Ecology, South China Sea Institute of Oceanology, Chinese Academy of Sciences, Guangzhou, China, [6] Department of Ocean Science, The Hong Kong University of Science and Technology, Kowloon, Hong Kong SAR, China, [7] University of Warwick, School of Life Sciences, Coventry, United Kingdom, [8] CNRS Research Federation (FR2022) Tara Océans GO-SEE, Paris, France

OPEN ACCESS

Edited by:
Susana Agusti, King Abdullah University of Science and Technology, Saudi Arabia

Reviewed by:
Alexandra Coello-Camba, IMEDEA (CSIC-UIB), Spain
Cristiana Callieri, National Research Council (CNR), Italy

***Correspondence:**
Laurence Garczarek
laurence.garczarek@sb-roscoff.fr

†Present address:
Hugo Doré, Department of Ecology, Evolution and Marine Biology, University of California, Santa Barbara, Santa Barbara, CA, United States

Specialty section:
This article was submitted to Aquatic Microbiology, a section of the journal Frontiers in Microbiology

Received: *10 March 2022*
Accepted: *31 March 2022*
Published: *09 May 2022*

Citation:
Ferrieux M, Dufour L, Doré H, Ratin M, Guéneuguès A, Chasselin L, Marie D, Rigaut-Jalabert F, Le Gall F, Sciandra T, Monier G, Hoebeke M, Corre E, Xia X, Liu H, Scanlan DJ, Partensky F and Garczarek L (2022) Comparative Thermophysiology of Marine Synechococcus CRD1 Strains Isolated From Different Thermal Niches in Iron-Depleted Areas. Front. Microbiol. 13:893413. doi: 10.3389/fmicb.2022.893413

Marine *Synechococcus* cyanobacteria are ubiquitous in the ocean, a feature likely related to their extensive genetic diversity. Amongst the major lineages, clades I and IV preferentially thrive in temperate and cold, nutrient-rich waters, whilst clades II and III prefer warm, nitrogen or phosphorus-depleted waters. The existence of such cold (I/IV) and warm (II/III) thermotypes is corroborated by physiological characterization of representative strains. A fifth clade, CRD1, was recently shown to dominate the *Synechococcus* community in iron-depleted areas of the world ocean and to encompass three distinct ecologically significant taxonomic units (ESTUs CRD1A-C) occupying different thermal niches, suggesting that distinct thermotypes could also occur within this clade. Here, using comparative thermophysiology of strains representative of these three CRD1 ESTUs we show that the CRD1A strain MITS9220 is a warm thermotype, the CRD1B strain BIOS-U3-1 a cold temperate thermotype, and the CRD1C strain BIOS-E4-1 a warm temperate stenotherm. Curiously, the CRD1B thermotype lacks traits and/or genomic features typical of cold thermotypes. In contrast, we found specific physiological traits of the CRD1 strains compared to their clade I, II, III, and IV counterparts, including a lower growth rate and photosystem II maximal quantum yield at most temperatures and a higher turnover rate of the D1 protein. Together, our data suggests that the CRD1 clade prioritizes adaptation to low-iron conditions over temperature adaptation, even though the occurrence of several CRD1 thermotypes likely explains why the CRD1 clade as a whole occupies most iron-limited waters.

Keywords: marine picocyanobacteria, *Synechococcus*, CRD1, thermotype, temperature adaptation

INTRODUCTION

Marine picocyanobacteria contribute to the biogeochemical cycling of various elements, most notably carbon, contributing ∼25% of ocean net primary productivity, of which the *Synechococcus* genus alone is responsible for about 16% (Flombaum et al., 2013). The large geographic distribution of these organisms, extending from the equator to subpolar waters, is largely attributable to their extensive genetic and functional diversity (Zwirglmaier et al., 2008; Farrant et al., 2016; Doré et al., 2020). Amongst the nearly 20 clades within subcluster (SC) 5.1, the most abundant and diversified *Synechococcus* lineage in oceanic ecosystems (Dufresne et al., 2008; Scanlan et al., 2009; Ahlgren and Rocap, 2012), only four (clades I, II, III, and IV) were thought to largely dominate *in situ*. Clades I and IV mainly thrive in temperate and cold, nutrient-rich waters, while clades II and III reside in warm, oligotrophic or mesotrophic areas (Zwirglmaier et al., 2008; Mella-Flores et al., 2011), suggesting the existence of cold (I/IV) and warm (II/III) *Synechococcus* "thermotypes." This hypothesis was subsequently confirmed by work demonstrating that strains representative of these different clades exhibit distinct thermal *preferenda* (Mackey et al., 2013; Pittera et al., 2014; Breton et al., 2020; Six et al., 2021), a feature notably linked to differences in the thermostability of light-harvesting complexes (Pittera et al., 2017), lipid desaturase gene content (Pittera et al., 2018) and the ability of some strains to induce photoprotective light dissipation at colder temperatures using the orange carotenoid protein (OCP; Six et al., 2021). Field studies using global ocean datasets have allowed to refine the respective ecological niches of the different thermotypes, with clade I extending further north than clade IV (Paulsen et al., 2016; Doré et al., 2022) and clades II and III predominating in N- and P-depleted waters, respectively, but also to highlight the importance of a fifth clade within SC 5.1, the CRD1 clade (Farrant et al., 2016; Sohm et al., 2016; Kent et al., 2019). Initially thought to be limited to the Costa Rica dome area (Saito et al., 2005; Gutiérrez-Rodríguez et al., 2014), the latter clade was recently found to be a major component of *Synechococcus* communities in iron (Fe)-depleted areas (Farrant et al., 2016; Sohm et al., 2016; Ahlgren et al., 2020). Furthermore, analysis of the global distribution of these organisms using high-resolution marker genes has highlighted large within-clade microdiversity associated with niche differentiation in marine *Synechococcus* (Farrant et al., 2016; Larkin and Martiny, 2017; Xia et al., 2019), as also observed in *Prochlorococcus* (Kashtan et al., 2014; Larkin et al., 2016). Using the *petB* gene encoding cytochrome b_6, Farrant et al. (2016) showed that most major clades encompassed several Ecologically Significant Taxonomic Units (ESTUs), i.e., genetically related subgroups within clades occupying distinct oceanic niches. This is notably the case for ESTU IIB that occupies a cold thermal niche in sharp contrast with IIA, the dominant ESTU within clade II that occupies warm, mesotrophic, and oligotrophic Fe-replete waters. Similarly, three distinct ESTUs with distinct thermal niches were identified within the CRD1 clade and the co-occurring clade EnvB (a.k.a. CRD2; Ahlgren et al., 2020): (i) CRD1B/EnvBB are found in cold mixed waters in co-occurrence with ESTUs IA, IVA and IVC, (ii) CRD1C/EnvBC dominate in warm, high-nutrient low-chlorophyll (HNLC) regions such as the central Pacific Ocean, and (iii) CRD1A/EnvBA are present in both environments and thus span a much wider range of temperatures than CRD1B and C (Farrant et al., 2016). This suggests that these three CRD1 ESTUs could correspond to different thermotypes.

In order to test this hypothesis, we used strains representative of each of the three CRD1 ESTUs to determine the fundamental thermal niches of these organisms as compared to typical cold (clades I and IV) and warm (clades II and III) thermotypes. Furthermore, given the strong influence of temperature on optimal functioning of the photosynthetic apparatus in marine *Synechococcus* (Pittera et al., 2014, 2017; Guyet et al., 2020), we also examined the effect of temperature acclimation on the photophysiology of CRD1 ESTUs compared to their clade I and IV counterparts and show that CRD1 thermotypes actually differ more strongly in this respect to members of clades I–IV than from each other.

MATERIALS AND METHODS

Strains and Growth Conditions

The eight *Synechococcus* spp. strains used in this study were retrieved from the Roscoff Culture Collection (RCC[1]), including representative strains of the three known CRD1 ESTUs (CRD1A—C) and one or two of each of the four dominant clades in the field (clades I—IV) used as controls (**Table 1** and **Supplementary Figure 1**). Cells were grown in 50 mL flasks (Sarstedt, Germany) in PCR-S11 culture medium (Rippka et al., 2000) supplemented with 1 mM sodium nitrate. Cultures were acclimated for at least 2 weeks in temperature-controlled chambers across a range of temperatures dependent on the thermal tolerance of each strain and under a continuous light of 75 μmol photons m^{-2} s^{-1} (hereafter μE m^{-2} s^{-1}) provided by a white-blue-green LED system (Alpheus, France). For each experiment, cultures were grown in triplicate, inoculated at an initial cell density of $\sim 3 \times 10^6$ cells mL^{-1}, and samples were harvested daily to measure growth rate and fluorescence parameters as described below.

In order to compare the capacity of strains to repair the D1 subunit of photosystem II (PSII; see "Measurement of PSII Repair Rate" section), cultures grown in 250 ml flasks at 75 μE m^{-2} s^{-1} were acclimated at 18, 22, and 25°C, temperatures at which all strains were able to grow, were subjected to high light stress (375 μE m^{-2} s^{-1}). Exponentially growing cultures were sampled at T0 and after 15, 30, 60, and 90 min of stress, before shifting cultures back to the initial light conditions and then sampling again after 15, 30, 60 min, and 24 h of recovery (R). While D1 repair measurements were performed at all-time points, cell concentrations were measured by flow cytometry only at T0, T30 min, T90 min, R30 min, and R24 h and liposoluble pigment content was determined only at T0.

[1]https://roscoff-culture-collection.org/

TABLE 1 | Characteristics of the *Synechococcus* strains used in this study.

Strains name	MVIR-18-1	A15-62	M16.1	WH8102	BL107	BIOS-E4-1	BIOS-U3-1	MITS9220
RCC #[a]	2,385	2,374	791	539	515	2,534	2,533	2,571
Subcluster[b]	5.1	5.1	5.1	5.1	5.1	5.1	5.1	5.1
Clade[b]	I	II	II	III	IV	CRD1	CRD1	CRD1
ESTU[b]	IA	IIA	IIA	IIIA	IVA	CRD1C	CRD1B	CRD1A
Pigment type[c]	3aA	3dB	3a	3c	3dA	3cA	3dA	3dA
Ocean	Atlantic	Atlantic	Atlantic	Atlantic	Med. Sea	Pacific	Pacific	Pacific
Region	North Sea	Offshore Mauritania	Gulf of Mexico	Caribbean Sea	Balearic Sea	South East Pacific	Chile upwelling	Equatorial Pacific
Isolation latitude	61°00' N	17°37' N	27°70' N	22°48' N	41°72' N	31°52' S	34°00' S	0°00' N
Isolation longitude	1°59' E	20°57' W	91°30' W	65°36' W	3°33' E	91°25' W	73°22' W	140°00' W

[a]*Roscoff Culture Collection,* [b]*Farrant et al. (2016),* [c]*Humily et al. (2013).*

Flow Cytometry

Culture aliquots (200 μl) sampled for flow cytometry were fixed using 0.25% (v/v) glutaraldehyde (grade II, Sigma Aldrich, United States) and stored at −80°C until analysis (Marie et al., 1999). Cell concentrations were estimated using a Guava easyCyte flow cytometer (Luminex Corporation, United States) and maximum growth rates (μ_{max}) were calculated as the slope of the linear regression of ln (cell density) vs. time during the exponential growth phase. *Synechococcus* cells were identified based on their red (695 nm) and orange (583 nm) fluorescence, proxies for their chlorophyll *a* and phycoerythrin content, respectively. Fluorescence, forward scatter and side scatter values were normalized to that of standard 0.95 μm beads using Guavasoft software (Luminex Corporation, United States).

Fluorescence Measurements

The maximum PSII quantum yield (F_V/F_M) was estimated using a Pulse Amplitude Modulation fluorimeter (Phyto-PAM II, Walz, Germany) during the exponential growth phase after 10 min dark acclimation followed by addition of 100 μM of the PSII blocker 3-(3,4-dichlorophenyl)-1,1-dimethylurea (DCMU, Sigma-Aldrich, United States; Campbell et al., 1998).

The PSII quantum yield was calculated as:

$$F_V/F_M = (F_M - F_0)/F_M$$

where F_0 is basal fluorescence, F_M maximal fluorescence level and F_V variable fluorescence (Campbell et al., 1998; Six et al., 2007).

Fluorescence excitation (with emission set at 580 nm) and emission (with excitation set at 530 nm) spectra were generated using a LS-50B spectrofluorometer (Perkin-Elmer, United States) as described in Six et al. (2004). The fluorescence excitation ratio ($Exc_{495:550\ nm}$) was used as a proxy for the PUB:PEB ratio. Phycobilisome (PBS) rod length and the degree of coupling of the PBS to PSII reaction center chlorophylls was then assessed using fluorescence emission spectra by calculating the phycoerythrin (PE, F_{max} = 565–575 nm) to phycocyanin (PC, F_{max} = 645–655 nm) ratio as well as the PC to PBS terminal acceptor (TA; F_{max} = 680 nm) ratio, respectively (Pittera et al., 2017).

Pigment Analyses

Triplicate cultures were harvested during the exponential phase when F_V/F_M was maximum for each temperature condition. Cultures (50 mL) were subjected to centrifugation in the presence of 0.01% (v/v) pluronic acid (Sigma-Aldrich, Germany) at 4°C, 14,000 × g for 7 min, using an Eppendorf 5804R (Eppendorf, France). Pellets were resuspended and transferred to 1.5 ml Eppendorf tubes and centrifuged at 4°C, 17,000 × g for 2 min using an Eppendorf 5417R centrifuge (Eppendorf, France). Once the supernatant was removed samples were stored at −80°C until further analysis. Pigment content was subsequently assessed using calibrated high-performance liquid chromatography (HPLC 1100 Series System, Hewlett Packard, St Palo Alto, CA), as previously described (Six et al., 2005).

Measurement of the Photosystem II Repair Rate

Each culture acclimated to 75 μE m^{-2} s^{-1} and 18, 22 or 25°C was split into two new 50 mL flasks (Sarstedt Germany) with one used as a control and the other flask supplemented with lincomycin (0.5 mg mL^{-1} final concentration, Sigma-Aldrich, United States) in order to inhibit protein synthesis and thus D1 repair (Guyet et al., 2020). Both sub-cultures were then subjected to light stress by exposing cultures to 375 μE m^{-2} s^{-1} continuous light (at the same temperature), and F_V/F_M measured at different time points as described above. The PSII repair rate for each strain at each temperature was determined from the coefficient differences between the exponential curves fitted over the 90 min time course of F_V/F_M measurements for control and +lincomycin samples. This light stress experiment was replicated on four independent cultures.

Determination of the Realized Environmental Niches of Major *Synechococcus* Ecologically Significant Taxonomic Units

The realized niches of CRD1 and clades I-IV ESTUs were determined using *petB* reads extracted from metagenomic data from the *Tara* Oceans and *Tara* Polar circle expeditions, the Ocean Sampling Day (OSD; June 21st 2014) campaign, and *petB* metabarcodes from (i) various oceanographic cruises (CEFAS,

BOUM, Micropolar, RRS Discovery cruise 368 and several in the northwestern Pacific Ocean as detailed in Xia et al., 2017), (ii) two individual sampling sites in the Mediterranean Sea (Boussole, Point B) as well as (iii) a bi-monthly sampling at the long-term observatory site SOMLIT ("Service d'Observation en Milieu Littoral")-Astan located 2.8 miles off Roscoff between July 2009 and December 2011 (**Supplementary Table 1**).

petB metagenomic recruitment using the *Tara* and OSD datasets was performed as described previously (Farrant et al., 2016). *Synechococcus petB* sequences from both metagenomes and metabarcodes were used to define operational taxonomic units (OTUs) at 97% identity using Mothur v1.34.4 (Schloss et al., 2009) that were then taxonomically assigned using a *petB* reference database (Farrant et al., 2016). OTUs encompassing more than 3% of the total *Synechococcus* reads for a given sample were grouped into ESTUs and used to determine the whole temperature range occupied by each of the five major *Synechococcus* ESTUs.

Comparative Genomics

The Cyanorak *v2.1* information system (Garczarek et al., 2021)[2] was used to compare the phyletic pattern i.e., the presence/absence pattern of each cluster of likely orthologous genes (CLOG) in each strain, for CRD1 strains and their clades I-IV counterparts for a number of selected genes potentially involved in adaptation to low temperature based on previous literature (see section "Results").

RESULTS

The Fundamental Thermal Niches of CRD1 vs. Clades I–IV Strains

In order to determine the temperature optima and boundary limits of the different CRD1 strains and to compare them to those of typical cold and warm *Synechococcus* thermotypes, representative strains of each of the three CRD1 ESTUs and strains of clades I, II, III, and IV were grown over a range of temperatures from 6 to 36°C. The growth responses of all strains to temperature followed a typical asymmetric bell-shaped curve over the selected temperature range (**Figure 1**), with a progressive rise in growth rate (μ) until T_{opt} (the temperature associated with maximum μ: μ_{max}) was reached, and a sharp decline above T_{opt}. BIOS-U3-1 (CRD1-B) was able to grow between 12 and 29°C with a T_{opt} at 25°C ($\mu_{max} = 0.78 \pm 0.02\ d^{-1}$), a growth pattern most similar to that of the clade IV strain BL107, while the clade I strain MVIR-18-1 was able to grow at much lower temperatures, down to 8°C but could not grow above 25°C (**Figure 1A**). MITS9220 (CRD1-A) and BIOS-E4-1 (CRD1-C) displayed thermal growth characteristics more similar to the clade II (A15-62 and M16.1) and III (WH8102) strains, representatives of warm thermotypes (**Figure 1B**). While most strains in this category displayed a minimal growth temperature of 16°C, large variations between strains were observed at the highest thermal boundary limit (T_{max}). Maximum growth temperature was obtained for M16.1 (II; T_{max}: 34°C), then A15-62 (II) and WH8102 (III; both with T_{max} at 32°C), MITS9220 (CRD1-A; T_{max}: 31°C) and finally for BIOS-E4-1 (CRD1-C; T_{max}: 30°C). The latter strain also displayed the highest minimal growth temperature (T_{min}: 18°C) and thus possesses the narrowest temperature range for growth of all the strains studied (12°C vs. 15–18°C). It is also worth noting that CRD1 strains display a lower maximum growth rate and more generally lower growth rates at most temperatures than their clade I, II, III, and IV counterparts.

The Environmental Realized Niches of CRD1 vs. Clades I–IV Strains

We then compared the fundamental thermal niches of all studied strains, i.e., the whole temperature range over which they can grow in a laboratory setting in the absence of biotic interactions (e.g., competition or predation), with environmental realized niches (*sensu* Pearman et al., 2008) of the corresponding ESTUs. For this, we determined the distribution limits of each of these ESTUs along the *Tara* Oceans and *Tara* Polar circle transects, 203 samples from OSD2014 and additional oceanographic cruises and individual sampling sites, altogether encompassing 413 samples worldwide covering a wide range of temperature conditions (**Figure 1**, **Supplementary Figure 2**, and **Supplementary Table 1**). This made it possible to have much finer estimates of the limits of the thermal niches of the different ESTUs than in the study performed by Farrant et al. (2016), in particular for the cold adapted ESTUs, which were poorly represented in the initial *Tara* Oceans dataset (**Supplementary Figure 2**).

This analysis showed that the CRD1B ESTU displayed a reduced thermal tolerance range in the environment (14–24.5°C) compared to the BIOS-U3-1 strain in culture (12–29°C), while the typical cold thermotypes colonized larger thermal niches *in situ* than their representative strains (**Figure 1A**). Environmental realized niches indeed ranged from 2.5 to 24°C for ESTU IA (compared to 8–25°C for MVIR-18-1) and from 8.5 to 25°C for ESTU IVA (compared to 12–29°C for BL107). Interestingly, the median temperature of the CRD1B ESTU is 3°C higher than that observed for ESTUs IA and IVA.

As concerns warm thermotypes, CRD1C displayed a fairly narrow thermal tolerance range *in situ* (22–29.5°C), which, similar to the cold thermotype CRD1B, was even narrower than for its representative strain BIOS-E4-1 (18–30°C; **Figure 1B**). Comparatively, the CRD1A ESTU was detected across a wider temperature range (14–30.5°C) than the other two CRD1 ESTUs and also slightly larger than the corresponding strain in culture (MITS9220, 16–31°C). Still, the most extended temperature range was observed for ESTU IIA and IIIA (12–32°C) that reached significantly lower temperature limits than the corresponding clade II (16 to 32–34°C) and III (16–32°C) strains. Of note, although both IIA and IIIA ESTUs displayed a similar temperature range, the median temperature of ESTU IIA (25°C) was about 3°C higher than that of ESTU IIIA (22°C) and the maximum median temperature was surprisingly observed for the CRD1C ESTU (26.5°C). In this context, it

[2]http://www.sb-roscoff.fr/cyanorak/

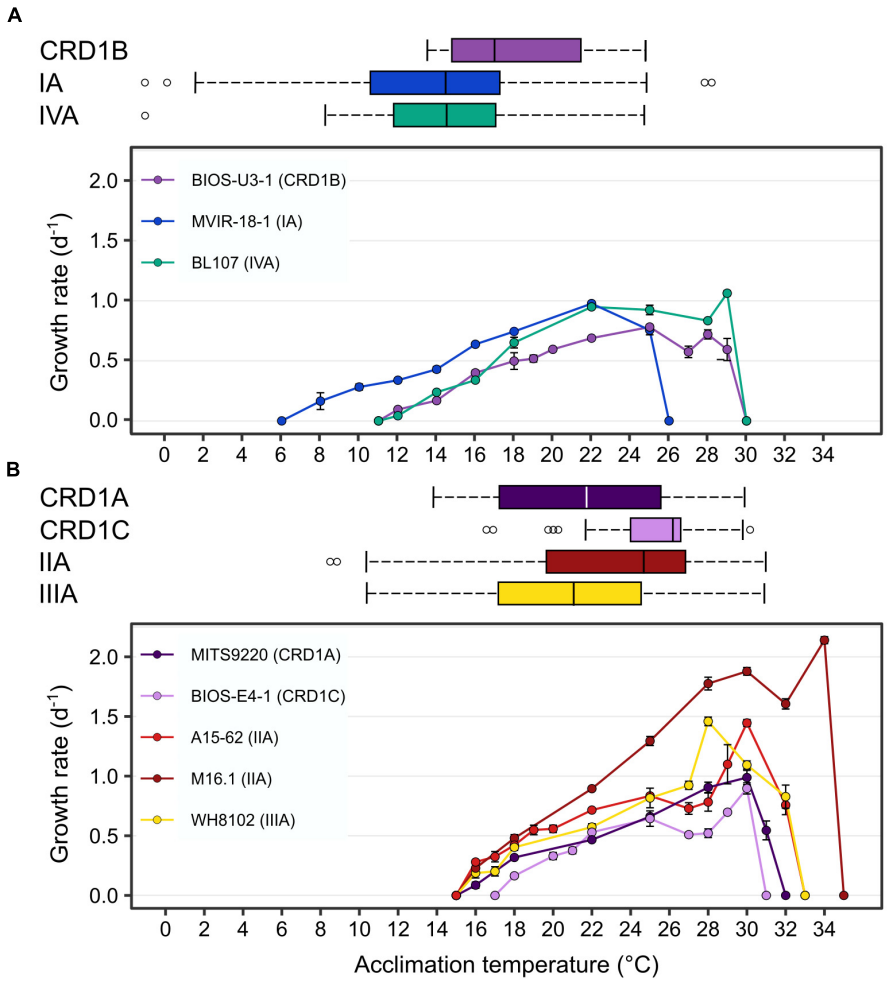

FIGURE 1 | Fundamental thermal niches of CRD1 vs. clade I, II, III, and IV strains and environmental realized niches of the corresponding ESTUs. **(A)** CRD1-B strain BIOS-U3-1 vs. cold thermotypes. **(B)** CRD1-A strain MITS9220 and the CRD1-C strain BIOS-E4-1 vs. warm thermotypes. The insert indicates the strain names and their corresponding ESTU (*sensu* Farrant et al., 2016) between brackets. Each data point is the average of at least 3 biological replicates. Environmental realized niches are indicated as horizontal boxplots for each ESTU above each graph with the whiskers corresponding to 1.5-fold the interquartile range and outliers being plotted as individual points.

is also worth mentioning that although clade II strains are clearly both warm thermotypes, M16.1 displays a significantly higher temperature limit for growth than A15-62 and more generally than all other strains. This suggests that ESTU IIA may encompass two distinct ESTUs, but such a high temperature niche (>32°C) where they could be discriminated is exceptional and not available in our dataset (**Supplementary Table 1**).

Comparative Genomics

In order to assess whether the cold, temperate thermotype BIOS-U3-1 (CRD1B) exhibits similar adaptation mechanisms to those previously described for the cold-adapted clades I and/or IV, we examined a number of clusters of likely orthologous genes (CLOGs) from all *Synechococcus* genomes belonging to clades I-IV and CRD1 present in the Cyanorak *v2.1* information system (Garczarek et al., 2021). First, we looked for the occurrence of two amino-acid substitutions in phycocyanin α- (RpcA) and β-subunits (RpcB), which were shown to differ between cold- (Gly in clades I and IV for RpcA43; Ser in RpcB42) and warm-thermotypes (Ala in clades II and III for RpcA43; Asp in RpcB42), these substitutions being potentially responsible for the differential thermotolerance of this phycobiliprotein between thermotypes (Pittera et al., 2017). In all three CRD1 strains, both sites displayed the warm-type residue (**Supplementary Figures 3A,B**), suggesting that in contrast to typical cold and warm thermotypes, the molecular flexibility of this phycobiliprotein does not differ between CRD1 thermotypes. We then looked at fatty acid desaturases that are essential for regulating membrane fluidity and thus the activity of integral membrane proteins, including photosynthetic complexes (Mikami and Murata, 2003; Pittera et al., 2018; Breton et al., 2020). All three CRD1 strains surprisingly possess in addition

to the core Δ9-desaturase gene *desC3*, a second Δ9-desaturase, *desC4* (**Supplementary Table 2**), previously thought to be specific to cold-adapted strains as well as the Δ12-desaturase *desA3* found in both cold-adapted clades I and IV as well as in clade III, a warm thermotype subjected to much stronger seasonal variability than its (sub) tropical clade II counterparts (Pittera et al., 2018). Furthermore, BIOS-U3-1 also possesses *desA2*, thought to be specific to warm environments, while this gene is in contrast absent from the other two CRD1 warm-adapted strains. Thus, CRD1 strains exhibit a different desaturase gene set and potentially display a larger capacity to regulate membrane fluidity than typical cold- or warm-adapted thermotypes. Finally, while all clades I, III and IV genomes possess the *ocp* operon, involved in the protection of PSII against photoinactivation through the dissipation of excess light energy (Kirilovsky, 2007) and which was recently shown in marine *Synechococcus* to play a key role at low temperature (Six et al., 2021), none of the three CRD1 genomes possess this operon.

Photosynthetic Activity and Pigment Content

PSII quantum yield (F_V/F_M), used as a proxy of photosynthetic activity, was measured for each strain over their whole temperature growth range. Most strains displayed a decrease in this parameter at both low and high boundary limits of their growth temperature range and this effect was particularly striking for BIOS-U3-1, reaching values down to 0.11 at 14°C and 0.32 at 28°C (**Figure 2A**). Besides MVIR-18-1 that exhibited a quite constant F_V/F_M over its whole temperature range, the decrease in F_V/F_M at high temperature was stronger for cold than warm thermotypes that are able to maintain a quite high F_V/F_M in the warmest growth conditions (**Figure 2B**). Finally, as for growth rate, CRD1 strains exhibited lower F_V/F_M at all temperatures than clade I to IV strains.

The $Exc_{495:550nm}$ fluorescence excitation ratio, used as a proxy for PUB:PEB ratio, was consistent with the pigment type of each strain (Humily et al., 2013; **Table 1** and **Supplementary Figure 4A**). This ratio remained pretty constant over the whole temperature range for all strains except for the chromatic acclimator BL107 (pigment type 3dA), for which a sharp increase was observed at its maximal growth temperature (28°C) to reach a value (1.35) intermediate between that typically observed in green light (or white light; 0.6–0.7) and blue light (1.6–1.7). This suggests that the chromatic acclimation process could be affected by growth temperature, at least in this strain. The phycobilisome (PBS) rod lengths and the degree of coupling of PBS to PSII reaction center chlorophylls, as estimated from PE:PC and PE:TA ratios, respectively, showed fairly limited variations over the temperature range, indicating that the phycobiliprotein composition of PBS is quite stable over the growth temperature range of each strain (**Supplementary Figures 4B,C**). One notable exception was a rise in both ratios for strain A15-62 at its minimal growth temperature, likely attributable to the partial decoupling of individual phycobiliproteins and of the whole PBS from PSII, a phenomenon typically observed under stressful conditions (Six et al., 2007; Guyet et al., 2020). It is also worth noting that MITS9220 and to some extent BIOS-E4-1, exhibited a significantly higher PE:PC ratio than the five other strains, potentially indicating a different phycobiliprotein composition and/or length of PBS rods.

In terms of liposoluble pigments, the β-carotene/chlorophyll *a* (β-car/Chl *a*) ratio tended to increase with temperature in BIOS-E4-1 and MITS9220, as observed for the other warm thermotypes, whilst this ratio was more stable in the cold thermotypes BIOS-U3-1 and BL107, and seemed to slightly increase in the lower part of the thermal range for the clade I strain MVIR-18-1 (**Figure 3**). For all strains, these ratios result from a concomitant increase with temperature of Chl *a* and β-car content per cell (**Supplementary Figure 5**), indicating an enhancement of the surface of thylakoids per cell at higher temperatures that was particularly marked for BIOS-E4-1 and A15-62, whilst this variation was fairly limited in the other two CRD1 strains. As these two pigments are present in different proportions in PSI and II (Umena et al., 2011; Xu and Wang, 2017), the higher β-car/Chl *a* ratio measured in clades I and IV strains also suggests that they may have a higher PSII:PSI ratio than all other strains, including BIOS-U3-1, and that this ratio might be more strongly affected by temperature in warm than cold thermotypes.

As concerns the zeaxanthin/chlorophyll *a* (Zea/Chl *a*) ratio, although an increase in this ratio was measured at low temperature for all strains, the amplitude was globally larger for cold than for warm thermotypes, with BIOS-U3-1 behaving very similarly to the clade IV strain BL107 that exhibits the largest variation in this ratio (**Figure 3**). Changes in this ratio likely originate partially from the decrease in Chl *a* content in response to cold, a strategy typically used by cells to regulate light utilization under slow growth conditions (Inoue et al., 2001). However, several strains also displayed an increase in their Zea content per cell at low temperature, a response particularly striking in BIOS-U3-1 and A15-62, but that also seems to occur in M16.1 and in the two other CRD1 strains BIOS-E4-1 and MITS9220 (**Supplementary Figure 5**). Thus, although Zea has been hypothesized to be involved in the photoprotection of cold-adapted strains by dissipating excess light energy under low temperature conditions (Kana et al., 1988; Breton et al., 2020), this process seems to be present in both cold and warm-adapted CRD1 strains and in most warm thermotypes as well. In this context, it is also worth noting that the two clade II strains, A15-62 and M16.1, displayed fairly distinct temperature-induced variations in their Zea:Chl *a* ratios and individual pigment contents, possibly linked to their different isolation temperatures (see section "Discussion" below).

Photosystem II Repair Capacity

The ability of the different strains to repair PSII in response to light stress (375 $\mu E\ m^{-2}\ s^{-1}$) was determined in cultures acclimated to 18, 22, and 25°C by measuring changes in F_V:F_M over time after adding the protein synthesis inhibitor lincomycin, or not (**Supplementary Figure 6**). While a decrease in F_V:F_M ratio during the 90 min light stress period was observed in both cultures supplemented with lincomycin and controls, this ratio

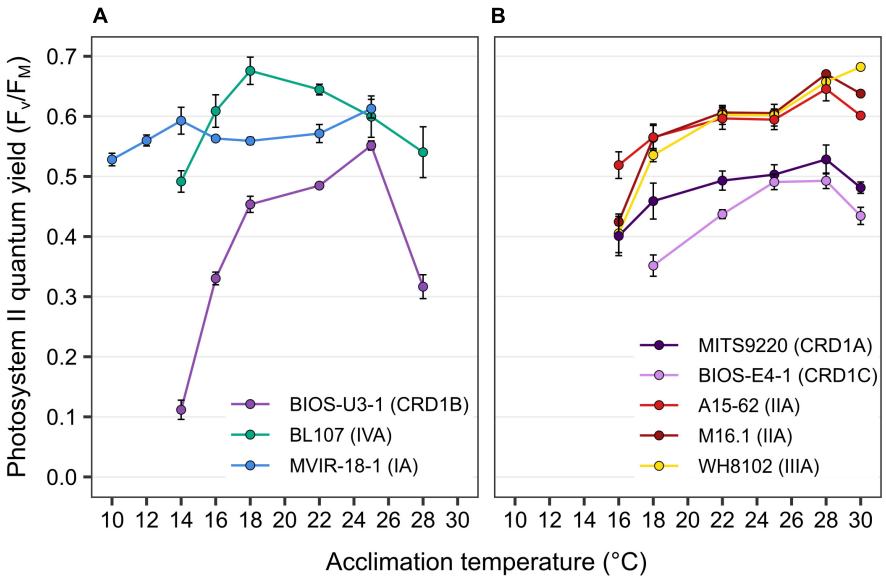

FIGURE 2 | Variation with growth temperature of photosystem II quantum yield (F_V/F_M) for CRD1 vs. clade I, II, III, and IV strains. **(A)** CRD1-B strain BIOS-U3-1 vs. cold thermotypes. **(B)** CRD1-A strain MITS9220 and the CRD1-C strain BIOS-E4-1 vs. warm thermotypes. The insert indicates the strain names and their corresponding ESTU (*sensu* Farrant et al., 2016) between brackets.

only re-increased back up to initial F_V:F_M values, after shifting cultures back to standard light conditions (75 μE m^{-2} s^{-1}), in the control group in most strains and temperature conditions. Thus, all studied strains were able to recover from this light stress, as long as the D1 repair cycle was not inactivated by inhibition of protein synthesis. Yet, a fast decrease in F_V:F_M was observed for all three CRD1 cultures supplemented with lincomycin, while the +/− lincomycin curves overlapped during the first 15–30 min of light stress in most other strains and conditions. This suggests that the initial decrease in F_V:F_M in clades I–IV strains was not due to D1 damage but rather to dissipation of light energy as heat through non-photochemical quenching (Campbell et al., 1998), whilst the damage and hence repair of D1 proteins only occurred later on.

The PSII repair rate (R_{PSII}), as calculated from the time course of F_V:F_M with and without lincomycin, increased with temperature in most strains, except for BIOS-U3-1 that displayed its highest rate at 22°C (**Figure 4**). Strikingly, all three CRD1 strains displayed significantly higher R_{PSII} than clade I-IV strains at all three tested temperatures, a difference ranging from 3- to nearly 40-fold at the lowest common temperature (18°C). Furthermore, CRD1 strains displayed fairly limited variation in R_{PSII} with temperature (ranging from 1.33 to 1.87-fold) compared to the other strains, the strongest increase in R_{PSII} being observed for the clade I strain MVIR-18-1 (21.5-fold) and the clade III strain WH8102 (5.5-fold). This indicates that CRD1 strains exhibit a constitutively high level of PSII repair compared to the other strains whatever the growth temperature and only trigger a moderate increase in R_{PSII} in response to temperature variations.

DISCUSSION

Temperature constitutes one the strongest driving factors that have shaped genetic diversification and niche partitioning in marine cyanobacteria (Scanlan et al., 2009; Flombaum et al., 2013; Biller et al., 2015) and phytoplankton at large (Sunagawa et al., 2015; Delmont et al., 2020). While temperature has caused one major diversification event in *Prochlorococcus*, resulting in the divergence of the cold-adapted HLI from the warm-adapted HLII clades (Johnson et al., 2006; Kettler et al., 2007), several independent temperature-related diversification events also occurred in the *Synechococcus* SC 5.1 radiation, leading to the emergence of clades I and IV (Dufresne et al., 2008; Zwirglmaier et al., 2008). Here, determination of the temperature optimum and boundary limits (i.e., the fundamental niche) of strains representative of the three CRD1 ESTUs identified in the field (Farrant et al., 2016) showed that different thermotypes can also be delineated within the CRD1 clade, which dominates the *Synechococcus* populations in low-Fe areas of the world Ocean. Comparison with representative strains of the cold-adapted *Synechococcus* ecotypes (clades I and IV) on the one hand, and warm-adapted ecotypes (clades II and III) on the other, made it possible to classify (i) the CRD1A strain MITS9220, isolated from the equatorial Pacific Ocean, as a warm thermotype, (ii) the CRD1B strain BIOS-U3-1, isolated from the Chilean upwelling, as a cold temperate thermotype, and finally (iii) the CRD1C strain BIOS-E4-1, isolated from the edge of the South Pacific gyre, a stable, warm, Fe-depleted oceanic region (Claustre et al., 2008), as a warm temperate stenotherm.

As expected from theory (Pearman et al., 2008), the realized environmental thermal niches of CRD1 ESTUs were narrower

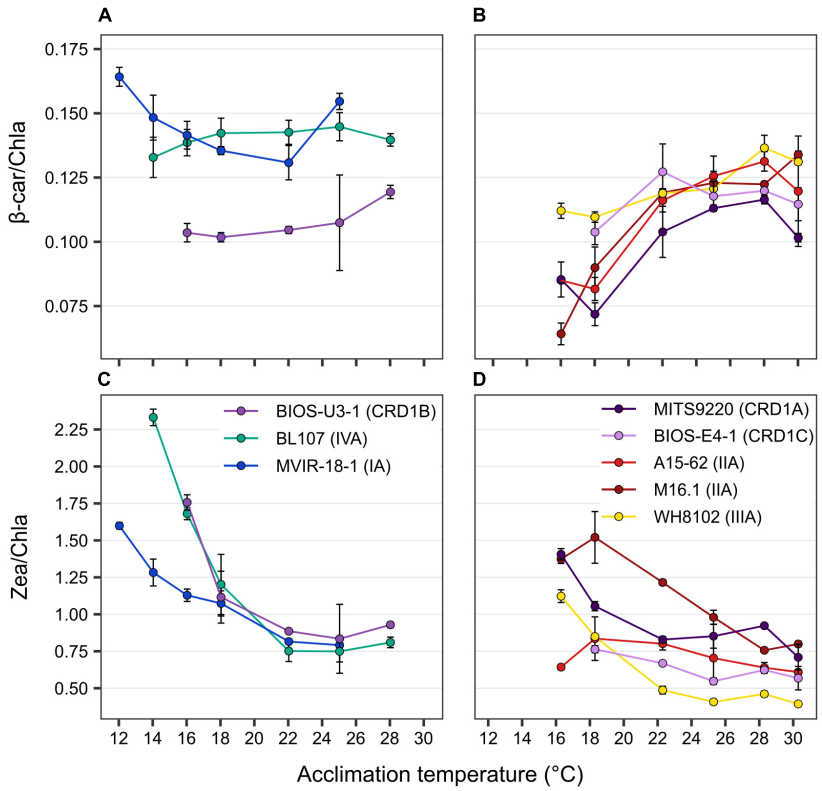

FIGURE 3 | Variation with growth temperature of cellular mass pigment ratios of CRD1 vs. clade I, II, III, and IV strains. **(A,B)** β-carotene (β-car) to chlorophyll *a* (Chla) ratio. **(C,D)** Zeaxanthin (Zea) to Chla ratio with **(A,C)** CRD1-B strain BIOS-U3-1 vs. cold thermotypes and **(B,D)** CRD1-A strain MITS9220 and the CRD1-C strain BIOS-E4-1 vs. warm thermotypes. Inserts indicate strain names and their corresponding ESTUs (*sensu* Farrant et al., 2016) between brackets.

than their fundamental niches (or similar for MITS9220). In contrast, for ESTUs IA to IVA, the realized environmental niche was significantly more extended toward the low thermal limit than the fundamental niches of their representative strains, this expansion being particularly marked for ESTU IA (**Figure 1**). This could be due to passive transport of *Synechococcus* populations by currents into water masses colder than their temperature limits for growth. Alternatively, these ESTUs may exhibit a greater microdiversity than previously assessed (Farrant et al., 2016) and could be subdivided into distinct ESTUs occupying slightly different thermal niches from the current ones, although representative strains to test this hypothesis remain to be isolated. In agreement with the latter hypothesis, Paulsen et al. (2016) measured a positive growth rate of *Synechococcus* natural populations dominated by clade I in waters as cold as 2°C in the vicinity of the Svalbard island. Thus, CRD1 ESTUs appear to be strongly outcompeted by their ESTU IA to IVA counterparts at their lower temperature limits. Consistent with this, comparison of their gene content showed that CRD1 ESTUs, including the cold thermotype CRD1B, lack the main adaptation mechanisms reported so far for typical cold thermotypes. Indeed, all CRD1 strains examined in this study (i) exhibit warm-type substitutions in their α and β-phycocyanin subunits, influencing the thermotolerance of this phycobiliprotein (Pittera et al., 2017; **Supplementary Figures 3A,B**); (ii) possess a different set of desaturase genes, involved in regulation of membrane fluidity (Pittera et al., 2018), than typical warm and cold thermotypes (**Supplementary Table 2**) and (iii) lack the OCP system, involved in the protection of PSII against photoinactivation, which seemingly plays a key role at low temperature (Kirilovsky, 2007; Six et al., 2021). Still, we cannot exclude that CRD1 strains could use alternative strategies to cope with temperature variations and notably to deal with the generation of reactive oxygen species, known to be generated by a variety of factors including low and high temperature (Nishiyama et al., 2006; Latifi et al., 2009). For instance, all CRD1 strains possess the *srxA* gene encoding sulfiredoxin catalyzing the reduction of 2-Cys peroxiredoxin involved in H_2O_2 detoxification (Findlay et al., 2005; Guyet et al., 2020) as well as *isiA* that, besides its role in increasing the light-harvesting efficiency of PSI under conditions of Fe-limitation, was also shown to provide photoprotection to PSII by dissipating excess light energy under oxidative stress conditions (Yeremenko et al., 2004; Ihalainen et al., 2005; **Supplementary Table 2**).

The ability of cyanobacteria to grow over a large temperature range largely relies on their capacity to optimize the functioning of their photosynthetic apparatus, notably at low temperature that induces a general slowing down of cell metabolism (Murata et al., 2007; Pittera et al., 2014, 2017). For this reason, we

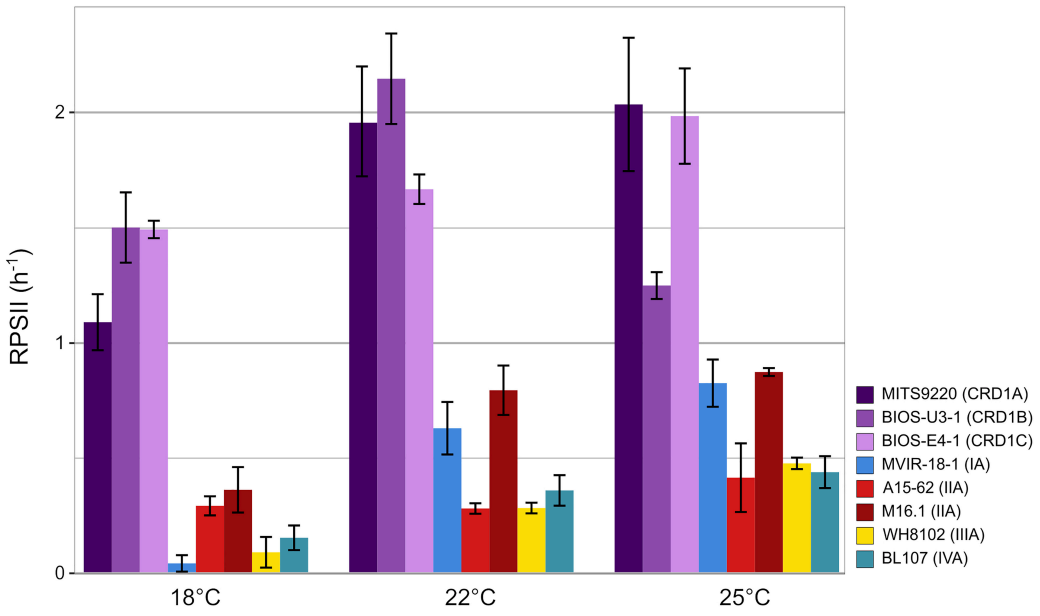

FIGURE 4 | Variation with growth temperature of cumulative photosystem II repair rate (RPSII) of CRD1 vs. clade I, II, III, and IV strains. The insert indicates the strain names and their corresponding ESTU (*sensu* Farrant et al., 2016) between brackets.

also compared the photophysiology of CRD1 and clades I-IV strains at three growth temperatures common to all strains. These analyses showed that all three CRD1 strains exhibit a lower growth rate at most temperatures than clade I to IV strains (**Figure 1**), possibly explaining why they are easily outcompeted by other taxa when Fe is no longer limiting, as observed for instance around the Marquesas Islands (Caputi et al., 2019). Moreover, CRD1 strains also display a lower PSII maximum quantum yield (**Figure 2**), suggesting that PSII is partially photoinactivated, that is their D1 repair cycle does not fully compensate damage to this protein, even under optimal growth temperatures. Consistent with this, the very high turnover rate of the D1 protein measured in all CRD1 strains indicates that their PSII is much more sensitive to light stress than other strains and can only trigger a moderate increase in R_{PSII} in response to both light and temperature variations, possibly indicating that they are adapted to live deeper in the water column than clades I to IV. This sensitivity could be partially linked to the abovementioned absence of the OCP, potentially reducing their ability to dissipate excess light energy, although it must be noted that the clade II strain A15-62 also lacks the OCP system. Interestingly in this context, all cold thermotypes including the CRD1B strain BIOS-U3-1, possess more copies of the D1:2 isoform (3–6 copies, average: 3.9 ± 1.1) than warm thermotypes (2–3 copies, average: 2.2 ± 0.4), this isoform providing a lower quantum yield but higher PSII resistance to photoinhibition than D1:1 (**Supplementary Table 2**; Clarke et al., 1993a,b; Campbell et al., 1995; Garczarek et al., 2008). Moreover, A15-62 is one of the only *Synechococcus* strains to possess two complete copies of the D1:1 isoform, a duplication which could partly explain why, despite the absence of OCP, this atypical clade II strain is able to maintain a high PSII quantum yield over its whole growth temperature range with fairly low D1 repair rates. Interestingly, CRD1 strains also possess a paralog of *psbN*, which was found to be required for the assembly of the PSII reaction center in *Nicotiana tabacum* and would play an important role in the D1 repair cycle (Torabi et al., 2014).

Taken together, both comparative genomics and photophysiological analyses highlighted a number of specificities of CRD1 strains compared to their clade I-IV counterparts, rather than them possessing traits distinctive of cold or warm thermotypes. In this context, it is worth noting that although strains representative of ESTUs IVA and CRD1B exhibit a similar fundamental thermal niche in culture, the higher median temperature of CRD1B in the field indicates that it preferentially thrives in temperate waters (about 18°C, **Figure 1**), where energetically costly temperature adaptation mechanisms might not be essential. This suggests that for members of the CRD1 clade, adaptation to low-Fe conditions likely prevails over adaptation to temperature variations, and/or that adaptation mechanisms to temperature variations might be more complex and diversified than previously thought. Still, in terms of a realized environmental thermal niche, the occurrence of several CRD1 thermotypes likely explains why the CRD1 clade as a whole occupies most Fe-limited areas, a vast ecosystem constituting about 30% of the world Ocean (Moore et al., 2013; Bristow et al., 2017). A notable exception is the Southern Ocean, for which from the little available data shows that *Synechococcus* is scarce south of the polar front (Wilkins et al., 2013; Farrant et al., 2016), consistent with the fairly high low-temperature limit (14°C) of the CRD1B environmental realized niche (**Figure 1**), while low-Fe availability likely limits the growth

of clades I and IV in this area. In contrast, CRD1 growth does not currently appear to be limited by warm temperatures since most oceanic waters display a temperature below 30°C (**Supplementary Figure 2B** and **Supplementary Table 1**). However, one cannot exclude that with global change, some areas of the world Ocean could become warmer than the highest limits determined here for representative strains of CRD1A and C, i.e., 31 and 30°C, respectively. In this context, it is worth mentioning that in the dataset used for this study, several coastal stations, sampled during the OSD campaign reached 31.5°C (**Supplementary Table 1**). Thus, although biogeochemistry global models predict that *Synechococcus* could be one of the winners of the phytoplankton community in a future world Ocean (Flombaum et al., 2013; Schmidt et al., 2020; Visintini et al., 2021), it might well not be able to survive in the warmest low-Fe areas, an ecological niche that is currently expanding (Polovina et al., 2008). Although a few studies have started to analyze the genomic bases of adaptation of *Synechococcus* cells to Fe-limitation in the field (Ahlgren et al., 2020; Garcia et al., 2020), further comparative genomic and physiological studies are still needed to decipher the specific capacity of CRD1 clade members to deal with Fe-limitation which should help predict the future distribution and dynamics of *Synechococcus* taxa in the world Ocean.

DATA AVAILABILITY STATEMENT

The datasets presented in the National Center for Biotechnology Information (NCBI) repository (https://www.ncbi.nlm.nih.gov; PRJNA811120).

AUTHOR CONTRIBUTIONS

MF, HD, and LG designed the experiments. MF, LD, HD, MR, AG, FR-J, TS, LC, and GM collected the samples and performed the physiological measurements. MF and DM ran the flow cytometry analyses. FL isolated several CRD1 strains used in this study. HD, XX, DS, HL, and LG performed sequencing and bioinformatics analyses of metabarcodes. MH, EC, FP, and LG developed and refined the Cyanorak *v2.1* database. MF, HD, FP, and LG made the figures. MF, LD, HD, FP, and LG interpreted results. All authors contributed to the preparation of the manuscript, read, and approved the final manuscript.

FUNDING

This work was supported by the French "Agence Nationale de la Recherche" Programs CINNAMON (ANR-17-CE02-0014-01) and EFFICACY (ANR-19-CE02-0019) as well as the European program Assemble Plus (H2020-INFRAIA-1-2016-2017; grant no. 730984).

ACKNOWLEDGMENTS

We would like to thank Thierry Cariou for providing physico-chemical parameters from the SOMLIT-Astan station and Gwenn Tanguy (Biogenouest genomics core facility) and Monica Moniz for their sequencing of *petB* metabarcodes. We are also most grateful to Nathalie Simon for coordinating the phytoplankton time-series at the SOMLIT-Astan station, Christophe Six for technical hints on PAM fluorimetry and HPLC analyses as well as Priscillia Gourvil and Martin Gachenot from the Roscoff Culture Collection (http://roscoff-culture-collection.org/) and Florian Humily for isolating and/or maintaining the *Synechococcus* strains used in this study. We also thank the support and commitment of the *Tara* Oceans coordinators and consortium, Agnès b. and E. Bourgois, the Veolia Environment Foundation, Région Bretagne, Lorient Agglomeration, World Courier, Illumina, the EDF Foundation, FRB, the Prince Albert II de Monaco Foundation, the *Tara* schooner and its captains and crew.

SUPPLEMENTARY MATERIAL

The Supplementary Material for this article can be found online at: https://www.frontiersin.org/articles/10.3389/fmicb.2022.893413/full#supplementary-material

REFERENCES

Ahlgren, N. A., and Rocap, G. (2012). Diversity and distribution of marine *Synechococcus*: multiple gene phylogenies for consensus classification and development of qPCR assays for sensitive measurement of clades in the ocean. *Front. Microbiol.* 3:213. doi: 10.3389/fmicb.2012.00213

Ahlgren, N. A., Belisle, B. S., and Lee, M. D. (2020). Genomic mosaicism underlies the adaptation of marine *Synechococcus ecotypes* to distinct oceanic iron niches. *Environ. Microbiol.* 22, 1801–1815. doi: 10.1111/1462-2920.14893

Biller, S. J., Berube, P. M., Lindell, D., and Chisholm, S. W. (2015). *Prochlorococcus*: the structure and function of collective diversity. *Nat. Rev. Microbiol.* 13, 13–27. doi: 10.1038/nrmicro3378

Breton, S., Jouhet, J., Guyet, U., Gros, V., Pittera, J., Demory, D., et al. (2020). Unveiling membrane thermoregulation strategies in marine picocyanobacteria. *New Phytol.* 225, 2396–2410. doi: 10.1111/nph.16239

Bristow, L. A., Mohr, W., Ahmerkamp, S., and Kuypers, M. M. M. (2017). Nutrients that limit growth in the ocean. *Curr. Biol.* 27, R431–R510. doi: 10.1016/j.cub.2017.03.030

Campbell, D., Hurry, V., Clarke, A. K., Gustafsson, P., and Öquist, G. (1998). Chlorophyll fluorescence analysis of cyanobacterial photosynthesis and acclimation. *Microbiol. Mol. Biol. Rev.* 62, 667–683. doi: 10.1128/mmbr.62.3.667-683.1998

Campbell, D., Zhou, G., Gustafsson, P., Oquist, G., and Clarke, A. K. (1995). Electron transport regulates exchange of two forms of photosystem II D1 protein in the cyanobacterium *Synechococcus*. *EMBO J.* 14, 5457–5466. doi: 10.1128/MMBR.62.3.667-683.1998

Caputi, L., Carradec, Q., Eveillard, D., Kirilovsky, A., Pelletier, E., Pierella Karlusich, J. J., et al. (2019). Community-level responses to iron availability in open ocean plankton ecosystems. *Glob. Biogeochem. Cycles* 33, 391–419. doi: 10.1029/2018GB006022

Clarke, A. K., Hurry, V. M., Gustafsson, P., and Oquist, G. (1993a). Two functionally distinct forms of the photosystem II reaction-center protein D1 in

the cyanobacterium *Synechococcus* sp. PCC 7942. *Proc. Natl. Acad. Sci. U.S.A.* 90, 11985–11989. doi: 10.1073/pnas.90.24.11985

Clarke, A. K., Soitamo, A., Gustafsson, P., and Oquist, G. (1993b). Rapid interchange between two distinct forms of cyanobacterial photosystem II reaction-center protein D1 in response to photoinhibition. *Proc. Natl. Acad. Sci. U.S.A.* 90, 9973–9977. doi: 10.1073/pnas.90.21.9973

Claustre, H., Sciandra, A., and Vaulot, D. (2008). Introduction to the special section bio-optical and biogeochemical conditions in the South East Pacific in late 2004: the BIOSOPE program. *Biogeosciences* 5, 679–691. doi: 10.5194/bg-5-679-2008

Delmont, T. O., Gaia, M., Hinsinger, D. D., Fremont, P., Guerra, A. F., Eren, A. M., et al. (2020). Functional repertoire convergence of distantly related eukaryotic plankton lineages revealed by genome-resolved metagenomics. *BioRxiv* [Preprint] BioRxiv: 2020.10.15.341214-2020.10.15.341214, doi: 10.1101/2020.10.15.341214

Doré, H., Farrant, G. K., Guyet, U., Haguait, J., Humily, F., Ratin, M., et al. (2020). Evolutionary mechanisms of long-term genome diversification associated with niche partitioning in marine picocyanobacteria. *Front. Microbiol.* 11:567431. doi: 10.3389/fmicb.2020.567431

Doré, H., Leconte, J., Breton, S., Demory, D., Hoebeke, M., Corre, E., et al. (2022). Global phylogeography of marine *Synechococcus* in coastal areas unveils strikingly different communities than in open ocean. *BioRxiv* [Preprint] doi: 10.1101/2022.03.07.483242

Dufresne, A., Ostrowski, M., Scanlan, D. J., Garczarek, L., Mazard, S., Palenik, B. P., et al. (2008). Unraveling the genomic mosaic of a ubiquitous genus of marine cyanobacteria. *Genome Biol.* 9:R90. doi: 10.1186/gb-2008-9-5-r90

Farrant, G. K., Doré, H., Cornejo-Castillo, F. M., Partensky, F., Ratin, M., Ostrowski, M., et al. (2016). Delineating ecologically significant taxonomic units from global patterns of marine picocyanobacteria. *Proc. Natl. Acad. Sci. U.S.A.* 113, E3365–E3374. doi: 10.1073/pnas.1524865113

Findlay, V. J., Tapiero, H., and Townsend, D. M. (2005). Sulfiredoxin: a potential therapeutic agent? *Biomed. Pharmacother.* 59, 374–379. doi: 10.1016/j.biopha.2005.07.003

Flombaum, P., Gallegos, J. L., Gordillo, R. A., Rincón, J., Zabala, L. L., Jiao, N., et al. (2013). Present and future global distributions of the marine Cyanobacteria *Prochlorococcus* and *Synechococcus*. *Proc. Natl. Acad. Sci. U. S. A.* 110, 9824–9829. doi: 10.1073/pnas.1307701110

Garcia, C. A., Hagstrom, G. I., Larkin, A. A., Ustick, L. J., Levin, S. A., Lomas, M. W., et al. (2020). Linking regional shifts in microbial genome adaptation with surface ocean biogeochemistry. *Philos. Trans. R. Soc. B Biol. Sci.* 375:20190254. doi: 10.1098/rstb.2019.0254

Garczarek, L., Dufresne, A., Blot, N., Cockshutt, A. M., Peyrat, A., Campbell, D. A., et al. (2008). Function and evolution of the *psbA* gene family in marine *Synechococcus*: *Synechococcus* sp. WH7803 as a case study. *ISME J.* 2, 937–953. doi: 10.1038/ismej.2008.46

Garczarek, L., Guyet, U., Doré, H., Farrant, G. K., Hoebeke, M., Brillet-Guéguen, L., et al. (2021). Cyanorak v2.1: a scalable information system dedicated to the visualization and expert curation of marine and brackish picocyanobacteria genomes. *Nucleic Acids Res.* 49, D667–D676. doi: 10.1093/nar/gkaa958

Gutiérrez-Rodríguez, A., Slack, G., Daniels, E. F., Selph, K. E., Palenik, B., and Landry, M. R. (2014). Fine spatial structure of genetically distinct picocyanobacterial populations across environmental gradients in the Costa Rica Dome. *Limnol. Oceanogr.* 59, 705–723. doi: 10.4319/lo.2014.59.3.0705

Guyet, U., Nguyen, N. A., Doré, H., Haguait, J., Pittera, J., Conan, M., et al. (2020). Synergic effects of temperature and irradiance on the physiology of the marine *Synechococcus* strain WH7803. *Front. Microbiol.* 11:1707. doi: 10.3389/fmicb.2020.01707

Humily, F., Partensky, F., Six, C., Farrant, G. K., Ratin, M., Marie, D., et al. (2013). A gene island with two possible configurations is involved in chromatic acclimation in marine *Synechococcus*. *PLoS One* 8:e84459. doi: 10.1371/journal.pone.0084459

Ihalainen, J. A., D'Haene, S., Yeremenko, N., van Roon, H., Arteni, A. A., Boekema, E. J., et al. (2005). Aggregates of the chlorophyll-binding protein IsiA (CP43') dissipate energy in cyanobacteria. *Biochemistry* 44, 10846–10853. doi: 10.1021/bi0510680

Inoue, N., Taira, Y., Emi, T., Yamane, Y., Kashino, Y., Koike, H., et al. (2001). Acclimation to the growth temperature and the high-temperature effects on photosystem II and plasma membranes in a mesophilic cyanobacterium *Synechocystis* sp. PCC6803. *Plant Cell Physiol.* 42, 1140–1148. doi: 10.1093/pcp/pce147

Johnson, Z. I., Zinser, E. R., Coe, A., McNulty, N. P., Woodward, E. M. S., and Chisholm, S. W. (2006). Niche partitioning among *Prochlorococcus* ecotypes along ocean-scale environmental gradients. *Science* 311, 1737–1740. doi: 10.1126/science.1118052

Kana, T. M., Glibert, P. M., Goericke, R., and Welschmeyer, N. A. (1988). Zeaxanthin and ß-carotene in *Synechococcus* WH7803 respond differently to irradiance. *Limnol. Oceanogr.* 33, 1623–1626. doi: 10.4319/lo.1988.33.6part2.1623

Kashtan, N., Roggensack, S. E., Rodrigue, S., Thompson, J. W., Biller, S. J., Coe, A., et al. (2014). Single-cell genomics reveals hundreds of coexisting subpopulations in wild *Prochlorococcus*. *Science* 344, 416–420. doi: 10.1126/science.1248575

Kent, A. G., Baer, S. E., Mouginot, C., Huang, J. S., Larkin, A. A., Lomas, M. W., et al. (2019). Parallel phylogeography of *Prochlorococcus* and *Synechococcus*. *ISME J.* 13, 430–441. doi: 10.1038/s41396-018-0287-6

Kettler, G. C., Martiny, A. C., Huang, K., Zucker, J., Coleman, M. L., Rodrigue, S., et al. (2007). Patterns and implications of gene gain and loss in the evolution of *Prochlorococcus*. *PLoS Genet.* 3:e231. doi: 10.1371/journal.pgen.0030231

Kirilovsky, D. (2007). Photoprotection in cyanobacteria: the orange carotenoid protein (OCP)-related non-photochemical-quenching mechanism. *Photosynth. Res.* 93:7. doi: 10.1007/s11120-007-9168-y

Larkin, A. A., and Martiny, A. C. (2017). Microdiversity shapes the traits, niche space, and biogeography of microbial taxa: the ecological function of microdiversity. *Environ. Microbiol. Rep.* 9, 55–70. doi: 10.1111/1758-2229.12523

Larkin, A. A., Blinebry, S. K., Howes, C., Lin, Y., Loftus, S. E., Schmaus, C. A., et al. (2016). Niche partitioning and biogeography of high light adapted *Prochlorococcus* across taxonomic ranks in the North Pacific. *ISME J.* 10, 1555–1567. doi: 10.1038/ismej.2015.244

Latifi, A., Ruiz, M., and Zhang, C. C. (2009). Oxidative stress in cyanobacteria. *FEMS Microbiol. Rev.* 33, 258–278. doi: 10.1111/j.1574-6976.2008.00134.x

Mackey, K. R. M., Paytan, A., Caldeira, K., Grossman, A. R., Moran, D., McIlvin, M., et al. (2013). Effect of temperature on photosynthesis and growth in marine *Synechococcus* spp. *Plant Physiol.* 163, 815–829. doi: 10.1104/pp.113.221937

Marie, D., Partensky, F., Vaulot, D., and Brussaard, C. (1999). Enumeration of phytoplankton, bacteria, and viruses in marine samples. *Curr. Protoc. Cytom* 10, 11.11.1–11.11.15. doi: 10.1002/0471142956.cy1111s10

Mella-Flores, D., Mazard, S., Humily, F., Partensky, F., Mahé, F., Bariat, L., et al. (2011). Is the distribution of *Prochlorococcus* and *Synechococcus* ecotypes in the Mediterranean Sea affected by global warming? *Biogeosciences* 8, 2785–2804. doi: 10.5194/bg-8-2785-2011

Mikami, K., and Murata, N. (2003). Membrane fluidity and the perception of environmental signals in cyanobacteria and plants. *Prog. Lipid Res.* 42, 527–543. doi: 10.1016/S0163-7827(03)00036-5

Moore, C. M., Mills, M. M., Arrigo, K. R., Berman-Frank, I., Bopp, L., Boyd, P. W., et al. (2013). Processes and patterns of oceanic nutrient limitation. *Nat. Geosci.* 6, 701–710. doi: 10.1038/ngeo1765

Murata, N., Takahashi, S., Nishiyama, Y., and Allakhverdiev, S. I. (2007). Photoinhibition of photosystem II under environmental stress. *Biochim. Biophys. Acta Bioenerg.* 1767, 414–421. doi: 10.1016/j.bbabio.2006.11.019

Nishiyama, Y., Allakhverdiev, S. I., and Murata, N. (2006). A new paradigm for the action of reactive oxygen species in the photoinhibition of photosystem II. *Biochim. Biophys. Acta BBA Bioenerg.* 1757, 742–749. doi: 10.1016/j.bbabio.2006.05.013

Paulsen, M. L., Doré, H., Garczarek, L., Seuthe, L., Müller, O., Sandaa, R.-A., et al. (2016). *Synechococcus* in the atlantic gateway to the arctic ocean. *Front. Mar. Sci.* 3:191. doi: 10.3389/fmars.2016.00191

Pearman, P. B., Guisan, A., Broennimann, O., and Randin, C. F. (2008). Niche dynamics in space and time. *Trends Ecol. Evol.* 23, 149–158. doi: 10.1016/j.tree.2007.11.005

Pittera, J., Humily, F., Thorel, M., Grulois, D., Garczarek, L., and Six, C. (2014). Connecting thermal physiology and latitudinal niche partitioning in marine *Synechococcus*. *ISME J.* 8, 1221–1236. doi: 10.1038/ismej.2013.228

Pittera, J., Jouhet, J., Breton, S., Garczarek, L., Partensky, F., Maréchal, É, et al. (2018). Thermoacclimation and genome adaptation of the membrane lipidome

in marine *Synechococcus*. *Environ. Microbiol.* 20, 612–631. doi: 10.1111/1462-2920.13985

Pittera, J., Partensky, F., and Six, C. (2017). Adaptive thermostability of light-harvesting complexes in marine picocyanobacteria. *ISME J.* 11, 112–124. doi: 10.1038/ismej.2016.102

Polovina, J. J., Howell, E. A., and Abecassis, M. (2008). Ocean's least productive waters are expanding. *Geophys. Res. Lett.* 35:L03618. doi: 10.1029/2007GL031745

Rippka, R., Coursin, T., Hess, W., Lichtle, C., Scanlan, D. J., Palinska, K. A., et al. (2000). *Prochlorococcus marinus Chisholm* et al. 1992 subsp. *pastoris* subsp. nov. strain PCC 9511, the first axenic chlorophyll *a2/b2*-containing cyanobacterium (*Oxyphotobacteria*). *Int. J. Syst. Evol. Microbiol.* 50, 1833–1847. doi: 10.1099/00207713-50-5-1833

Saito, M. A., Rocap, G., and Moffett, J. W. (2005). Production of cobalt binding ligands in a *Synechococcus* feature at the Costa Rica upwelling dome. *Limnol. Oceanogr.* 50, 279–290. doi: 10.4319/lo.2005.50.1.0279

Scanlan, D. J., Ostrowski, M., Mazard, S., Dufresne, A., Garczarek, L., Hess, W. R., et al. (2009). Ecological genomics of marine picocyanobacteria. *Microbiol. Mol. Biol. Rev.* 73, 249–299. doi: 10.1128/MMBR.00035-08

Schloss, P. D., Westcott, S. L., Ryabin, T., Hall, J. R., Hartmann, M., Hollister, E. B., et al. (2009). Introducing Mothur: Open-source, platform-independent, community-supported software for describing and comparing microbial communities. *Appl. Environ. Microbiol.* 75, 7537–7541. doi: 10.1128/AEM.01541-09

Schmidt, K., Birchill, A. J., Atkinson, A., Brewin, R. J. W., Clark, J. R., Hickman, A. E., et al. (2020). Increasing picocyanobacteria success in shelf waters contributes to long-term food web degradation. *Glob. Change Biol.* 26, 5574–5587. doi: 10.1111/gcb.15161

Six, C., Joubin, L., Partensky, F., Holtzendorff, J., and Garczarek, L. (2007). UV-induced phycobilisome dismantling in the marine picocyanobacterium *Synechococcus* sp. WH8102. *Photosynth. Res.* 92, 75–86. doi: 10.1007/s11120-007-9170-4

Six, C., Ratin, M., Marie, D., and Corre, E. (2021). Marine *Synechococcus* picocyanobacteria: light utilization across latitudes. *Proc. Natl. Acad. Sci. U.S.A.* 118:e2111300118. doi: 10.1073/pnas.2111300118

Six, C., Thomas, J., Brahamsha, B., Lemoine, Y., and Partensky, F. (2004). Photophysiology of the marine cyanobacterium *Synechococcus* sp. WH8102, a new model organism. *Aquat. Microb. Ecol.* 35, 17–29. doi: 10.3354/ame035017

Six, C., Thomas, J.-C., Thion, L., Lemoine, Y., Zal, F., and Partensky, F. (2005). Two novel phycoerythrin-associated linker proteins in the marine cyanobacterium *Synechococcus* sp. strain WH8102. *J. Bacteriol.* 187, 1685–1694. doi: 10.1128/JB.187.5.1685-1694.2005

Sohm, J. A., Ahlgren, N. A., Thomson, Z. J., Williams, C., Moffett, J. W., Saito, M. A., et al. (2016). Co-occurring *Synechococcus* ecotypes occupy four major oceanic regimes defined by temperature, macronutrients and iron. *ISME J.* 10, 333–345. doi: 10.1038/ismej.2015.115

Sunagawa, S., Coelho, L. P., Chaffron, S., Kultima, J. R., Labadie, K., Salazar, G., et al. (2015). Structure and function of the global ocean microbiome. *Science* 348, 1261359–1261359. doi: 10.1126/science.1261359

Torabi, S., Umate, P., Manavski, N., Plöchinger, M., Kleinknecht, L., Bogireddi, H., et al. (2014). PsbN is required for assembly of the photosystem II reaction center in *Nicotiana tabacum*. *Plant Cell* 26, 1183–1199. doi: 10.1105/tpc.113.120444

Umena, Y., Kawakami, K., Shen, J.-R., and Kamiya, N. (2011). Crystal structure of oxygen-evolving photosystem II at a resolution of 1.9 Å. *Nature* 473, 55–60. doi: 10.1038/nature09913

Visintini, N., Martiny, A. C., and Flombaum, P. (2021). *Prochlorococcus*, *Synechococcus*, and picoeukaryotic phytoplankton abundances in the global ocean. *Limnol. Oceanogr. Lett.* 6, 207–215. doi: 10.1002/lol2.10188

Wilkins, D., Lauro, F. M., Williams, T. J., Demaere, M. Z., Brown, M. V., Hoffman, J. M., et al. (2013). Biogeographic partitioning of Southern Ocean microorganisms revealed by metagenomics. *Environ. Microbiol.* 15, 1318–1333. doi: 10.1111/1462-2920.12035

Xia, X., Cheung, S., Endo, H., Suzuki, K., and Liu, H. (2019). Latitudinal and vertical variation of *Synechococcus* assemblage composition along 170°W transect from the South Pacific to the Arctic Ocean. *Microb. Ecol.* 77, 333–342. doi: 10.1007/s00248-018-1308-8

Xia, X., Partensky, F., Garczarek, L., Suzuki, K., Guo, C., Cheung, S. Y., et al. (2017). Phylogeography and pigment type diversity of *Synechococcus* cyanobacteria in surface waters of the northwestern Pacific Ocean. *Environ. Microbiol.* 19, 142–58. doi: 10.1111/1462-2920.13541

Xu, W., and Wang, Y. (2017). "Function and structure of cyanobacterial photosystem I," in *Photosynthesis: Structures, Mechanisms, and Applications*, eds H. J. M. Hou, M. M. Najafpour, G. F. Moore, and S. I. Allakhverdiev (Cham: Springer International Publishing), 111–168. doi: 10.1007/978-3-319-48873-8_7

Yeremenko, N., Kouřil, R., Ihalainen, J. A., D'Haene, S., van Oosterwijk, N., Andrizhiyevskaya, E. G., et al. (2004). Supramolecular organization and dual function of the IsiA chlorophyll-binding protein in cyanobacteria. *Biochemistry* 43, 10308–10313. doi: 10.1021/bi048772l

Zwirglmaier, K., Jardillier, L., Ostrowski, M., Mazard, S., Garczarek, L., Vaulot, D., et al. (2008). Global phylogeography of marine *Synechococcus* and *Prochlorococcus* reveals a distinct partitioning of lineages among oceanic biomes. *Environ. Microbiol.* 10, 147–161. doi: 10.1111/j.1462-2920.2007.01440.x

Conflict of Interest: The authors declare that the research was conducted in the absence of any commercial or financial relationships that could be construed as a potential conflict of interest.

Publisher's Note: All claims expressed in this article are solely those of the authors and do not necessarily represent those of their affiliated organizations, or those of the publisher, the editors and the reviewers. Any product that may be evaluated in this article, or claim that may be made by its manufacturer, is not guaranteed or endorsed by the publisher.